Dissertation zur Erlangung des Doktorgrades
der Fakultät für Chemie und Pharmazie
der Ludwig-Maximilians-Universität München

Pulmonary Delivery of Pharmaceutical Proteins by Means of Vibrating Mesh Nebulization

Sebastian Peter Hertel
aus
Berlin, Deutschland

2014

Erklärung

Diese Dissertation wurde im Sinne von § 7 der Promotionsordnung vom 28. November 2011 von Herrn Prof. Dr. Gerhard Winter betreut.

Eidesstattliche Versicherung

Diese Dissertation wurde eigenständig und ohne unerlaubte Hilfe erarbeitet.

München, 28.05.2014

.... ..

(Sebastian Peter Hertel)

Dissertation eingereicht am 04.06.2014

1. Gutachter: Prof. Dr. Gerhard Winter
2. Gutachter: Prof. Dr. Wolfgang Frieß

Mündliche Prüfung am 07.07.2014

Acknowledgements

The work reported in this thesis would not have been possible without the help of many people who have supported me throughout this pursuit and beyond.

Prof. Gerhard Winter has been a great supervisor. His wealth of knowledge and ideas, which he is happy to share, is inspirational. I want to particularly thank him for the independence and trust and lately the patience I experienced during the years.

Prof. Wolfgang Frieß co-supervised my thesis and deserves my thanks for his expert advice not only in the field of pulmonary delivery.

Together, they manage to create the framework for the great team and productive working atmosphere that made the preparation of this thesis in their labs very much worthwhile.

The core project of this thesis arose through SuppreMol, who merged two fascinating topics biopharmaceuticals and pulmonary delivery into an awesome project that I enjoyed working on from the first day to the last. While I want to name Dr. Thomas Pohl and Dr. Peter Sondermann, my gratitude for scientific guidance and discussions, a welcoming atmosphere and, very important, generous supply of precious SM101 material is extended to the entire team. I appreciate the unique opportunity that I had during the years, to accompany SuppreMol on their mission to enable novel treatment options for autoimmune diseases. I wish them success to achieve their goal.

Otmar Schmid and his team at the Comprehensive Pneumology Center (CPC) conducted all in vivo experiments reported in this thesis. I am grateful for the opportunity to participate in *in vivo* lab work at the CPC and our nebulizer handovers at the local grocery store. Juliane Freitag deserves a special acknowledgment, as her master thesis provided important input for my thesis.

Many thanks are due for the equally valuable contributions to this thesis, made by the students I supervised during their bachelor thesis or internships: Markus Rotter, Melanie Patzak, Franziska Wurst, Claudia Menzel und Bernhard Lohrer.

Financial support of large parts of this work is acknowledged to the BMBF grant "KMU-innovativ: Biotechnologie BioChance".

I am happy to have shared the labs with very generous and supportive colleagues. Thank you, not only for the lively discussions but especially for the merry times I had in and out of the lab, be it on the soccer field or at the barbeques, the ski slope or the Dorf-Alm dance floor. Special thanks go to Thomas, Raimund, Angelika, Elsa, Markus, Gerd, Christian and Veronika.

My favorite (and only) lab-mate Alice deserves thanks for a lot of reasons. I really lived off her constant supply of sweets and "Ohrwürmer" for our lab.

Special thanks go to Matthias Lamberti who let me experience some startup culture while sharing his office where the majority of these pages have been written.

All that would not have happened without the everlasting support, love and education I receive from my parents and my sister. Thank you for baby-sitting as I am writing these lines and for the constant bugging about the stage of this work.

I want to conclude with expressing my indescribable gratitude to my best (and most beautiful) "cooperation partner", who always covers my back when needed and beyond. Anna, you and Emil always gave me a good reason and a place to escape from experiments and thesis writing.

Table of Content

List of Abbreviations

AAD	adaptive aerosol delivery
AATD	alpha-1-antitrypsin deficiency
ADA	anti-drug antibody
ADCC	antibody dependent cellular cytotoxicity
aDE	active delivery efficiency
AF	aerosol formulation
aIAR	active inhalable aerosol rate
AM	alveolar macrophages
ANOVA	one-way analysis of variance
anti-OVA IgG	anti-chicken egg albumin antibody
API	active pharmaceutical ingredient
aRF	active respirable fraction
BAL	bronchoalveolar lavage
BALF	bronchoalveolar lavage fluid
BSA	bovine serum albumin
CCF	central-composite-face centered design
CEX-HPLC	cation exchange high performance liquid chromatography
CF	cystic fibrosis
COPD	chronic obstructive pulmonary disease
CPC	Comprehensive Pulmonology Center
d[v,50]	see VMD
DAC	Deutscher Arzneimittel Codex (German Pharmaceutical Codex)
DE	delivery efficiency
>DL	above detector limit
DoE	design of experiment
DP	drug product
DPI	dry powder inhaler
DSC	differential scanning calorimetry
µDSC	microcalorimetry
DSMZ	Deutsche Sammlung von Mikroorganismen und Zellkulturen
ELISA	enzyme-linked immunosorbent assay
F/T	freeze/thaw
FACS	fluorescence activated cell sorting
FcγR	receptor for the Fc part of immunoglobulin G
FDA	US Food and Drug Administration
FDKP	fumaryl diketopiperazine
FNU	formazine nephelometric units
FPF	fine particle fraction

G-CSF	granulocyte-colony stimulating factor
GSD	geometric standard deviation
HBS	histidine buffered saline
HCC	Home Cage Control
HPβCD	hydroxypropyl-β-cyclodextrin
HSC	hematopoietic stem cells
i.t.	intratracheal
i.v.	intravenous
IAR	inhalable aerosol rate
IC	immune complex
IgG/ IgE	immunoglobulin G
IL	interleukin
IL	initial load
IM	intermittent
INF	interferon
ITP	primary immune thrombocytopenia
IVIS	*in vivo* imaging system
IVN	vented intubated nebulization
LDH	lactic dehydrogenase
mAb	monoclonal antibody
MDI	metered dose inhaler
MMAD	mass median aerodynamic diameter
MnSOD	manganese superoxide dismutase
MOPS	3-(N-Morpholino) propanesulfonic Acid
MWCO	molecular weight cut-off
NADH	reduced form of nicotinamide adenine dinucleotide
NDA	new drug application
o.t.	oro-tracheal
OD	optical density
OL	overloaded
OR	output rate
OVA	ovalbumin, chicken egg albumin
PBS	phosphate buffered saline
PC	pre-cooled
PEG	polyethylene glycol
PF	parenteral formulation
pI	isoelectric point
pMDI	pressurized metered dose inhaler
PP	polypropylene

PS80, PS20	polysorbate (80 and 20)
psig	pound-force per square inch
PVDF	polyvinylidene fluoride
rAAT	recombinant alpha-1-antitrypsin
RBC	red blood cells
RC	reflux condenser
ref.	reference
RF	respirable fraction
rh	recombinant human
rhConINF	recombinant human consensus interferon
ROI	region of interest
RP-HPLC	reversed phase high performance liquid chromatography
RSV	respiratory syntactical virus
SCOP	structural classification of proteins
SD	standard deviation
SDS	sodium dodecyl sulfate
SE-HPLC	size exclusion high performance liquid chromatography
sFcγR	soluble Fc receptor for immunoglobulin G (ectodomain)
SLE	systemic lupus erythematosus
SLPI	secretory leukoprotease inhibitor
SM101	soluble extracellular domain of FcγRIIB developed by SuppreMol GmbH
T_{agg}	protein aggregation temperature
TFA	trifluoric acid
T_m	protein unfolding temperature
TOR	total output rate
T_{RES}	reservoir temperature
$T_{RES\ AVG}$	average reservoir temperature
$T_{RES\ MAX}$	maximum reservoir temperature
TSI	twin stage impinger
US nebulizer	ultrasonic nebulizer
VM nebulizer	vibrating mesh nebulizer
VMD	volume median diameter
VMN	vibrating mesh nebulization

Chapter I Aim of the Thesis

The objective of this thesis was to investigate the suitability of vibrating mesh (VM) nebulization for the pulmonary delivery of sensitive pharmaceutical proteins.

Vibrating mesh nebulization has proven to enable efficient, fast and with the latest generation of inhaler devices highly reproducible pulmonary delivery of small molecular drugs. These performance properties are very interesting for the pulmonary delivery of costly biopharmaceuticals and VM nebulizers have been used to nebulize a range of proteins. Detailed studies on the possible impact of VM nebulization on protein stability an obligatory requirement and a major issue concerning all aerosol generating methods have not yet been published though. Many of the proteins successfully nebulized with VM devices so far, can be considered rather stable (DNase, α1-AT, IL) [1]. Hence, the suitability of VM nebulization for the pulmonary delivery of more delicate pharmaceutical proteins has not been conclusively assessed.

A major aim of this thesis was therefore a thorough characterization of VM nebulization in order to evaluate its feasibility to aerosolize liquid formulations of delicate pharmaceutical proteins. This included an investigation to identify forces causing protein degradation encountered during VM nebulization. Furthermore the influence of proteins and their formulations on nebulizer performance was examined. Based on the gathered data, procedures to mitigate respective detrimental forces were developed and evaluated for their efficiency (**Chapter IV**).

Another objective was the integration of the nebulization process into formulation development in a high throughput fashion. A surrogate screening method was developed to predict protein stability after VM nebulization while consuming only a fraction of valuable time and API material necessary for actual nebulization. The method was evaluated for three different proteins (**Chapter V**).

The initial stimulus and the pivotal and connecting element of this work was the assessment of feasibility for the local pulmonary delivery of the biopharmaceutical SM101 via nebulization and

the development of a respective formulation. SM101 is a soluble human FcγRIIB receptor currently in development by SuppreMol (Martinsried, Germany) for the treatment of primary immune thrombocytopenia and systemic lupus erythematosus and potential candidate for topical pulmonary delivery. A final objective was the evaluation of SM101 *in vivo* efficacy for the treatment of pulmonary type III hypersensitivity reaction. This included the identification of suitable aerosol delivery methods for administration to small laboratory animals and the development of a disease model applicable for SM101 efficacy testing (**Chapter VI**).

Chapter II Introduction

1 Rationale for pulmonary delivery of biopharmaceuticals

The rationale for pulmonary delivery of biopharmaceuticals can be ascribed to two different aims. On the one hand, systemic delivery through the lungs has been suggested to be a very promising non-invasive alternative to intravenous delivery of biopharmaceuticals featuring the unique combination of a highly disperse dosage form and a huge absorptive area directly interfacing with the blood circulation system [2, 3]. Additionally the level of metabolizing enzymes is reduced compared to the GI tract [4] and absorbed molecules do not undergo a first pass effect [5]. Accordingly, bioavailability for proteins was reported to be the highest for any non-invasive route [6]. While insulin has been a driving force for research in the field, the withdrawal of Exubera® has also demonstrated some of the difficulties accompanying this approach [7-9].

On the other hand, motivation for biopharmaceutical delivery to the lungs is the topical treatment of respiratory diseases. Direct access to the site of action allows for high local API concentrations while minimizing systemic exposure to the drug [10-12], making therapies more effective and safe. In 1996 Pulmozyme® (Dornase alfa, DNase) became available for the treatment of cystic fibrosis as the first inhaled biopharmaceutical. Unlike Exubera® it is also a market success with annual sales topping $600 million in 2011 and 2012 [13]. Local pulmonary delivery is an interesting opportunity for the treatment of respiratory diseases like CF, COPD, asthma or pulmonary fibrosis [14]. Various peptides and proteins are under development for the treatment of lung malignancies [15], lung transplant rejection [16], α1-antitrypsin deficiency (genetic emphysema) [17-20] or for pulmonary vaccination. An inhalative measles vaccination was reported to be superior to a parenteral vaccination in 4 million children [21].

Despite the advantageous biological situation and the successful example of Pulmozyme®, no other inhaled biopharmaceutical is approved to date. A selection of biopharmaceuticals in development for inhalation is listed in Table II-1. Many of the challenges of successful inhalation

of a biopharmaceutical apply for both, local and systemic delivery [22] although local treatment may seem an easier target [7].

Table II-1: Examples of proteins for inhalation, in parts taken from [23] and [24].

Peptide/Protein	Disease State	Device	Reference; clinical trial number
Dornase alfa (DNase)	Cystic fibrosis (CF)	approved for nebulization; AERx	Genenzyme NCT01712334; [25-29] [30]
recombinant Alpha-1-antitrypsin (rAAT), Alpha-1-proteinase inhibitor	Alpha-1-antitrypsin deficiency (AATD), CF	Nebulization	NCT00486837, Talecris, Phase III; [17] NCT01217671, Kamada, Phase III; [31-33]
IgG1	lung cancer	nebulization DPI	[15, 34] [35-37]
BIO-11006	COPD	Nebulization	NCT00648245; [38]; BioMarck, Phase II
IL-4/IL-13 antagonist (Pitrakinra)	asthma	DPI	NCT00801853; [39]; [43], Aerovance; Phase II
rh-IL-4 receptor	asthma	AERx	[40]
Bikunin (Aerolytic®)	CF, COPD	nebulization	Aerovance; Phase II
Secretory leukoprotease inhibitor (SLPI)	Emphysema/CF	Nebulization DPI	[41] [42]
Interferon-α	Tuberculosis, lung metastases	Nebulizer AERx	[43, 44] [45]
Interferon-β	asthma Respiratory viruses Multiple sclerosis Lung cancer	i-neb AAD	NCT01126177, Synairgen, phase II
Interferon-γ	IPF; tuberculosis; lung cancer Cancer/Pneumocystis carinii	i-neb AAD	[46]
Interferon-ω	viral infections	Respimat®	[47]
Interleukin-2	Cancer	Jet nebulizer	[48, 49]
Anti-IgE mAb (Omalizumab®)	Asthma	Jet nebulizer DPI	[50] [51]
Catalase	Oxidative stress		[52]
Liposomal rh-Cu/Zn–Superoxide dismutase	Acute lung Injury	eFlow	[53]
Mn-Superoxide dismutase	anti-inflammatory	Respimat®	[47]
Calcitonin	Osteoporosis	DPI	[54]
Parathyroid hormone	Osteoporosis	i.t.	[55]
Human growth hormone	Growth deficiency	DPI	[56]

Peptide/Protein	Disease State	Device	Reference; clinical trial number
Insulin	Diabetes		
Exubera®		DPI	[57], Nektar/Pfizer withdrawn
AFREZZA®		DPI	[58], NCT01451398
Adagio™			Mannkind, NDA submitted
		nebulizer	Dance Biopharm Inc
			EudraCT: 2012-002071-34
insulin-like growth factor-I	Diabetes	nebulizer	[59]
GLP-1	Diabetes	i.t.	[60]
rhG-CSF	Neutropenia	Nebulizer	[61]
GM-CSF	Pulmonary alveolar proteinosis; lung metastases	AKITA Jet nebulizer	[62] [63-66]
EPO-Fc	Anemia	Nebulizer	[67, 68]
IFN-α-Fc	Lung cancer, tuberculosis	Nebulizer	[69]
IFN-β-Fc	Lung cancer Multiple sclerosis	Nebulizer	[70]
FSH-Fc	Infertility treatment	Nebulizer	[71]

2 The challenges of pulmonary delivery

A major obstacle is the achievement of sufficient and reproducible pulmonary API deposition, which is complicated by a highly branched lung geometry, different clearance mechanisms that prevent prolonged residence times and the great, yet uncontrolled impact of the patients breathing maneuver on aerosol deposition and distribution. At the same time aerosol generation must not corrupt the fragile stability of biopharmaceuticals to prevent a loss of biologic activity or unwanted toxic or immunogenic side effects. As demonstrated by the Exubera® failure, user-friendly and convenient operation of delivery devices is another requirement to gain market acceptance [7-9].

For aerosols to deposit into the lungs, the branched geometry of the airways, mucociliary clearance and phagocytosis by alveolar macrophages [72, 73], that evolved to prevent the deposition of foreign material into the lungs, need to be overcome. This is achieved by the generation of an aerosol of sufficiently small particles by means of an inhaler device. The

probability of aerosol deposition in the lungs is determined by the diameter (d) of the generated aerosol particles and the breathing maneuver performed by the patient [74] (v = speed ~ respiratory flow rate; t = time ~ breath holding time), which both influence the forces relevant for aerosol deposition mechanics [10, 22, 75, 76]:

Inertial Impaction	$\sim d^2 * v$
Gravitational Sedimentation	$\sim d^2 * t$
Diffusion by Brownian motion	$\sim t / d$

Since breathing patterns differ substantially among individuals but are beyond control of common inhalers, pulmonary deposition of an aerosol is commonly predicted based on its particle size distribution [77-79] which is easily accessible by in vitro analytics. According to deposition models, it is assumed that particles in a range of 1-5 µm deposit in the small respiratory airways, while larger droplets deposit on the throat and conducting airways and smaller aerosol particles may be exhaled. These predictions might not be very accurate though [10] since they are based on deposition models of monodisperse environmental aerosols in healthy male subjects instead of more polydisperse pharmaceutical aerosols of higher density [10].

Various inhaler types have been developed to achieve pulmonary delivery and with them pulmonary delivery has been established for the treatment of respiratory diseases with small molecule drugs. Indications include asthma, chronic obstructive pulmonary disease (COPD) and other respiratory ailments like cystic fibrosis or emphysema. Apart from these common inhalation therapies, pulmonary delivery is also used in the treatment of RSV infections, tuberculosis, croup, primary pulmonary hypertension, influenza and schizophrenia [80]. Metered dose inhalers (MDI) and especially dry powder inhalers (DPI) are the dominant devices types for small molecule drug administration to the lungs. In contrast the only marketed inhaled biological Pulmozyme® is exclusively available for nebulization. Likewise, with a few exceptions, biopharmaceuticals in development for inhalation are designated for nebulization (see Table II-1). Otherwise, nebulizers are confined to treatments requiring frequent administration of large doses, e.g. in cystic fibrosis or for aerosol delivery to children and elderly patients. Nebulizers are employed during stationary treatments in hospitals and are the only possibility to administer aerosols to intubated patients. All prevalent device types have been available for 50 years or more and each type has its eligibility

Table II-2: Attributes of an ideal medical inhaler, taken from [81].

Reliable, reproducible and accurate dosing and particle generation
Generation of small particles of 1-5 µm
Simple use and handling
Multiple dose capability
Resistance to bacterial contamination
Durability
Cost effectiveness
Product stability

while none can combine all the properties proposed for an ideal medical inhaler by Wolff and Niven [81] (Table II-2).

The shortcoming with respect to exact dosing is tolerated for treatment with small molecular drugs, as they usually possess a large therapeutic index and can achieve a safe and effective therapeutic treatment even if the pulmonary delivered dose is variable and contains only a fraction of the charged amount [10, 82]. Biopharmaceutical inhalation may require stricter rules in order to be successful. Especially the high costs of biopharmaceuticals call for a more efficient and less wasteful delivery. High potency and specificity may also make a better control over the deposited dose and the spatial distribution within different lung regions mandatory.

An aspect of paramount importance for biopharmaceuticals is their delicate stability whose conservation is essential for biologic activity. Protein degradation can occur at any given stage including production, processing, formulation or shipping and storage. Many excellent and comprehensive reviews have been published that describe the diverse manifestations of protein degradation and elucidate various factors and influences provoking such [83-88]. These include elevated temperature, extreme pH, shaking and shearing stress, light exposure, freezing or drying which may results in physical or chemical protein degradation. Chemical degradation relates to alterations in the primary structure of protein, which among other mechanisms may be caused by deamidation, oxidation or hydrolysis. Physical degradation on the other hand, manifests as aggregation, adsorption or loss of secondary, tertiary or quaternary protein structure.

Given the relative robustness of small molecular drugs, the impact of aerosol generation on molecular integrity has not been a major focus during the development or optimization of aerosol delivery devices but is of utmost importance for successful inhalation of biopharmaceuticals.

3 Metered dose inhalers and dry powder inhalers

The currently available inhaler device classes differ significantly in the requirements for the formulation of the biopharmaceutical to be delivered.

In MDIs, the API is dissolved or suspended in a propellant such as HFA 134a which raises concerns regarding protein solubility and especially protein stability. Consequentially this approach is less promising for biopharmaceutical inhalation than DPI or nebulizer based delivery. Nevertheless, the feasibility of MDI suspensions for biopharmaceutical delivery was demonstrated with spray-dried [89] or lyophilized [90] BSA formulations as well as lyophilized nanoparticles containing lysozyme [91] or thymopentin [92]. Considering the high cost of biopharmaceuticals, a further disadvantage of pMDIs is their low lung deposition efficiency in the range of 10-20% of the metered dose [93, 94] and the significant inter- and intra-individual dose variability in the range of 40-80% [95-97]. When used without a spacer, up to 75% of the metered dose deposit on the oropharynx and may be swallowed. Furthermore, the complicated handling of pMDIs has been documented with reports of 76% of patients making at least one error in MDI handling [98].

Unlike MDIs, DPIs do not require coordination of breathing and actuation by the patient since particle disaggregation relies on the patients inspiratory flow rate instead of a propellant [1, 7]. This may prove unfavorable though for young children, elderly patients or patients with severe conditions or acute exacerbations when inspiratory flow may be too low for powder deagglomeration. Consequently, handling problems observed in 4-94% of the patients, depending on the DPI model used, were especially prevalent with young children [99]. Lung doses range between 10-30% [93, 100] and also underlie individual variations in a range of 8-47% [95-97].

Biopharmaceutical delivery via DPIs requires the precedent drying of the API since it is usually initially available as a liquid drug substance. Protein stability is usually improved in the solid state wherefore DPI is considered a promising approach for biopharmaceutical delivery to the

lungs with some drug candidates being in clinical development (see table 1). Various techniques for protein drying and particle generation have been reviewed for pulmonary delivery [12, 101]. These include spray drying and lyophilization as were used for the insulin formulations of Exubera® and AFREZZA® respectively. Prior to its withdrawal, Exubera® was the first and only approved and marketed DPI for biopharmaceutical inhalation. AFREZZA® is one of only two inhalable insulin developments still active after Pfizer stopped Exubera® sales (the second being Adagio™ by Dance Biopharm based on nebulization). In the aftermath additional data on AFREZZA® was demanded by the FDA. In October 2013 Mannkind Corporation submitted the third new drug application (NDA) for AFREZZA®. A decision is expected in July 2014, after an FDA advisory committee had recommended to grant AFREZZA® approval in April 2014.

On the downside, DPI development and manufacture is more complex and costly [1]. The formulation is a crucial determinant of deposition efficiency. Particles must be small for optimum lung deposition while at the same time the powder must be free flowing for disaggregation during inhalation [94]. However fine powders are cohesive and have poor flow properties [94]. The conflict is usually solved by the addition of large inert carrier particles which improve powder flowability. As a consequence, the maximum amount of API deliverable in a single inhalation is significantly reduced [102]. The amount of powder inhaled is limited since high powder doses may induce cough [1]. Humidity poses a problem for particle disaggregation and protein stability [103].

Several proprietary particle formulation technologies have addressed these problems by means of large porous particles that have advantageous aerodynamic properties and can significantly enhance the lung dose of a single inhalation [7] with reported lung deposition of 50% [104]. The already mentioned AFREZZA® is built on Technosphere® microparticles, made from fumaryl diketopiperazine (FDKP). Arcus® formerly known as AIR® are large porous particles made from PLGA generated by spray drying [104]. They were originally intended for the pulmonary delivery of insulin (Alkermes in cooperation with Eli Lilly) and are now developed as a pulmonary delivered Parkinson therapy by Civitas therapeutics. Finally the PulmoSphere® technology has gained FDA approval as part of Novartis' TOBI podhaler in March 2013. These large porous particles are based on long-chain phospholipids [105]. Besides insulin, these large porous particle platforms have also been employed for the pulmonary delivery of other biopharmaceuticals like PTH [106], hGH [107], sCT [108], GLP-1 [109] and immunoglobulins [110, 111].

4 Nebulizers

If protein stability permits the use of a liquid formulation, nebulizers are the device of choice for atomization, while the API may be formulated either in solutions or in a suspensions. Liquid formulations are usually available in early stages of biopharmaceutical development and nebulizers are readily available to atomize virtually any liquid formulation. Avoiding additional process steps like drying, formulation development for nebulization is usually simpler, less expensive and faster than for dry powder formulations, allowing for a faster progression to clinical trials. Nebulizers can be categorized according to the mechanism of atomization into jet, ultrasonic or vibrating mesh nebulizers. Factors relevant for protein degradation and inactivation depend on the underlying mechanism of aerosol generation.

4.1 Proteins and the Air-liquid interface

A feature inherent for any nebulizer regardless of its atomization principle is the generation of a huge air-liquid interface during dispersion of the bulk liquid into micron-sized aerosol droplets. Since proteins are amphiphilic molecules they have the tendency to interact with interfaces, which is often associated with protein adsorption, (partial) unfolding and aggregation.

The very hydrophobic air-liquid interface is ubiquitous during protein manufacturing, processing, handling or storage [85, 112, 113] and stress testing involving a forced exposition to the air-liquid interface by agitation is routinely conducted during formulation development to predict protein stability. The extent of interface generated during such agitation experiments can be sufficient to provoke severe protein aggregation. Shaking of insulin elicited distinct aggregation [114]. IgG1 antibody agitation led to the formation of soluble aggregates and subvisible particles [115, 116]. After shaking of recombinant factor XIII [117] and vortexing of human growth hormone [118] non-covalent, insoluble aggregates were formed to a large extent.

Protein interaction with the air-liquid interface does not always result in protein degradation though [119]. The extent of protein aggregation and the formed species rather depend on individual protein characteristics determining its aggregation propensity and the probability and intensity of interface interaction. Aggregation propensity is ultimately governed by the primary structure [83], e.g. the proportion and distribution of hydrophobic residues and charge [120] in

the amino acid sequence, as well as secondary structure motifs [121]. The probability and intensity of interaction with interfaces is determined by the surface area available, surface tension and the surface activity of the protein [86, 122], which is influenced by various properties including molecule size, charge, hydrophobicity, stability and structural features [123].

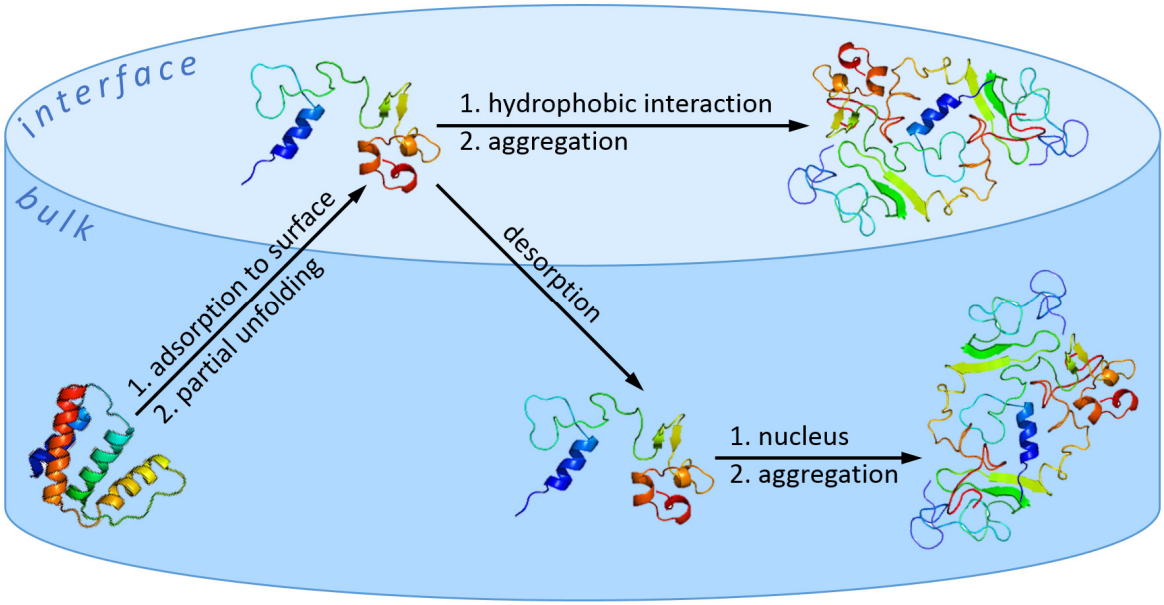

Figure II-1: Mechanism of air-liquid interface induced aggregation. Protein models are reprinted (adapted) with permission from [124](Copyright (2012) American Chemical Society).

Air-liquid interface induced aggregation is a mechanism involving multiple phases [87, 125] (Figure II-1). Initially monomer is adsorbed to the interface. Upon contact, molecules align to the interface thereby taking a flat confirmation [125, 126]. This involves at least partial unfolding of the monomer and hydrophobic residues which are normally buried within the native structure [127, 128] now interact with the gaseous phase. A monolayer of partially unfolded molecules is formed until allocation of the entire surface area available. This step proceeds fast [129, 130], occurring within one second for lysozyme [131] and can be speeded up with increasing protein concentration [125]. The exposition of hydrophobic residues is associated with an increase in surface activity and a decrease in biological activity [129].

In a subsequent step occurring at a much slower rate [129, 130], molecules may undergo changes in their secondary structure depending on the protein [125, 129, 132] and on the layer of adsorption. While lysozyme molecules located in the primary layer with direct contact to the interface take mainly antiparallel beta-sheet conformation, molecules in the secondary and additional layers interact with the hydrophilic residues of the unfolded molecules and assume a loose confirmation dominated by random coil [125].

Aggregation may occur directly in the interface where the proximity of hydrophobic residues increases the probability of inter-molecular interactions. Additionally, non-native protein molecules may serve as nuclei for aggregation in the bulk solution after desorption from the interface [86, 87]. Aggregated species may be detected as oligomers and soluble aggregates or grow further to form insoluble aggregates including subvisible and visible particles. The respective pathways are very complex and differentiate from protein to protein and for different formulations [117, 133].

Partial unfolding in the interface also impacts on thermal protein degradation. Instead of the sharp transition between the folded and unfolded state observable during T_m measurements of bulk solutions, thermal unfolding of protein adsorbed to an interface occurs over a broad range of temperatures lower than the bulk T_m [128].

It has been estimated that the nebulization of 10 mL solution with a jet nebulizer is associated with the generation of air-liquid interface greater than 24 m^2 [134] or even 1500 m^2 [135]. The plentiful emergence of air-liquid interface during nebulization is therefore presumably a major detrimental impact on protein stability.

The actual extent of protein degradation by air-liquid interface effects or other detrimental factors present during nebulization also depends on the nebulizer type used. While dedicated studies are available for jet and US nebulizers, less information is available for VM devices.

4.2 Aerosolization of Proteins by Jet Nebulizers

Jet nebulizers apply the energy of a compressed gas – usually air – to atomize a liquid. The liquid is forced through a nozzle by means of a high-velocity air-stream (Venturi effect; see Figure II-2). The liquid entrained into the stream is sheared into a thin film which breaks up into primary aerosol droplets. This primary aerosol has a very broad droplet size distribution ranging from <1 to 600 µm [134]. An array of baffles is used to filter all droplets of inadequate size so only droplets in the desired size range are delivered to the nebulizer's mouthpiece. Larger droplets, which make up more than 97% of the primary aerosol [1, 26], are recycled into the fluid reservoir and undergo repeated atomization. On average each API molecule undergoes the process 10 to 15 times before leaving the device in an aerosol droplet [1, 136, 137].

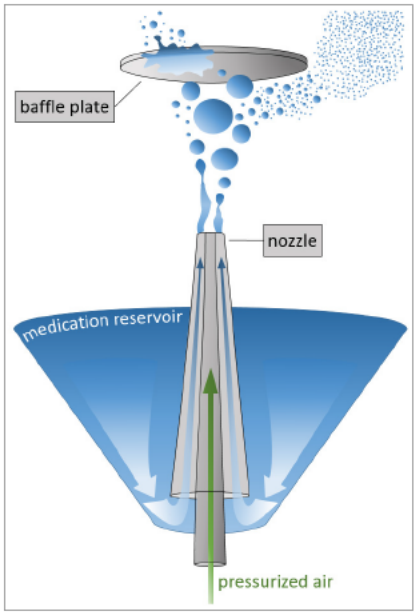

Figure II-2: Illustration of jet nebulization - larger droplets are recycled into the medication reservoir by baffles.

As hinted above, jet nebulizers suffer from low deposition efficiency. A significant amount of medication is wasted since these devices have a residual "dead" volume of 0.5 to 1.5 mL and usually operate continuously also during exhalation phases. Thus while the respirable fraction of the generated aerosol is in a range of 30-70% [138], only 5-15% of the initial charge actually deposits in the lung [139-143] which is comparable to a pMDI. On the other hand, peripheral deposition is improved [141, 142] and deposition on the throat is almost completely prevented as opposed to up to 85% throat deposition in pMDIs [139]. In a study comparing jet nebulization to a pMDI and spacer, lung doses were comparable in children, while jet nebulization delivered up to 73% more dose per minute [142]. The poor delivery efficiency is a significant disadvantage considering the comparably high value of biopharmaceuticals.

Protein degradation during jet nebulization has been subject of detailed investigations, which yielded the generation of air-liquid interface as the main detrimental factor. Repeated aerosol recirculation multiplies the amount of generated air-liquid interface with ongoing operation and thus further amplifies the detrimental impact. Solvent evaporation from the droplet surface locally increases the protein concentration. This may create a closer proximity of partially unfolded protein molecules and thus promote protein aggregation. Although often mentioned as a detrimental factor, shear forces did not directly cause protein degradation.

Niven et al. found that operating the nebulizer in the absence of any air-liquid interface, which was achieved by submerging the nebulizer jets in protein solution, prevented all G-CSF

degradation observed during normal nebulization [134]. On the other hand, careful bubbling of air at 0.5 psig through G-CSF solution resulted in the aggregation of 10% of the protein. The detrimental impact of interface generation by bubbling was also reported by Maa et al. for hGH [119].

Applying DoE to examine the impact of jet nebulizer settings on protein degradation, Fängmark et al. found that low liquid feed rates and low relative humidity of the atomizing gas were negative influences on the stability of urease [144]. Decreasing the relative humidity of the atomizing gas from 70% to <5% increased urease degradation, which was attributed to an increased extent of solvent evaporation and resulting up-concentration of the protein and excipients. A low liquid feed rate, i.e. a low ratio of liquid volume per gas volume amplified both evaporation and generation of air-liquid interface as it was responsible for the formation of smaller aerosol droplets.

Increased operating air pressure, which Niven et al. [135] associated with higher shear forces did not alter the extent of urease degradation in the primary aerosol [144] when there was no aerosol recirculation. The interaction of shear and air-liquid interface during protein denaturation was examined by Maa et al. [119]. Shearing experiments were performed with a rotor stator homogenizer. In the absence of any air-liquid interface, hGH remained intact even if homogenized at the highest shear rate. In the presence of an air-liquid interface, the extent of hGH aggregation increased with higher shear rates during homogenization. At the highest rate all hGH monomer content was lost after less than 20 minutes shearing. Higher shear generated more surface area by finer dispersion of the air in the liquid phase.

Fängmark et al. also investigated the impact of aerosol recirculation for an IgG antibody and found that in the investigated range of up to 9 cycles, aerosol recirculation was the most detrimental factor of jet nebulization [34]. Repeated atomization multiplies all other stress encountered during jet nebulization.

Solvent evaporation is a common phenomenon in jet nebulization [145, 146] and protein up-concentration of up to 33% has been reported [25]. In parallel an up-concentration of excipients added for protein stabilization has to be expected. A detrimental impact of oxidation as could be promoted by radical formation from cavitation was ruled out [144].

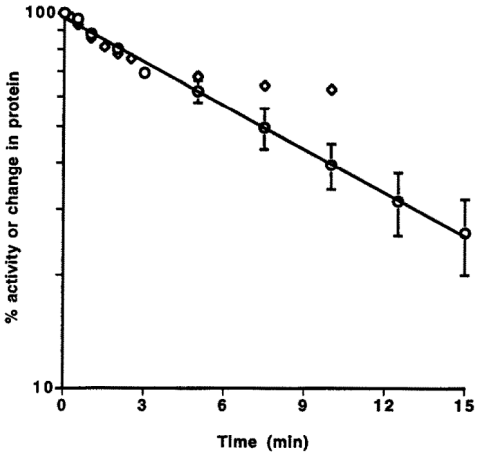

Figure II-3: Degradation profile of LDH (circles) and G-CSF (diamonds) during jet nebulization. Taken from [135].

Two different time profiles of protein degradation were observed for jet nebulization. For LDH [135] and urease [144] a log-linear degradation was reported, i.e. an equal fraction of protein is degraded with every recirculation (Figure II-3). In contrast, the time course of IgG [34] and G-CSF [135] degradation was marked by a rapid initial decline in native protein reaching a plateau after 5 to 10 minutes. Niven proposed that G-CSF aggregates formed at the air-liquid interface may saturate the interface and prevent migration of native molecules to the interface. Fängmark observed that the IgG degradation profile (compare G-CSF in Figure II-3) matched well with the temperature profile in the medication reservoir. He concluded that IgG degradation was mainly influenced by evaporation effects, apparently assuming that the extent of evaporation followed the same profile as the reservoir temperature. While a comparable temperature drop within the initial 2-4 minutes before reaching a plateau was also observed in two further studies [147, 148], neither found a corresponding plateau in concentration change. Instead concentration increased linearly throughout the entire nebulization.

Beyond that, rhDNase did not show any signs of degradation during shear and interfacial stress [119] or jet nebulization [25], demonstrating that interfacial protein degradation does not only depend on the available surface area but also on properties of the protein like surface activity. Surface tension measurements affirm this suggestion as the less stable rhGH (<50 mN/m; [119]) and G-CSF (~48mN/m;[134]) are more surface active than the more stable rhDNase (68 mN/m; [119]). Jet nebulization has also been reported for other proteins, including hGH [149], alpha1-antitrypsin (α1-AT) [150, 151], insulin [149], interleukin 2 (IL-2) in lung metastases [48, 152] and interferon-γ [153, 154].

4.3 Aerosolization of Proteins by Ultrasonic Nebulizers

Ultrasonic (US) nebulizers are second generation inhalers invented in the 1960s. While they were developed to eliminate the weaknesses of jet nebulizers, a gentler mode of aerosol generation was not an objective at that time. Instead, US nebulizers are more portable and operate quietly. Treatment times are reduced since output rates are usually higher with ultrasonic nebulizers [155-157] but pulmonary deposition efficiency remains comparable to jet nebulizers. A substantial amount of material is lost as residual "dead" volume which is equal [155] or slightly lower [156, 157] than for jet nebulizers. Atomization relies on high frequency ultrasonic vibration. A piezo-electric crystal oscillating at frequencies usually above 1 MHz is embedded in the bottom of the medication reservoir. The ultrasonic vibration is transmitted through the liquid in the reservoir and creates a geyser or standing wave (Figure II-4). Two different mechanisms are assumed to be responsible for primary aerosol generation [158]. Capillary waves form on the liquid surface and create droplets on their crest. Another theory attributes droplet emission by cavitation effects of collapsing microscopic air bubbles. Both phenomena have been observed and fascinating photos and videos are available [159, 160]. Comparable to jet nebulization, the primary aerosol is more polydisperse than desired (Figure II-4) entailing the use of an internal baffling system to deliver adequately sized droplets to the mouthpiece and recirculate larger droplets into the medication reservoir.

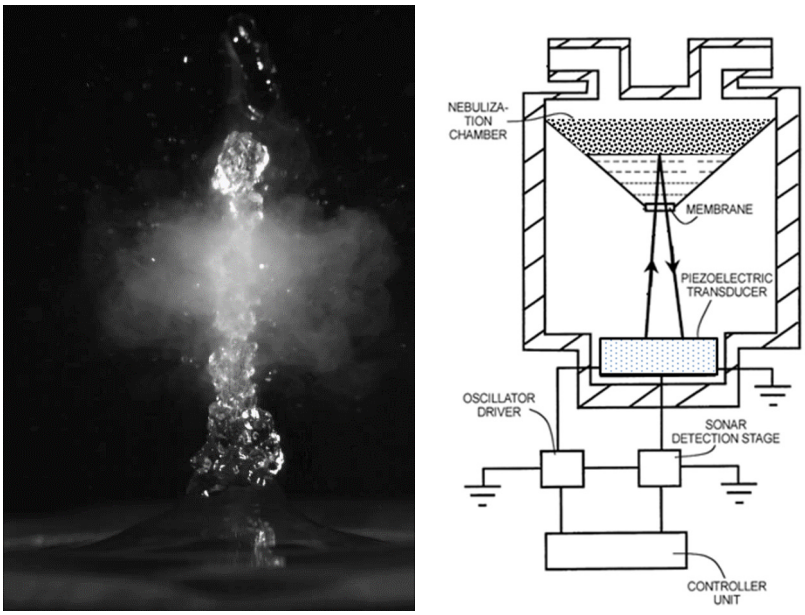

Figure II-4: Standing wave as generated inside an US nebulizer (A). The fine mist is delivered to the mouthpiece while the larger droplets are recycled into the medication reservoir by baffles. Still frame taken from [160]. Schematic drawing of an US nebulizer (B) modified from patent US6357671 [161].

As observed for jet nebulizers, aerosol recirculation plays a pivotal role in biopharmaceutical degradation during US nebulization. Besides the aerosol inherent air-liquid interface, additional detrimental influences were suggested in relation to ultrasound and cavitation [162-164]. A byproduct of ultrasonic radiation is the heating of the inhaler solution. A large part of the introduced energy is dissipated as heat and does not contribute to aerosol generation. Temperature in the medication reservoir has been reported to rise with ongoing nebulization [147, 165]. Temperatures reaching above 50°C in the medication reservoir and up to 75°C within the geyser pose a significant limitation for the nebulization of thermolabile proteins [166]. Together heating and aerosol recirculation invoke evaporation that may be less [167, 168] or more pronounced than by jet nebulization [147].

Niven et al. conducted a detailed investigation of factors relevant for LDH degradation during US nebulization [166]. The kinetic of LDH activity loss during US nebulization differed from the apparent first order kinetic observed during jet nebulization [135]. Degradation followed a sigmoidal progression instead, indicating that more than one factor was involved in LDH degradation (Figure II-5 A). To identify the involved factors, Niven applied three different modes of operation (apart from normal operation) for US nebulization of LDH (Figure II-5 B). One modification was to maintain the temperature inside the medication reservoir at 25°C throughout nebulization by means of a cooling coil. In the absence of heating, LDH activity declined in a log-linear jet nebulizer like fashion. In a second experiment, normal heating was allowed but generation of new air-liquid interface was minimized by blocking the geyser with a baffle. LDH remained stable for ten minutes but suddenly lost most of its activity within just a few minutes presumably when the temperature within the geyser approached the unfolding temperature (T_m) of LDH at 56°C. Additionally the device was operated while both, heating and interface generation were prevented. Over a time span of 40 minutes, no more than 15% of LDH activity was lost. In a different study, formation of hydroxyl radicals resulting from cavitation increased as a function of nebulization time, which may furthermore induce protein oxidation [163].

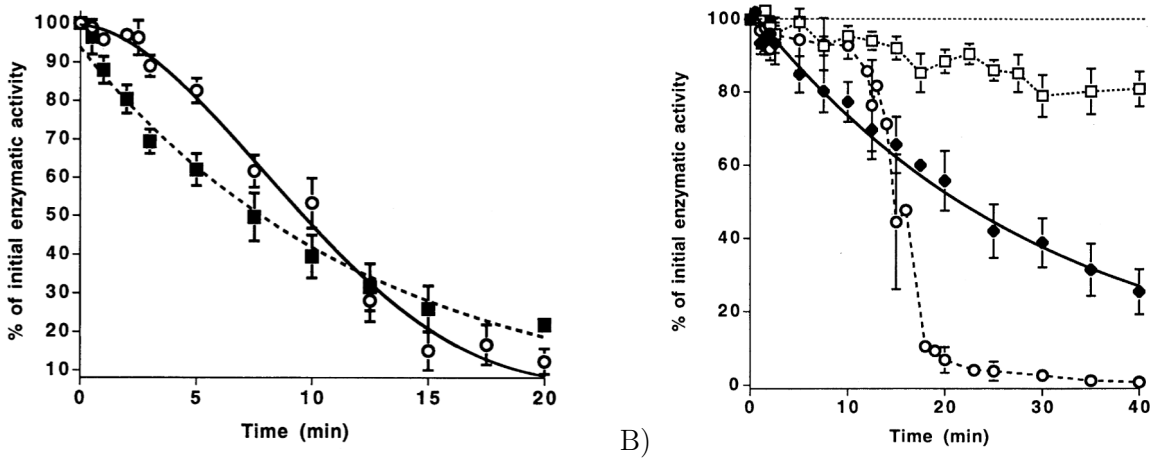

Figure II-5 A: LDH degradation profile after jet (filled squares) or ultrasonic nebulization (empty circles). B: Isolation of individual factors for LDH inactivation during US nebulization. LDH activity during nebulization at 25°C (filled circles), during normal heating but without aerosol production (empty circles) or operated at 25°C without aerosol production (empty squares) are shown. Taken form [166].

Protein degradation by US nebulization can be predominantly attributed to thermal and interfacial stress. Additional factors like cavitation are of minor importance. The use of the unfolding temperature to predict susceptibility to degradation during nebulization has been suggested [169]. It should be noted though, that proteins absorbed to the air-liquid interface exhibit onset temperatures for unfolding that are significantly lower compared to bulk solutions [128]. T_m values determined for bulk solutions may thus not be appropriate for the definition of threshold temperatures in nebulization but rather serve to roughly categorize proteins into more or less susceptible to the encountered thermal stress. For example Steckel et al. had to realize that US nebulization significantly destabilized aviscumine although the temperature inside the medication reservoir was not allowed to rise above 35°C and was thus kept well below the T_m of aviscumine at 50°C [145].

Niven et al. found that nebulizer cooling did not only reduce protein degradation but also markedly reduced the output rate [166]. He concluded that cooling was not feasible for routine operation as already long treatment times would be further extended, which is inacceptable as prolonged treatment times may have a negative impact on life quality of chronically ill patients and are associated with reduced compliance [75, 170]. In general US nebulizers are considered not suitable for the pulmonary delivery of proteins [1].

Contrary to this notion, Ip et al. have compared one jet and three different US nebulizers for the nebulization of rhConINF and found that the extent of rhConINF degradation varied greatly among the tested US nebulizers [165]. A Microstat nebulizer caused complete monomer loss

within 10 minutes of nebulization, while nebulization with a DeVilbiss Aerosonic® device resulted in 75% monomer recovery. Contrary to the Aerosonic® which automatically stopped operation when T_{RES} rose above 52°C to cool down, temperature rise in the Microstat was unrestricted and topped 80°C within 10 minutes of nebulization. A third device, the Medix Easimist nebulizer did not negatively affect rhConINF monomer content or in vitro activity. This device is equipped with an internal fan to remove aerosol from the reservoir and cool the solution. Similarly Khatri et al. tested jet and US nebulizers with the model protein LDH and also reported a significant difference between two US nebulizers regarding heating and protein degradation [171]. While the Sonix 2000® nebulizer exhibited the expected temperature rise and 80% loss in LDH activity within the medication reservoir, the reservoir temperature only negligibly changed for the Omron U1 and LDH activity was mostly recovered. This US nebulizer operates at only 67 kHz to prevent heating. On the other hand, the aerosol performance of the Omron U1 was poor which was also observed by Munster et al. during urokinase plasminogen activator nebulization [172]. Nebulization of an equal volume took twice as long with the Omron U1 compared to a Sonix 2000® and the aerosol droplet diameter was also 40% larger for the Omron device.

Parallel to the determination of LDH activity inside the medication reservoir, Khatri et al. also collected the aerosol in the two stages of a twin-stage glass impinger. The cutoff diameter between the upper and the lower stage is 6.4 µm so that all aerosol deposited in the lower stage may be considered as the respirable fraction. Interestingly, while the LDH activity of the residual volume remaining in the medication reservoir after nebulization with the OMRON U1 was close to 100%, so was the result for LDH deposited in the upper stage but in the lower stage only 3% of the LDH activity could be recovered although 30% of the protein had deposited there. Khatri et al. attributed the pronounced LDH deactivation to the smaller aerosol size and the hence larger air-liquid interface. Such a distinct effect of droplet size with 100% LDH activity remaining in droplets greater 6.4 µm compared to only 10% LDH activity remaining in droplets below 6.4 µm seems rather unlikely and has not been reported elsewhere. Instead, the aerosol collection conditions significantly differ for the upper and the lower stage of the twin-stage impinger. Only in the lower stage does aerosol collection involve bubbling of the aerosol through a buffer solution. The disruptive effects of bubbling on protein stability have been laid out above, indicating that

the results may be corrupted by unsuitable aerosol collection conditions. A critical evaluation of methods used for aerosol collection is not yet available in literature.

Besides the already mentioned proteins, ultrasonic nebulization has also been reported for platelet activating factor [173], G-CSF and PEG-G-CSF [61], rh-SOD [174] and alpha1-protease inhibitor [20]. G-CSF and PEG-G-CSF remained active when the US nebulizer was cooled with a coil. Rh-SOD exhibited 97% activity after nebulization with a modified US neb.

4.4 Aerosolization of Proteins by Vibrating Mesh Nebulizers

In the early 2000s a new class of nebulizers became available, so called vibrating mesh (VM) nebulizers (also called vibrating membrane nebulizer, Figure II-6). Since then, various reviews about VM nebulizers have been published [10, 157, 175-178]. The VM technology is an advancement of the ultrasonic nebulization principle, developed to improve the efficiency and speed of nebulization as well as device handling whereas optimized protein stability was no primary concern. Vibrating mesh nebulizers are small, battery powered and portable. Operation is silent [179, 180]. VM nebulization is reported to be more efficient and faster than nebulization with other types [27, 140, 179, 181]. Treatment times could be reduced 3-4 fold compared to a jet nebulizer [179, 181, 182]. In direct comparison to jet nebulizers, lung deposition was found to be doubled [181-183] or more than quadrupled in 3-year old children [184]. The residual volume of usually < 0.3 mL is a major reason for the observed efficiency increase. VM nebulizers employ a piezoelectric actuator coupled to a mesh that is set into vibration by the high frequent oscillation of the actuator. The liquid in the reservoir is forced through thousands of micron sized holes in the vibrating mesh, which has been described as a “micro-pump action” [185]. This generates a slow moving primary aerosol that is characterized by a narrow size distribution and thus does not require a baffling system to deliver an aerosol of the desired size range. Aerosol recirculation is therefore not necessary and even ruled out by design [186] which is a major improvement over jet and ultrasonic devices. While the generated air-liquid interface is still huge, it is greatly reduced compared to the repeatedly recirculated aerosols of jet or US nebulizers. This eliminates the main cause of solvent evaporation and the resulting solute up-concentration. Accordingly, no significant changes in solvent concentrations during VM nebulization were reported [27, 148].

Figure II-6: Nebulizers with vibrating mesh technology (upper left to lower right): OMRON MicroAIR® NE-22, Aerogen Aeroneb® Pro, Aeroneb® Go, PARI eFlow® (all reprinted with permission from [177]), AKITA® APIXNEB (reprinted with permission form [10]), Respironics i-neb AAD™ (reprinted with permission from [157]).

Devices are categorized according to the mode of vibration transmission from the piezo element as either active or passive. In active models like the PARI eFlow® and the Aeroneb® Go and Pro the mesh is directly attached to the piezoelectric element (Figure II-7 left). In passive devices like the Omron MicroAIR® and the i-neb AAD, the piezoelectric actuator is not directly attached to the mesh, instead the mesh is static and the vibrations are transmitted by a transducer horn [185](Figure II-7 right). Droplet size distribution and output rate of VM nebulizers can be optimized and adjusted to meet specific requirements by manipulating the diameter and the number of apertures in the mesh [179, 187]. This is offered by PARI for the eFlow® platform, reaching respirable fractions in a range of 60-98% [188]. VM technology also provides the basis for two devices that incorporate control of the users breathing pattern to achieve high and very reproducible pulmonary deposition. The AKITA² APIXNEB builds on PARI's eFlow® aerosol head but incorporates breath triggered operation and additionally regulates the inhalation flow and volume of the user. The i-neb AAD extends OMRON based passive VM technology by adaptive aerosol delivery (AAD) algorithms and breath triggered aerosol generation. Both devices enable high lung deposition of approximately 70% and very short inhalation times [32, 188, 190].

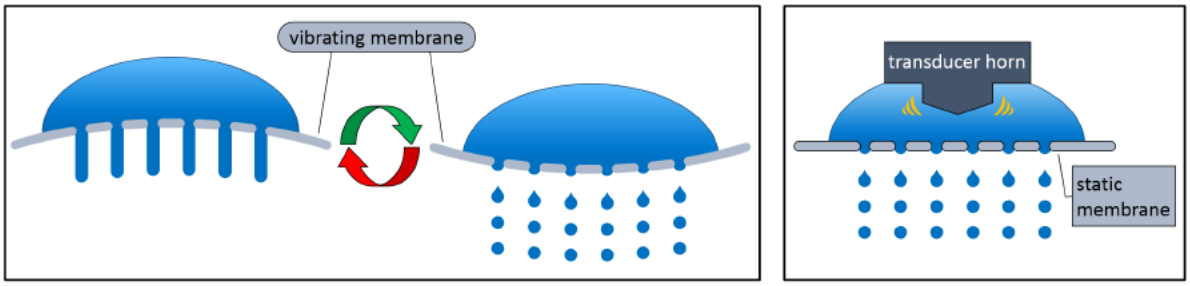

Figure II-7: Illustration of the operating principle of vibrating mesh technology: active devices with direct membrane vibration (left) or passive devices with a static mesh and a transducer horn (right), adapted from [189].

VM nebulization has been associated with low shear [187] and is generally expected to enable gentle aerosol generation suitable for biopharmaceuticals [10, 175, 176]. But reports on reservoir heating are inconsistent. No or negligible temperature changes have been reported for passive VM nebulizers (OMRON MicroAIR®, i-neb ADD) and also the Aeroneb® pro [148]. In contrast, mesh heating was observed with the Nano Spray Dryer B90 (BÜCHI Labortechnik GmbH, Essen, Germany) - which also relies on VM technology. Under otherwise equal conditions changing spray intensity from 25% to 100%, i.e. operating the mesh continuously instead of only 25% of the time, resulted in a rise in the mesh temperature by up to 21°C, indicating that mesh vibration is responsible for heating [189]. A comprehensive investigation to identify potentially detrimental forces encountered during VM nebulization, which may also shed some light on this apparent discrepancy, is not available from the literature. Nevertheless, the feasibility of biopharmaceutical nebulization via VM devices has been reported for several proteins.

The stability and activity of the marketed product Pulmozyme® has been studied with a variety of nebulizer types. Consistently, the highest remaining activity is reported for VM nebulization with 90-100% recovery [27, 28]. After jet nebulization, lower activity values of 80-96% were recovered [25, 27, 28]. Neither jet nor VM nebulization caused aggregation of DNase. In contrast, degradation was observed after US nebulization causing aggregation [26] and up to 40% activity loss [28] which was associated to reservoir heating. For Pulmozyme® the true benefit of the eFlow® over jet nebulizers is a reduction of treatment times by as much as 50% [27] due to a higher output rate. Another study demonstrated an improved treatment response when the AKITA² was used to target DNase deposition to the small airways [29].

Due to high API cost of α1-antitrypsin (AAT) which is currently in clinical phase III for topical treatment of AAT-deficiency, efficient pulmonary delivery is important. Nebulization with a PARI eFlow® preserved 90-95% AAT activity and did not generate soluble aggregates according

to SEC analysis. Insoluble aggregate formation was not addressed in the study [191]. Many studies rely on pulmonary delivery of AAT by jet nebulization [17], but data on biologic activity or aggregation are not available. Short treatment times and efficient AAT deposition have been reported for the AKITA² [32] and the i-neb AAD [31] VM nebulizers.

Maillet et al. investigated the feasibility of local pulmonary administration of the antibody Cetuximab® for lung cancer treatment and directly compared the impact of jet, US and VM nebulization regarding aggregation and biologic activity [15]. They found that subvisible particle formation was distinct for US and jet nebulization. The particle count after US nebulization was approximately twice as high as that after jet nebulization, whereas VM nebulization with an Aeroneb® Pro resulted in negligible subvisible particle counts. Cetuximab® binding activity and inhibitory action analyzed in cell assays was preserved after jet and especially VM nebulization. Data variability was very high for the US nebulized sample, which was attributed to the sedimentation of protein aggregate particles onto the cells. Maillet et al. claim that protein aggregation observed during US nebulization was not caused by the noted temperature increase since no aggregation occurred during still storage at comparable conditions. This does not take into account a possible reduction of the unfolding temperature [128] by interface adsorption.

A direct comparison of jet and VM nebulization was also performed by Germershaus et al. for insulin-like growth factor-I, finding no difference in protein stability for a PARI LC® Sprint jet nebulizer and the PARI eFlow® nebulizer [59]. After nebulization a 7% decrease in IGF-I peak was observed after nebulization with either device. The formation of aggregates or particles was suggested to be responsible for the loss. While no covalent aggregation was observed via non-reducing SDS PAGE, non-covalent aggregation or particle formation was not analyzed in this study. Besides protein stability, nebulizer performance significantly differed. Output rate with the eFlow® increased more than fourfold compared to the jet nebulizer. On the other hand the FPF reached more than 80% for the jet nebulizer but remained below 60% for the eFlow®.

Preservation of binding potency and no soluble aggregation or degradation were also reported for eFlow® nebulization of a formulation of PA401 (IL-8 decoy chemokine) [192]. While providing no detailed information on the impact on API stability, successful VM nebulization has further been reported for GM-CSF [62], IL-4 mutein [193] and INF-γ [46], for liposomal formulations of

rh-Cu/Zn SOD [53] and for the Fc-fusion proteins EPO-Fc [67, 68], INF-β-Fc [70], INF-α-Fc [69] and FSH-Fc [71].

5 Aerosolization of Proteins by Metered Dose Liquid Inhalers

Within the last decades, a number of delivery device technologies emerged which generate aerosol from pre-metered liquids without the application of a propellant gas. Their different underlying principles of aerosol generation are covered in a number of reviews [10, 22, 157, 176, 178]. For the AERx® system and the Respimat® device aerosolization of proteins has been reported.

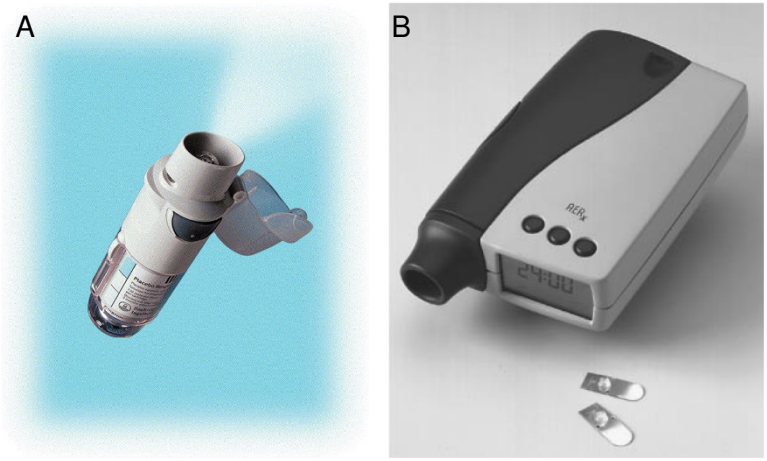

Figure II-8 A: Respimat® by Boehringer Ingelheim [194]; B: Aradigm's AERx® inhaler system [10]

The AERx® system is a hand held device generating a fine aerosol cloud by mechanically extruding a pre-metered solution through an array of micron sized nozzles (Figure II-8 B). Each pre-metered dose is contained in the medication reservoir on a disposable strip that also hosts the nozzle array. The technology had been licensed to Novo Nordisk for pulmonary insulin delivery [195, 196] but the partnership was discontinued after Pfizer's withdrawal of Exubera®. The feasibility of pulmonary biopharmaceutical delivery with the AERx® inhaler has also been demonstrated for INF-α-2b [45] and the superior delivery efficiency of the AERx® over a common jet nebulizer has been demonstrated for DNase [30] and rh-IL-4 receptor [40]. Comparing AUC data after rh-IL-4 receptor delivery with the AERx® or a PARI LC STAR® jet nebulizer revealed significantly higher systemic delivery after AERx® inhalation, which was attributed to a higher respirable dose and better peripheral aerosol distribution in the lung. A contribution of API

degradation by the delivery devices and potential differences between the devices was not assessed though.

The Respimat® Soft Mist Inhaler is approved for the pulmonary delivery of tiotropium bromide and a combination of ipratropium bromide and fenoterol both used for the treatment of asthma and COPD (Figure II-8 A). Energy for aerosol generation is provided mechanically by a loaded spring. Upon actuation, an aqueous formulation is forced through nozzles, forming two colliding jets that break up into a fine, slow aerosol mist. One puff aerosolizes 13µL solution with a viscosity of up to 1.6 mPa*s enabling the spraying of concentrated formulations for the delivery of high API doses in a single or few breathes. For example the spraying of 35 mg/mL insulin has been reported [47]. Respimat® impact on protein stability has been investigated for interferon omega (INF-ω) and manganese superoxide dismutase (MnSOD) [47]. MnSOD formulated at 3.3 mg/mL in PBS was aerosolized and the mist collected in a trap. Remaining MnSOD activity was determined enzymatically and by an ELISA assay. According to ELISA, 78-89% of MnSOD activity remained while no activity loss was observed with the enzymatic xanthine / xanthine oxidase reaction. Interferon omega formulated in 50 mM sodium citrate and 150 mM NaCl at pH 5.5 was aerosolized at either 5 mg/mL or 53 mg/mL. At the lower concentration 77-98% of the activity of a reference sample remained after aerosolization according to an ELISA assay or 47-81% as determined by a cell based activity assay. Remaining activity was in a comparable range for the high INF-ω concentration with 60-100% and 61-98% according to ELISA and cell based assays respectively. The inhalable fractions were 61% for MnSOD and 67-70% for INF-ω as determined by an ACI.

6 Formulation of Proteins for Nebulization

Biopharmaceuticals are usually formulated with a range of excipients to avoid degradation and a loss of efficacy which they might face during any stage from production or processing over storage and shipment to application and delivery. Protein formulation is extensively covered in the literature with excellent reviews available [83, 197-199]. When it comes to formulations for pulmonary application a number of restrictions has to be considered. According to the Ph. Eur. the pH of inhaled drugs must be in a range of 3.5 to 8.0 [200] and should ideally be above pH

5.0 [201], which must be considered during selection of the buffering agent. Osmolality was well tolerated in a range of 150-549 mOsmol but isotonicity has been recommended for pulmonary formulations [201]. This limits the maximum concentration of osmotically active excipients (e.g. salts, sugars, polyols) often used in protein formulations. Another potentially limiting aspect found with many inhaler types is the impact of the formulation on the characteristics of the generated aerosol. It has been demonstrated that physicochemical properties like viscosity, surface tension or ionic strength can significantly affect important aerosol properties like the FPF, the total output or the output rate [185, 202-204]. Further complicating matters, the range of excipients currently approved for pulmonary delivery is very limited (FDA inactive ingredient database for approved drugs, [205]). Nevertheless a number of reviews deals with the topic of formulation for pulmonary drug delivery [12, 24, 206, 207].

Surfactants are most protective at interfaces [86] and thus are commonly incorporated in protein formulations for nebulization, as the air-liquid interface has been identified as the main site of protein degradation. Polysorbate 80 (PS80) and polysorbate 20 (PS20) (approved in Sanasthmax, Chiesi) are among the approved excipients and can be found in many biopharmaceutical formulations as they displace protein molecules from the air-liquid interface [208]. Niven et al. reported for PS80 and two other nonionic detergents (Zwittergent 3-08 and 3-16) that their applied concentration must lie above the respective critical micelle concentration in order to stabilize the protein during nebulization [134]. Accordingly for a range of proteins stabilization was reported for PS80 concentrations of 0.01% or above (G-CSF [134], LDH [135], rhConINF [165], t-Pa [209]). Reduced degradation of rhConINF has been reported after addition of 0.01% PS20 [165]. A comparable stabilizing potential was observed for the nonionic detergents PS80, poloxamer 188 and solutol H515 during aviscumine nebulization [210].

Stabilization of various proteins including LDH [135], G-CSF [134], rhConINF [165], aviscumine [210] and urease [144] was also observed for formulation with polyethylene glycol (PEG) depending on PEG molecular weight. PEG 1000 and especially PEG 8000 were found to be more protective than PEG 400 at an equal concentration of 1% [134]. Addition of PEG results in preferential hydration of proteins by steric exclusion of the PEG molecules from native proteins [211, 212]. In order to explain the improved stabilization with larger PEG molecular weight, it has been suggested that PEG sterically hinders monomer to monomer interactions at the air-

water interface thus preventing further aggregation [134]. Unlike nonionic detergents, PEGs have a distinct impact on viscosity, which can limit their use in nebulization. During US nebulization Niven et al. observed that both PS80 and PEG 8000 stabilized LDH activity at the beginning of nebulization but lost their stabilizing potency with ongoing operation and rising reservoir temperature [166]. When heating was prevented full LDH activity was maintained by the addition of PS80 or PEG 8000.

7 References

[1] R. Siekmeier, G. Scheuch, Systemic Treatment by inhalation of Macromolecules - Principles, Problems and Examples, J Physiol Pharmacol, 59 (2008) 53-65.

[2] J.S. Patton, Mechanisms of macromolecule absorption by the lungs, Advanced Drug Delivery Reviews, 19 (1996) 3-36.

[3] J.S. Patton, P.R. Byron, Inhaling medicines: delivering drugs to the body through the lungs, Nat Rev Drug Discov, 6 (2007) 67-74.

[4] A. Tronde, B. Nordén, H. Marchner, A.-K. Wendel, H. Lennernäs, U.H. Bengtsson, Pulmonary absorption rate and bioavailability of drugs in vivo in rats: Structure absorption relationships and physicochemical profiling of inhaled drugs, J Pharm Sci, 92 (2003) 1216-1233.

[5] A.L. Adjei, P.K. Gupta, Inhalation Delivery of Therapeutic Peptides and Proteins, M. Dekker, New York, 1997.

[6] J.S. Patton, C.S. Fishburn, J.G. Weers, The Lungs as a Portal of Entry for Systemic Drug Delivery, Proceedings of the American Thoracic Society, 1 (2004) 338-344.

[7] J.G. Weers, J. Bell, H.K. Chan, D. Cipolla, C. Dunbar, A.J. Hickey, I.J. Smith, Pulmonary formulations: what remains to be done?, J Aerosol Med Pulm Drug Deliv, 23 (2010) S5-23.

[8] L. Heinemann, The failure of exubera: are we beating a dead horse?, Journal of diabetes science and technology, 2 (2008) 518-529.

[9] R. Siekmeier, G. Scheuch, Inhaled insulin--does it become reality?, J Physiol Pharmacol, 59 (2008) 81-113.

[10] D.E. Geller, The science of aerosol delivery in cystic fibrosis, Pediatric Pulmonology, 43 (2008) S5-S17.

[11] A. Maillet, L. Guilleminault, E. Lemarié, S. Lerondel, N. Azzopardi, J. Montharu, N. Congy-Jolivet, P. Reverdiau, B. Legrain, C. Parent, D.-H. Douvin, J. Hureaux, Y. Courty, M. Monte, P. Diot, G. Paintaud, A. Pape, H. Watier, N. Heuzé-Vourc'h, The Airways, a Novel Route for Delivering Monoclonal Antibodies to Treat Lung Tumors, Pharmaceutical Research, 28 (2011) 2147-2156.

[12] G. Pilcer, K. Amighi, Formulation strategy and use of excipients in pulmonary drug delivery, International Journal of Pharmaceutics, 392 (2010) 1-19.

[13] Pulmozyme Worldwide Sales, Evaluate Ltd, Retrieved 2013-02-12 from http://www.evaluategroup.com/Universal/View.aspx?type=Search&query=pulmozyme.

[14] N. Canavan, New Tools, Old Concerns in Inhalation Therapies, Pharmaceutical Formulation & Quality, (2012) 4-6.

[15] A. Maillet, N. Congy-Jolivet, S. Le Guellec, L. Vecellio, S. Hamard, Y. Courty, A. Courtois, F. Gauthier, P. Diot, G. Thibault, E. Lemarié, N. Heuzé-Vourc'h, Aerodynamical, Immunological and Pharmacological Properties of the Anticancer Antibody Cetuximab Following Nebulization, Pharmaceutical Research, 25 (2008) 1318-1326.

[16] A.T. Iacono, B.A. Johnson, W.F. Grgurich, J.G. Youssef, T.E. Corcoran, D.A. Seiler, J.H. Dauber, G.C. Smaldone, A. Zeevi, S.A. Yousem, J.J. Fung, G.J. Burckart, K.R. McCurry, B.P. Griffith, A Randomized Trial of Inhaled Cyclosporine in Lung-Transplant Recipients, New England Journal of Medicine, 354 (2006) 141-150.

[17] M. Griese, P. Latzin, M. Kappler, K. Weckerle, T. Heinzlmaier, T. Bernhardt, D. Hartl, α1-Antitrypsin inhalation reduces airway inflammation in cystic fibrosis patients, European Respiratory Journal, 29 (2007) 240-250.

[18] C. Vogelmeier, I. Kirlath, S. Warrington, N. Banik, E. Ulbrich, R.M. Du Bois, The intrapulmonary half-life and safety of aerosolized alpha1-protease inhibitor in normal volunteers, American Journal of Respiratory and Critical Care Medicine, 155 (1997) 536-541.

[19] M.P. Flament, P. Leterme, T. Burnouf, A. Gayot, Influence of formulation on jet nebulisation quality of α1 protease inhibitor, International Journal of Pharmaceutics, 178 (1999) 101-109.

[20] M.P. Flament, P. Leterme, A. Gayot, Influence of the technological parameters of ultrasonic nebulisation on the nebulisation quality of α1 protease inhibitor (α1PI), International Journal of Pharmaceutics, 189 (1999) 197-204.

[21] A.B. Sabin, A. Arechiga, J. de Castro, et al., Successful immunization of children with and without maternal antibody by aerosolized measles vaccine: I. different results with undiluted human diploid cell and chick embryo fibroblast vaccines, JAMA, 249 (1983) 2651-2662.

[22] G. Taylor, M. Gumbleton, Aerosols for Macromolecule Delivery: Design Challenges and Solutions, American Journal of Drug Delivery, 2 (2004) 143-155.

[23] S.-A. Cryan, Carrier-based strategies for targeting protein and peptide drugs to the lungs, The AAPS Journal, 7 (2005) E20-E41.

[24] F. Depreter, G. Pilcer, K. Amighi, Inhaled proteins: Challenges and perspectives, International Journal of Pharmaceutics, 447 (2013) 251-280.

[25] D. Cipolla, I. Gonda, S.J. Shire, Characterization of Aerosols of Human Recombinant Deoxyribonuclease I (rhDNase) Generated by Jet Nebulizers, Pharmaceutical Research, 11 (1994) 491-498.

[26] D.C. Cipolla, A.R. Clark, H.K. Chan, I. Gonda, S.J. Shire, Assessment of Aerosol Delivery Systems for Recombinant Human Deoxyribonuclease, STP Pharma Sci., 4 (1994) 50-62.

[27] T. Scherer, D.E. Geller, L. Owyang, M. Tservistas, M. Keller, N. Boden, K.C. Kesser, S.J. Shire, A technical feasibility study of dornase alfa delivery with eflow® vibrating membrane nebulizers: Aerosol characteristics and physicochemical stability, J Pharm Sci, 100 (2011) 98-109.

[28] M. Tservistas, F.-C. Lintz, M. Keller, Impact of the Nebulization principle on the biological activity of labile formulations containing liposomes, peptides and proteins, in: R.N. Dalby, P.R. Byron, J. Peart, J.D. Suman, S.J. Farr (Eds.) Respiratory Drug Delivery IX, Palm Desert, CA, USA, 2004, pp. 613 - 616.

[29] E.M. Bakker, S. Volpi, E. Salonini, E.C. van der Wiel-Kooij, C.J.J.C.M. Sintnicolaas, W.C.J. Hop, B.M. Assael, P.J.F.M. Merkus, H.A.W.M. Tiddens, Improved treatment response to dornase alfa in cystic fibrosis patients using controlled inhalation, European Respiratory Journal, 38 (2011) 1328-1335.

[30] D. Geller, J. Thipphawong, B. Otulana, D. Caplan, D. Ericson, L. Milgram, J. Okikawa, J. Quan, C.M. Bowman, Bolus inhalation of rhDNase with the AERx system in subjects with cystic fibrosis, J. Aerosol Med.-Depos. Clear. Eff. Lung, 16 (2003) 175-182.

[31] D.E. Geller, K.C. Kesser, The I-neb Adaptive Aerosol Delivery System enhances delivery of alpha1-antitrypsin with controlled inhalation, J Aerosol Med Pulm Drug Deliv, 23 (2010) S55-59.

[32] P. Brand, M. Schulte, M. Wencker, C.H. Herpich, G. Klein, K. Hanna, T. Meyer, Lung deposition of inhaled α1-proteinase inhibitor in cystic fibrosis and α1-antitrypsin deficiency, European Respiratory Journal, 34 (2009) 354-360.

[33] S. Pnina, S. Jan, M. Gerry, P. Eeva, S. Niels, R.C. Kenneth, H. Nick, M. William, R. Michale, V. Claus, G. Timm, B. Robert, A. Raja, K.E. Richard, A.S. Robert, Phase II/III, Double-Blind, Randomized, Placebo-Controlled, International Study Evaluating The Safety And Efficacy Of Inhaled, Human, Alpha-1 Antitrypsin (AAT) In Alpha-1 Antitrypsin Deficient Patients (AATD), in: D38. UPDATE IN ALPHA ONE DEFICIENCY, American Thoracic Society, 2014, pp. A5790-A5790.

[34] I. Fängmark, J.C. Carpin, Protein nebulization, Journal of Aerosol Science, 27, Supplement 1 (1996) S231-S232.

[35] S. Schüle (2005): Stabilization of Antibodies in Spray-dried Powders for Inhalation. PhD thesis, Ludwig Maximilian University Munich: Faculty of Chemistry and Pharmacy.

[36] S. Schüle, T. Schulz-Fademrecht, P. Garidel, K. Bechtold-Peters, W. Frieß, Stabilization of IgG1 in spray-dried powders for inhalation, European Journal of Pharmaceutics and Biopharmaceutics, 69 (2008) 793-807.

[37] R. Fuhrherr (2005): Spray-dried antibody powders for pulmonary application. PhD thesis, Ludwig Maximilian University Munich: Faculty of Chemistry and Pharmacy.

[38] A. Agrawal, E.C. Murphy III, J. Park, K.B. Adler, I. Parikh, Aerosolized BIO-11006, a novel MARCKS-related peptide, improves airway obstruction in a mouse model of mucus hypersecretion, Journal of Epithelial Biology and Pharmacology, 4 (2011) 1-6.

[39] S. Wenzel, D. Wilbraham, R. Fuller, E.B. Getz, M. Longphre, Effect of an interleukin-4 variant on late phase asthmatic response to allergen challenge in asthmatic patients: results of two phase 2a studies, The Lancet, 370 (2007) 1422-1431.

[40] S. Sangwan, J.M. Agosti, L.A. Bauer, B.A. Otulana, R.J. Morishige, D.C. Cipolla, J.D. Blanchard, G.C. Smaldone, Aerosolized protein delivery in asthma: gamma camera analysis of regional deposition and perfusion, Journal of aerosol medicine : the official journal of the International Society for Aerosols in Medicine, 14 (2001) 185-195.

[41] A. Gibbons, N.G. McElvaney, C.C. Taggart, S.-A. Cryan, Delivery of rSLPI in a liposomal carrier for inhalation provides protection against cathepsin L degradation, Journal of Microencapsulation, 26 (2009) 513-522.

[42] A. Gibbons, N. McElvaney, S.-A. Cryan, A Dry Powder Formulation of Liposome-Encapsulated Recombinant Secretory Leukocyte Protease Inhibitor (rSLPI) for Inhalation: Preparation and Characterisation, AAPS PharmSciTech, 11 (2010) 1411-1421.

[43] V. Kinnula, K. Mattson, K. Cantell, Pharmacokinetics and toxicity of inhaled human interferon-alpha in patients with lung cancer, Journal of interferon research, 9 (1989) 419-423.

[44] S. Giosue, M. Casarini, F. Ameglio, P. Zangrilli, M. Palla, A.M. Altieri, A. Bisetti, Aerosolized interferon-alpha treatment in patients with multi-drug-resistant pulmonary tuberculosis, European cytokine network, 11 (2000) 99-104.

[45] G. Balwani, B. Boyd, J. Whatley, J. Thipphawong, R. Morishige, J. Okikawa, B. Otulana, E. Tamches, T. Buclin, J. Biollaz, Evaluation of the AERx system for the pulmonary delivery of recombinant human interferon alfa-2b to healthy subjects, in: 29th Annual Meeting of the Controlled Release Society, Seoul, Korea, 2002.

[46] K.T. Diaz, S. Skaria, K. Harris, M. Solomita, S. Lau, K. Bauer, G.C. Smaldone, R. Condos, Delivery and safety of inhaled interferon-gamma in idiopathic pulmonary fibrosis, J Aerosol Med Pulm Drug Deliv, 25 (2012) 79-87.

[47] H. Lamche, C.J.M. Meade, B. Zierenberg, R.C. Reimholz, Process for nebulizing aqueous compositions containing highly concentrated insulin, U.S. Patent US20030064032 A1, issued 6. Nov. 2002.

[48] O. Merimsky, E. Gez, R. Weitzen, H. Nehushtan, R. Rubinov, H. Hayat, T. Peretz, M. Ben-Shahar, H. Biran, R. Katsenelson, V. Mermershtein, D. Loven, N. Karminsky, A.

Neumann, D. Matcejevsky, M. Inbar, Targeting pulmonary metastases of renal cell carcinoma by inhalation of interleukin-2, Annals of Oncology, 15 (2004) 610-612.

[49] E. Esteban-González, J. Carballido, V. Navas, Z. Torregrosa, A. Muñoz, M. Álvarez de Mon, Retrospective review in patients with pulmonary metastases of renal cell carcinoma receiving inhaled recombinant interleukin-2, Anti-Cancer Drugs, 18 (2007) 291-296.

[50] J.V. Fahy, D.W. Cockcroft, L.-P. Boulet, H.H. Wong, F. Deschesnes, E.E. Davis, J. Ruppel, J.Q. Su, D.C. Adelman, Effect of Aerosolized Anti-IgE (E25) on Airway Responses to Inhaled Allergen in Asthmatic Subjects, Am. J. Respir. Crit. Care Med., 160 (1999) 1023-1027.

[51] J. Andya, Y.-F. Maa, H. Costantino, P.-A. Nguyen, N. Dasovich, T. Sweeney, C. Hsu, S. Shire, The Effect of Formulation Excipients on Protein Stability and Aerosol Performance of Spray-Dried Powders of a Recombinant Humanized Anti-IgE Monoclonal Antibody1, Pharmaceutical Research, 16 (1999) 350-358.

[52] V.R. Muzykantov, Delivery of antioxidant enzyme proteins to the lung, Antioxidants & redox signaling, 3 (2001) 39-62.

[53] A. Wagner, K. Vorauer-Uhl, H. Katinger, Nebulization of Liposomal rh-Cu/Zn SOD with a Novel Vibrating Membrane Nebulizer, Journal of Liposome Research, 16 (2006) 113-125.

[54] L.J. Deftos, J.J. Nolan, B.L. Seely, P.L. Clopton, G.J. Cote, C.L. Whitham, L.J. Florek, T.A. Christensen, M.R. Hill, Intrapulmonary Drug Delivery of Salmon Calcitonin, Calcif Tissue Int, 61 (1997) 345-347.

[55] J.S. Patton, Pulmonary delivery of drugs for bone disorders, Advanced Drug Delivery Reviews, 42 (2000) 239-248.

[56] E.C. Walvoord, A. de la Peña, S. Park, B. Silverman, L. Cuttler, S.R. Rose, G. Cutler, S. Drop, J.J. Chipman, Inhaled Growth Hormone (GH) Compared with Subcutaneous GH in Children with GH Deficiency: Pharmacokinetics, Pharmacodynamics, and Safety, Journal of Clinical Endocrinology & Metabolism, 94 (2009) 2052-2059.

[57] S. White, D.B. Bennett, S. Cheu, P.W. Conley, D.B. Guzek, S. Gray, J. Howard, R. Malcolmson, J.M. Parker, P. Roberts, N. Sadrzadeh, J.D. Schumacher, S. Seshadri, G.W. Sluggett, C.L. Stevenson, N.J. Harper, EXUBERA: pharmaceutical development of a novel product for pulmonary delivery of insulin, Diabetes Technol Ther, 7 (2005) 896-906.

[58] A. Rossiter, C.P. Howard, N. Amin, D.J. Costello, A.H. Boss, Technosphere® Insulin: Safety in Type 2 Diabetes Mellitus, in: A.D. Association (Ed.) ADA Scientific Sessions, American Diabetes Association, Orlando, FL, USA, 2010, pp. 1.

[59] O. Germershaus, I. Schultz, T. Lühmann, M. Beck-Broichsitter, P. Högger, L. Meinel, Insulin-like growth factor-I aerosol formulations for pulmonary delivery, European Journal of Pharmaceutics and Biopharmaceutics, 85 (2013) 61-68.

[60] K.C. Lee, S.Y. Chae, T.H. Kim, S. Lee, E.S. Lee, Y.S. Youn, Intrapulmonary potential of polyethylene glycol-modified glucagon-like peptide-1s as a type 2 anti-diabetic agent, Regulatory Peptides, 152 (2009) 101-107.

[61] R. Niven, K.L. Whitcomb, L. Shaner, A. Ip, O. Kinstler, The Pulmonary Absorption of Aerosolized and Intratracheally Instilled rhG-CSF and monoPEGylated rhG-CSF, Pharmaceutical Research, 12 (1995) 1343-1349.

[62] M. Luisetti, P. Kroneberg, T. Suzuki, Z. Kadija, B. Muellinger, I. Campo, J. Gleske, G. Rodi, W.C. Zimlich, F. Mariani, F. Ferrari, M. Frey, B.C. Trapnell, Physical properties, lung deposition modeling, and bioactivity of recombinant GM-CSF aerosolised with a highly efficient nebulizer, Pulmonary Pharmacology & Therapeutics, 24 (2011) 123-127.

[63] R.D. Rao, P.M. Anderson, C.A.S. Arndt, P.J. Wettstein, S.N. Markovic, Aerosolized Granulocyte Macrophage Colony-Stimulating Factor (GM-CSF) Therapy in Metastatic Cancer, American Journal of Clinical Oncology, 26 (2003) 493-498.

[64] R. Tazawa, B.C. Trapnell, Y. Inoue, T. Arai, T. Takada, Y. Nasuhara, N. Hizawa, Y. Kasahara, K. Tatsumi, M. Hojo, H. Ishii, M. Yokoba, N. Tanaka, E. Yamaguchi, R. Eda, Y. Tsuchihashi, K. Morimoto, M. Akira, M. Terada, J. Otsuka, M. Ebina, C. Kaneko, T. Nukiwa, J.P. Krischer, K. Akazawa, K. Nakata, Inhaled granulocyte/macrophage-colony stimulating factor as therapy for pulmonary alveolar proteinosis, Am J Respir Crit Care Med, 181 (2010) 1345-1354.

[65] S.N. Markovic, V.J. Suman, W.K. Nevala, L. Geeraerts, E.T. Creagan, L.A. Erickson, K.M. Rowland, Jr., R.F. Morton, W.L. Horvath, M.R. Pittelkow, A dose-escalation study of aerosolized sargramostim in the treatment of metastatic melanoma: an NCCTG Study, Am J Clin Oncol, 31 (2008) 573-579.

[66] M.E. Wylam, R. Ten, U.B.S. Prakash, H.F. Nadrous, M.L. Clawson, P.M. Anderson, Aerosol granulocyte-macrophage colony-stimulating factor for pulmonary alveolar proteinosis, European Respiratory Journal, 27 (2006) 585-593.

[67] A.J. Bitonti, J.A. Dumont, S.C. Low, R.T. Peters, K.E. Kropp, V.J. Palombella, J.M. Stattel, Y. Lu, C.A. Tan, J.J. Song, A.M. Garcia, N.E. Simister, G.M. Spiekermann, W.I. Lencer, R.S. Blumberg, Pulmonary delivery of an erythropoietin Fc fusion protein in non-human primates through an immunoglobulin transport pathway, Proc Natl Acad Sci U S A, 101 (2004) 9763-9768.

[68] J.A. Dumont, A.J. Bitonti, D. Clark, S. Evans, M. Pickford, S.P. Newman, Delivery of an Erythropoietin-Fc Fusion Protein by Inhalation in Humans through an Immunoglobulin Transport Pathway, Journal of aerosol medicine : the official journal of the International Society for Aerosols in Medicine, 18 (2005) 294-303.

[69] A.J. Bitonti, J.A. Dumont, Pulmonary administration of therapeutic proteins using an immunoglobulin transport pathway, Advanced Drug Delivery Reviews, 58 (2006) 1106-1118.

[70] S. Vallee, S. Rakhe, T. Reidy, S. Walker, Q. Lu, P. Sakorafas, S. Low, A. Bitonti, Pulmonary administration of interferon Beta-1a-fc fusion protein in non-human primates using an immunoglobulin transport pathway, Journal of interferon & cytokine research : the official journal of the International Society for Interferon and Cytokine Research, 32 (2012) 178-184.

[71] S.C. Low, S.L. Nunes, A.J. Bitonti, J.A. Dumont, Oral and pulmonary delivery of FSH Fc fusion proteins via neonatal Fc receptor-mediated transcytosis, Human Reproduction, 20 (2005) 1805-1813.

[72] K.C. Stone, R.R. Mercer, P. Gehr, B. Stockstill, J.D. Crapo, Allometric Relationships of Cell Numbers and Size in the Mammalian Lung, American Journal of Respiratory Cell and Molecular Biology, 6 (1992) 235-243.

[73] C. Lombry, D.A. Edwards, V. Preat, R. Vanbever, Alveolar macrophages are a primary barrier to pulmonary absorption of macromolecules, Am J Physiol Lung Cell Mol Physiol, 286 (2004) L1002-1008.

[74] T. Martonen, I. Katz, Deposition Patterns of Aerosolized Drugs Within Human Lungs: Effects of Ventilatory Parameters, Pharmaceutical Research, 10 (1993) 871-878.

[75] G. Scheuch, M.J. Kohlhaeufl, P. Brand, R. Siekmeier, Clinical perspectives on pulmonary systemic and macromolecular delivery, Advanced Drug Delivery Reviews, 58 (2006) 996-1008.

[76] K. Bechtold-Peters, H. Luessen, Pulmonary Drug Delivery: Basics, Applications and Opportunities for Small Molecules and Biopharmaceutics, ECV Editio Cantor Verlag, Aulendorf, 2007.

[77] A.J. Hickey, T.B. Martonen, Y. Yang, Theoretical relationship of lung deposition to the fine particle fraction of inhalation aerosols, Pharmaceutica Acta Helvetiae, 71 (1996) 185-190.

[78] T. Martonen, I. Katz, K. Fults, A. Hickey, Use of Analytically Defined Estimates of Aerosol Respirable Fraction to Predict Lung Deposition Patterns, Pharmaceutical Research, 9 (1992) 1634-1639.

[79] G. Scheuch, W. Stahlhofen, Deposition and Dispersion of Aerosols in the Airways of the Human Respiratory Tract: The Effect of Particle Size, Experimental Lung Research, 18 (1992) 343-358.

[80] R. Liste, ROTE LISTE® 2013 Buchausgabe - Einzelausgabe: Arzneimittelverzeichnis für Deutschland (einschließlich EU-Zulassungen und bestimmter Medizinprodukte), Rote Liste Service GmbH, Frankfurt/Main, 2013.

[81] R.K. Wolff, R.W. Niven, Generation of aerosolized drugs, Journal of aerosol medicine : the official journal of the International Society for Aerosols in Medicine, 7 (1994) 89-106.

[82] N.R. Labiris, M.B. Dolovich, Pulmonary drug delivery. Part II: The role of inhalant delivery devices and drug formulations in therapeutic effectiveness of aerosolized medications, British Journal of Clinical Pharmacology, 56 (2003) 600-612.

[83] W. Wang, Instability, stabilization, and formulation of liquid protein pharmaceuticals, International Journal of Pharmaceutics, 185 (1999) 129-188.

[84] W. Wang, Protein aggregation and its inhibition in biopharmaceutics, International Journal of Pharmaceutics, 289 (2005) 1-30.

[85] H.-C. Mahler, W. Friess, U. Grauschopf, S. Kiese, Protein aggregation: Pathways, induction factors and analysis, J Pharm Sci, 98 (2009) 2909-2934.

[86] M. Manning, D. Chou, B. Murphy, R. Payne, D. Katayama, Stability of Protein Pharmaceuticals: An Update, Pharmaceutical Research, 27 (2010) 544-575.

[87] J.S. Philo, T. Arakawa, Mechanisms of Protein Aggregation, Current Pharmaceutical Biotechnology, 10 (2009) 348-351.

[88] W. Wang, S. Nema, D. Teagarden, Protein aggregation Pathways and influencing factors, International Journal of Pharmaceutics, 390 (2010) 89-99.

[89] H.-Y. Li, P.C. Seville, Novel pMDI formulations for pulmonary delivery of proteins, International Journal of Pharmaceutics, 385 (2010) 73-78.

[90] R.O. Williams Iii, J. Liu, Formulation of a protein with propellant HFA 134a for aerosol delivery, European Journal of Pharmaceutical Sciences, 7 (1999) 137-144.

[91] Y. Tan, Z. Yang, X. Peng, F. Xin, Y. Xu, M. Feng, C. Zhao, H. Hu, C. Wu, A novel bottom-up process to produce nanoparticles containing protein and peptide for suspension in hydrofluoroalkane propellants, International Journal of Pharmaceutics, 413 (2011) 167-173.

[92] Y. Tan, Z. Yang, X. Pan, M. Chen, M. Feng, L. Wang, H. Liu, Z. Shan, C. Wu, Stability and aerosolization of pressurized metered dose inhalers containing thymopentin nanoparticles produced using a bottom-up process, International Journal of Pharmaceutics, 427 (2012) 385-392.

[93] R. Pauwels, S. Newman, L. Borgstrom, Airway deposition and airway effects of antiasthma drugs delivered from metered-dose inhalers, European Respiratory Journal, 10 (1997) 2127-2138.

[94] A.R. Clark, Medical Aerosol Inhalers: Past, Present, and Future, Aerosol Science and Technology, 22 (1995) 374-391.

[95] P.J. Thompson, Drug Delivery to the Small Airways, American Journal of Respiratory and Critical Care Medicine, 157 (1998) S199-S202.

[96] O. Aswania, S. Ritson, S.M. Iqbal, J. Bhatt, A.S. Rigby, M.L. Everard, Intra-subject variability in lung dose in healthy volunteers using five conventional portable inhalers, Journal of aerosol medicine : the official journal of the International Society for Aerosols in Medicine, 17 (2004) 231-238.

[97] L. Borgström, T. Bengtsson, E. Derom, R. Pauwels, Variability in lung deposition of inhaled drug, within and between asthmatic patients, with a pMDI and a dry powder inhaler, Turbuhaler®, International Journal of Pharmaceutics, 193 (2000) 227-230.

[98] M. Molimard, C. Raherison, S. Lignot, F. Depont, A. Abouelfath, N. Moore, Assessment of handling of inhaler devices in real life: an observational study in 3811 patients in primary care, Journal of aerosol medicine : the official journal of the International Society for Aerosols in Medicine, 16 (2003) 249-254.

[99] F. Lavorini, A. Magnan, J. Christophe Dubus, T. Voshaar, L. Corbetta, M. Broeders, R. Dekhuijzen, J. Sanchis, J.L. Viejo, P. Barnes, C. Corrigan, M. Levy, G.K. Crompton, Effect of incorrect use of dry powder inhalers on management of patients with asthma and COPD, Respiratory medicine, 102 (2008) 593-604.

[100] I.J. Smith, M. Parry-Billings, The inhalers of the future? A review of dry powder devices on the market today, Pulmonary Pharmacology & Therapeutics, 16 (2003) 79-95.

[101] S.A. Shoyele, S. Cawthorne, Particle engineering techniques for inhaled biopharmaceuticals, Advanced Drug Delivery Reviews, 58 (2006) 1009-1029.

[102] J.G. Weers, T.E. Tarara, A.R. Clark, Design of fine particles for pulmonary drug delivery, Expert Opinion on Drug Delivery, 4 (2007) 297-313.

[103] M. Irngartinger, V. Camuglia, M. Damm, J. Goede, H.W. Frijlink, Pulmonary delivery of therapeutic peptides via dry powder inhalation: effects of micronisation and manufacturing, European Journal of Pharmaceutics and Biopharmaceutics, 58 (2004) 7-14.

[104] D.A. Edwards, J. Hanes, G. Caponetti, J. Hrkach, A. Ben-Jebria, M.L. Eskew, J. Mintzes, D. Deaver, N. Lotan, R. Langer, Large Porous Particles for Pulmonary Drug Delivery, Science, 276 (1997) 1868-1872.

[105] D.E. Geller, J. Weers, S. Heuerding, Development of an inhaled dry-powder formulation of tobramycin using PulmoSphere technology, J Aerosol Med Pulm Drug Deliv, 24 (2011) 175-182.

[106] V. Codrons, F. Vanderbist, B. Ucakar, V. Préat, R. Vanbever, Impact of formulation and methods of pulmonary delivery on absorption of parathyroid hormone (1?34) from rat lungs Journal of Pharmaceutical Sciences Volume 93, Issue 5, J Pharm Sci, 93 (2004) 1241-1252.

[107] C. Bosquillon, V. Préat, R. Vanbever, Pulmonary delivery of growth hormone using dry powders and visualization of its local fate in rats, Journal of Controlled Release, 96 (2004) 233-244.

[108] S.S. Steiner, R. Feldstein, H. Lian, C.A. Rhodes, G.S. Shen, Method for drug delivery to the pulmonary system, issued 03/12/2013.

[109] M.T. Marino, D. Costello, R. Baughman, A. Boss, J. Cassidy, C. Damico, S. van Marle, A. van Vliet, P.C. Richardson, Pharmacokinetics and Pharmacodynamics of Inhaled GLP-1 (MKC253): Proof-of-Concept Studies in Healthy Normal Volunteers and in Patients With Type 2 Diabetes, Clin Pharmacol Ther, 88 (2010) 243-250.

[110] A. Bot, T. Tarara, D. Smith, S. Bot, C. Woods, J. Weers, Novel Lipid-Based Hollow-Porous Microparticles as a Platform for Immunoglobulin Delivery to the Respiratory Tract, Pharmaceutical Research, 17 (2000) 275-283.

[111] L. Dellamary, D.J. Smith, A. Bloom, S. Bot, G.-R. Guo, H. Deshmuk, M. Costello, A. Bot, Rational design of solid aerosols for immunoglobulin delivery by modulation of aerodynamic and release characteristics, Journal of Controlled Release, 95 (2004) 489-500.

[112] A. Hawe, M. Wiggenhorn, M. van de Weert, J.H.O. Garbe, H.-C. Mahler, W. Jiskoot, Forced degradation of therapeutic proteins, J Pharm Sci, 101 (2012) 895-913.

[113] A. Eppler, M. Weigandt, A. Hanefeld, H. Bunjes, Relevant shaking stress conditions for antibody preformulation development, European Journal of Pharmaceutics and Biopharmaceutics, 74 (2010) 139-147.

[114] V. Sluzky, A.M. Klibanov, R. Langer, Mechanism of insulin aggregation and stabilization in agitated aqueous solutions, Biotechnology and Bioengineering, 40 (1992) 895-903.

[115] Sylvia Kiese, Astrid Papppenberger, Wolfgang Friess, Hanns-Christian Mahler, Shaken, not stirred: Mechanical stress testing of an IgG1 antibody, J Pharm Sci, 97 (2008) 4347-4366.

[116] H.-C. Mahler, R. Müller, W. Frie, A. Delille, S. Matheus, Induction and analysis of aggregates in a liquid IgG1-antibody formulation, European Journal of Pharmaceutics and Biopharmaceutics, 59 (2005) 407-417.

[117] L. Krielgaard, L.S. Jones, T.W. Randolph, S. Frokjaer, J.M. Flink, M.C. Manning, J.F. Carpenter, Effect of tween 20 on freeze-thawing- and agitation-induced aggregation of recombinant human factor XIII, J Pharm Sci, 87 (1998) 1593-1603.

[118] M. Katakam, L.N. Bell, A.K. Banga, Effect of surfactants on the physical stability of recombinant human growth hormone, J Pharm Sci, 84 (1995) 713-716.

[119] Y.-F. Maa, C.C. Hsu, Protein denaturation by combined effect of shear and air-liquid interface, Biotechnology and Bioengineering, 54 (1997) 503-512.

[120] M. Calamai, N. Taddei, M. Stefani, G. Ramponi, F. Chiti, Relative Influence of Hydrophobicity and Net Charge in the Aggregation of Two Homologous Proteins, Biochemistry, 42 (2003) 15078-15083.

[121] E. Querol, J.A. Perez-Pons, A. Mozo-Villarias, Analysis of protein conformational characteristics related to thermostability, Protein Engineering, 9 (1996) 265-271.

[122] T.W. Randolph, L.S. Jones, Surfactant-Protein Interactions, in: J.F. Carpenter, M.C. Manning (Eds.) Rational Design of Stable Protein Formulations, Springer US, New York, 2002, pp. 159-175.

[123] S. Magdassi, Surface Activity of Proteins: Chemical and Physicochemical Modifications, Taylor & Francis, New York, 1996.

[124] V.A. Voelz, M. Jäger, S. Yao, Y. Chen, L. Zhu, S.A. Waldauer, G.R. Bowman, M. Friedrichs, O. Bakajin, L.J. Lapidus, S. Weiss, V.S. Pande, Slow Unfolded-State Structuring in Acyl-CoA Binding Protein Folding Revealed by Simulation and Experiment, Journal of the American Chemical Society, 134 (2012) 12565-12577.

[125] Y.F. Yano, T. Uruga, H. Tanida, H. Toyokawa, Y. Terada, M. Takagaki, H. Yamada, Driving Force Behind Adsorption-Induced Protein Unfolding: A Time-Resolved X-ray Reflectivity Study on Lysozyme Adsorbed at an Air/Water Interface, Langmuir, 25 (2008) 32-35.

[126] A.K. Hüsecken, F. Evers, C. Czeslik, M. Tolan, Effect of Urea and Glycerol on the Adsorption of Ribonuclease A at the Air−Water Interface, Langmuir, 26 (2010) 13429-13435.

[127] M.D. Lad, F. Birembaut, J.M. Matthew, R.A. Frazier, R.J. Green, The adsorbed conformation of globular proteins at the air/water interface, Physical Chemistry Chemical Physics, 8 (2006) 2179-2186.

[128] R.J. Green, I. Hopkinson, R.A.L. Jones, Unfolding and Intermolecular Association in Globular Proteins Adsorbed at Interfaces, Langmuir, 15 (1999) 5102-5110.

[129] A. Tronin, T. Dubrovsky, S. Dubrovskaya, G. Radicchi, C. Nicolini, Role of Protein Unfolding in Monolayer Formation on Air−Water Interface, Langmuir, 12 (1996) 3272-3275.

[130] A. Singh, O. Konovalov, J. Novak, A. Vorobiev, The sequential growth mechanism of a protein monolayer at the air-water interface, Soft Matter, 6 (2010) 3826-3831.

[131] Y.F. Yano, E. Arakawa, W. Voegeli, T. Matsushita, Real-time investigation of protein unfolding at an air-water interface at the 1 s time scale, Journal of Synchrotron Radiation, 20 (2013) 980-983.

[132] A.H. Martin, M.B.J. Meinders, M.A. Bos, M.A. Cohen Stuart, T. van Vliet, Conformational Aspects of Proteins at the Air/Water Interface Studied by Infrared Reflection−Absorption Spectroscopy, Langmuir, 19 (2003) 2922-2928.

[133] B.R. Simler, G. Hui, J.E. Dahl, B. Perez-Ramirez, Mechanistic complexity of subvisible particle formation: Links to protein aggregation are highly specific, J Pharm Sci, 101 (2012) 4140-4154.

[134] R.W. Niven, S.J. Prestrelski, M.J. Treuheit, A.Y. Ip, T. Arakawa, Protein nebulization II. Stabilization of G-CSF to air-jet nebulization and the role of protectants, International Journal of Pharmaceutics, 127 (1996) 191-201.

[135] R.W. Niven, A.Y. Ip, S.D. Mittelman, C. Farrar, T. Arakawa, S.J. Prestrelski, Protein nebulization: I. Stability of lactate dehydrogenase and recombinant granulocyte-colony stimulating factor to air-jet nebulization, International Journal of Pharmaceutics, 109 (1994) 17-26.

[136] R.W. Niven, Delivery of Biotherapeutics by Inhalation Aerosol, Critical Reviews™ in Therapeutic Drug Carrier Systems, 12 (1995) 151-231.

[137] R. Uchenna Agu, M. Ikechukwu Ugwoke, M. Armand, R. Kinget, N. Verbeke, The lung as a route for systemic delivery of therapeutic proteins and peptides, Respiratory Research, 2 (2001) 198-209.

[138] D.T. Loffert, D. Ikle, H.S. Nelson, A comparison of commercial jet nebulizers, CHEST Journal, 106 (1994) 1788-1792.

[139] R.A. Lewis, J.S. Fleming, Fractional deposition from a jet nebulizer: How it differs from a metered dose inhaler, British Journal of Diseases of the Chest, 79 (1985) 361-367.

[140] A.L. Coates, M. Green, K. Leung, J. Chan, N. Ribeiro, F. Ratjen, M. Charron, A comparison of amount and speed of deposition between the PARI LC STAR(R) jet nebulizer and an investigational eFlow(R) nebulizer, J Aerosol Med Pulm Drug Deliv, 24 (2011) 157-163.

[141] B.M. Zainudin, M. Biddiscombe, S.E. Tolfree, M. Short, S.G. Spiro, Comparison of bronchodilator responses and deposition patterns of salbutamol inhaled from a pressurised metered dose inhaler, as a dry powder, and as a nebulised solution, Thorax, 45 (1990) 469-473.

[142] J.H. Wildhaber, N.D. Dore, J.M. Wilson, S.G. Devadason, P.N. LeSouëf, Inhalation therapy in asthma: Nebulizer or pressurized metered-dose inhaler with holding chamber? In vivo comparison of lung deposition in children, The Journal of Pediatrics, 135 (1999) 28-33.

[143] P. Brand, S. Häußermann, B. Müllinger, A. Fischer, B. Wachall, J. Stegemann, Reduction of drug-dose and therapy-costs in the inhalation therapy with high dose tobramycin,

Journal of cystic fibrosis : official journal of the European Cystic Fibrosis Society, 5 (2006) S40.

[144] I. Fängmark, J.C. Carpin, Stability of urease during aerosolization: The effect of operating conditions, Journal of Aerosol Science, 29 (1998) 279-288.

[145] H. Steckel, F. Eskandar, K. Witthohn, Effect of Excipients on the Stability and Aerosol Performance of Nebulized Aviscumine, Journal of Aerosol Medicine, 16 (2003) 417-432.

[146] P.R. Phipps, I. Gonda, Evaporation of aqueous aerosols produced by jet nebulizers: effects on particle size and concentration of solution in the droplets, Journal of aerosol medicine : the official journal of the International Society for Aerosols in Medicine, 7 (1994) 239-258.

[147] H. Steckel, F. Eskandar, Factors affecting aerosol performance during nebulization with jet and ultrasonic nebulizers, European Journal of Pharmaceutical Sciences, 19 (2003) 443-456.

[148] M. Beck-Broichsitter, P. Kleimann, T. Schmehl, T. Betz, U. Bakowsky, T. Kissel, W. Seeger, Impact of lyoprotectants for the stabilization of biodegradable nanoparticles on the performance of air-jet, ultrasonic, and vibrating-mesh nebulizers, European Journal of Pharmaceutics and Biopharmaceutics, 82 (2012) 272-280.

[149] J.S. Patton, R.M. Platz, (D) Routes of delivery: Case studies: (2) Pulmonary delivery of peptides and proteins for systemic action, Advanced Drug Delivery Reviews, 8 (1991) 179-196.

[150] R.C. Hubbard, N.G. McElvaney, S.E. Sellers, J.T. Healy, D.B. Czerski, R.G. Crystal, Recombinant DNA-produced alpha 1-antitrypsin administered by aerosol augments lower respiratory tract antineutrophil elastase defenses in individuals with alpha 1-antitrypsin deficiency, The Journal of clinical investigation, 84 (1989) 1349-1354.

[151] R.C. Hubbard, M.A. Casolaro, M. Mitchell, S.E. Sellers, F. Arabia, M.A. Matthay, R.G. Crystal, Fate of aerosolized recombinant DNA-produced alpha 1-antitrypsin: use of the epithelial surface of the lower respiratory tract to administer proteins of therapeutic importance, Proceedings of the National Academy of Sciences, 86 (1989) 680-684.

[152] E. Huland, H. Heinzer, H. Huland, R. Yung, Overview of interleukin-2 inhalation therapy, The cancer journal from Scientific American, 6 Suppl 1 (2000) S104-112.

[153] T.S. Hallstrand, H.D. Ochs, Q. Zhu, W.C. Liles, Inhaled IFN-γ for persistent nontuberculous mycobacterial pulmonary disease due to functional IFN-γ deficiency, European Respiratory Journal, 24 (2004) 367-370.

[154] R.B. Moss, N. Mayer-Hamblett, J. Wagener, C. Daines, K. Hale, R. Ahrens, R.L. Gibson, P. Anderson, G. Retsch-Bogart, S.Z. Nasr, I. Noth, D. Waltz, P. Zeitlin, B. Ramsey, K. Starko, Randomized, double-blind, placebo-controlled, dose-escalating study of

aerosolized interferon gamma-1b in patients with mild to moderate cystic fibrosis lung disease, Pediatric pulmonology, 39 (2005) 209-218.

[155] K.M.G. Taylor, O.N.M. McCallion, Ultrasonic nebulisers for pulmonary drug delivery, International Journal of Pharmaceutics, 153 (1997) 93-104.

[156] T. Gessler, T. Schmehl, M.M. Hoeper, F. Rose, H.A. Ghofrani, H. Olschewski, F. Grimminger, W. Seeger, Ultrasonic versus jet nebulization of iloprost in severe pulmonary hypertension, European Respiratory Journal, 17 (2001) 14-19.

[157] M.B. Dolovich, R. Dhand, Aerosol drug delivery: developments in device design and clinical use, The Lancet, 377 (2011) 1032-1045.

[158] B. Avvaru, M.N. Patil, P.R. Gogate, A.B. Pandit, Ultrasonic atomization: Effect of liquid phase properties, Ultrasonics, 44 (2006) 146-158.

[159] B. Howard (2010): High speed photography of ultrasonic atomization. Master thesis, Brown University: School of Engineering.

[160] B. Howard, Ultrasonic Atomization, Brown University, Retrieved 11/18/2013 from http://ultrasoundatomization.com/15.html.

[161] G. Cewers, Ultrasonic nebulizer, U.S. Patent US6357671 B1, issued 03/19/2002.

[162] L. Huamao, L. Yuhua, L. Zhouhua, The heating phenomenon produced by an ultrasonic fountain, Ultrasonics Sonochemistry, 4 (1997) 217-218.

[163] J.A. Giarratano, J. Carpenter, C.S. Lengsfeld, Protein Aggregation during Ultrasonic Nebulization, in: I. Americas (Ed.) 24rd Annual Conference on Liquid Atomization and Spray Systems, ILASS Americas, San Antonio, Texas, USA, 2012.

[164] H.I. Elsner, E.B. Lindblad, Ultrasonic degradation of DNA, DNA (Mary Ann Liebert, Inc.), 8 (1989) 697-701.

[165] A.Y. Ip, T. Arakawa, H. Silvers, C.M. Ransone, R.W. Niven, Stability of recombinant consensus interferon to air-jet and ultrasonic nebulization, J Pharm Sci, 84 (1995) 1210-1214.

[166] R.W. Niven, A.Y. Ip, S. Mittelman, S.J. Prestrelski, T. Arakawa, Some Factors Associated with the Ultrasonic Nebulization of Proteins, Pharmaceutical Research, 12 (1995) 53-59.

[167] G.A. Ferron, K.F. Kerrebijn, J. Weber, Properties of aerosols produced with three nebulizers, The American review of respiratory disease, 114 (1976) 899-908.

[168] S.P. Newman, P.G. Pellow, S.W. Clarke, In vitro comparison of devilbiss jet and ultrasonic nebulizers, CHEST Journal, 92 (1987) 991-994.

[169] M. Zeles-Hahn, T.J. Anchordoquy, C.S. Lengsfeld, Observations on the impact of aerosolization on macromolecular therapeutics, in: European Conference on Liquid Atomization and Spray Systems, Como Lake, Italy, 2008, pp. 8-3.

[170] Z.M. Corden, C.M. Bosley, P.J. Rees, G.M. Cochrane, Home Nebulized Therapy for Patients with COPD Patient Compliance With Treatment and Its Relation to Quality of Life, CHEST Journal, 112 (1997) 1278-1282.

[171] L. Khatri, K.M.G. Taylor, D.Q.M. Craig, K. Palin, An assessment of jet and ultrasonic nebulisers for the delivery of lactate dehydrogenase solutions, International Journal of Pharmaceutics, 227 (2001) 121-131.

[172] A.M. Munster, E. Bendstrup, J.I. Jensen, J. Gram, Jet and ultrasonic nebulization of single chain urokinase plasminogen activator (scu-PA), Journal of aerosol medicine : the official journal of the International Society for Aerosols in Medicine, 13 (2000) 325-333.

[173] T. Kosugi, S. Saitoh, N. Tamaki, K. Hanashiro, K. Nakahodo, M. Nakamura, Inhalation of platelet-activating factor increases respiratory resistance in rats: Determination by means of an astograph under nonanesthetized conditions, The Laryngoscope, 103 (1993) 428-430.

[174] E.G. Langenback, J.M. Davis, C. Robbins, N. Sahgal, R.J. Perry, S.R. Simon, Improved pulmonary distribution of recombinant human Cu/Zn superoxide dismutase, using a modified ultrasonic nebulizer, Pediatric Pulmonology, 27 (1999) 124-129.

[175] J.C. Waldrep, R. Dhand, Advanced Nebulizer Designs Employing Vibrating Mesh/Aperture Plate Technologies for Aerosol Generation, Current Drug Delivery, 5 (2008) 114-119.

[176] A.B. Watts, J.T. McConville, R.O. Williams, Current therapies and technological advances in aqueous aerosol drug delivery, Drug Development and Industrial Pharmacy, 34 (2008) 913-922.

[177] L. Vecellio, The mesh nebuliser: a recent technical innovation for aerosol delivery, Breathe, 2 (2006) 252-260.

[178] H.W. Frijlink, A.H. de Boer, Trends in the technology-driven development of new inhalation devices, Drug Discovery Today: Technologies, 2 (2005) 47-57.

[179] J.S. Lass, A. Sant, M. Knoch, New advances in aerosolised drug delivery: vibrating membrane nebuliser technology, Expert Opinion on Drug Delivery, 3 (2006) 693-702.

[180] Y. Saeki Adachi, T. Itazawa, M. Nakabayashi, T. Fuchizawa, Y. Okabe, Y. Ito, Y. Adachi, G. Murakami, T. Miyawaki, Safety and usefulness of a novel eMotion electric mesh nebulizer in children with asthma, Allergology international : official journal of the Japanese Society of Allergology, 55 (2006) 167-171.

[181] L. Pitance, L. Vecellio, T. Leal, G. Reychler, H. Reychler, G. Liistro, Delivery efficacy of a vibrating mesh nebulizer and a jet nebulizer under different configurations, J Aerosol Med Pulm Drug Deliv, 23 (2010) 389-396.

[182] A.L. Coates, M. Green, K. Leung, J. Chan, N. Ribeiro, E. Louca, F. Ratjen, M. Charron, M. Tservistas, M. Keller, Rapid pulmonary delivery of inhaled tobramycin for Pseudomonas infection in cystic fibrosis: A pilot project, Pediatric Pulmonology, 43 (2008) 753-759.

[183] A.L. Coates, M. Green, K. Leung, E. Louca, M. Tservistas, J. Chan, N. Ribeiro, M. Charron, The challenges of quantitative measurement of lung deposition using 99mTc-DTPA from delivery systems with very different delivery times, Journal of aerosol medicine : the official journal of the International Society for Aerosols in Medicine, 20 (2007) 320-330.

[184] K.G. Schuepp, S. Devadson, C. Roller, J.H. Wildhaber, A complementary combination of delivery device and drug formulation for inhalation therapy in preschool children, Swiss medical weekly, 134 (2004) 198-200.

[185] T. Ghazanfari, A.M.A. Elhissi, Z. Ding, K.M.G. Taylor, The influence of fluid physicochemical properties on vibrating-mesh nebulization, International Journal of Pharmaceutics, 339 (2007) 103-111.

[186] R. Dhand, New Frontiers in Aerosol Delivery during mechanical Ventilation, Respiratory Care, 49 (2004) 666-677.

[187] M. Knoch, M. Keller, The customised electronic nebuliser: a new category of liquid aerosol drug delivery systems, Expert Opinion on Drug Delivery, 2 (2005) 377-390.

[188] R. Stangl, S. Seemann, M. Knoch, Customizing an Electronic Nebulizer in: ISAM 15th, Perth, Australia, 2005.

[189] K. Schmid (2011): Spray drying of protein precipitates and Evaluation of the Nano Spray Dryer B-90. PhD thesis, Ludwig Maximilian University Munich: Faculty of Chemistry and Pharmacy.

[190] K. Nikander, I. Prince, S. Coughlin, S. Warren, G. Taylor, Mode of breathing-tidal or slow and deep-through the I-neb Adaptive Aerosol Delivery (AAD) system affects lung deposition of (99m)Tc-DTPA, J Aerosol Med Pulm Drug Deliv, 23 (2010) S37-43.

[191] M. Keller, M. Tservistas, E. Bitterle, S. Bauer, Aerosol Characterization of Alpha-1 Antitrypsin After Nebulization with the eFlow(R): A Novel Vibrating Perforated Membrane Nebulizer, in: R.N. Dalby, P.R. Byron, J. Peart, J.D. Suman, S.J. Farr (Eds.) Respiratory Drug Delivery X, Boca Raton, FL, USA, 2006, pp. 733-736.

[192] A. Poncin, M. Tservistas, C. Zankl, T. Gerlza, A. Luithlen, R. Egle, R. Doornbos, M. Knoch, A. Kungl, a novel formulation of an il-8 decoy chemokine, pa401, with potential application for the treatment of copd can be nebulized by eflow (r) technology, in:

Journal Of Aerosol Medicine And Pulmonary Drug Delivery, Mary Ann Liebert, Inc 140 Huguenot Street, 3rd Fl, New Rochelle, Ny 10801 USA, 2013, pp. A248-A249.

[193] J. Tepper, A. Tomkinson, Methods for treating asthma in human and non human primates using IL-4 mutant compositions, U.S. Patent 7947648, issued 05/24/2011.

[194] R. Dalby, M. Spallek, T. Voshaar, A review of the development of Respimat® Soft Mist™ Inhaler, International Journal of Pharmaceutics, 283 (2004) 1-9.

[195] S.J. Farr, A. McElduff, L.E. Mather, J. Okikawa, M.E. Ward, I. Gonda, V. Licko, R.M. Rubsamen, Pulmonary insulin administration using the AERx system: physiological and physicochemical factors influencing insulin effectiveness in healthy fasting subjects, Diabetes Technol Ther, 2 (2000) 185-197.

[196] J. Thipphawong, B. Otulana, P. Clauson, J. Okikawa, S.J. Farr, Pulmonary insulin administration using the AERx insulin diabetes system, Diabetes Technol Ther, 4 (2002) 499-504.

[197] T.J. Kamerzell, R. Esfandiary, S.B. Joshi, C.R. Middaugh, D.B. Volkin, Protein excipient interactions: Mechanisms and biophysical characterization applied to protein formulation development, Advanced Drug Delivery Reviews, 63 (2011) 1118-1159.

[198] S. Frokjaer, D.E. Otzen, Protein drug stability: a formulation challenge, Nat Rev Drug Discov, 4 (2005) 298-306.

[199] S.P. Sellers, Y.-F. Maa, Principles of Biopharmaceutical Protein Formulation: An Overview, in: C.M. Smales, D.C. James (Eds.) Therapeutic Proteins, Humana Press Inc., Totowa, NJ, 2005, pp. 243-263.

[200] Ph.EUR., Preparations for Inhalation, in: B. European Directorate for the quality of Medicine (EDQM), Belgium (Ed.) 0671, European Directorate for the quality of Medicine (EDQM), Ph.Eur., 2008, pp. 1048-1053.

[201] R. Beasley, P. Rafferty, S.T. Holgate, Adverse reactions to the non-drug constituents of nebuliser solutions, British Journal of Clinical Pharmacology, 25 (1988) 283-288.

[202] O.N.M. Mc Callion, K.M.G. Taylor, M. Thomas, A.J. Taylor, The influence of surface tension on aerosols produced by medical nebulisers, International Journal of Pharmaceutics, 129 (1996) 123-136.

[203] O.M. McCallion, K.G. Taylor, M. Thomas, A. Taylor, Nebulization of Fluids of Different Physicochemical Properties with Air-Jet and Ultrasonic Nebulizers, Pharmaceutical Research, 12 (1995) 1682-1688.

[204] O.N.M. Mccallion, K.M.G. Taylor, M. Thomas, A.J. Taylor, Ultrasonic Nebulisation of Fluids with Different Viscosities and Surface Tensions, Journal of Aerosol Medicine, 8 (1995) 281-284.

[205] FDA, Inactive Ingredient Database for Approved Drug Products, FDA, Center for Drug Evaluation and Research, Office of Generic Drugs, Silver Spring, MD, USA. Retrieved 09/03/2013 from http://www.accessdata.fda.gov/scripts/cder/iig/index.cfm.

[206] S.A. Shoyele, A. Slowey, Prospects of formulating proteins/peptides as aerosols for pulmonary drug delivery, International Journal of Pharmaceutics, 314 (2006) 1-8.

[207] L. Garcia-Contreras, H.D.C. Smyth, Liquid-Spray or Dry-Powder Systems for Inhaled Delivery of Peptide and Proteins?, American Journal of Drug Delivery, 3 (2005) 29-45.

[208] T. Serno, E. Hartl, A. Besheer, R. Miller, G. Winter, The role of polysorbate 80 and HPbetaCD at the air-water interface of IgG solutions, Pharm Res, 30 (2013) 117-130.

[209] J. Dunn, R. Nayar, J. Campos, B. Hybertson, Y. Zhou, M. Manning, J. Repine, K. Stringer, Feasibility of Tissue Plasminogen Activator Formulated for Pulmonary Delivery, Pharmaceutical Research, 22 (2005) 1700-1707.

[210] H. Steckel, F. Eskandar, K. Witthohn, The effect of formulation variables on the stability of nebulized aviscumine, International Journal of Pharmaceutics, 257 (2003) 181-194.

[211] R. Bhat, S.N. Timasheff, Steric exclusion is the principal source of the preferential hydration of proteins in the presence of polyethylene glycols, Protein Science, 1 (1992) 1133-1143.

[212] T. Arakawa, S.N. Timasheff, Mechanism of polyethylene glycol interaction with proteins, Biochemistry, 24 (1985) 6756-6762.

Chapter III Materials and Methods

1 Materials

1.1 Proteins

1.1.1 SM101

SM101 was provided by SuppreMol GmbH (Martinsried, Germany). SM101 is the soluble Fc gamma receptor IIB (sFcγRIIB) produced by expression of the extracellular domain of human FcγRIIB in E. coli. The molecule is unglycosylated and has a molecular weight of approximately 20 kDa. The crystal structure was revealed by Sondermann et al. [1, 2]. SM101 belongs to the immunoglobulin superfamily and exhibits mainly beta-sandwich tertiary structure (Figure III-1).

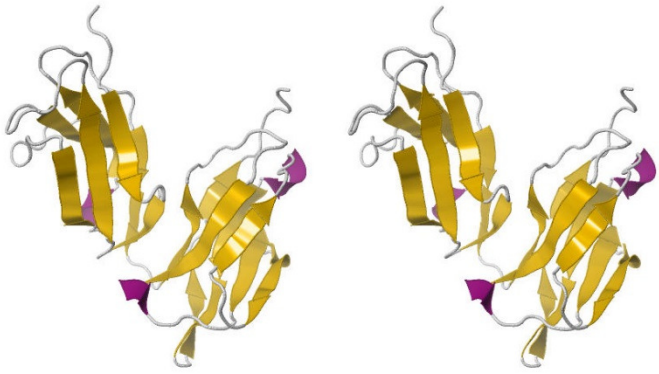

Figure III-1: Stereoscopic view of the crystal structure of human Fc gamma receptor IIb ectodomain (cd32). Secondary structure elements are color coded: beta strand (yellow), 3/10 helix (violet) and random coil (grey).

Receptors of the Fc region of immunoglobulins mediate the effects of antibodies and immune complexes (IC) and thereby link the humoral and the cellular immune system [3]. FcRs binding IgG antibodies are labeled FcγR. Different FcγR subclasses occur endogenously in humans as type I transmembrane proteins or in a soluble form of which FcγRIIB is the only inhibitory receptor. FcγR are expressed on most immune cells, except T-cells and are involved in the activation and regulation of immune responses. FcγRIIB is involved in down regulation and control of antibody or IC mediated phagocytosis, antigen presentation, antibody dependent

cellular cytotoxicity (ADCC) and release of pro-inflammatory cytokines. Additionally FcγRIIB downregulate B-cell activity and thereby reduce antibody production. The absence or insufficient ratio of inhibitory FcγRIIB was related to autoimmune diseases like arthritis and systemic lupus erythematosus (SLE) in mice and in humans.

SM101 competes with FcR bearing immune cells for autoantigen/autoantibody complexes and thus prevents autoantibody production by plasma-cells and the triggering of the inflammatory cascade. This suggests the efficacy of SM101 for the treatment of various autoimmune diseases. Clinical studies evaluating the potential of intravenously administered SM101 for the treatment of primary immune thrombocytopenia (ITP) and SLE are currently in phases IIb and IIa respectively [4] and "excellent safety and long lasting pharmacodynamic effects" have been shown. Local pulmonary delivery of SM101 would enable the treatment of immune related diseases or symptoms occurring in the lungs. Possible conditions include farmer's lung, SLE alveolitis or COPD.

Since SM101 is homologous to the endogenously occurring sFcγRIII, a rise of anti-drug antibodies (ADA) might have serious consequence involving depletion of the natural counterpart [5-7] with serious impact on the immune system. Notably no ADA against SM101 were found in patients repeatedly receiving SM101 infusions [8].

Bulk drug substance was supplied in 5.3 mM NaH_2PO_4, 1.96 mM KH_2PO_4 and 150 mM NaCl, pH 6.5 at a SM101 concentration of 8.2 mg/mL. Each batch of API material was reformulated and the phosphate buffer was quantitatively exchanged via cation-exchange chromatography (CEX) on an ÄKTA Explorer 100 (GE Healthcare). CEX buffer exchange yielded SM101 in histidine buffered saline (HBS) of 20 mM histidine and 216-264 mM sodium chloride at pH 6.5 with SM101 concentrations ranging from 7.2-14.1 mg/mL. Sodium chloride content was calculated from the conductivity, normalized to the values of the loading and elution buffer employed. SM101 concentration in the eluate was determined via UV/Vis spectroscopy at 280nm with an extinction coefficient of 1.51625 g/L*cm used for calculation. Aliquots of reformulated SM101 stock were stored at -80°C until used.

SM101 formulations were made up from concentrated excipient stock solutions and aliquoted SM101 stock and then filtered through 0.2 µm PVDF syringe filters (Acrodisc® LC 25mm Syringe

Filter, PALL Life Science, Dreieich, Germany), whereas surfactant stock was added afterwards. Surfactant stock was filtered separately whereby the first syringe volume was discarded for filter saturation. SM101 was used in several formulations and concentrations throughout different stages of this thesis as indicated in Table III-1. Sodium chloride content was adjusted to either 75 or 150 mM and the SM101 concentration was set to the desired value in a range of 0.25 to 20.0 mg/mL.

To obtain SM101 concentrations of 10 mg/mL or above SM101 stock was concentrated by ultracentrifugation with Vivaspin 15 units with a molecular weight cut-off (MWCO) of 5kDa (Sartorius Stedim Biotech GmbH, Goettingen, Germany) in a swing bucket centrifuge at 4000 g and 4°C (Sigma 4K15, Osterode am Harz, Germany). Concentrator membranes were flushed with a unit volume of placebo buffer prior to use. Recovered SM101 was syringe filtered (Puradisc™ PVDF, Whatman, Whatman International, Kent, UK), SM101 concentration determined via UV/Vis spectroscopy and adjusted to a desired value with a respective buffer solution. To reduce sodium chloride content of formulation candidate C to 0 mM, the buffer was exchanged by repeated dilution and ultrafiltration of the SM101 stock solution.

At a later stage of the project, SuppreMol GmbH had established a new manufacturing process that yielded SM101 drug substance formulated directly in the newly developed (Chapter V) parenteral formulation (Table III-1: parenteral formulation / candidate B). Using this as a starting material, the aerosol formulation (Table III-1) used in the *in vivo* studies (Chapter VI) was generated by 1:1 dilution with an excipient stock solution containing 20 mM histidine, 0 mM NaCl, pH 6.5, 3.33% sucrose and 1.67% mannitol. This was done under aseptic conditions, under a laminar airflow and the final formulation was sterile filtered into pyrogen-free and sterile falcon tubes.

Table III-1: SM101 formulations used throughout the experiments.

Formulation	Excipients	Concentration		Experiments
		mg/mL	mM	(SM101 concentration in mg/mL)
drug product (DP)	NaH_2PO_4	0.731	5.3	Chapter V:
	KH_2PO_4	0.272	2.0	parenteral formulation
	NaCl	8.766	150	development (5.0)
	D-Mannitol	20.0	109.8	
	Polysorbate 20	0.05	0.04	
histidine buffered saline (HBS)	L-Histidine	3.103	20.0	Chapter IV:
	NaCl	8.766	150.0	aerosol cloud collection (3.0)
				T_m and T_{agg} measurement (1.0)
				Chapter V:
				surrogate screening method (5.0)
				excipient screening (2.0 or 8.0)
candidate A	L-Histidine	3.103	20.0	Chapter V:
	NaCl	8.766	150.0	parenteral formulation
	D-Mannitol	20.0	109.8	development (10.0 or 20.0)
	Polysorbate 20	0.05	0.04	
parenteral formulation = candidate B	L-Histidine	3.103	20.00	Chapter IV:
	NaCl	8.766	150.00	T_m measurement (1.0)
	D-Mannitol	10.000	54.90	Chapter V:
	Sucrose	20.000	58.40	parenteral formulation
	Polysorbate 20	0.050	0.04	development (10.0 or 20.0)
				excipient screening (2.0 or 8.0)
				AKITA² nebulization (20.0)
candidate C	L-Histidine	3.103	20.0	Chapter V:
	D-Mannitol	20.0	109.8	parenteral formulation
	Sucrose	60.0	175.3	development (10.0 or 20.0)
	Polysorbate 20	0.05	0.04	
candidate 1	L-Histidine	3.103	20.00	Chapter V:
	NaCl	8.766	150.00	AKITA² nebulization (10.0 or 20.0)
	D-Mannitol	10.000	54.90	
	Sucrose	20.000	58.40	
	Polysorbate 20	0.400	0.32	
aerosol formulation (AF) = candidate 2	L-Histidine	3.103	20.00	Chapter V:
	NaCl	4.383	75.00	AKITA² nebulization (10.0)
	D-Mannitol	13.333	73.20	Chapter VI:
	Sucrose	26.667	77.90	MicroSprayer® (0.25, 0.5, 1.0)
	Polysorbate 20	0.400	0.32	Aeroneb® Pro nebulization (10.0)
				in vivo experiments (10.0)

1.1.2 L-lactic dehydrogenase (LDH)

L-lactic dehydrogenase (LDH) was employed as a model protein in the investigations described in chapter IV and V. LDH is very sensitive to interfacial stress and has previously been used as a sensitive model protein during nebulization, spray drying and lyophilization [9-14]. LDH is

naturally occurring in the cytoplasm of virtually all living beings, where it catalyzes the reduction of pyruvate to lactate under concomitant regeneration of the reduced β-NADH/H+ to β-NAD+ during anaerobic glycolysis (lactic acid fermentation). Another motivation for LDH application throughout this thesis was its readily available activity assay, which is based on the spectrophotometric monitoring of this enzymatic reaction. LDH is a tetrameric protein made up of two different sub-units the M- and the H-type. All five possible isoforms are distributed in an organ specific manner in the human body. Serum levels of LDH isozymes are therefore used to diagnose damage of particular organs or tissue.

According to the structural classification of proteins (SCOP), LDH belongs to the alpha and beta proteins class. Rabbit muscle lactic dehydrogenase (LDH) with a total molecular weight of 140 kDa was purchased from Sigma Aldrich (LDH, Cat. # L2500, Sigma-Aldrich Chemie GmbH, Munich, Germany). Prior to use, LDH was dialyzed against an excess of 20 mM potassium phosphate buffer, pH 7.4 with 12-30 mL Slide-a-Lyzer® casettes (Thermo Fisher Scientific, Rockford, Il, USA) of 30 kDa MWCO. Dialysis buffer was exchanged twice before overnight dialysis. LDH solution was filtered through 0.2 µm PVDF syringe filters (Puradisc PVDF, Whatman, Whatman International, Kent, UK) after removal from the dialysis cassette. LDH concentration was determined spectrophotometrically at 280nm with an extinction coefficient $\varepsilon = 1.49$ mL*mg^{-1}*cm^{-1}. During surrogate screening studies (Chapter V), formulations containing one additional excipient were made from excipient stock solutions and LDH stock of 1.0 mg/mL. LDH was used in a final concentration of 0.2 mg/mL throughout all experiments.

1.1.3 Granulocyte-colony stimulating factor (G-CSF)

Recombinant human granulocyte-colony stimulating factor (G-CSF) material from two sources was used throughout this thesis. Studies evaluating the feasibility of systemic pulmonary delivery of G-CSF revealed its sensitivity to nebulization [15, 16]. Therefore, G-CSF was chosen as a second model protein. Its surface activity and its distinct pH sensitive stability made it the ideal model protein for the investigation about the impact of proteins on nebulizer performance (Chapter IV) and for the surrogate screening method (Chapter V).

Physiologically, it is a cytokine involved in hematopoiesis, controlling the production, differentiation and function of neutrophil and basophile granulocytes from bone marrow.

Recombinant human G-CSF is used to treat febrile neutropenia, prevent neutropenia after chemotherapy and to increase the count of hematopoietic stem cells (HSC) before HSC donation. Besides the original Neupogen® (Amgen GmbH, Thousand Oaks, CA, USA), several biosimilars are marketed. G-CSF has a molecular weight of 19.6 kDa and belongs to the all alpha proteins class (SCOP) with a four-helix bundle tertiary structure.

G-CSF was provided at 4.04 mg/mL G-CSF in 10 mM acetate buffer, 0.005% PS20 at pH 4.0. It was excessively dialyzed to a 100mM acetate buffer pH 3.5 to eliminate PS20 content following the dialysis procedure described above. Dialyzed G-CSF was filtered through 0.2 µm PVDF syringe filters (Puradisc PVDF, Whatman, Whatman International, Kent, UK) and adjusted to a concentration of 0.3 or 3.0 mg/mL. Sodium hydroxide was added to adjust pH to 4.0, 4.5 or 5.0. The experiments described in chapter IV were conducted with this material. Surrogate screening experiments reported in chapter V were carried out with 1.0 mg/mL G-CSF in 20 mM potassium hydrogen phosphate buffer at pH 4.4. Formulations with one additional excipient were made from stock solutions. G-CSF starting material for this experiment was provided at 4 mg/mL G-CSF in 20 mM $KHPO_4$ pH 4.0. At pH 4.4, G-CSF remained sufficiently storage stable but was very sensitive to nebulization and interfacial stress.

1.1.4 Monoclonal immunoglobulin G (IgG)

The monoclonal antibody of the IgG 1 class was a gift from Roche Diagnostics GmbH (Penzberg, Germany). Degradation of this IgG has been described after vortexing [17] and freeze/thawing [18] which indicates its sensitivity towards interfacial stress. It was therefore selected as a more thermostable model protein for nebulization at high protein concentrations (Chapter IV).

IgG starting material was formulated in 10 mM potassium phosphate buffer at pH 6.9. 15 mg/mL IgG were used to investigate the impact of aerosol cloud collection and nebulization on protein stability. IgG formulations at 15 mg/mL or 40 mg/mL IgG served as models to investigate the impact of protein induced viscosity increase on nebulizer performance. In the case of 40 mg/mL, IgG was concentrated by ultrafiltration (Vivaspin 20, 30.000 kDa MWCO, Sartorius Stedim, Göttingen, Germany). All IgG formulations were syringe filtered through 0.2 µm PVDF filters (Puradisc PVDF, Whatman, Whatman International, Kent, UK).

1.1.5 Anti-chicken egg albumin antibody (Anti-OVA IgG)

Polyclonal anti-chicken egg albumin antibody (anti-OVA IgG) was used to initiate an immediate immune response to OVA antigen in the passive pulmonary Arthus reaction model in mice as described by Skokowa [19] (Chapter VI). Polyclonal anti-OVA IgG in whole serum was bought from Sigma Aldrich (Munich, Germany, Cat. # C5634). The serum contained a total protein fraction of 70.8 mg/mL mainly made up of albumin and immunoglobulins, while the specific anti-OVA IgG concentration was 4.2 mg/mL. The formulation was used undiluted during in vitro stability/activity assessment and for *in vivo* studies.

1.1.6 Ovalbumin (OVA, chicken egg albumin)

Endotoxin free OVA (lot # 11785, Hyglos GmbH, Bernried am Starnberger See, Germany) was used as an antigen in the Arthus reaction model in mice (Chapter VI). OVA was purchased as a lyophilized powder and a stock solution of 19.3 mg/mL OVA in 20 mM histidine, 150 mM NaCl, 2% sucrose, 1% mannitol, 0.005% polysorbate 20 was prepared. Prior to instillation, OVA concentration was diluted to 0.8 mg/mL with respective placebo buffer. For preliminary stability testing, OVA grade 5 was bought from Sigma Aldrich (Steinheim, Germany). Formulations of 4.0-10.0 mg/mL OVA in PBS or 10 mM or 100 mM sodium phosphate buffer at pH 7.0, 7.4 or 8.0 were subjected to *in vitro* stability determination after nebulization.

OVA is the main protein component in chicken egg white. OVA belongs to the serpin superfamily and has a molecular weight of 43-45 kDa. It is commonly used as a model antigen to induce immune reactions in animal models. Available commercial OVA material is often contaminated with endotoxic LPS which interferes with the inflammatory response.

1.2 Excipients

Table III-2 lists all excipients used in formulations throughout this thesis. Excipients used for purposes other than formulation are summarized in Table III-3.

Table III-2: Excipients used for protein formulation.

Excipient	Quality	Vendor
L-Histidine	EMPROVE® exp Ph. Eur., USP	Merck KGaA (Darmstadt, Germany)
Sodium chloride (NaCl)	EMPROVE® exp Ph. Eur.	Merck KGaA (Darmstadt, Germany)
Polysorbate 20 (PS20)	Super Refined ®	CRODA GmbH (Nettetal, Germany)
Hydroxypropyl-β-cyclodextrin	Pharmaceutical Grade	Wacker-Chemie GmbH (Burghausen, Germany)
Polyethyleneglycol 8000	Pharmaceutical Grade	Clariant GmbH (Wiesbaden, Germany)
L-Arginine	Pharmaceutical Grade	Boehringer Ingelheim Pharma GmbH (Ingelheim, Germany)
Sucrose	USP	Sigma Aldrich (Steinheim, Germany)
D-Mannitol	Ph. Eur.	Riedel de Haen (Seelze, Germany)
Polysorbate 80 (PS80)	Ph. Eur.	Merck KGaA (Darmstadt, Germany)
Pluronic® F68 = P188	Pharmaceutical Grade	BASF AG (Ludwigshafen, Germany)
Poloxamer® 407	Cell culture	Sigma Aldrich (Steinheim, Germany)
Brij® E35	PRACT grade	Serva Electrophoresis GmbH (Heidelberg, Germany)
Sorbitol	Ph. Eur.	Caesar & Lorentz GmbH (Hilden, Germany)
D(+)-Trehalose	For biochemistry	VWR International GmbH (Darmstadt, Germany)
Glycine	Ph. Eur.	Merck KGaA (Darmstadt, Germany)
Disodium hydrogen phosphate (Na_2HPO_4)	p.a.	Applichem GmbH (Darmstadt, Germany)
Sodium dihydrogen phosphate (NaH_2PO_4)	p.a.	Applichem GmbH (Darmstadt, Germany)
Dipotassium hydrogen phosphate (K_2HPO_4)	p.a.	Applichem GmbH (Darmstadt, Germany)
Potassium dihydrogen phosphate (KH_2PO_4)	p.a.	Applichem GmbH (Darmstadt, Germany)
Sodium Acetate	p.a.	VWR International GmbH (Darmstadt, Germany)
Glacial acetic acid (100%)	p.a.	VWR International GmbH (Darmstadt, Germany)

Table III-3: Excipients applied for non-formulation purposes.

Excipient	Quality	vendor
5/6-Carboxyfluorescein	BioReagent, suitable for fluorescence	Sigma Aldrich (Steinheim, Germany)
Bovine serum albumin (BSA)	min 96%	Sigma Aldrich (Steinheim, Germany)
Na-pyruvate	99%	Sigma Aldrich (Steinheim, Germany)
β-NADH	98%	Sigma Aldrich (Steinheim, Germany)
Sodium dodecyl sulfate (SDS)	>99%, ACS	Sigma Aldrich (Steinheim, Germany)
3-(N-Morpholino) propanesulfonic Acid (MOPS)	molecular biology grade	Merck KGaA (Darmstadt, Germany)
Acetonitrile	HPLC grade	Merck KGaA (Darmstadt, Germany)

2 Methods

2.1 Nebulization

Throughout this thesis, various vibrating mesh (VM) and a jet nebulizer have been employed. The nebulization conditions applied are mentioned below and referred to the respective chapter and section.

2.1.1 Nebulizer performance

Three different VM nebulizers a PARI eFlow® (PARI GmbH, Starnberg, Germany, Cat. # 678G200), an Aeroneb® Go (Aerogen, Galway, Ireland) and a MicroAIR U22 (OMRON Healthcare Europe, Hoofddorp, Netherlands) were charged with 1 mL solution and operated until complete nebulization. Nebulized solutions contained physiologic saline with or without the addition of sucrose or PS20 to manipulate viscosity or surface tension respectively. Furthermore, the impact of proteins and excipients on VM nebulizer performance was examined with a PARI eFlow® loaded with 4 mL solution, which were completely nebulized. The same conditions were applied for the evaluation of protein aggregation on VM nebulizer performance.

2.1.2 Aerosol collection method evaluation

Aerosol collection procedures were evaluated for aerosols of either 3 mg/mL SM101 or 15 mg/mL IgG1 generated with a PARI® eFlow loaded with 4mL solution.

2.1.3 Nebulizer heat up

A PARI eFlow® was charged with either 1, 2, 3 or 4 mL saline and completely nebulized to assess the impact of initial load (IL) on reservoir temperature progression during nebulization.

2.1.4 Normal and passively cooled nebulization

A PARI eFlow® was used to compare different nebulization procedures regarding their effect on the temperature in the medication reservoir (T_{RES}). The impact on aerosol characteristics was assessed by physiologic saline nebulization. Resulting protein degradation was studied for three

different proteins including LDH, IgG and SM101. For all nebulization procedures, 3 mL solution were nebulized. Further details of the nebulization procedures were as follows:

Normal

During 'Normal' nebulization the PARI eFlow® was charged with 3 mL solution at room temperature and then nebulized completely.

Pre-cooled (PC)

Nebulizer solution was 'pre-cooled' (PC) in a refrigerator and 3mL of pre-cooled solution were charged into the reservoir and nebulized completely without prior equilibration to room temperature.

Overloaded (OL)

Another approach included loading the medication reservoir with 4 mL solution of which only 3 mL were nebulized. Overloading was performed either with solutions equilibrated to room temperature (OL) or in combination with pre-cooled solution (PC-OL). Nebulization time was used to determine the moment when 3mL solution had been nebulized and operation had to be terminated.

Intermittent (IM)

Intermittent nebulization (IM) was achieved manually with a frequency of 5s nebulization followed by 5s pausing. 3mL solution equilibrated to room temperature was completely nebulized.

2.1.5 Nebulization of the parenteral SM101 formulation

A PARI eFlow® was overloaded with 2.2 mL pre-cooled parenteral formulation containing 20 mg/mL SM101. 1.2 mL were nebulized and collected in 2 mL PP tubes as described in section 2.5. The nebulized-collected and the residual fraction were analyzed for SM101 stability and activity.

2.1.6 Surrogate method development

During surrogate screening method development and parameter tuning for the proteins LDH and G-CSF, reference nebulization was performed with a PARI eFlow®. For SM101 and LDH

reservoir overloading as described above (section 2.1.4) was applied and a total of 4 mL solution was charged into the medication reservoir. For G-CSF the loaded 4mL were completely nebulized. All protein aerosols were collected in either 2 mL or 0.65 mL PP caps as described in section 2.5.

2.1.7 Aerosol formulation candidate nebulization

The candidates for the SM101 aerosol formulation were nebulized with an AKITA² vibrating mesh nebulizer and an AKITA jet (both Activaero GmbH, Gemünden, Germany) nebulizer. Both devices were operated in an intermittent mode consisting of a 5 s inhalation and 5 s exhalation phase. Aerosol was only generated during the first 4 s of the inhalation phase. AKITA² nebulization conditions followed the PC-OL procedure mentioned above (section 2.1.4). The formulations were pre-cooled to 10-15°C. And 2.0-2.5 mL of the 4.0 mL charge were nebulized and collected in 2 mL PP tubes and pooled prior analysis.

Nebulization conditions for the AKITA jet were designed to generate a comparable amount of aerosol as the AKITA². Aiming for approximately 2 mL to remain inside the medication reservoir for subsequent analysis of SM101 activity and stability, 5 mL were loaded in the reservoir and the device was operated for 20 minutes.

2.1.8 Pneumatic and manual in vitro MicroSprayer® use

A MicroSprayer® Aerosolizer Model IA-1C-M with a FMJ-250 High Pressure Syringe (both Penn-Century. Inc., Wyndmoor, PA, USA) was used to generate aerosols from 100-250µL solutions, previously filtered through 0.2 µm syringe filters (Puradisc PVDF, Whatman, Whatman International, Kent, UK). After spraying of protein formulations, the MicroSprayer® was cleaned with filtered 1% SDS solution. Actuation of the MicroSprayer® was either done manually or with a pneumatic actuator device operated with pressurized air, set to a defined pressure in a range of 2.0-8.0 bar. The pneumatic actuator was developed by Otmar Schmid and his group (CPC, Neuherberg, Germany).

2.1.9 *In vitro* stability to small volume vibrating mesh nebulization

Prior to selection of the nebulizer employed for vented intubated inhalation in *in vivo* studies, three prospect vibrating mesh nebulizers were compared regarding aerosol characteristics and operating temperature. Therefore, a PARI eFlow®, an Aeroneb® Pro and an Aeroneb® Solo were loaded with 1 mL placebo aerosol formulation and operated until dryness.

The stability of SM101 and anti-OVA IgG after complete nebulization in small volume samples was investigated with an Aeroneb® Pro. Therefore, 100 µL 10 mg/mL SM101 in HBS or in the aerosol formulation was nebulized. The solution was dispensed directly onto the mesh of the nebulizer. Five aliquots were pooled into one sample for stability analysis. For anti-OVA IgG, 400 µL samples were completely nebulized.

2.2 Temperature measurement during nebulization

Nebulizer reservoir temperature was recorded with a Data Logger (OMEGA HH147U, Newport Electronics GmbH, Deckenpfronn, Germany). A thin wire thermocouple was placed at the bottom of the reservoir in proximity to the membrane while not touching it, to measure reservoir temperature during the entire nebulization. The heating rate was calculated as the slope of the linear regression of the T_{RES} curve. The temperature of the vibrating membrane itself was approximated by temperature measurements on the metal substrate holding both the membrane and the vibrating piezo element [20]. A wire thermocouple was connected to the metal substrate with thermal adhesive (Conrad Electronic SE, Hirschau, Germany), so that neither piezo nor membrane operation were impaired (Figure III-2).

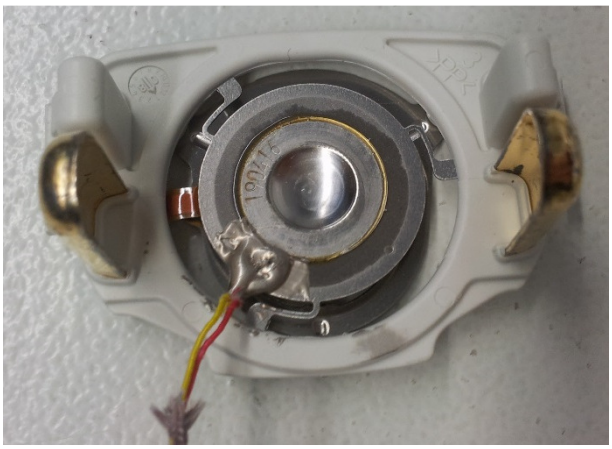

Figure III-2: Thermo couple attached to PARI eFlow® aerosol head.

2.3 Actively cooled nebulization

A custom built system for cooling the PARI eFlow® reservoir was developed based on a micro Peltier element (Figure III-3). The setup consisted of a custom molded heat transfer module made of nickel silver alloy connecting the back of the eFlow reservoir with the cold side of a 5 cm² Peltier element (QC-71-1.0-3.9, Quick-Ohm Küpper & Co. GmbH, Wuppertal, Germany). A fan-cooled heat sink was attached to the hot side of the Peltier element. Thermal grease (KERATHERM KP92, Conrad Electronic SE, Hirschau, Germany) was applied to fill thermo conductive interfaces. The extent of cooling was controlled via the voltage applied to the Peltier element with a controllable power adaptor (VOLTCRAFT PSP 12010, Conrad Electronic SE, Hirschau, Germany). With this setup the reservoir could be equilibrated to a minimum of -20°C, generating enough cooling power to compensate heating during mesh vibration.

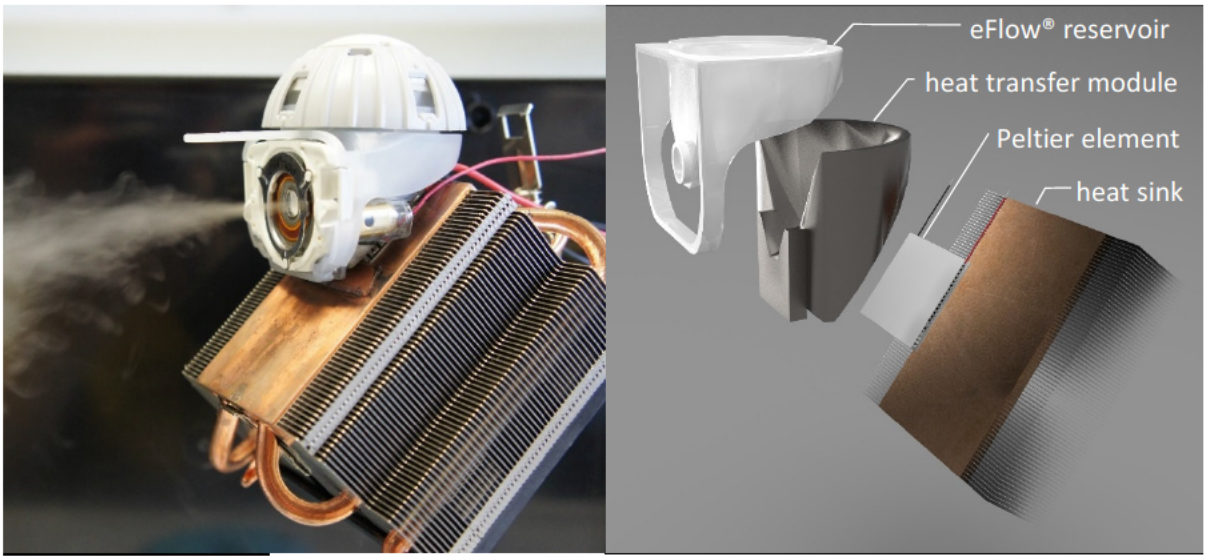

Figure III-3: Actively cooled nebulizer in operation (left). Exploded view of the Peltier cooler setup (right): eFlow® reservoir, custom molded metallic heat transfer module, Peltier element and heat sink.

2.4 Nebulizer Performance

Throughout this work, the characteristics of the generated aerosols have been analyzed. The performance of different nebulizers was compared (Chapter IV.2) and the influence of excipients, proteins and nebulization temperature (Chapter IV.4) on aerosol properties was evaluated. Therefore nebulizer performance was assessed as the aerosol droplet size distribution and the output rate.

2.4.1 Output rate

The output rate (OR) of a nebulizer was determined gravimetrically as evaporation was negligible [21]. Therefore, nebulizer weight was determined before and after nebulization and the nebulization time was recorded. OR was calculated according to Equation III-1.

$$output\ rate\ (OR) = \frac{m_{charged\ nebulizer} - m_{after\ nebulization}}{t_{nebulization}}$$ *Equation III-1*

2.4.2 Time resolved output rate

Time resolved output rate data was generated by operating a PARI eFlow® placed on an analytical balance (Mettler-Toledo GmbH, Gießen, Germany). The weight loss upon nebulization was recorded on a computer and plotted over nebulization time. The weight was also monitored before and after nebulization to assure a balanced setup. The output rate at any time point was calculated as the first derivative of the mass loss over time curve. ORIGIN v8.0 was used to generate the first derivative in a three step process. Initially the raw data was smoothed with a 5 point Savitzky-Golay filter. The first derivative was calculated and the data set smoothed with a percentile filter set to 50% percentile and a 25 point window.

2.4.3 Aerosol droplet size distribution

Aerosol droplet size distribution was determined via laser diffraction on a MasterSizer X (Malvern Instruments GmbH, Herrenberg, Germany) equipped with a 300 mm lens. Nebulizers were placed such that the aerosol passed the lens at a distance of 4 cm before being cleared by a vacuum suction system. Measurements were performed continuously every 3 seconds during the entire duration of nebulization. Results are either presented time-resolved by plotting the single values over nebulization time or as a mean value calculated from all single values of the entire duration of nebulization.

Aerosol size distribution was characterized as the volume median diameter (d[v,50] or VMD) and the geometric standard deviation (GSD). The respirable fraction (RF, also: fine particle fraction (FPF)) was calculated as the fraction of nebulized volume within 1.0-5.0 µm sized droplets.

For the MicroSprayer®, a modified setup was used since the atomization process lasted only few seconds not minutes as during nebulization. Time resolved data of up to 100 measurements were recorded in the internal buffer of the MasterSizer for each atomization. The duration of a single measurement was adjusted such that the entire atomization process was recorded in no more than 100 measurements. Therefore, the number of sweeps (1 sweep = 2 µs) was set in a range of 1-50 depending on the spray duration (sprayed volume and the applied actuation pressure).

2.4.4 Calculation of derived aerosol characteristics

Additional aerosol parameters derived from OR, RF and remaining protein activity were calculated as follows.

The inhalable aerosol rate (IAR) was calculated from OR and RF:

$$Inhalable\ aerosol\ rate\ (IAR) = OR * RF \qquad \textit{Equation III-2}$$

The fraction of protein aerosols which is both respirable and biologically active is indicated by the active respirable fraction (aRF), i.e. the product of RF and remaining protein activity:

$$Active\ respirable\ fraction\ (aRF) = RF * protein\ activity \qquad \textit{Equation III-3}$$

Finally, the rate at which active and respirable aerosol is generated can be calculated as the product of OR, RF and remaining activity the active inhalable aerosol rate (aIAR).

$$Active\ inhalable\ aerosol\ rate\ (aIAR) = OR * RF * ACT \qquad \textit{Equation III-4}$$

2.5 Aerosol Cloud Collection

In order to analyze protein stability after nebulization, generated aerosol clouds had to be re-collected. By default, re-collection of aerosols from VM nebulizers and the MicroSprayer® was achieved by condensation in 2 mL polypropylene (PP) caps (VWR International, Darmstadt, Germany), which were placed directly in front of the vibrating mesh or the MicroSprayer® tip. No more than 1 mL condensate was collected per cap to ensure enough space for aerosol droplet

formation. Larger aerosol quantities were collected in multiple caps and the fractions subsequently pooled prior to analysis. The amount of aerosol collected was determined by weighing the caps. In chapter IV.4, smaller fractions of 300-600 µL condensate were collected and not pooled but analyzed fraction-wise in order to monitor protein degradation over nebulization time.

Additional collection procedures for VM nebulizers were evaluated in chapter IV.3 regarding the impact on protein degradation and collection efficiency (Figure III-4). Collection efficiency was defined as the fraction of the initial reservoir charge recovered by the collection procedure and determined gravimetrically. If the collection procedure included dilution, solvent evaporation or washing steps (TSI and RC collection method), collection efficiency was calculated from the recovery of an inert marker. The use of SM101 itself was not feasible since SM101 concentration may also be altered by degradation. Instead, 1 µg/mL 5/6-carboxyfluorescein (CF) was added to the formulation to retrace the extent of dilution and solvent evaporation. The factor f(CF) was calculated as the CF amount recovered after sample collection divided by the initial CF amount and used to correct results of stability indicating assays for sample dilution or solvent evaporation.

$$f(CF) = \frac{CF_{recovered}}{CF_{initially\ charged}}$$ *Equation III-5*

2.5.1 Fluorescence (CF)

CF fluorescence was determined in a 96 well plate on a FLUOstar Omega (BMG LABTECH GmbH, Offenburg, Germany). The excitation filter was set to 485nm and emission was recorded at 520 nm. Calibration was performed with CF standards at 0.078, 0.156, 0.312, 0.625, 1.25 and 2.50 µg/mL.

2.5.2 Collection procedures

Collection in test tubes of different size

PP caps of 2 mL, 4 mL and 15 mL and 4 mL glass cuvettes (Nephla turbidity tube, Hach Lange, Düsseldorf, Germany) were used to collect aerosol clouds by placing the collectors directly in front of the vibrating mesh.

Collection inside the aerosol chamber

The aerosol chamber of a PARI eFlow® was used to collect its aerosol by simply exchanging the mouthpiece with a tightly sealing cap [22], so that the emitted aerosol condensed inside the aerosol chamber. Aerosol chambers of 27.4 mL (small) or 48 mL (large) were compared [23].

Collection in a twin-stage impinger (TSI)

A twin-stage glass impinger (TSI) was used for aerosol collection [11, 13, 24]. Air-flow through the impinger was set to 30 L/min. Depending on droplet size, the aerosol deposits in the placebo buffer filled first or second stage of the collector. The stages were filled with 7 mL or 30 mL placebo buffer respectively.

Collection in a reflux condenser (RC)

Inspired by the methods proposed by Ip et al. [25] and Steckel et al. [26], aerosol was collected in a modified reflux condenser. Aerosol was drawn through a water cooled RC by a vacuum at a flow rate of 15 L/min and condensed on the walls of the internal coil. Condensed liquid collected in a PP tube below the RC. After nebulization, the internal coil was flushed with 3 mL of placebo buffer and the washing fraction was collected separately.

Collection negative controls

In order to discriminate nebulizer induced protein degradation from collection artifacts, both nebulized and non-nebulized protein formulation were collected by the same methods and protein stability compared. For test tube and aerosol chamber collection protein solution was pipetted repeatedly along test tube walls for five minutes, to simulate surface related stress without nebulization. Additionally, the data for the different sized tubes were compared to evaluate the impact of collector surface on protein degradation. TSI induced protein degradation was controlled by the addition of 4 mL protein solution directly into the 30 mL placebo buffer of the second stage and applying an air-flow of 30 L/min for 5 minutes. Non-nebulized protein solution was drawn through the reflux condenser at an air-flow of 15 L/min. Approximately 0.5 mL protein solution were added to the RC per minute for a total of five minutes. The solution was collected in a PP tube and a 3mL wash fraction was collected separately.

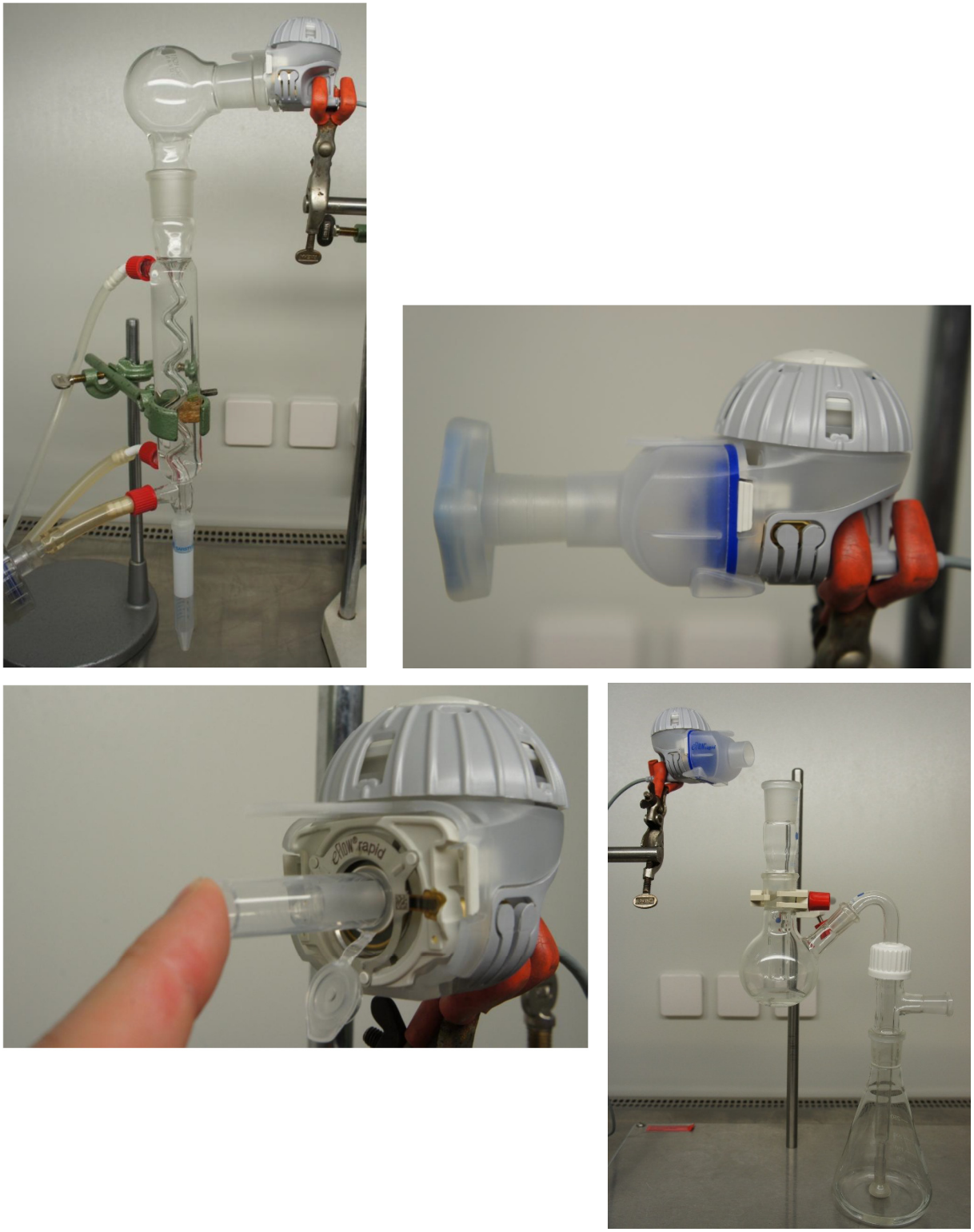

Figure III-4: Pictures of the evaluated aerosol collection methods, including collection in a reflux condenser (top left), in a buffer filled twin-stage impinger (bottom right), inside the aerosol chamber of the nebulizer (top right) or in test tubes (bottom left).

2.6 Formulation Development

2.6.1 Parenteral formulation development

1 mL of each SM101 formulation candidate was filled into 2R glass vials (FIOLAX 35.0 x 16.00 x 1.00 mm, klar HGB1/ISO719, Zscheile & Klinger, Hamburg, Germany) under a laminar air-flow and sealed with rubber stoppers (Ø=13mm, Chlorobutyl Typ11044/VII/703, Zscheile & Klinger, Hamburg, Germany) and an aluminum cap (Ø=13mm, Zscheile & Klinger, Hamburg, Germany).

Freeze/thaw (-20°C/+25°C)

Freeze/thaw stability was determined after 0, 1, 2, 4 and 6 cycles. Therefore, 2R vials were placed into a freezer at -20°C for at least 2h. Frozen samples were thawed under gentle agitation (150rpm) at room temperature. Respective placebo controls were handled accordingly, while non-frozen reference samples were stored at 2-8°C until analyzed.

Accelerated storage stability at 25°C and 40°C

Storage stability was assessed under accelerated stress conditions. Therefore, SM101 samples and respective placebos in 2R vials were stored at 25±0.5°C and analyzed after 0, 1, 7, 14 and 28 days, while samples stored at 40±1°C were analyzed at day 0, 1, 2 and 7.

2.6.2 Aerosol formulation development

Surrogate method (Agitation at elevated temperatures)

2.0 mL or 0.65 mL PP caps (VWR International, West Chester, Cat.# 20170-170 and Cat.# 20170-293) half-filled with 1.0 mL or 0.325 mL sample respectively were agitated at 1450 rpm on a shaker platform (Eppendorf Mixer 5432, Eppendorf AG, Hamburg, Germany), which was modified to hold caps horizontally. Shaking was performed inside an incubator. During method development (Chapter V.3 for SM101 and Chapter V.4 for LDH and G-CSF) shaking time ranged from 5 to 60 minutes while incubator temperatures were set to 25±1°C, 30±1°C, 35±1 or 40±1°C.

Settings used during surrogate based formulation development for SM101 were 10 minute agitation at 30°C. For G-CSF and LDH, agitation times were prolonged to 45 and 60 minutes

respectively. Additional experiments involving 60 minute agitation of SM101 and G-CSF at 30°C were performed.

Design of experiment for aerosol formulation candidate selection

Design and evaluation of the experiments for formulation optimization was done with Modde 9.0 software (Umetrics, Umeå, Sweden). A central-composite-face centered design (CCF) including four factors with three levels each (high, average, low) was used, giving a total of 27 runs a centered triplicate included. Investigated factors were SM101 concentration, sodium chloride concentration, total sugar content (fixed sucrose:mannitol ratio of 2:1 (w:w)) and polysorbate concentration. Turbidity after application of the surrogate method was the response parameter, whereby turbidity of equally treated placebo was subtracted as blank.

2.7 Protein stability

2.7.1 Size exclusion chromatography (SE-HPLC)

Size exclusion chromatography (SE-HPLC) was used to determine the extent of soluble protein aggregation and monitor changes in protein monomer content. Soluble protein aggregates and protein fragment content was calculated from respective peak area under the curve ratios. Deviations in protein monomer content were calculated dividing sample monomer peak area by monomer peak area of respective unstressed standards.

Protein samples were diluted to 2.0 mg/mL (Chapter V - SM101 formulation development) or 1.0 mg/mL protein (all other experiments) with respective formulation buffer. Samples with lower protein concentration were analyzed without prior dilution. After 5 minutes centrifugation at 18.000g, 100 µL of supernatant was injected onto a SE-HPLC column and eluted.

SM101

During parenteral formulation development for SM101 (Chapter V.2), SE-HPLC analytics were performed on an Agilent Series 1200 HPLC system by T. Pohl at SuppreMol. All consecutive SE-HPLC analyses were performed on a Merck Hitachi LaChrom 7000 HPLC system. Elution was monitored over a range of 200-400nm by a diode array detector to discriminate between proteinaceous and non-proteinaceous peaks. Calculations based on 280nm chromatogram data.

For separation, SM101 samples were injected onto a Superdex 75 300/10GL column (GE Healthcare Europe GmbH, Freiburg, Germany) and eluted with 20 mM histidine, 150 mM NaCl, pH 6.5 buffer at a flow rate of 0.5 mL/min. The column was calibrated with SM101 reference standard at 0.17, 0.39, 0.69, 1.39 and 2.8 mg/mL.

G-CSF

G-CSF samples were also separated with a Superdex 75 300/10GL column but 100 mM potassium phosphate buffer at pH 6.9 was used for elution at a flow rate of 0.5 mL/min.

LDH

LDH samples were injected onto a Superose 12 300/10GL column (GE Healthcare Europe GmbH, Freiburg, Germany) and eluted with 50 mM phosphate, 150 mM NaCl, pH 6.9 at 0.8 mL/min.

IgG

A Superose 12 column and 50 mM phosphate, 150 mM NaCl, pH 6.9 elution buffer were also used for the separation of monoclonal IgG samples at a flow rate of 0.8 mL/min.

OVA

OVA samples and mixtures of OVA and SM101 were separated on a Superose 12 column and eluted with a 50 mM phosphate, 150 mM NaCl, pH 6.9 buffer at a flow rate of 0.8 mL/min.

Anti-OVA IgG

Anti-OVA IgG and mixtures of anti-OVA IgG and SM101 were analyzed on a Dionex HPLC System (P680 pump, ASI100 autosampler, UVD170U UV/Vis detector, all Sunnyvale, CA, USA). For better results two Superose 12 columns were connected serially and samples eluted with 50 mM phosphate, 150 mM NaCl, pH 7.0 at a flow rate of 0.8 mL/min. On this HPLC system elution was monitored at 215 nm, 254 nm and 280 nm while calculations based on 280 nm chromatogram data.

2.7.2 Reverse phase chromatography (RP-HPLC)

Chemical degradation of SM101 was analyzed by reverse phase chromatography (RP-HPLC). Therefore, samples were run over a Knauer Eurosil Bioselect 300-5 C4 column attached to a Dionex HPLC system (see above, SE-HPLC of anti-OVA IgG). The column was equilibrated in

30% acetonitrile, 0.1% TFA. Samples were diluted to 1.0 mg/mL SM101 with respective placebo buffer and centrifuged at 18.000 g for 5 min. 35 µL of the supernatant was injected. Separation and elution followed an acetonitrile gradient (Table III-4) at a flow rate of 1.0 mL/min. The column was calibrated by the injection of 5, 15, 25, 35 and 50 µL SM101 reference standard at 1.0 mg/mL.

Table III-4: RP-HPLC gradient. Solvent A: water + 0.1% TFA, solvent B: acetonitrile + 0.09% TFA.

time	Solvent B
[min]	[%]
0	30
3	30
4	35
14	45
14.01	100
18	100
18.01	30
22	30

2.7.3 Cation exchange chromatography (CEX-HPLC)

SM101 deamidation was monitored by cation exchange chromatography on a Dionex ProPac WCX-10 column equilibrated in 10 mM MOPS, 20 mM NaCl, pH 6.9 attached to a Merck-Hitachi LaChrom 7000 HPLC system. Samples were diluted to 2 mg/mL with respective placebo buffer, then further diluted to 1 mg/mL with 10mM MOPS, pH 6.9 and finally centrifuged (18.000 g, 5 min). 20 µL of the supernatant were injected onto the column and separated by a sodium chloride gradient (Table III-5) at a flow rate of 1.0 mL/min.

Table III-5: CEX-HPLC gradient. Solvent A: 10 mM MOPS, pH 6.9; solvent B: 10 mM MOPS, 1000 mM NaCl, pH 6.9.

time	Solvent B
[min]	[%]
0	2
1	2
26	13
26.1	75
32	75
32.1	2
38	2

2.7.4 UV/Vis spectroscopy

UV/Vis spectra were recorded with a Nanodrop 2000 (PEQLAB Biotechnologie GmbH, Erlangen, Germany) from 4µL undiluted samples. The OD_{280} was corrected for scattering by subtraction of the baseline at 340 nm. Values were measured in triplicate and the protein concentration was calculated by division by the respective extinction coefficient of the protein as listed in Table III-6:

Table III-6: Extinction coefficients of the proteins used.

protein	extinction coefficient [$L \cdot g^{-1} \cdot cm^{-1}$]
SM101	1.5625
LDH	1.49
G-CSF	0.815
IgG1	1.415
OVA	0.70

2.7.5 Protein unfolding temperature (T_m) by µDSC

Protein unfolding temperature (T_m) was determined via differential scanning calorimetry on a VP-DSC (MicroCal Inc., MA, USA). Protein sample was measured at 1 mg/mL against respective placebo solution. Samples were heated from 20-90°C at a rate of 1 K/min. For baseline runs, both sample and reference cell were loaded with the reference sample solution. A baseline run was subtracted from sample data and T_m was calculated by Origin DSC data analysis software.

2.7.6 Protein aggregation temperature (T_{agg}) by UV/Vis spectroscopy

Analogously to T_m, T_{agg} is the temperature at which 50% of the protein is aggregated [27]. For T_{agg} measurements, the sample was heated from 25°C to 80°C at approximately 1 K/min in a cuvette sealed with a lid (UV-Cuvette micro, BRAND GmbH + CO KG, Wertheim, Germany) and the OD_{350} was recorded (Agilent 8453 UV-Visible Spectrophotometer, Agilent Technologies Deutschland GmbH, Böblingen, Germany). T_{agg} was determined as the peak of the first derivative curve of OD_{350} over temperature.

2.7.7 Light obscuration

Light obscuration performed on a PAMAS particle counter (PAMAS SVSS-C, PAMAS GmbH, Rutesheim) was used to determine subvisible particle counts in a range of 1 to 200 µm. After 0.5 mL rinsing volume, three consecutive measurements of 0.3 mL sample were performed. Results were averaged and normalized to particle count in 1 mL of sample. Prior to each measurement, the system was flushed with ultra clean water until less than a total of 100 particles per milliliter and no particle greater 10 µm were observed.

Samples were measured without dilution except during SM101 parenteral formulation development (Chapter V.2) and during investigation of SM101 and anti-OVA IgG stability to small volume VM nebulization (Chapter VI.3), where the measurements were performed after fivefold or 15-fold dilution with corresponding placebo buffer respectively to yield a total of 1500 µL. The subvisible particle count in the undiluted sample was calculated by the following equation:

Equation III-6

$$particle\ count_{undiluted\ sample} = \frac{V_{measured} * particle\ count_{measured} - V_{diluent} * particle\ count_{diluent}}{V_{sample}}$$

Particle count data was also used to estimate the mass of protein aggregated in subvisible particles. According to Barnard et al. [28], the average bin diameter was used to calculate the particle volume for each bin size assuming spherical particles. The density of protein particles was reported as 1.43 g/mL. Barnard assumed particles to contain 25% water and 75% protein, thus an additional factor is introduced into the equation. Bin particle count, bin volume and protein particle density are multiplied to give the particle mass in each size bin, which is integrated over the whole particle range to give the total mass of aggregates in the sample.

Equation III-7

$$Total\ aggregate\ protein\ mass = \int 0.75 * 1.43 \left[\frac{g}{mL}\right] * bin\ volume\ [mL] * bin\ particle\ count$$

2.7.8 Turbidity

Sample turbidity was determined as the optical density at 350nm (OD_{350}), where no chromophore in the used formulations absorbs and apparent absorbance can be attributed to scattering effects of suspended insoluble protein aggregates [29, 30]. For anti-OVA IgG in rabbit whole serum, turbidity was determined at 500 nm instead, where absorbance of the serum was reduced. Measurements were carried out with undiluted sample in a 96 well quartz microplate (Hellma GmbH & Co KG, Mühlheim) on a microplate reader (FLUOstar Omega, BMG LABTECH GmbH, Offenburg) with 300 µL sample volume. OD_{350} of a single well was determined as the mean of three scans and the OD_{350} of ultraclean water or respective placebo buffers was subtracted as blank measurement.

Turbidity determination by attenuation (OD_{350}) was compared to nephelometric turbidity measurements (NEPHLA, Dr. Bruno Lange GmbH & Co. KG, Düsseldorf) (Figure III-5). Turbidity data of both methods was linearly correlated for a dilution series of aggregated SM101 (R^2=0.9936), as well as for a dilution series of formazine standard (VWR International) (R^2=0.9972). The conversion factors to calculate FNU from OD350 were 0.245 and 0.255 for SM101 and formazine respectively.

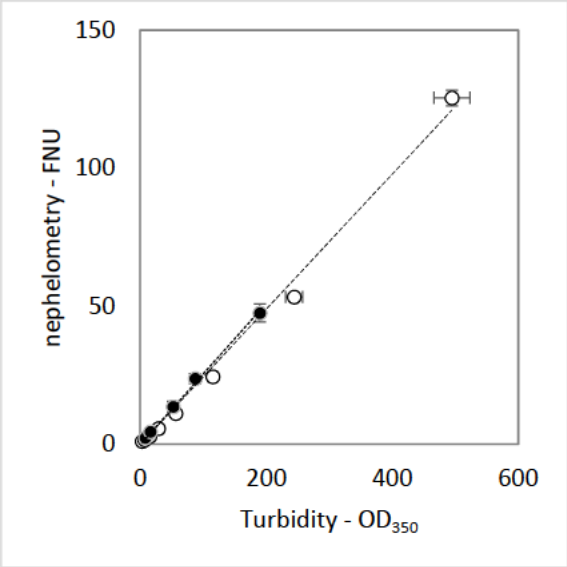

Figure III-5: Turbidity data determined by OD_{350} linearly correlates to nephelometric measurements for dilution series of a formazine standard (filled symbols, R^2=0.9972) according to Ph. Eur. and for a dilution series of aggregated SM101 (empty symbols, R^2=0.9936), n=3 (mean ± SD).

2.7.9 Visual inspection

Visual inspection was performed in front of a white and black background under diffuse and direct illumination as outlined in European Pharmacopoeia method 2.9.20. Samples were classified according to Deutscher Arzneimittelkodex (DAC 2006). Categories are 0: no visible particles; 1: hardly visible particles within 5 seconds of inspection; 2: clearly visible particles within 5 seconds of inspection; 10: instantly visible large numbers of particles.

2.7.10 OVA gel weight determination

To quantify the extent of OVA gelation, formed gels were collected from container walls and transferred into fresh 1.5 mL PP reaction caps. Samples were than centrifuged for 5 minutes at 18.000 g and the supernatant discarded. The gel pellets were transferred to small aluminum cups and dried for 1h at 80°C. Dried pellet weight was determined on a microbalance (Mettler Toledo, Gießen, Germany).

2.8 Protein activity

SM101 activity determination was performed by Thomas Pohl at the SuppreMol Laboratories in Martinsried, Germany.

2.8.1 SM101 FACS potency assay

The activity of SM101 after nebulization was measured using a FACS based cellular assay according to SuppreMol's internal protocol. Raji cells (DSMZ # ACC319, human Burkitt Lymphoma) were incubated with a constant amount of aggregated human IgG (ligands for FcγRIIB) and varying amounts of SM101 (sFcγRIIB). In this setting, the soluble FcγRIIB-receptor SM101 competes with the cell-bound FcγRIIB receptor, being the sole Fcγ receptor expressed on Raji cells, for binding to human aggregated IgG. Cell-bound aggregated IgGs can subsequently be detected by means of fluorescence labeled polyclonal secondary antibody binding to the heavy and light chain of human IgG. By applying varying amounts of SM101 to a set amount of cells and aggregated IgG a progressive inhibition of IgG binding to membrane-bound FcγRIIB (being a function of SM101 concentration) can be determined. Parallel control samples

with unstained cells and cells incubated with secondary antibody only are used to determine the auto-fluorescence of the cells as well as unspecific binding of secondary antibody. FACS-analysis was carried out by recording 1x104 gated viable cells on a BD-FACS-Canto-II using BD FACS-Diva software (BD Biosciences, San Jose, CA, USA). Data was subsequently evaluated using FlowJo Software (Treestar Inc., OR, USA). For calculation of the IC50 the logistic function (Origin 6.0, Microcal, Northampton, MA, USA) was fitted to the raw data. For calculations, the SM101 concentration was determined by UV/Vis spectroscopy.

2.8.2 LDH activity assay

LDH enzymatic activity assay was adapted from the method described by Niven et al. [14] to work with a microplate reader. Wells were preloaded with 50 µL of diluted LDH sample. 250 µL of freshly prepared pyruvate-β-NADH mixture was added and measurement started immediately, monitoring the decrease of absorption at 340 nm for at least 60 s. Sample dilution and pyruvate-β-NADH mixture were done with 1% BSA solution to prevent LDH adsorption to surfaces. Each set of simultaneous measurements contained one well 1% BSA as blank and a LDH reference standard. LDH activity was calculated from the linear segment of the slope of absorption decrease. Remaining LDH activity was calculated as the fraction of activity after nebulization or agitation compared to simultaneously determined activity of non-stressed (non-nebulized and non-agitated) LDH standard.

2.8.3 ELISA

The OVA binding activity of anti-OVA IgG was determined by an ELISA kit (Mybiosource, San Diego, CA, USA) in 96 well format according to the instructions. A standard calibration curve was recorded with 0.0, 0.5, 1.0, 2.5, 5.0 and 10.0 mg/mL anti-OVA IgG with every measurement.

2.9 Other *in vitro* analytics

2.9.1 pH

Sample pH was determined with a Mettler Toledo Inlab Micro pH electrode in 100µL sample solution.

2.9.2 Osmolality measurements

Formulation osmolality was determined on an automatic semi-micro cryo-osmometer (Knauer, Berlin, Germany) with 200 µL of sample. Before each measurement, the device was calibrated against standard solutions of 0 mOsm/kg (highly purified water) and 400 mOsm/kg (217 mM NaCl) real osmolality, which corresponds to 434 mOsm/kg ideal osmolality.

2.9.3 Viscosity

Viscosity of placebo and protein formulations was determined with a cone plate rheometer (Anton Paar, Graz, Austria) at 25°C. A fixed shear rate of 100 s^{-1} was used.

2.9.4 Surface tension

Surface tension of placebo and protein formulations was determined with an automatic Wilhelmy plate tensiometer (Krüss K100, Hamburg, Germany). The plate and the sample cup were thoroughly cleaned prior to each measurement. The surface tension of de-ionized water was determined at least once a day as a reference.

2.9.5 Microscopy / Coomassie staining

Coomassie staining was used to determine if material deposited on the vibrating mesh was of proteinaceous nature. The meshes were covered with premixed coomassie staining solution (Serva Electrophoresis GmbH, Heidelberg, Germany) and incubated for 60 minutes on a laboratory shaker. The meshes were then rinsed with ultraclean water and agitated in ultraclean water overnight. Stained and unstained nebulizer membranes were observed under a digital microscope (Keyence, Neu-Isenburg, Germany) at a range of 100 fold to 1000 fold magnification.

2.10 Statistical evaluation of results

Significance levels of the results were calculated by one-way Analysis of variance (ANOVA) including post-hoc testing by Tukey to calculate individual p-values. The symbols and significance levels displayed are listed in Table III-7.

Table III-7: Significance levels and symbols to indicate them throughout this study.

Symbol	Meaning
ns	$P > 0.05$
*	$P \leq 0.05$
**	$P \leq 0.01$
***	$P \leq 0.001$

2.11 *In vivo* animal study

All *in vivo* experiments were performed by Otmar Schmid and his group at the Comprehensive Center of Pulmonology (Neuherberg, Germany). Lung deposition and distribution investigation described in Chapter VI.2.3 are part of the master thesis of Juliane Freitag [31].

2.11.1 *In vivo* pulmonary application methods

Administration of aerosols or solutions into the lungs of mice was achieved by either oro-tracheal instillation (o.t.), intubated MicroSprayer® aerosolization or vented intubated inhalation with an Aeroneb® Pro nebulizer. Prior to aerosol/solution application, mice were anaesthetized.

Oro-tracheal instillation

Mice were fixed onto a plane tilted by 45° and intubated by a non-surgical technique. An intubation tube was introduced through the mouth into the trachea and positioned right before the carina. With a 1 mL syringe inserted through the intubation tube, 50 µL solution and a 200 µL air bolus were instilled as the animal inhaled [32]. The actually applied volume was determined gravimetrically by weighing the cannula and syringe before and after administration.

MicroSprayer®

Anaesthetized mice were intubated and the MicroSprayer® aerosolizer tip was inserted through the intubation tube. 50 µL solution were sprayed into the lung by pneumatic actuation at a pressure of 2.2 bar. During a study comparing lung deposition and distribution in one group of mice pneumatic MicroSprayer® actuation was performed at a pressure of 4.0 bar instead.

Intubated vented inhalation with a vibrating mesh nebulizer

Anaesthetized mice were attached to a respirator working with volume controlled overpressure, allowing for spontaneous exhalation. Ventilation frequency was set to 120/min at an air volume

of 0.4 mL. An Aeroneb® Pro VM nebulizer operating in an intermittent mode adjusted to the respirator was connected to the ventilation circuit via a T-piece. Ventilation of the mice was performed until the loaded solution was completely nebulized.

Further procedure

Immediately after the administration procedure, the intubation tube was removed and the mice were sacrificed by exsanguination. Lung and trachea were excised for analysis and the rest of the animal was discarded.

2.11.2 *In vivo* study of pulmonary application methods for small animals

C57BL/6 mice (age 8-14 weeks, all female, weight 18-27 g) were sorted into seven groups according to the application method used to delivery fluorescently labelled SM101 to the lung. A 1 mg/mL stock of SM101 covalently bound to the fluorophore Alexa Fluor® 750 (provided by SuppreMol GmbH) was diluted 1:20 or 1:40 for pulmonary administration. The application method, administered volume and the number of mice per group are listed in Table III-8. For intubated ventilated inhalation, a larger volume was applied to compensate for the expected lower deposition efficiency of this procedure.

Table III-8: Animal groups by pulmonary application method.

group	volume [µL]	animals
placebo instillation	50	4
instillation, undiluted	50	4
instillation, 1:2 dilution	50	3
MicroSprayer® 2.0 bar	50	4
MicroSprayer® 4.4 bar	50	4
intubated ventilated inhalation (Aeroneb® Pro)	100	4

Mice were kept in isolated, ventilated cages (IVC-Racks; BioZone, Margate, UK) supplied with filtered air in a 12-hr light/12-hr dark cycle (lights on from 06:00-18:00). Food (standard chow) and water were available ad libitum. All procedures for animal handling and experiments were performed in accordance with protocols approved by the Regierung von Oberbayern (District Government of Upper Bavaria).

The excised lungs were separated into the trachea and the five lobes and analyzed regarding deposition and distribution of the fluorescent dye by IVIS imaging and by fluorescence spectroscopy of the homogenized lung.

Lung imaging by IVIS

The freshly excised lobes and the trachea were placed on a microscope slide, which was placed into the imaging chamber and aligned to the field of view of the *in vivo* imaging system (IVIS Lumina, Xenogen Corporation, CA, USA). An excitation wavelength of 745 nm and an emission range of 810-875 nm were used for Alexa Fluor® 750. The outline of the lobes as seen in the white light images were used to mark the region of interest (ROI) for calculation of the fluorescence signal of the single lobes and the entire lung.

Lung homogenate

After IVIS imaging, the lung tissue was stored at -20°C for several days until preparation of lung homogenates according to an optimized protocol based on MacLoughlin et al. [33]. Lung lobes were thawed and the mass was determined gravimetrically. Each lobe was homogenized separately. Therefore, 300 µL minus the lobe weight of a formamide-water (1:3) mixture was added and the sample was then homogenized with an ultra-turrax homogenizer at level 5-6 (IKA T 10 basic, IKA®-Werke GmbH & CO. KG, Staufen, Germany) for 3 minutes at room temperature. The homogenizer was rinsed with the solvent mixture and the wash collected and pooled with the sample. As a reference 50µL fluorescent dye were added to a pristine lung that was treated alike. The homogenized samples were incubated at 60°C for 14-18 h while shaking at 300 rpm. Finally, the lysed samples were vortexed. Sample fluorescence was determined with a Tecan Safire 2 plate reader (Tecan Group Ltd., Männedorf, Switzerland). Therefore, 50 µL aliquots of each sample were loaded into 4 wells of a black, flat bottom 96 well plate. Formamide-water (1:3) mixture served as a blank and a standard calibration series was recorded with every well plate measured. An excitation wavelength of 745 nm and an emission range of 765-799 nm was used for Alexa Fluor® 750 and Alexa Fluor® 750 conjugated SM101. The measured fluorescence intensity was corrected for dilution with formamide-water during homogenization by the factor $f_{dilution}$ (Equation III-8) and extrapolated to the intensity of the entire lobe (I_{lobe}) (Equation III-9).

$$f_{dilution} = \frac{m_{lobe} + V_{solvent}}{m_{lobe}}$$ *Equation III-8*

$$I_{lobe} = I_{measured} * f_{dilution} * \left(\frac{m_{lobe}}{V_{measured}}\right) = I_{measured} * \frac{m_{lobe} + V_{solvent}}{V_{measured}}$$ *Equation III-9*

Fluorescence intensity of an entire lung (I_{lung}) was calculated by addition of the intensities of all five lobes and the trachea. The relative deposition efficiency for the application method was calculated as a percentage of the intensity of the reference lung ($I_{reference}$) (Equation III-10). Sample homogenization and measurement was not completed in a single day. The fluorescence yield of SM101 bound Alexa Fluor® 750 declined during storage, so that the reference values determined on the first day were not applicable to later day samples. Therefore, fluorescence data of the instilled lungs/lobes homogenized on each day served as the 100% reference value for all other application methods.

$$relative\ deposition\ efficiency\ [\%] = \frac{I_{lung}}{I_{reference}}$$ *Equation III-10*

To determine the amount of dye deposited in each lobe, the intensity of 1 µL dye (I_{dye}) was calculated from the reference sample.

$$Intensity\ of\ 1\ \mu L\ dye\ (I_{dye}) = \frac{I_{reference}}{V_{reference}}$$ *Equation III-11*

The dye volume (V_{dye}) deposited in each lobe was then calculated by Equation III-12.

$$dye\ volume\ per\ lobe\ (V_{dye})[\mu L] = \frac{I_{lobe}}{I_{dye}}$$ *Equation III-12*

Finally, the amount of dye deposited in a lobe was normalized for relative lung mass (Equation III-13).

$$V_{normalized} = \frac{V_{dye}}{\%\ lung\ mass} = \frac{V_{dye}}{\frac{m_{lobe}}{m_{lung}} * 100}$$ *Equation III-13*

Aerosol distribution was judged by inter-lobe variability, which was calculated as the standard deviation of $V_{normalized}$ between all five lobes of a lung.

2.11.3 *In vivo* study of SM101 efficacy

In a preliminary experiment, C57BL/6 mice (age 8-14 weeks, all female, weight 18-27 g) received a reverse or a non-reverse protocol to induce a pulmonary Arthus reaction (Table III-9). The reverse protocol included the o.t. instillation of 150 µg anti-OVA IgG followed by the i.v. administration of 20 mg/kg OVA antigen. For induction of the non-reverse Arthus reaction 420 µg anti-OVA IgG (100 µL) were i.v. injected followed by o.t. instillation of 40 µg OVA antigen (50 µL). Mice in the home cage control group did not receive any agents but otherwise underlay identical conditions. Bronchoalveolar lavage (BAL) was performed after 6 h and after 24 h for all animal groups.

Table III-9: Animal groups for the preliminary experiment.

#	n	Group Name	1st application (anti-OVA IgG)	2nd application (OVA Ag)
1	3	Home Cage Control	-	-
2	4	reverse protocol	150 µg o.t.	20 mg/kg i.v.
3	4	non-reverse protocol	420 µg i.v.	40 µg o.t.

In the first inhalation experiment, C57BL/6 mice (age 8-14 weeks, all female, weight 18-27 g) received the protocol for induction of a non-reverse pulmonary Arthus reaction as described above. The animals were divided into 5 groups receiving treatment or different control treatments as listed in Table III-10. With a third application, mice received either placebo or a 100 µg dose of SM101 by vented intubated inhalation.

Repetition of the inhalation experiment was carried out under the same conditions and protocols. One animal group was added, receiving the 100 µg SM101 dose via o.t. instillation instead of nebulization as the third application (Table III-11).

Table III-10: Animal groups for the first inhalation experiment.

#	n	Group Name	1st application (i.v.) anti-OVA IgG (100µl)	2nd application (o.t.) OVA-Antigen (50µl)	3rd application (nebulization) (100µl)
1	3	Home Cage Control	-	-	-
2	4	OVA Control	-	40µg	Placebo
3	5	Lung Control	-	40µg	SM101 (100µg)
4	5	Positive Control	420µg	40µg	Placebo
5	5	Treatment	420µg	40µg	SM101 (100µg)

Table III-11: Animal groups for the second inhalation experiment.

#	n	Group Name	1st application (i.v.) anti-OVA IgG (100µl)	2nd application (o.t.) OVA-Antigen (50µl)	3rd application (nebulization) (100µl)
1	4	Home Cage Control	-	-	-
2	5	OVA Control	-	40µg	Placebo
3	5	Lung Control	-	40µg	SM101 (100µg)
4	5	Positive Control	420µg	40µg	Placebo
5	5	Treatment	420µg	40µg	SM101 (100µg)
6	5	Treatment	420µg	40µg	SM101 (100µg) (i.t.)

Bronchoalveolar lavage and total and differential cell counts

24 h after induction of the Arthus reaction, mice were sacrificed by an overdose of ketamine/xylazine followed by exsanguination. The trachea was cannulated, BAL was performed with PBS (4*0.5 mL) and the collected volume of bronchoalveolar lavage fluid (BALF) was determined for each sample. Total cell counts were determined in a hemocytometer (Neubauer Zählkammer), whereas the erythrocyte count (RBC=red blood cells) were accounted for hemorrhage. Differential cell counts were performed on May Grünwald Giemsa stained cytospins (10 min at 400 g) to quantify the inflammatory recruitment of neutrophils, macrophages and lymphocytes.

3 References

[1] P. Sondermann, R. Huber, U. Jacob, Crystal structure of the soluble form of the human Fcg-receptor IIb: a new member of the immunoglobulin superfamily at 1.7 Å resolution, EMBO J, 18 (1999) 1095-1103.

[2] P. Sondermann, R. Huber, V. Oosthuizen, U. Jacob, The 3.2-AÊ crystal structure of the human IgG1 Fc fragment±FcgRIII complex, Nature, 406 (2000) 267-273.

[3] T. Takai, Roles of Fc receptors in autoimmunity, Nat Rev Immunol, 2 (2002) 580-592.

[4] SuppreMol, SuppreMol Pipeline, SuppreMol GmbH, http://www.suppremol.com/pipeline.html. Retrieved 15.09.2013 from http://www.suppremol.com/pipeline.html.

[5] N. Casadevall, J. Nataf, B. Viron, A. Kolta, J.-J. Kiladjian, P. Martin-Dupont, P. Michaud, T. Papo, V. Ugo, I. Teyssandier, B. Varet, P. Mayeux, Pure Red-Cell Aplasia and Antierythropoietin Antibodies in Patients Treated with Recombinant Erythropoietin, New England Journal of Medicine, 346 (2002) 469-475.

[6] A. Kromminga, H. Schellekens, Antibodies against Erythropoietin and Other Protein-Based Therapeutics: An Overview, Annals of the New York Academy of Sciences, 1050 (2005) 257-265.

[7] H. Schellekens, W. Jiskoot, Erythropoietin-Associated PRCA: Still an Unsolved Mystery, Journal of Immunotoxicology, 3 (2006) 123-130.

[8] T.S. Konstaninova, I.V. Leonidovna, A. Hellmann, S. Kyrcz-Krzemien, S. Tillmanns, P. Sondermann, P. Buckel, Interim Results From a Phase Ib/IIa Clinical Trial with the Soluble Fc-Gamma IIb Receptor SM101 for the Treatment of Primary Immune Thrombocytopenia, in: A.S.o.H. (ASH) (Ed.) 2012 ASH Annual Meeting and Exposition, Atlanta, GA, 2012.

[9] K. Schersch, O. Betz, P. Garidel, S. Muehlau, S. Bassarab, G. Winter, Systematic investigation of the effect of lyophilizate collapse on pharmaceutically relevant proteins, part 2: Stability during storage at elevated temperatures, J Pharm Sci, 101 (2012) 2288-2306.

[10] M. Adler, G. Lee, Stability and surface activity of lactate dehydrogenase in spray-dried trehalose, J Pharm Sci, 88 (1999) 199-208.

[11] Y.Y. Albasarah, S. Somavarapu, K.M.G. Taylor, Stabilizing protein formulations during air-jet nebulization, International Journal of Pharmaceutics, 402 (2010) 140-145.

[12] B.S. Chang, B.S. Kendrick, J.F. Carpenter, Surface-induced denaturation of proteins during freezing and its inhibition by surfactants, J Pharm Sci, 85 (1996) 1325-1330.

[13] L. Khatri, K.M.G. Taylor, D.Q.M. Craig, K. Palin, An assessment of jet and ultrasonic nebulisers for the delivery of lactate dehydrogenase solutions, International Journal of Pharmaceutics, 227 (2001) 121-131.

[14] R.W. Niven, A.Y. Ip, S.D. Mittelman, C. Farrar, T. Arakawa, S.J. Prestrelski, Protein nebulization: I. Stability of lactate dehydrogenase and recombinant granulocyte-colony stimulating factor to air-jet nebulization, International Journal of Pharmaceutics, 109 (1994) 17-26.

[15] R. Niven, K.L. Whitcomb, L. Shaner, A. Ip, O. Kinstler, The Pulmonary Absorption of Aerosolized and Intratracheally Instilled rhG-CSF and monoPEGylated rhG-CSF, Pharmaceutical Research, 12 (1995) 1343-1349.

[16] R.W. Niven, S.J. Prestrelski, M.J. Treuheit, A.Y. Ip, T. Arakawa, Protein nebulization II. Stabilization of G-CSF to air-jet nebulization and the role of protectants, International Journal of Pharmaceutics, 127 (1996) 191-201.

[17] C. Mück (2002): Analytik von Proteinaggregation mittels Coulter-Prinzip: Vergleich mit der Lichtblockade-Messung. Diploma Thesis, Ludwig Maximilian University Munich / University of Applied Sciences Albstadt-Sigmaringen, Germany.: Department of Pharmacy.

[18] K. Hellerbrand, A. Papadimitriou, G. Winter, Process for stabilizing proteins, US 6,238,664 B1, issued May 29, 2001.

[19] J. Skokowa, S.R. Ali, O. Felda, V. Kumar, S. Konrad, N. Shushakova, R.E. Schmidt, R.P. Piekorz, B. Nurnberg, K. Spicher, L. Birnbaumer, J. Zwirner, J.W.C. Claassens, J.S. Verbeek, N. van Rooijen, J. Kohl, J.E. Gessner, Macrophages Induce the Inflammatory Response in the Pulmonary Arthus Reaction through Gαi2 Activation That Controls C5aR and Fc Receptor Cooperation, J Immunol, 174 (2005) 3041-3050.

[20] J.S. Lass, A. Sant, M. Knoch, New advances in aerosolised drug delivery: vibrating membrane nebuliser technology, Expert Opinion on Drug Delivery, 3 (2006) 693-702.

[21] R. Tandon, M. McPeck, G.C. Smaldone, Measuring Nebulizer Output Aerosol Production vs Gravimetric Analysis, CHEST Journal, 111 (1997) 1361-1365.

[22] T. Scherer, D.E. Geller, L. Owyang, M. Tservistas, M. Keller, N. Boden, K.C. Kesser, S.J. Shire, A technical feasibility study of dornase alfa delivery with eflow® vibrating membrane nebulizers: Aerosol characteristics and physicochemical stability, J Pharm Sci, 100 (2011) 98-109.

[23] M. Keller, Paediatric Inhaled Products An Unmet Challenge for the Industry, in, http://www.paripharma.com/studies/posters_publications.html, 2006.

[24] A.M.A. Elhissi, M. Faizi, W.F. Naji, H.S. Gill, K.M.G. Taylor, Physical stability and aerosol properties of liposomes delivered using an air-jet nebulizer and a novel micropump

device with large mesh apertures, International Journal of Pharmaceutics, 334 (2007) 62-70.

[25] A.Y. Ip, T. Arakawa, H. Silvers, C.M. Ransone, R.W. Niven, Stability of recombinant consensus interferon to air-jet and ultrasonic nebulization, J Pharm Sci, 84 (1995) 1210-1214.

[26] H. Steckel, F. Eskandar, K. Witthohn, The effect of formulation variables on the stability of nebulized aviscumine, International Journal of Pharmaceutics, 257 (2003) 181-194.

[27] G.A. Senisterra, J.P.J. Finerty, High throughput methods of assessing protein stability and aggregation, Molecular BioSystems, 5 (2009) 217-223.

[28] J.G. Barnard, S. Singh, T.W. Randolph, J.F. Carpenter, Subvisible particle counting provides a sensitive method of detecting and quantifying aggregation of monoclonal antibody caused by freeze-thawing: Insights into the roles of particles in the protein aggregation pathway, J Pharm Sci, 100 (2011) 492-503.

[29] B.M. Eckhardt, J.Q. Oeswein, D.A. Yeung, T.D. Milby, T.A. Bewley, A Turbidimetric Method to Determine Visual Appearance of Protein Solutions, PDA Journal of Pharmaceutical Science and Technology, 48 (1994) 64-70.

[30] H.-C. Mahler, R. Müller, W. Frie, A. Delille, S. Matheus, Induction and analysis of aggregates in a liquid IgG1-antibody formulation, European Journal of Pharmaceutics and Biopharmaceutics, 59 (2005) 407-417.

[31] J. Freitag (2012): Quantitative Bestimmung von fluoreszenz-gekoppelten Nanopartikeln und Proteinen in biologischen Materialien. Master Thesis, Universität Rostock: UMR/ZIM, Klinik I, Abt. Pneumologie.

[32] K. Ganguly, S. Upadhyay, M. Irmler, S. Takenaka, K. Pukelsheim, J. Beckers, E. Hamelmann, H. Schulz, T. Stoeger, Pathway focused protein profiling indicates differential function for IL-1B, -18 and VEGF during initiation and resolution of lung inflammation evoked by carbon nanoparticle exposure in mice, Particle and Fibre Toxicology, 6 (2009) 1-14.

[33] R.J. MacLoughlin, B.D. Higgins, J.G. Laffey, T. O'Brien, Optimized Aerosol Delivery to a Mechanically Ventilated Rodent, Journal of Aerosol Medicine and Pulmonary Drug Delivery, 22 (2009) 323-332.

Chapter IV Characterization of vibrating mesh nebulization

1 Introduction

The initial decision to develop a liquid formulation for the pulmonary delivery of SM101 instead of a dry powder aerosol entailed the application of vibrating mesh (VM) nebulization for the aerosol generation. VM nebulizers, although originally not designed for proteins, have been reported to be promising for protein nebulization for their gentle aerosol generation, efficient delivery and improved usability. As explained in the introduction, successful protein nebulization relies on a suitable combination of the aerosol generating device and the protein formulation. This chapter will approach the objective to evaluate the feasibility of VM nebulization for pulmonary protein delivery from the device's side. Aiming to prepare for efficient protein delivery, VM nebulization was investigated and aspects relevant for protein stability or aerosol performance were identified and characterized.

The circumstance that the nebulized solution can influence the aerosol characteristics, depending on its physicochemical properties like viscosity or surface tension, has been reported for VM nebulizers. Resulting consequences however have only been demonstrated for model excipients that are of low relevance for protein formulation like silicon oils, glycerol or alcohol [1]. The influence of excipients commonly used for protein formulation on nebulizer performance of three different VM nebulizers was investigated. The device capable of the most efficient pulmonary delivery was selected, based on comparison under these relevant conditions. Furthermore, the effect of proteins aggregation on vibrating mesh functioning was evaluated.

On the other hand, the impact of VM nebulization on proteins was investigated. To gain a better understanding of how VM nebulization affects protein stability, potential stress factors were identified and characterized. On this basis, procedures to mitigate these stress factors were developed in order to enable advantageous VM nebulization for sensitive proteins.

An important prerequisite for the evaluation of protein stability after nebulization is a procedure to re-condense the generated aerosol cloud back into a bulk liquid, so standard stability and activity analytics may be applied. Different procedures have been mentioned for aerosol collection but not all suggested methods may be appropriate for atomized proteins. Therefore, collection procedures were evaluated regarding the impact on protein stability, collection efficiency and ease of handling with the aim to select a suitable method for subsequent use.

2 Impact of the formulation on vibrating mesh nebulization

2.1 Introduction

Three vibrating mesh nebulizers, which were available as retail including PARI's eFlow® rapid, the Aeroneb® Go (Aerogen) and OMRON's MicroAIR were compared regarding their aerosol performance. Taking into account that the nebulized solution influences these characteristics [1], the effects on nebulizer performance were evaluated for two model excipients commonly employed in protein formulation and for two model proteins. Sucrose served as an example of a viscosity enhancing excipient, which like other sugars or polyols is used to improve protein storage stability [2]. Polysorbate 20 (PS20) on the other hand, represented the class of nonionic surfactants often added to protect proteins from interfacial stress by surface exclusion, which is concomitant with a reduction in surface tension [3]. G-CSF served as a surface-active model protein and an IgG1 antibody was used to manipulate formulation viscosity. Based on the results for nebulizer performance under relevant conditions, the most suitable nebulizer was selected for further application.

During preliminary experiments, prolonged nebulization times were observed when some protein solutions were nebulized. Prolongation exceeded a dimension that could be explained by changes in physicochemical properties alone, according to literature [1, 4]. Instead, another mechanism is suggested. Insufficient stabilization led to protein degradation during nebulization. Subsequently, insoluble protein aggregates occluded some of the micron sized holes of the vibrating mesh. Obstruction and constriction of the mesh would explain distinct reduction of the output rate (OR) and may also affect other aerosol properties like droplet size distribution. To investigate

this hypothesis, a model was used that allowed the adjustment of protein stability, while maintaining equal physicochemical properties. Therefore narrow pH changes were used to control protein stability to nebulization. The formulation remained basically unchanged, so that an impact on nebulizer performance could be attributed to protein stability, while formulation properties could be ruled out. G-CSF is an ideal model due to its very pH sensitive stability. In acidic environment of pH 4.0 or below G-CSF remains stable, whereas above pH 4.5 significant G-CSF degradation was observed after interfacial stress [5, 6].

Nebulizer performance was judged by the size distribution of the generated aerosol droplets and the OR. The OR is a measure of the speed of nebulization. A higher OR results in a shorter treatment time, which is desirable since prolonged treatment times may have negative impacts on life quality of chronically ill patients and are associated with reduced compliance [7, 8]. The aerosol droplet size distribution was determined by laser diffraction, which delivers results that are in good agreement to cascade impactor determined values for aqueous aerosols of unit density [9]. Droplet size is represented by the volume median diameter (VMD, also d[v,50]), which under these conditions concurs with the mass median aerodynamic diameter (MMAD) [10]. The width of the distribution is reported as the geometric standard deviation (GSD) or the relative span.

$$GSD = \sqrt{\frac{d(v,84)}{d(v,16)}}$$ *Equation IV-1*

$$Span = \frac{d(v,90) - d(v,10)}{d(v,50)}$$ *Equation IV-2*

The aerosol droplet size distribution affects the fine particle fraction (FPF) of nebulized volume within droplets of 1-5 µm diameter. It is considered as a simplistic *in vitro* measure of the respirable fraction of the aerosol [11]. A promising nebulizer would generate aerosols of large respirable fractions at a high OR.

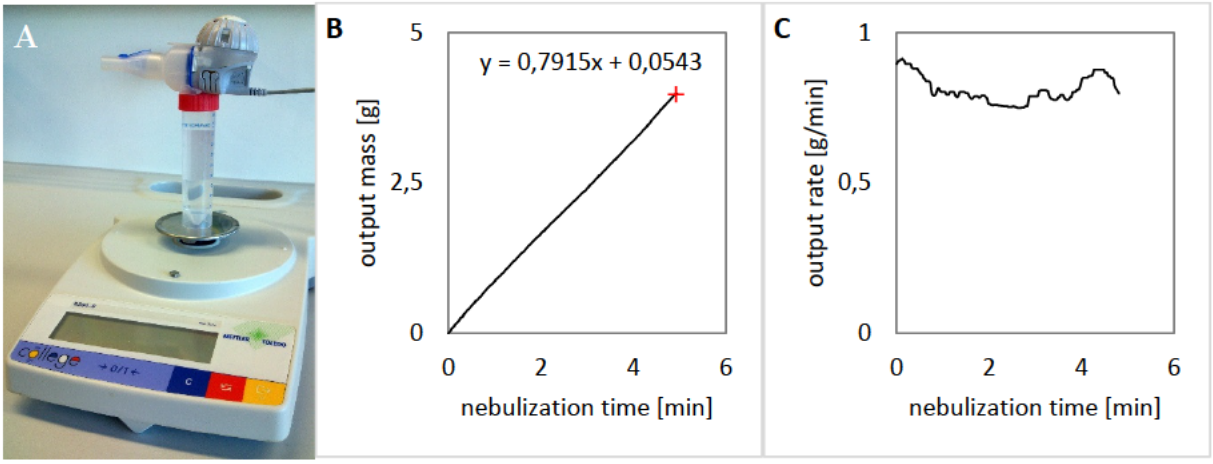

Figure IV-1: Picture of the setup for time resolved OR data generation (A) and the nebulized mass over nebulization time plot (B) recorded for 4 mL of 100 mM acetate buffer pH 4.0. Data for total output rate calculation is marked with (red cross; OR=0.809). The first derivative of this plot (C) reveals the OR at any given time point (average OR=0.810).

Aiming to gather more detailed data of the influence of excipients, aerosol characteristics were also monitored in a time resolved manner. While time resolved aerosol size distribution data was easily generated with laser diffraction, a method for time resolved OR data had to be developed. Therefore, a commonly employed gravimetric method for OR determination was modified. Instead of weighing the nebulizer only before and after operation and calculating the total OR as the quotient of output mass and nebulization time, the nebulizer was actually weighted constantly during operation and the data read out to a computer (Figure IV-1 A). Gravimetric determination of OR is feasible for VM nebulization as evaporation was negligible [12]. From the resulting data set, the nebulized mass over time can be plotted (Figure IV-1 B), whereas the last data pair of the plot corresponds to the total OR as determined by the usual procedure (OR = 0.809 mg/mL). With the extended data set, the OR at any given time point is accessible as the first derivative of this plot (Figure IV-1 C). Averaging all time resolved OR data points yields the same OR value (average OR = 0.810 mg/mL) as the previous procedure. With this method, OR can be characterized in much more detail, since changes in OR over the entire duration of nebulization can be monitored.

2.2 Nebulizer performance with physiologic saline

Initially, all nebulizers were characterized regarding their aerosol performance with 0.9% saline. With approximately 55% of the generated aerosol being in the respirable range, the eFlow® clearly outperformed the Aeroneb® Go and the MicroAIR with 31% and 24% respirable aerosol

Table IV-1: Volume median diameter (d[v,50]), geometric standard deviation (GSD), respirable fraction (FPF) and output rate (OR) of PARI eFlow®, Aeroneb® Go, OMRON MicroAIR as determined by laser diffraction and gravimetrically, n=3 (mean ± SD).

nebulizer	d(v,50) [µm]	GSD	FPF [%]	OR [g/min]
eFlow® rapid	4.76 ± 0.05	1.44 ± 0.05	55.2 ± 1.1	0.865
Aeroneb® Go	6.51 ± 0.34	1.66 ± 0.03	31.2 ± 3.5	0.536
MicroAIR	7.35 ± 0.17	1.71 ± 0.02	23.8 ± 1.4	0.385

respectively (Table IV-1). The same is true for the OR, where the eFlow® nebulizes 0.865 g/min while Aeroneb and MicroAIR operate slower at 0.536 g/min and 0.385 g/min respectively.

2.3 Impact of excipients on nebulizer performance

Subsequently, the influence of the formulation on nebulizer performance was taken into consideration to evaluate the devices under more relevant conditions. The resulting changes in the physicochemical properties viscosity and surface tension were monitored and the effect on the aerosol properties was evaluated.

2.3.1 Viscosity

Aerosols of five formulations of increasing sucrose content of 0%, 10%, 20%, 30% or 40% (w/v) were generated and characterized with the three nebulizers. Viscosity increased with sucrose concentration, while surface tension remained unchanged. Viscosity increase strongly affected OR (Figure IV-2) and the aerosol droplet size distribution. The extent of OR decrease by increasing viscosity is comparable for the PARI eFlow® and the MicroAIR® but about twice as pronounced for the Aeroneb Go®. Overall, the eFlow® nebulizes faster than the other devices. The Aeroneb Go® and the MicroAIR® failed to nebulize solutions with viscosities greater than 2.37 mPa*s (30% sucrose), whereas 40% sucrose (3.51 mPa*s) was successfully nebulized with the eFlow®.

With respect to VMD and GSD, an increased viscosity led to smaller droplets and slightly narrower size distributions for all devices. Accordingly, the FPF increased with increasing viscosity, which was more distinctive for the eFlow® and the MicroAIR than for the Aeroneb® Go.

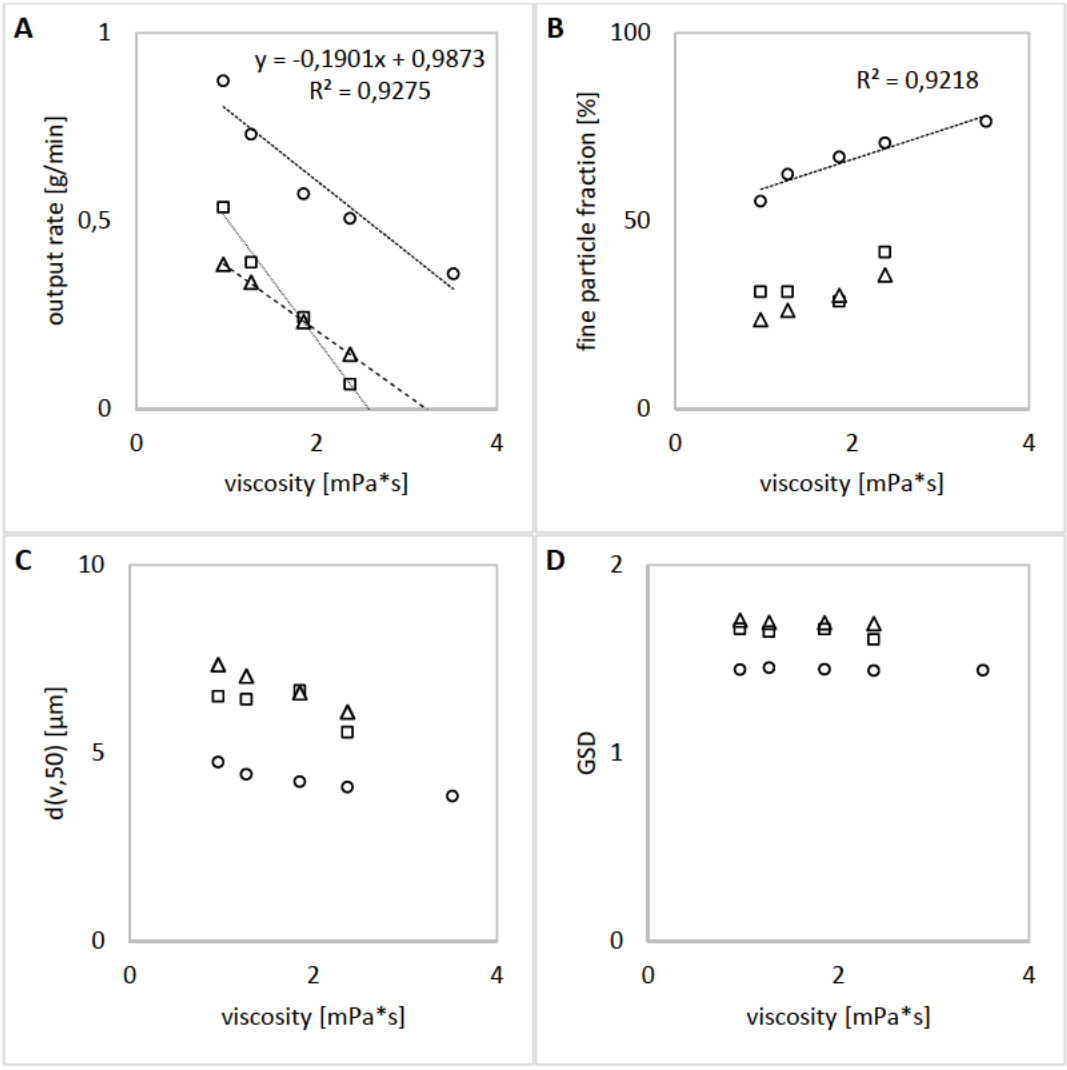

Figure IV-2: Influence of viscosity on OR (A), FPF (B), VMD (C) and GSD (D) of the PARI eFlow® (circle), Aeroneb® Go (square) and OMRON MicroAIR (triangle) nebulizer, n=3 (mean ± SD).

2.3.2 Surface tension

The impact of surface tension on the aerosol characteristics of the three nebulizers was investigated for four formulations including PS20 concentrations of 0%, 0.001%, 0.005% and 0.05%. PS20 mediated surface tension changes did not affect the aerosol droplet size distribution, i.e. VMD and GSD, or the respirable fraction, i.e. FPF, of any of the three nebulizers (Figure IV-3). OR on the other hand, was reduced by decreased surface tension, i.e. increased PS20 concentration, for the Aeroneb® Go and the MicroAIR but did not affect nebulization speed of the eFlow®.

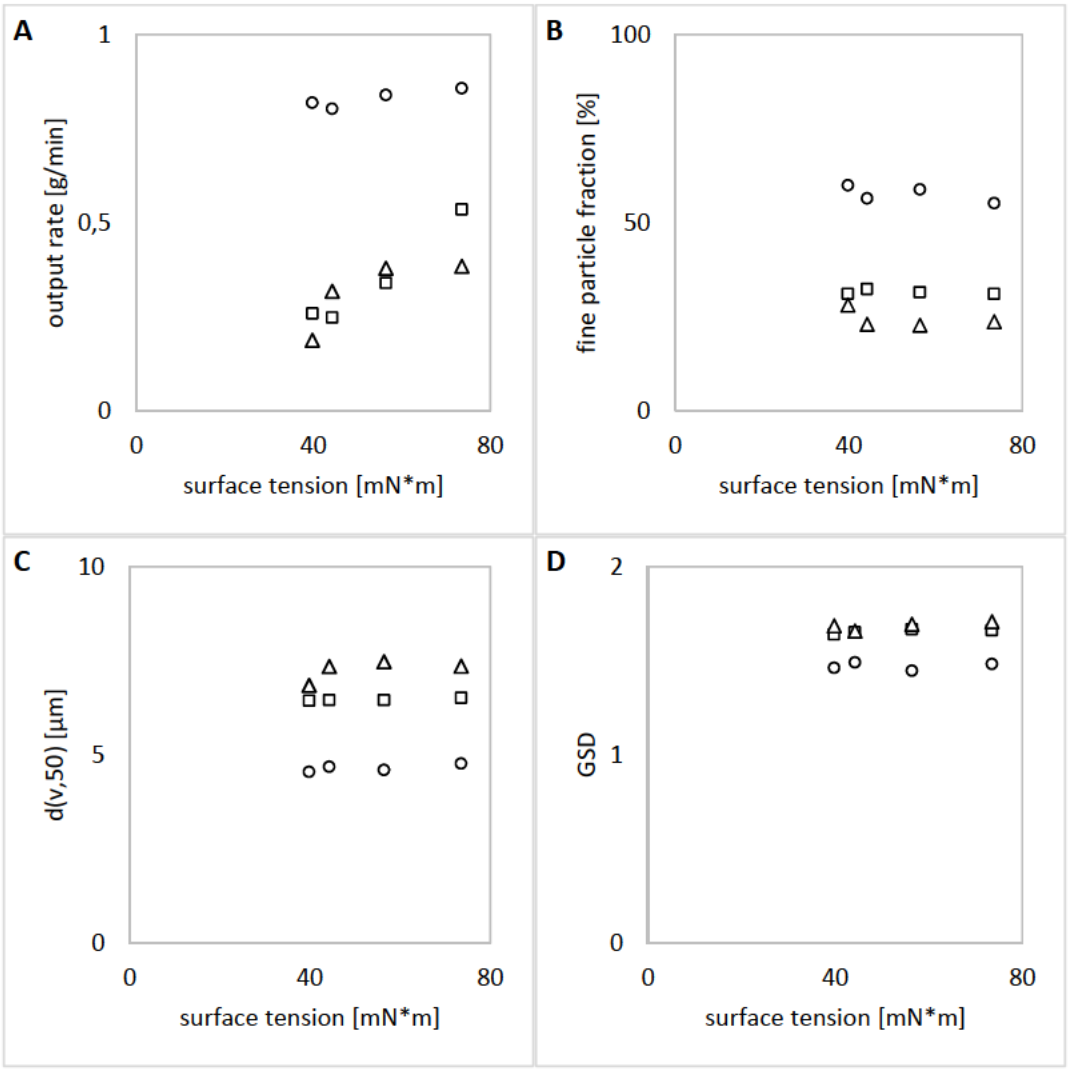

Figure IV-3: Influence of surface tension on OR (A), FPF (B), VMD (C) and GSD (D) of the PARI eFlow® (circle), Aeroneb® Go (square) and OMRON MicroAIR (triangle) nebulizer, n=3 (mean ± SD).

These observations are in accordance with literature. OR reduction by surface active drugs was reported for the Aeroneb® Pro nebulizer [13], while no such impact was observed for the PARI eFlow® when nebulizing solutions of polysorbate 80 [4]. The observed effect of viscosity on OR and FPF was previously reported for glucose solutions nebulized with a PARI eFlow® [4] and glycerol solutions nebulized with an OMRON MicroAIR and an Aeroneb® Pro [1]. OR of jet and ultrasonic (US) nebulizers also decreased with increasing viscosity [14]. On the other hand, aerosol droplet size has been reported to either increase or decrease for jet as well as US nebulizers [15-18]. This inconsistency was suggested to result from varying nebulizer designs and operation parameters [1].

2.4 Impact of proteins on nebulizer performance

2.4.1 Surface tension

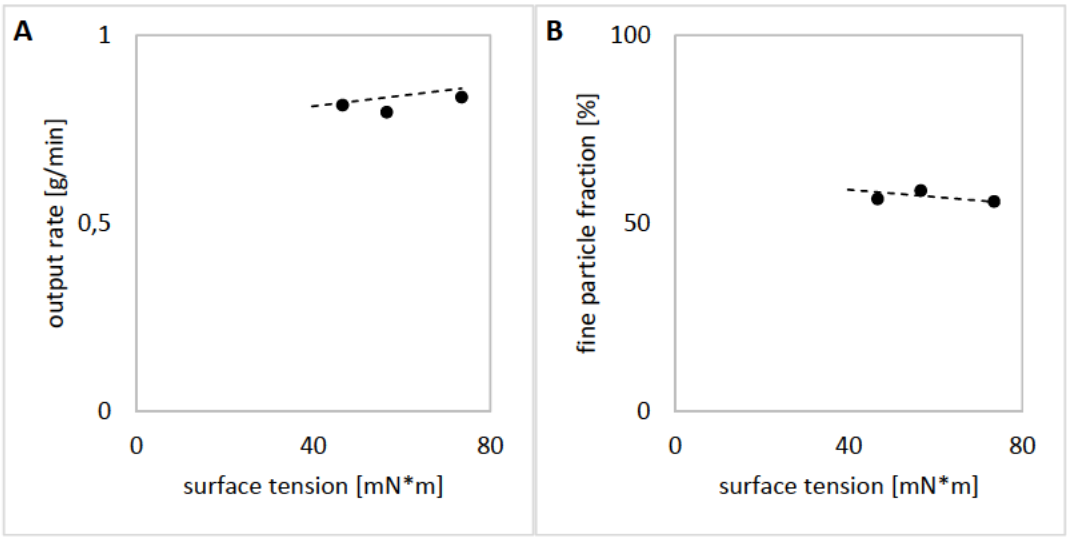

Figure IV-4: Impact of 0 mg/mL, 0.3 mg/mL and 3.0 mg/mL G-CSF surface tension on OR (A) and FPF (B) of a PARI eFlow® compared to PS20 induced surface tension (linear trend line), n=3 (mean ± SD).

Protein induced reduction of surface tension was achieved with different concentrations of G-CSF. The addition of 0.3 mg/mL G-CSF led to a decrease in surface tension from 73.5 mN/m for the respective placebo to 56.6 mN/m, while 3.0 mg/mL G-CSF resulted in a surface tension of 46.6 mN/m. Comparable to PS20 induced changes in surface tension, neither OR nor FPF of the PARI eFlow® were significantly affected by G-CSF addition (Figure IV-4).

2.4.2 Viscosity

High viscosities are a common phenomenon encountered during formulation of highly concentrated proteins like antibodies. Therefore an IgG1 antibody was nebulized at different concentrations to study its impact on nebulizer performance. The addition of 15 mg/mL or 40 mg/mL IgG resulted in viscosities of 1.15 mPa*s and 1.95 mPa*s respectively compared to 0.96 mPa*s for the placebo formulation.

The impact of IgG1 induced viscosity on nebulizer performance was comparable to excipient mediated effects. The addition of 15 mg/mL IgG1 had a minor impact on OR whereas it decreased by 30% for the 40 mg/mL IgG1 formulation (Figure IV-5). The 55% FPF of the nebulized placebo increased with IgG1 concentration to 58% and 65% FPF for 15 mg/mL and 40 mg/mL respectively.

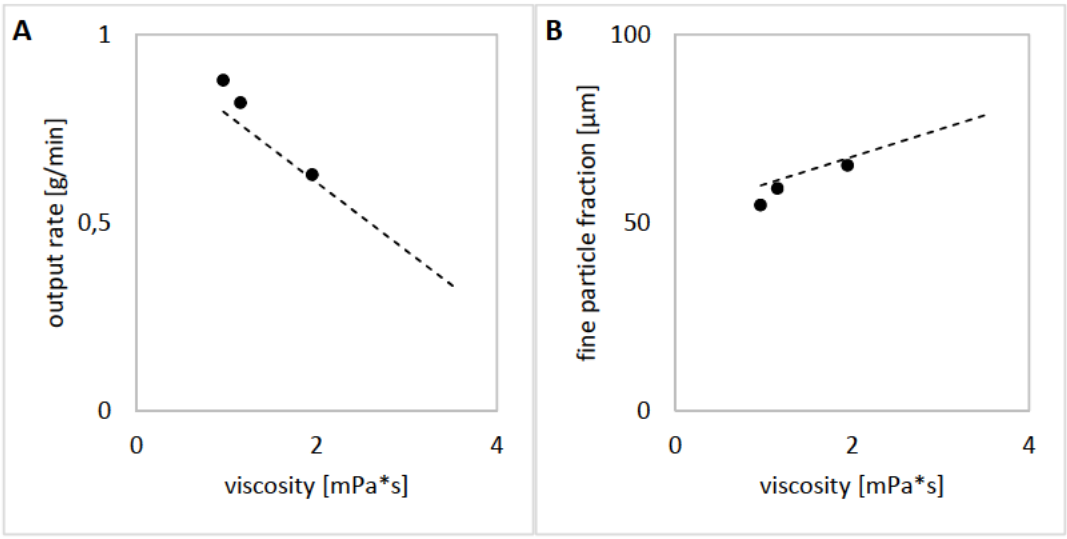

Figure IV-5: Impact of 0 mg/mL (n=5), 15 mg/mL (n=3) and 40 mg/mL (n=2) IgG1 viscosity on OR (A) and FPF (B) of a PARI eFlow® compared to the effect of sucrose induced viscosity (linear trend line) (mean ± SD).

Protein induced effects on nebulizer performance resemble those observed after excipient addition. While many proteins are surface active, no impact on aerosol properties was observed for the PARI eFlow®. Other vibrating mesh nebulizers may respond with reduced OR as observed for the Aeroneb® Go and MicroAIR and reported for the Aeroneb® Pro [13].

On the other hand, VM nebulizer performance is sensitive to formulation viscosity. Formulations of increased viscosities may seriously reduce OR. Reliable nebulization with a PARI eFlow® may not be guaranteed for formulations with viscosities above 3.5 mPa*s. This has to be considered for highly concentrated protein formulations. If the viscosity cannot be adjusted to an acceptable range by excipient addition [19], jet nebulization may serve as an alternative technology less affected by high viscosities [14].

2.5 Time resolved analysis of aerosol characteristics

Time resolved analysis of aerosol characteristics of the PARI eFlow® revealed that neither OR nor droplet size distribution were constant throughout the duration of one nebulization. OR increased by 20-30% while FPF decreased by 10-11% with ongoing nebulization of sucrose and IgG1 solutions (Figure IV-6). If, as observed above, viscosity is considered responsible for changes in aerosol properties, this behavior suggests a reduction of viscosity during nebulization. The pseudoplastic (shear thinning) viscosity behavior of IgG solutions [20, 21] could result in shear-thinning from vibration and ongoing nebulization and thus affect the aerosol characteristics. But then sucrose solutions should not exhibit the same phenomenon as they are Newtonian fluids [22,

23] and do not exhibit shear-thinning. Accounting for the temperature dependency of viscosity [24], a gradual increase of the temperature inside the nebulizer reservoir, as observed for ultrasonic nebulizers, could explain these observations. A respective increase in reservoir temperature was verified for the PARI eFlow® (section 4.2).

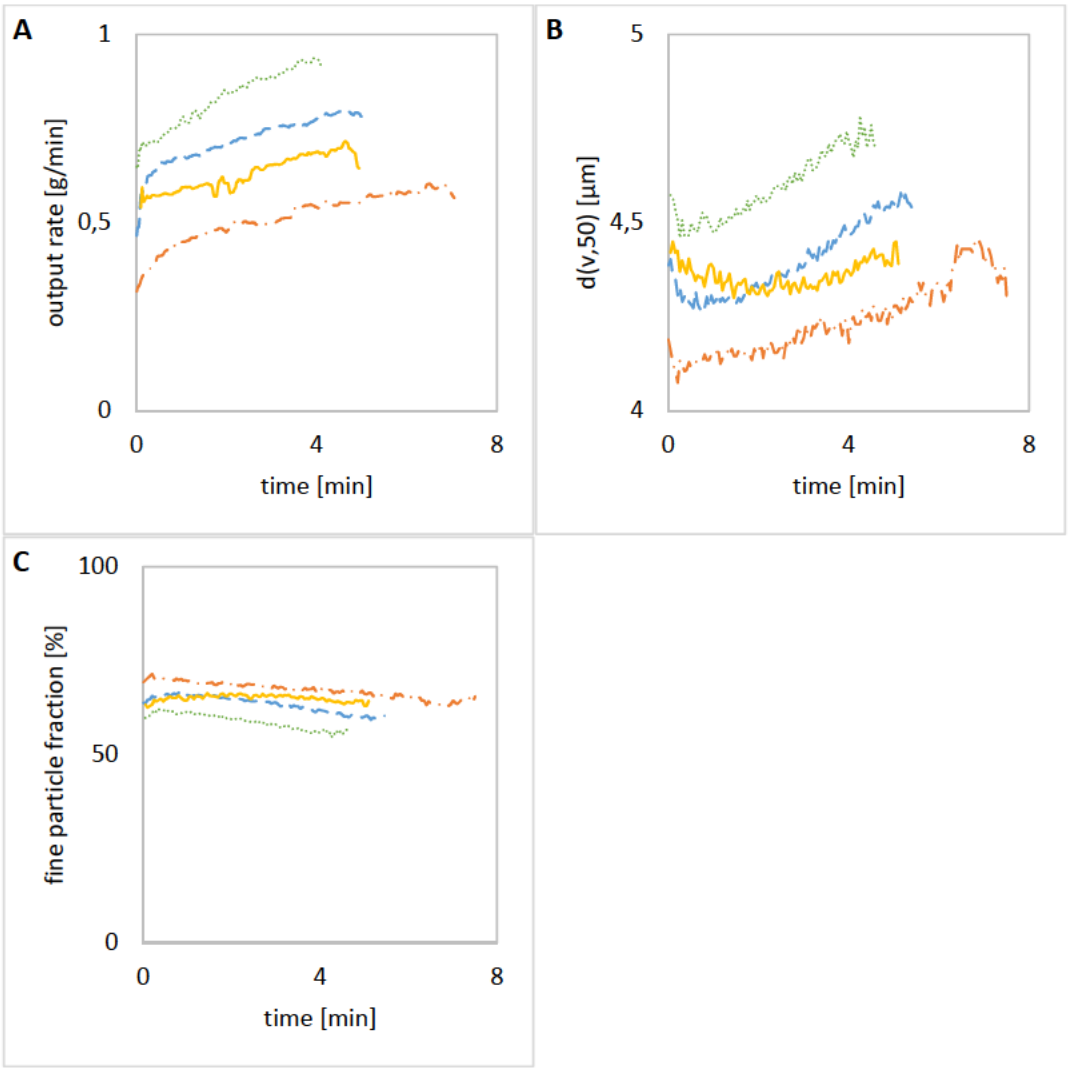

Figure IV-6: Time resolved data of OR (A), VMD (B) and FPF (C) for 100 mg/mL (blue dashed line, n=3) and 200 mg/mL (red dot dashed line, n=3) sucrose and 15 mg/mL (green dotted line, n=3) and 40 mg/mL (yellow solid line, n=2) IgG1 nebulized with a PARI eFlow® (error bars were omitted to retain clarity).

2.6 Impact of protein aggregation on vibrating mesh nebulization

2.6.1 Control of G-CSF stability to nebulization by pH adjustment

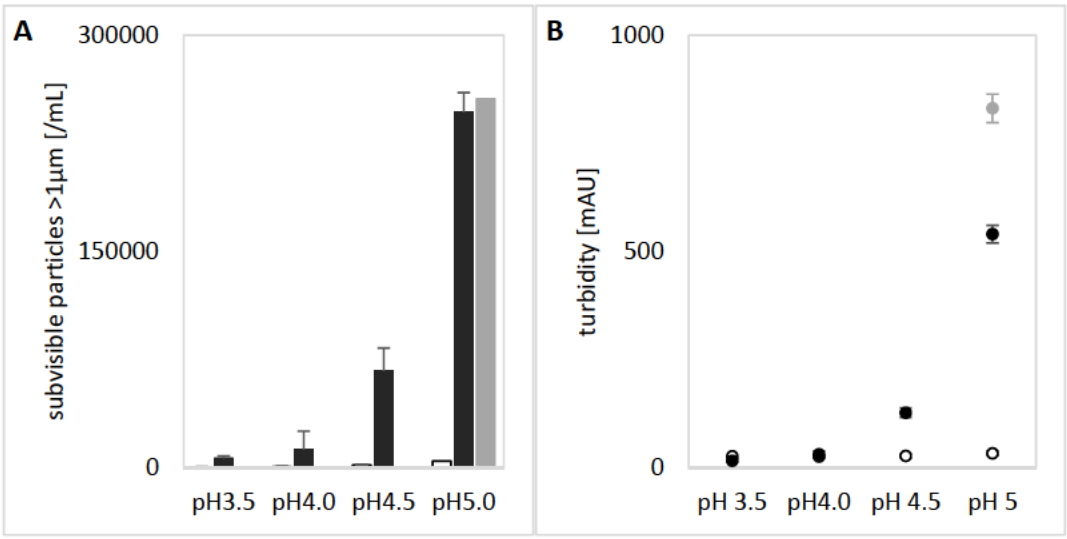

Figure IV-7: G-CSF aggregation after nebulization in dependence of formulation pH. Subvisible particles >1 µm (A) and turbidity (B) are displayed for placebo (white), nebulized G-CSF (black) and the residual reservoir volume (grey) for the pH 5.0 formulation, n=3 (mean ± SD).

Investigating the impact of protein stability on nebulizer performance relied on the adjustability of G-CSF stability by pH shift rather than qualitative changes in formulation composition. To discriminate stable from instable pH values, G-CSF aggregation was monitored after nebulization. G-CSF remained stable after nebulization if formulated at pH 3.5 or 4.0. Increasing pH to 4.5 resulted in rising turbidity and subvisible particle counts, which drastically escalated at pH 5.0 (Figure IV-7). These findings confirm reports of pH dependent G-CSF stability after thermal ramping and agitation [5, 6].

While pH adjustments did not affect placebo buffer viscosity or surface tension, it caused a slight increase in viscosity and decrease in surface tension for G-CSF formulations of increasing acidity (Table IV-2). These observations may be explained by the shift of the pH closer toward the pI of G-CSF at pH 5.65 [25, 26]. Proteins may exhibit increased surface activity the closer they are to their pI, as weaker electrostatic repulsion between protein molecules allows for more molecules to bind to the air-water surface [27]. The omission of electrostatic repulsive forces and the emerging dominance of attractive interactions, as formulation pH shifts toward the proteins pI, was also suggested to be the reason for increasing viscosity, which has been observed for several antibodies [28].

Table IV-2: Viscosity and surface tension of 0.3 mg/mL G-CSF in dependence of formulation pH, n=3 (mean ± SD).

	pH	viscosity [mPa*s]	surface tension [mN/m]
placebo	3.5	0.96 ± 0.00	73.5 ± 0.3
	4.5	0.97 ± 0.00	73.1 ± 0.1
G-CSF	3.5	0.96 ± 0.00	56.6 ± 1.0
	4.0	1.03 ± 0.01	53.6 ± 1.0
	4.5	1.08 ± 0.02	52.4 ± 0.4
	5.0	1.16 ± 0.01	n.d.

2.6.2 Impact of G-CSF stability on nebulizer performance

Characterizing the different G-CSF formulations regarding OR and FPF and benchmarking the results against the viscosity mediated effects determined for sucrose solutions (section 2.3) revealed that changing the pH of the G-CSF formulation provoked consequences of far greater magnitude than can be explained by the concomitant subtle rise in viscosity. Stable G-CSF formulations (pH 3.5 and pH 4.0) were nebulized at ORs consistent with sample viscosity. For the instable G-CSF formulations (pH 4.5 and pH 5.0) OR dropped considerably, whereby the decline was related to the extent of G-CSF aggregation rather than viscosity. The most instable formulation with pH 5.0 nebulized at 50% the OR of the stable formulations, which is comparable to a stable formulation with a viscosity about 3.0 mPa*s, whereas the sample had a viscosity of only 1.2 mPa*s (Figure IV-8). As observed before, the reduced OR was accompanied by an increased FPF, which was also more pronounced than the subtle rise in viscosity.

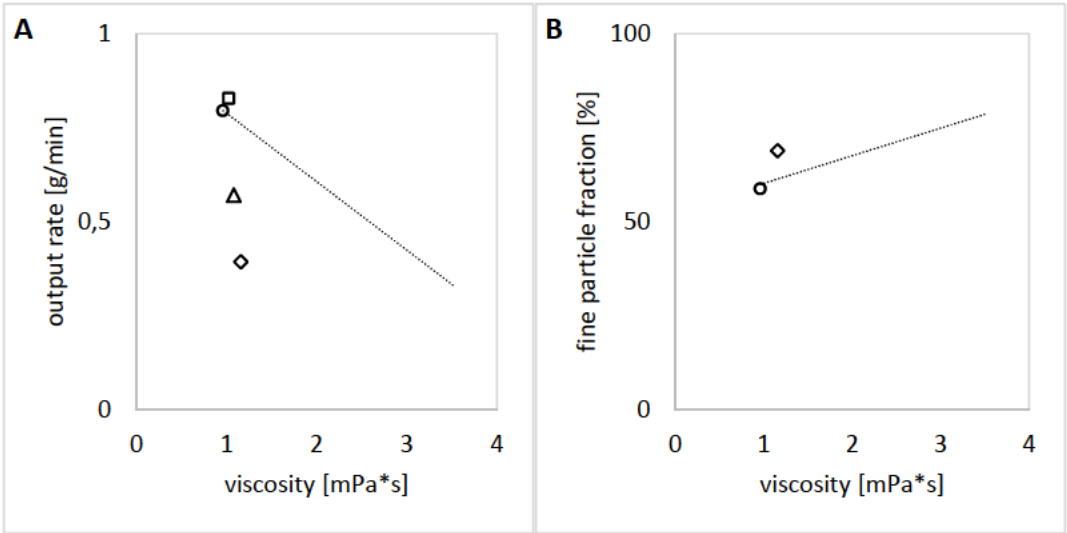

Figure IV-8: OR (A) and FPF (B) after nebulization of G-CSF at pH 3.5 (circle), 4.0 (square), 4.5 (triangle) and 5.0 (diamond) in respect to sample viscosity compared to the viscosity related impact of sucrose solutions on OR and FPF (linear trend line), n=3 (mean ± SD).

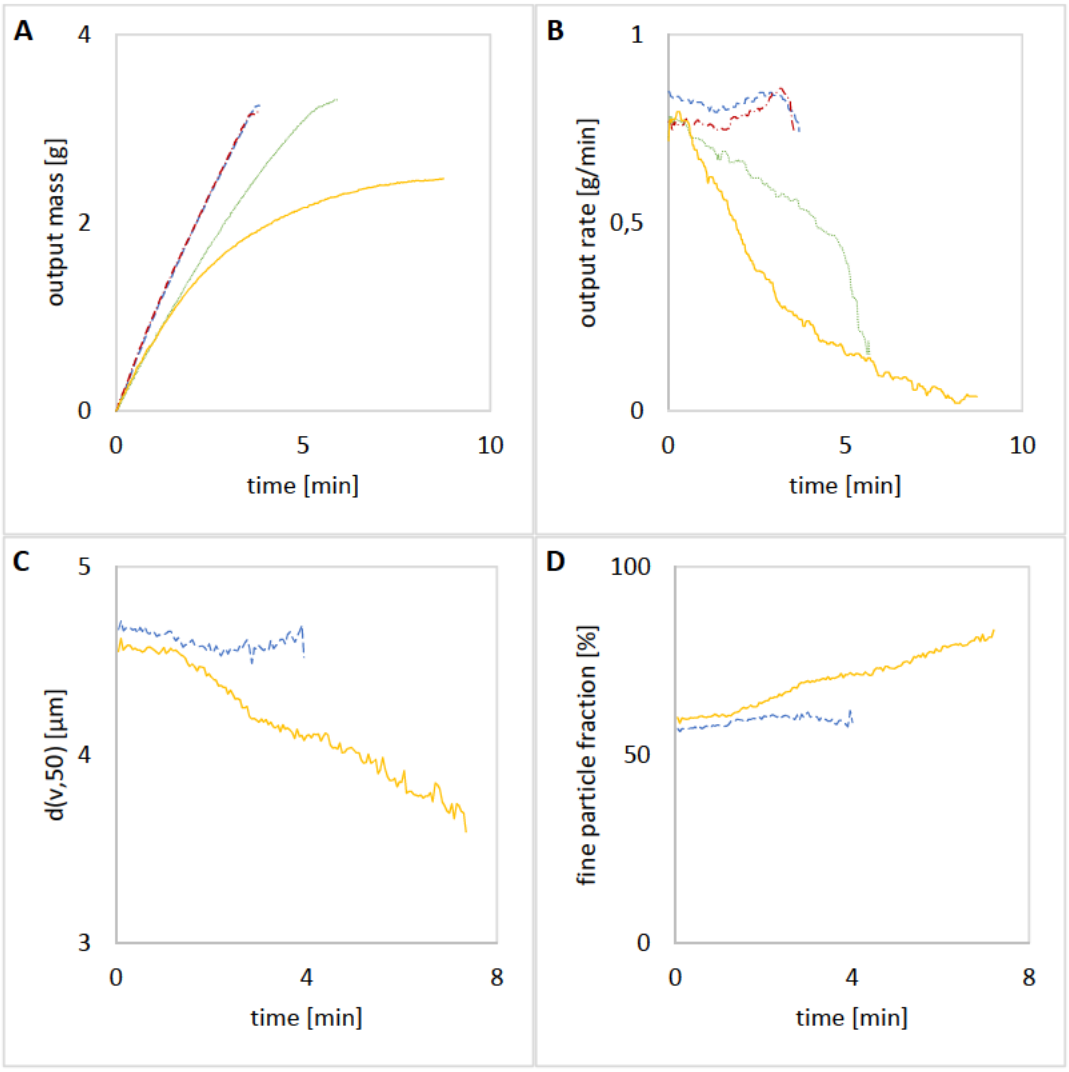

Figure IV-9: Time resolved data for nebulized mass (A), OR (B), VMD (C) and FPF (D) for G-CSF nebulized at pH 3.5 (blue dashed line), 4.0 (red dot dashed line), 4.5 (green dotted line) and 5.0 (yellow solid line).

Time resolved aerosol data provided some explanation for the severe impact of G-CSF stability on nebulizer performance. Stable, aggregate free G-CSF samples of pH 3.5 and pH 4.0 were nebulized at a constant rate of approximately 0.8 g/min (Figure IV-9 B). When nebulized at pH 4.5 the OR was no longer constant but steadily declined from 0.8 g/min below 0.4 g/min within five minutes of operation. As OR decreased nebulization times were prolonged. G-CSF at pH 5.0 suffered from a rapid drop in OR and completely ceased output after nebulization of less than 2.5 mL of the solution.

At pH 5.0, the declining OR was accompanied with a droplet size shrinking from initial 4.6 µm to final 3.6 µm (Figure IV-9 C) and therefore an FPF increasing from 60% to 83% (Figure IV-9 D). VMD and FPF remained constant throughout the nebulization of stable G-CSF at pH 3.5.

Both the shrinking droplets and the sloping OR in relation to the extent of G-CSF aggregation lead to the reasonable presumption that nebulizer performance is impaired by an obstruction of the vibrating mesh with G-CSF aggregate matter. Insoluble aggregates adhere to the mesh and constrict the micron sized apertures, so that progressively smaller droplets are extruded. As more and more G-CSF molecules degrade with ongoing nebulization, more apertures get clogged resulting in reduced OR and cessation of nebulization upon congestion of the entire vibrating mesh.

Presumably occluded meshes were observed under a digital microscope to confirm this hypothesis. Therefore, the mesh was rinsed with ultrapure water to rid non adhering protein material and stained with coomassie blue to confirm the proteinaceous nature of deposited matter.

The apertures are conically shaped [29]. On the inner side of the mesh, facing the reservoir, the holes have a diameter of approximately 30 µm and are easily visible even at low magnification (Figure IV-10 A). While coomassie staining revealed the adsorption of a proteinaceous layer to the metal membrane, aperture obstruction is not obvious from the inner side of the mesh (Figure IV-10 B). On the outer side, delivering the aerosol, the apertures are approximately 4µm wide. After nebulization of instable G-CSF samples (pH 5.0) the microscopic images of the mesh show small, white, elevated clusters of aggregated G-CSF evenly distributed over the entire perforated region of the membrane (Figure IV-10 D). In contrast, the mesh seemed free of such debris if stable G-CSF (pH 3.5) was nebulized (Figure IV-10 C). The clusters could be stained by coomassie blue confirming their proteinaceous nature (Figure IV-10 E+F). The regular pattern of the aggregate deposition on the mesh resembled the distribution of the apertures. Virtually all holes were clogged by aggregate matter that had been extruded from the tiny apertures to form elevated shapes. G-CSF seems to have heavily aggregated during its passage through the vibrating mesh.

These illustrative pictures confirm the theory that mesh occlusion by protein aggregates is the reason for severe break down of nebulizer performance observed for instable protein samples.

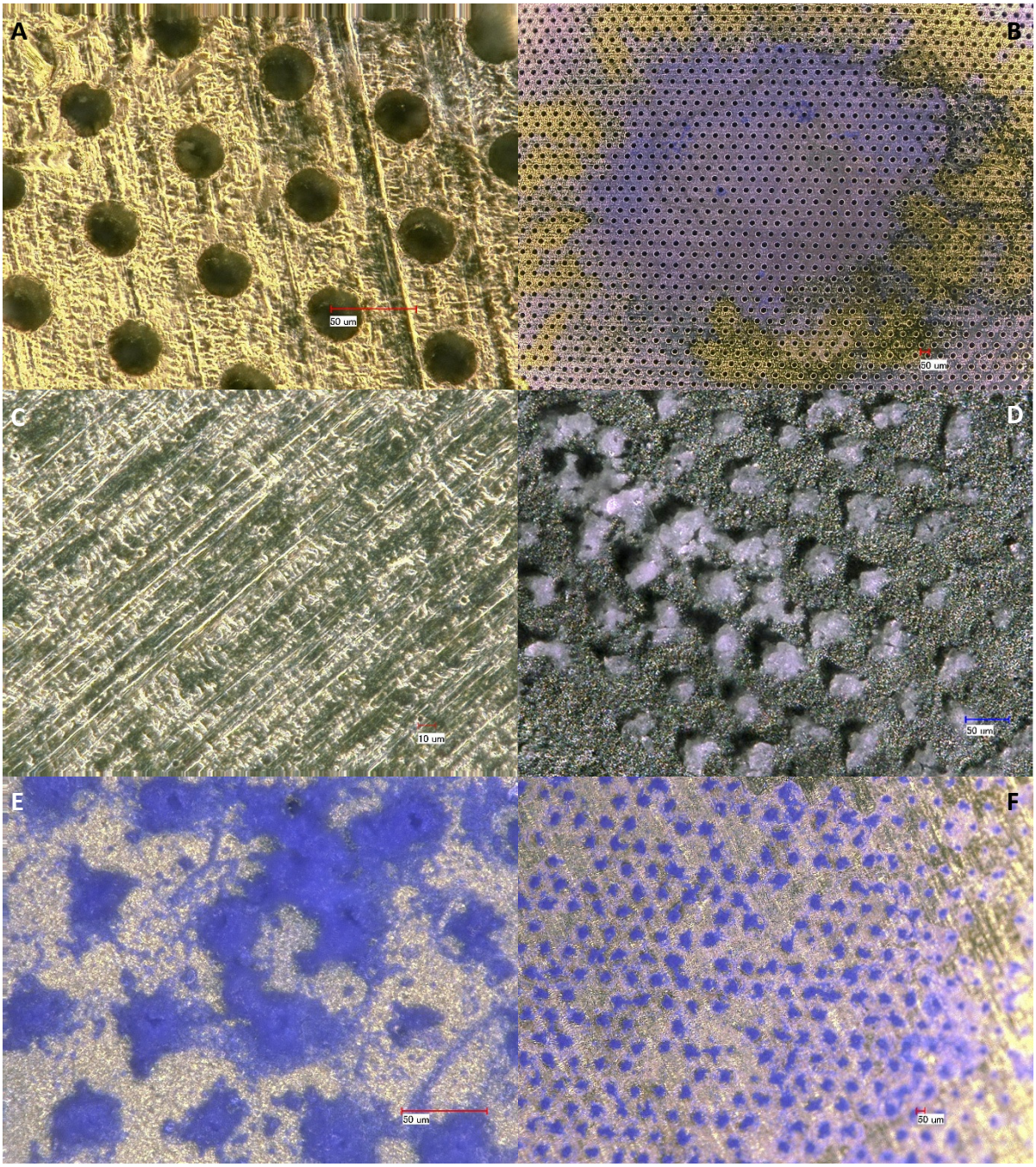

Figure IV-10: Inner side of the vibrating mesh at 1000 fold (A) and 100 fold (B) magnification after the nebulization of G-CSF at pH 5.0. Outer side of the mesh after nebulization of G-CSF at pH 3.5 (1000 fold magnification) (C) and pH 5.0 (500 fold magnification) (D). Coomassie stained GCSF aggregates on the outer side of the mesh after nebulization at pH 5.0 at 1000 fold (E) and 100 fold magnification (F).

2.7 Conclusion

The presented investigation revealed that nebulizer performance is influenced by both proteins and excipients commonly employed in protein formulation, as they alter the physicochemical properties of the formulation. A decrease in surface tension led to a slowdown in OR for two nebulizers, which is unfavorable for the nebulization of surface active proteins and stabilizing

surfactants. Only the PARI eFlow® was not negatively affected. Viscosity, on the other hand, had an impact on the OR and droplet size of all tested devices. This has to be considered for formulations containing viscosity increasing excipients like sugars or polyols as well as for elevated protein concentrations. While the respirable fraction was improved, OR was markedly reduced if the formulation viscosity rose above 1.2 mPa*s. Two nebulizers even failed to operate at higher viscosities.

The PARI eFlow® exhibited the best aerosol performance and was therefore selected for further application. This also allows to seamlessly switch to the AKITA² APIXNEB nebulizer (Activaero, Gemünden/Wohra, Germany) at a later stages of the project, as it is also powered by the eFlow® VM technology.

The AKITA² system controls the users breathing pattern, one of the most important factors regarding aerosol deposition [7, 30] and thus allows for a more efficient and reproducible aerosol delivery [31, 32]. Additionally, treatment compliance can be monitored, which is beneficial during clinical trials.

Aerosol characteristics are not constant but change throughout the duration of one nebulization, which can be explained by a gradual increase of the temperature inside the reservoir during operation and the temperature dependency of viscosity. This heat up may pose a challenge for the nebulization of heat sensitive proteins and has to be investigated further.

Protein aggregation was demonstrated to disrupt proper VM nebulizer operation by the occlusion of the mesh apertures. Even if protein aggregation is effectively prevented, thorough mesh cleaning procedures and a regular assessment of mesh function are vital for the reproducible generation of protein aerosols with VM nebulizers. The newly developed method for time resolved OR data can be used to detect early mesh occlusion and may be a valuable tool for the development of suspensions or nanoparticle or liposome formulations for VM nebulization, where mesh occlusion is of concern.

3 Aerosol cloud collection procedures

3.1 Introduction

As is evident from literature, nebulization may inflict significant degradation to sensitive protein molecules [33, 34]. In order to assess protein activity and stability after nebulization with common analytical methods, it becomes necessary to re-collect the aerosol cloud and condense it into a bulk liquid. Such a procedure must not induce protein denaturation by the collection itself, as it would be impossible to differentiate it from nebulizer induced protein degradation and thus corrupt subsequent stability data. Secondly, a collection procedure should collect the entire aerosol population generated by the nebulizer, since theoretically, aerosol deposition and protein degradation are affected by droplet diameter and a systemic disregard of certain aerosol populations might bias follow up stability analytics. All forces associated with aerosol deposition are influenced by droplet diameter (d): inertial impaction ($\sim d^2$), gravitational sedimentation ($\sim d^3$) and diffusion ($\sim 1/d$) [30]. Smaller droplets are less affected by these forces and are therefore more likely to evade collection. On the other hand, droplet diameter also determines the specific surface area ($\sim 1/d$) and may therefore influence the extent of protein degradation. Smaller droplets possess a higher specific surface area, thus protein molecules are more likely to interact with the hydrophobic air-liquid interface and suffer from interfacial stress [35]. Protein molecules in smaller aerosol droplets may therefore exhibit a different stability profile and lead to potentially biased protein stability data if overlooked. Finally, an ideal procedure should be simple to handle and not rely on an elaborate setup.

Aerosol cloud collection has been achieved by a variety of methods described in literature including liquid collection in a twin-stage impinger (TSI) [36-39], condensation in a vacuum vented reflux condenser (RC) [34, 40], collection in the nebulizer's aerosol chamber [41] or in test tubes [42, 43] of various volume and material. Collection efficiency and impact on protein stability were not reported although there is evidence of considerable detrimental influence of at least some of the listed procedures like TSI collection. Khatri et al. [39], already mentioned in chapter I, found protein collected in the lower TSI stage significantly less active than the fraction collected in the upper stage. Khatri et al. attributed this to a remarkable impact of aerosol droplet size on protein degradation. An effect of such extent has not been reported elsewhere and it seems more

likely that different collection procedures in the upper and the lower stage can explain the observations. Only in the lower stage, aerosol collection involves bubbling of the aerosol through a buffer solution. The disruptive effects of bubbling on protein stability have been laid out in chapter I, indicating that the results may be corrupted by unsuitable aerosol collection conditions. Therefore, the above listed procedures were evaluated regarding collection efficiency and their impact on protein degradation. In order to discriminate nebulizer induced protein degradation from collection induced artifacts, non-nebulized protein formulation was collected as control.

While aerosol collection has also been described by simply placing a glass slide in front of the nebulizer outlet to achieve aerosol condensation [44], this approach was not included into the experiments as the aerosol collection is incomplete, disregarding a large fraction of the aerosol.

3.2 Collection efficiency

Table IV-3: Collection efficiency and impact of collection procedure on reservoir temperature (T_{RES}) during nebulization, n=3 (mean ± SD).

collection method	collection efficiency [%] = recovery	ΔT_{RES} [°C]
no aerosol collection	--	10.3 ± 1.2
PP test tube 2 mL	98.5 ± 0.3	10.5 ± 0.7
PP test tube 4 mL	97.7 ± 1.2	9.4 ± 0.5
PP test tube 15 mL	99.2 ± 0.5	10.5 ± 2.0
glass test tube 4 mL	98.5 ± 0.6	9.6 ± 1.5
nebulizer chamber small	99.4 ± 0.3	9.9 ± 0.9
nebulizer chamber large	99.5 ± 0.0	10.6 ± 1.1
Twin-stage impinger (TSI)	95.7 ± 2.4	4.4 ± 1.1
Reflux condenser (RC)	93.3 ± 0.6	5.9 ± 0.6

The efficiency of aerosol cloud collection of the different procedures was compared for a 3 mg/mL SM101 solution containing 10 µg/mL carboxyfluorescein (CF). Since SM101 concentration may not only be altered by collection induced dilution or solvent evaporation but might also undergo degradation, CF was used as an inert concentration marker.

Aerosol collection inside of test tubes or the aerosol chambers was very effective with recoveries of no less than 98.5% (Table IV-3). 6.7% of the aerosol escaped collection when using an RC.

Additionally, the CF concentration increased by 11% after collection, which likely resulted from solvent evaporation caused by the vacuum induced air-flow through the collector. After collection with a TSI 95.7%, aerosol was recovered in placebo buffer. The simultaneous occurrence of dilution, evaporation and unaccounted aerosol losses prevented the calculation of the extent of solvent evaporation, which can be assumed to be comparable to RC collection.

Nebulization without aerosol collection performed as a reference procedure resulted in a 10°C increase in reservoir temperature (T_{RES}). A similar extent of reservoir heat up was observed for test tube or aerosol chamber collection. In contrast, TSI and RC collection exhibited reservoir heat up of about 4-6°C respectively, which can likely be accounted to a cooling effect of the observed solvent evaporation. This deviation from normal nebulization conditions may significantly alter protein stability of likewise collected samples and thereby generate misleading data.

3.3 Impact of aerosol collection on protein stability

3.3.1 SM101

SM101 stability was affected by the collection procedures. After RC or TSI collection, even non-nebulized SM101 was degraded, which reveals the detrimental nature of these collection procedures. Especially collection with a TSI led to the loss of 20% SM101 according to dilution corrected monomer recovery data and was accompanied by the formation of large amounts of subvisible particles and high turbidities for non-nebulized controls and collected SM101 aerosols alike (Figure IV-11).

The fraction of condensate that directly drained into a tube below the RC (direct) exhibited low subvisible particle and turbidity values. Monomer recovery of aerosol and control were slightly above 100% accounting for solvent evaporation and CF correction. A small fraction of condensed aerosol did not drain from the RC but was recovered after rinsing the RC with a fixed volume of placebo buffer (rinse). This fraction contained a highly increased turbidity and particle count compared to the first fraction.

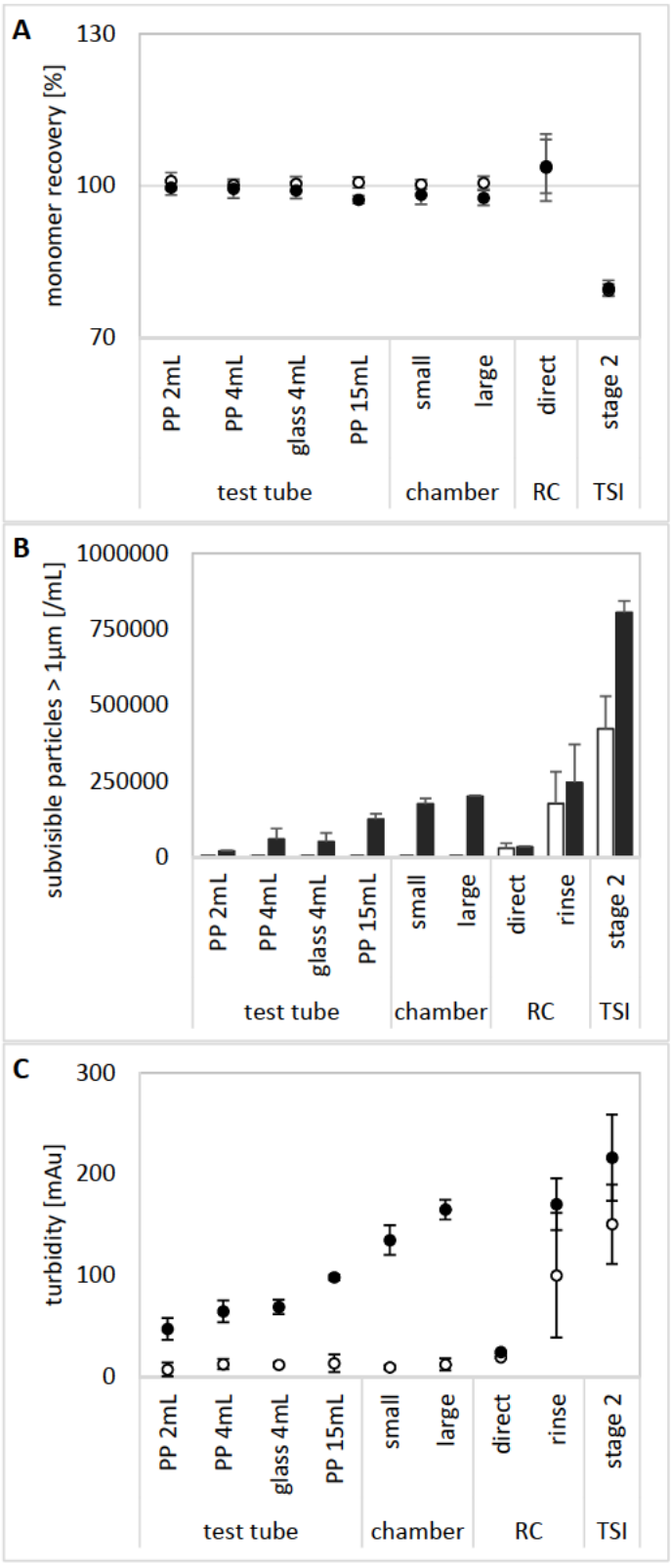

Figure IV-11: Impact of the aerosol collection procedure on the stability of 3 mg/mL SM101 after nebulization with a PARI eFlow®. SM101 monomer recovery (A), subvisible particles > 1 µm/mL (B) and turbidity (C) after the collection of non-nebulized control (white) and nebulized aerosol (black) in test tubes, aerosol chambers, reflux condenser (RC) or a twin-stage impinger (TSI), n=3 (mean ± SD). Values for RC and TSI are corrected for up-concentration or dilution respectively. RC samples yielded a direct fraction and a rinse fraction.

Non-nebulized controls were not negatively affected by collection in test tubes or aerosol chambers. SM101 monomer recovery was at 100% and subvisible particle counts and turbidity

remained very low. In contrast, subvisible particle and turbidity data for collected SM101 aerosols indicated that the extent of SM101 degradation after collection correlates to the size of test tubes or aerosol chambers used for collection. While monomer recovery was generally high, an equal trend was observable too. Using PP or glass containers of equal volume did not affect the extent of protein degradation. Increasing the collector volume from 2 mL, over 4 mL to 15 mL resulted in increased subvisible particle counts and turbidity values. If collected in 15 mL PP tubes, the sample contained six times the number of subvisible particles after collection in a 2 mL PP tube. Collection in an aerosol chamber resulted in up to tenfold that particle count. Though less distinct, the same situation was found for turbidity results.

3.3.2 IgG1

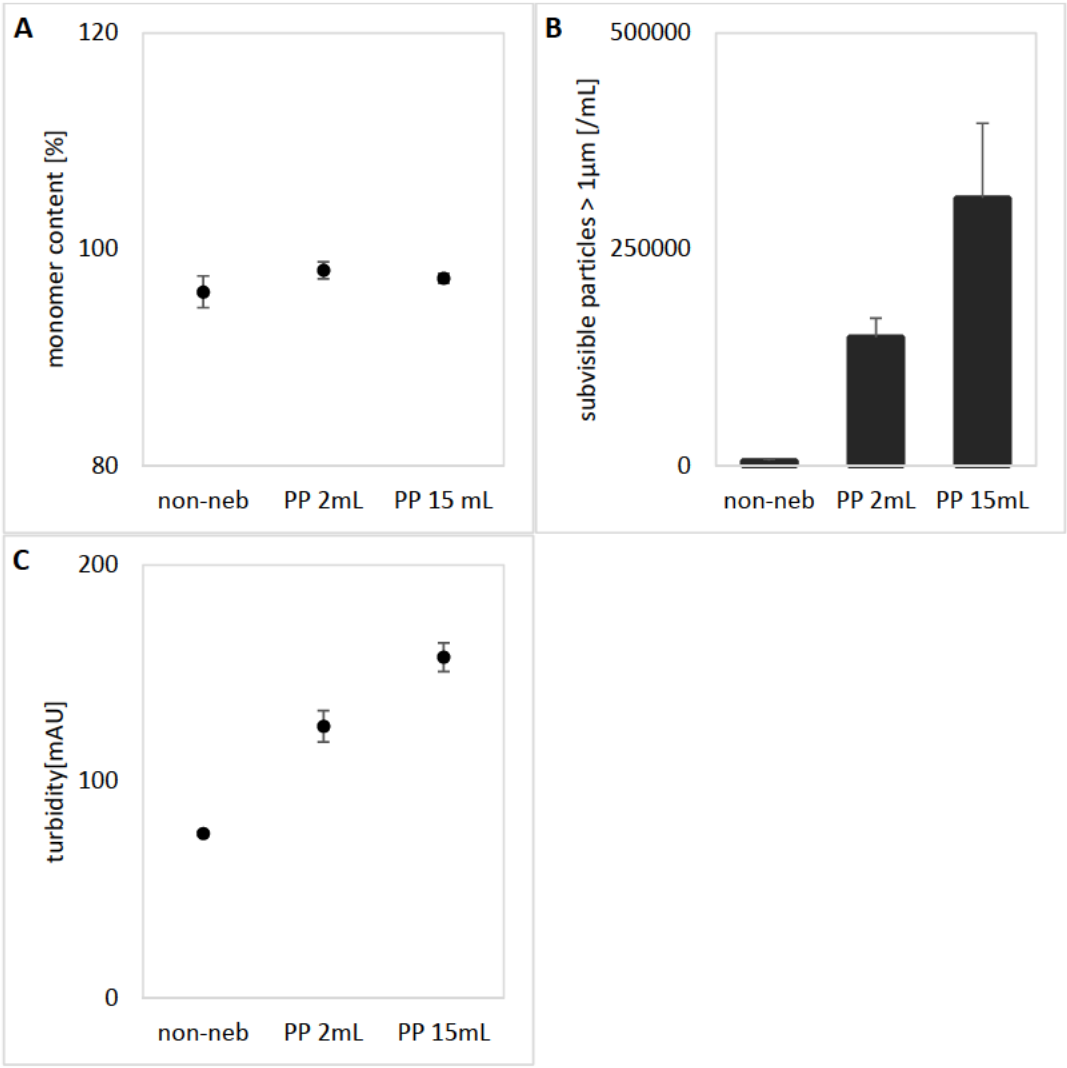

Figure IV-12: Impact of the aerosol collection container volume on monomer recovery (A), subvisible particles > 1µm/mL (B) and turbidity (C) of 15mg/mL IgG1 after nebulization with a PARI eFlow®, n=3 (mean ± SD).

The observed impact of aerosol collector size on protein stability was quickly investigated for an IgG1 antibody as a second protein. Collector size dependent aggregation propensity was confirmed for the IgG1. The increment in subvisible particles and turbidity after nebulization was approximately twice as large for aerosols collected in 15 mL PP tubes than for aerosols collected in 2mL PP tubes. Monomer recovery was not affected by collector size (Figure IV-12).

3.4 Conclusion

Virtually complete aerosol cloud collection can be achieved with various approaches. However, the compared procedures differ in respect to ease of handling and their impact on protein stability. Collection in test tubes or in the aerosol chamber stands out for easy handling since no additional equipment is needed. Neither aerosol concentration nor T_{RES} were altered by this approach. In contrast, collection with an RC or a TSI requires special glass ware that needs to be thoroughly cleaned before each collection. Both procedures rely on a vacuum induced stream of air through the collector. This leads to solvent evaporation and a reduced T_{RES}, which may both corrupt protein stability data after nebulization. In the TSI, the aerosol is collected in a highly diluted form possibly introducing further sources of error. The TSI was very unsuitable for the collection of SM101 aerosols, since the collection procedure alone was very detrimental and caused far more SM101 degradation than inflicted by actual nebulization. The observed degradation was probably a result of the air bubbling through the collection buffer filled second stage, which posed a significant interfacial stress for the collected protein molecules [37, 45].

While RC collection seemed less detrimental, resulting stability data for SM101 was not reliable. On the one hand, SM101 degradation was induced by the collection procedure itself, probably due to a combination of solvent evaporation and deposition on the large glass interface. On the other hand, SM101 aggregates were restrained inside the collector and only appeared in the washing fraction, thus leading to biased protein stability data.

Collection of non-nebulized control in test tubes did not cause any SM101 degradation, which is reasonable since no detrimental force is introduced by the procedure (unlike air-bubbling or evaporation on large interfaces). However, the size of the container used for collection affected

the resulting stability of both tested proteins, such that collection in the smallest PP tube resulted in less protein degradation than in the larger containers evaluated.

A possible explanation for the relation of collector size and protein degradation may involve the life time of the aerosol droplets. As aerosol droplets exhibit a large specific surface area, contained protein molecules are more likely to interact with the air-liquid interface and suffer from interfacial stress, which is reduced after droplet coalescence into a bulk liquid. Small collection containers provide less volume for aerosol expansion, leading to reduced droplet life times and therefore, less exposition of protein molecules to the detrimental air-liquid interface. Aerosol collection in small containers might therefore result in too positive protein stability data. Alternatively the amount of hydrophobic surface area available for aerosol deposition may control the extent of protein aggregation. Protein molecules situated in the air-liquid interface of aerosol droplets are partially unfolded and prone to further irreversible aggregation [46, 47] upon contact with glass or PP surface of the collector, while contact with already wet or protein covered surface or the liquid bulk leads to less aggregation. Accordingly, wetting the surface of a 4mL PP tube with placebo buffer before aerosol collection reduced SM101 turbidity by 4.4%. Using PEG400 or a 1% BSA solution for wetting, reduced SM101 aggregation by up to 11% or 18% according to turbidity and subvisible particle counts (Table IV-4). Since aerosol deposition in the lung occurs in the lining fluid, the reduction of hydrophobic surface availability during *in vitro* collection might deliver more realistic results regarding protein stability. An additional observation indicates a participation of the collector surface in protein aggregation as proposed by the second theory. During the collection of highly concentrated but insufficiently stabilized SM101 or ovalbumin (OVA) aerosols, the formation of large visible aggregate patches on the collector walls could be observed, whereas the collected bulk liquid remained free of visible particles.

Table IV-4: Effect of collection container coating on SM101 aggregation, n=2.

coating	turbidity	subvisible particles
placebo buffer	- 4.4%	n.d.
1% BSA	- 2 %	- 16 %
PEG 400	- 11 %	- 18 %

The procedure of aerosol collection has a significant impact on subsequently generated protein stability data. An unsuitable method may corrupt results, e.g. falsely attribute protein degradation to nebulization that actually resulted from the collection process. It is therefore crucial to carefully select and exclusively use one collection procedure to obtain meaningful and comparable datasets. Aerosol cloud collection in 2 mL PP tubes interfered least with protein stability and was therefore chosen as the standard procedure for all further experiments involving aerosol cloud collection.

4 Impact of vibrating mesh nebulization on protein stability

4.1 Introduction

Previous investigations yielded evidence for a significant rise of the temperature inside the reservoir (T_{RES}) of the PARI eFlow® during operation (section 3.2). The temperatures reached toward the end of nebulization can be detrimental for thermolabile protein drugs, provoking the loss of therapeutic activity and potentially leading to aggregation, which may result in unwanted side effects like increased immunogenicity [48, 49]. In contrast, various authors state that heating of the drug reservoir inside the VM nebulizer is limited and less pronounced as compared to US nebulizers [50, 51]. Therefore, eFlow® operation was investigated with respect to heating and the T_{RES} profile within the reservoir was recorded.

Temperature may not only influence the stability of the nebulized proteins as reported for US nebulizers or for vibrating mesh spray drying but also seems to have an effect on the characteristics of the generated aerosol via temperature dependent viscosity changes. Additionally, degradation of nebulized proteins may have dramatic consequences for the proper aerosol generation by VM nebulization due to occlusion of the mesh apertures (section 2.6). The prevention of protein degradation is therefore a prerequisite for efficient VM nebulization.

The relevance of thermal stress for protein degradation during VM nebulization was investigated with proteins of different susceptibility to thermal degradation. The contribution of thermal stress was discriminated from other stress factors relevant for VM nebulization. This is mainly

interfacial stress by the atomization immanent creation of a vast new air/liquid interface [37, 45], whereas shear or cavitation [52] by the mesh vibration have been ruled out.

In order to benefit from the advantages of VM nebulization with thermolabile protein drugs, different ways to prevent or reduce heating during nebulization were investigated. These approaches included simple 'passive' procedures to reduce reservoir heat-up, like nebulization of pre-cooled solutions, nebulizer pausing to cool down as well as reservoir overloading, i.e. nebulization of only a fraction of the loaded volume. Furthermore, active cooling of the nebulizer reservoir with a micro Peltier element was tested. All nebulization procedures were evaluated with respect to their capability to reduce T_{RES} during operation as well as their impact on nebulizer performance. Protein degradation after nebulization and the contribution of thermal stress were studied for three different proteins. Lactic dehydrogenase (LDH) served as a model protein, due to its sensitivity toward thermal and interfacial stress during nebulization [53, 54] and the availability of an activity assay. An IgG1 antibody was employed to investigate the effects of cooled nebulization on a more thermostable protein. Finally, the feasibility to protect SM101 during nebulization was tested. SM101 is rather sensitive to elevated temperatures, wherefore control of T_{RES} during VM nebulization appears highly important.

4.2 Temperature during operation

4.2.1 Impact of initial load on temperature profile

The temperature profile of the PARI eFlow® was measured in dependence of the initial reservoir load (IL) (1 mL, 2 mL, 3 mL or 4 mL saline). The IL had a significant impact on the reservoir temperature (Figure IV-13 A). Although the OR was constant and smaller volumes were nebulized in shorter times, the maximum reservoir temperature ($T_{RES\,MAX}$) only slightly increased with increased IL. Consequently, the average heating rate is inversely proportional to the IL (Figure IV-13 B). Energy dissipated from the circular piezo element heats the metallic substrate and the attached membrane to temperatures above 40°C almost immediately upon commencing operation and steadily rises with advancing nebulization. While a T_{RES} of 40°C is only reached toward the end of nebulization, this temperature stress during nebulization with a VM nebulizer may already be detrimental for thermolabile proteins of low T_m.

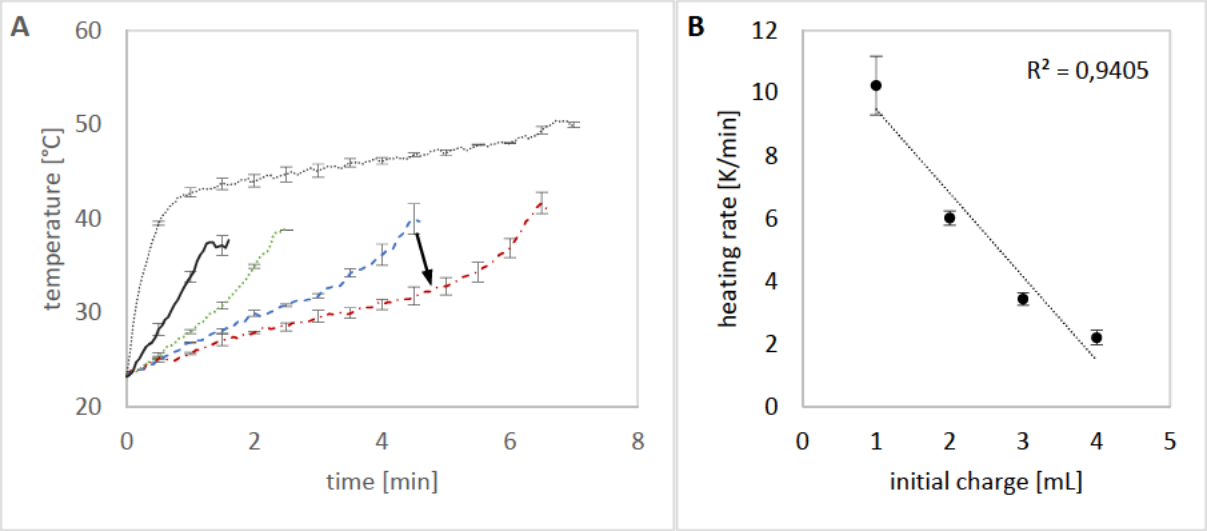

Figure IV-13, A: Progression of T_{RES} during nebulization of 1 mL (black solid line), 2 mL (green dotted line), 3 mL (blue dashed line) or 4 mL (red dot dashed line) saline and the temperature of the vibrating membrane during nebulization of 4 mL saline (dotted) with a PARI eFlow®, n≥3 (mean ± SD, error bars are displayed every 30 s to retain clarity). The arrow indicates the reduction of T_{RES} after the nebulization of 3mL saline with an initial load of 4 mL instead of 3 mL. B: Correlation of the heating rates to the initial reservoir load (R^2=0.9405), n≥3 (mean ± SD).

4.3 Effects of procedures to reduce reservoir heating during nebulization on reservoir temperature

In order to be able to nebulize temperature sensitive proteins with the PARI eFlow®, various modifications to the nebulization procedure were compared for their capability to reduce T_{RES} during nebulizer operation. One approach can be deduced from the observed dependency of the heating rate on IL. If 4 mL saline is loaded into the reservoir, of which only 3 mL are nebulized, T_{RES} should stay well below 35°C compared to approximately 40°C if only 3 mL had been loaded and nebulized (Figure IV-13 A, T_{RES} after nebulization of 3 ml marked by the arrow). Normal nebulization of 3 mL saline (Figure IV-13 A and Figure IV-14 A) served as a reference exhibiting a $T_{RES\ MAX}$ of 42.7°C and an average reservoir temperature ($T_{RES\ AVG}$) of 32.6°C (Table IV-5). In contrast, with reservoir overloading (OL) a $T_{RES\ MAX}$ of only 33.3 °C was reached. The moment for premature abortion of nebulization can be determined via the nebulization time. Alternatively, a reservoir with a built-in retained volume, as implemented in the PARI eFlow rapid®, may be used. The eFlow rapid® reservoir is designed to retain approximately 1 mL, thus mimicking common jet nebulizers to avoid patient overdosing [55]. The reduction of reservoir heat up may have been an additional reason for this design.

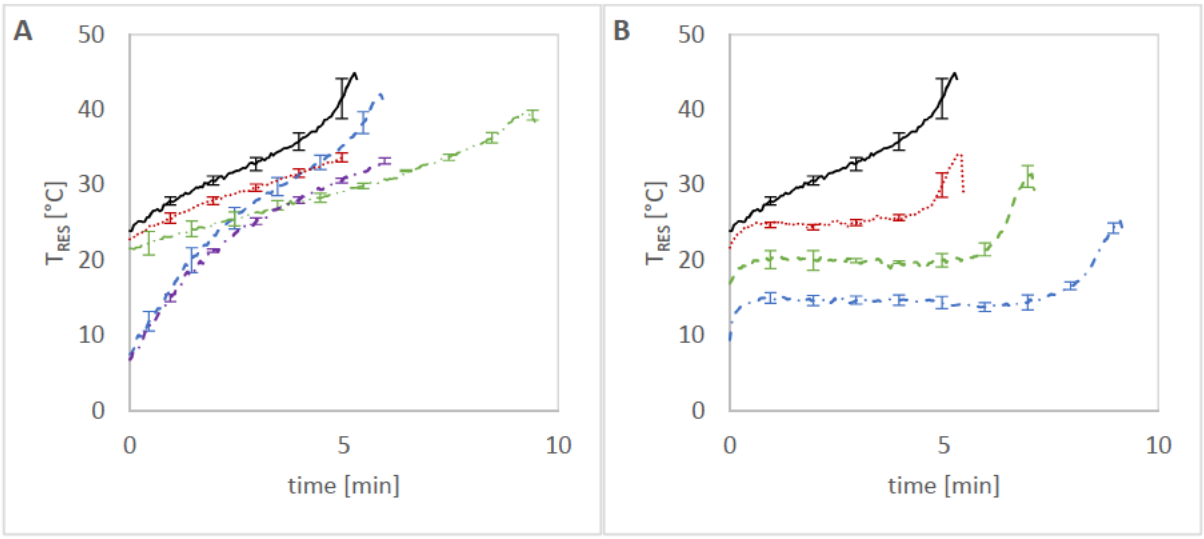

Figure IV-14: T_{RES} progression for different nebulization procedures. A: 'Passive' procedures include normal nebulization (black solid line), nebulization of pre-cooled solutions (PC, blue dashed line), reservoir overloading (OL, red dotted line), intermittent mode (IM, green double dot dashed line) and a combination of pre-cooling and overloading (PC-OL, purple dot dashed line). B: Active cooling during nebulization at 25°C (red dotted line), 20°C (green dashed line) and 15°C (blue dot dashed line) is compared to normal nebulization (black), n≥3 (mean ± SD, error bars are displayed every 60s to retain clarity).

Another obvious method which may enable to limit T_{RES} increase during nebulization, is to charge previously cooled solution (PC) into the nebulizer and immediately start operation. Since refrigerated storage of nebulizer solutions is usually required, this approach can easily be integrated into the normal routine. Nebulization of pre-cooled saline effectively reduced $T_{RES\ AVG}$ to 27.4°C by lowering the starting temperature. This had only little impact on $T_{RES\ MAX}$ due to an increased heating rate (Figure IV-14 A, Table IV-5).

A method previously described for ultrasonic nebulizers [34, 40] to limit warming of the reservoir includes automatic or manual pausing of nebulization upon reaching a threshold temperature and commencing operation after device cool down. Instead of pausing at the threshold temperature, the approach may be adapted to an intermittent mode, i.e. switching between short phases of operation and pausing during nebulization, thus resembling the mode of operation already implemented in breath controlled nebulizers. Using the nebulizer in an intermittent mode (IM) did not have great impact on neither $T_{RES\ MAX}$ nor $T_{RES\ AVG}$, which is in accordance with in lab experiences made with a respectively operating device (Activaero AKITA² APIXNEB®).

All these approaches may also be combined to achieve an even greater reduction of T_{RES}. Correspondingly, the combination of overloading the reservoir with pre-cooled solution (PC-OL) led to the most effective temperature reduction. $T_{RES\ MAX}$ and $T_{RES\ AVG}$ decreased to 31.2°C and 24.2°C respectively (Figure IV-14 A, Table IV-5).

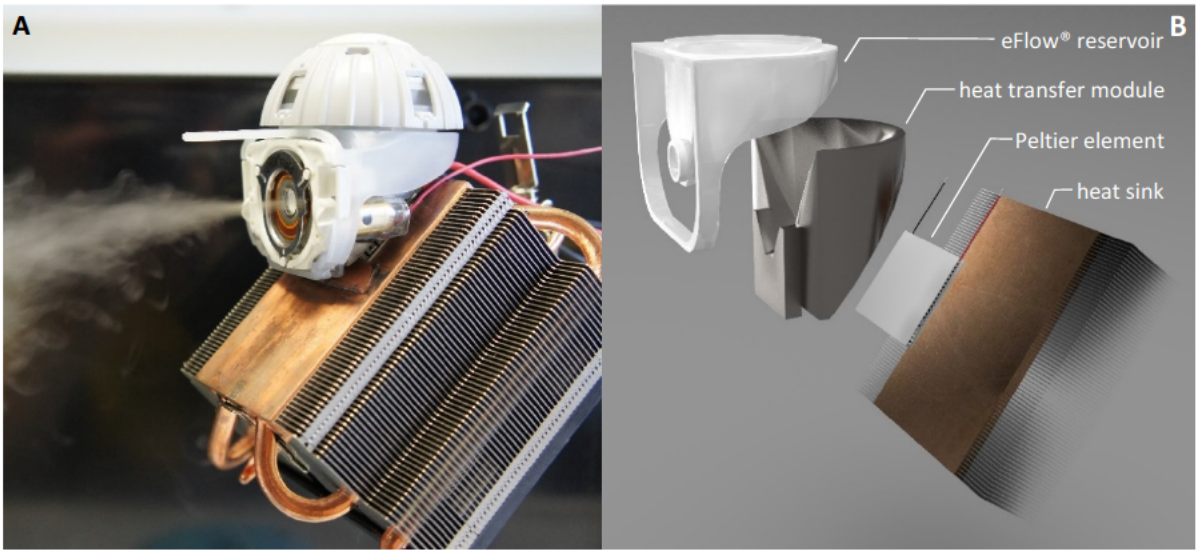

Figure IV-15: Actively cooled nebulizer in operation (A). Exploded view of the Peltier cooler setup (B): eFlow® reservoir, custom molded metallic heat transfer module, Peltier element and heat sink.

Besides these simple methods to manipulate T_{RES}, the feasibility of actively cooling the eFlow® reservoir was investigated. Active cooling was based on the use of a micro Peltier cooled eFlow® reservoir (Figure IV-15). With active cooling, a defined temperature could be set and kept constant throughout most of the operation, which was demonstrated for 25°C, 20°C and 15°C (Figure IV-14 B, Table IV-5). The reduction of the liquid level inside the reservoir with ongoing nebulization led to continual loss of contact area to the Peltier cooled back of the reservoir while the contact to the heating membrane remained unchanged. This was compensated by a gradual increase in Peltier performance. Toward the end of nebulization, T_{RES} sharply increased as Peltier performance was at the maximum and the contact area between the remaining solution and the cooled parts of the reservoir became too small to provide sufficient cooling. Therefore, $T_{RES\ MAX}$ values ranged 9-12°C above the predefined $T_{RES\ AVG}$.

Thus, a significant reduction in heat generation during nebulization is achievable by simple means including solution pre-cooling and reservoir overloading. Best control over T_{RES} was provided by active micro Peltier based cooling, enabling constant nebulization temperatures over most of the nebulization period. Combining active cooling with reservoir overloading would prevent the sharp rise toward the end of nebulization.

Table IV-5: Maximum ($T_{RES\ MAX}$) and average reservoir temperature ($T_{RES\ AVG}$) observed during nebulization of 4mL saline with a PARI eFlow® and different cooling procedures, n=3 (mean ± SD). Pre-cooling (PC), overloading (OL), intermittent operation (IM).

	$T_{RES\ MAX}$ [°C]	$T_{RES\ AVG}$ [°C]
normal	42.7 ± 2.3	32.6 ± 1.2
passive cooling		
PC	39.8 ± 2.6	27.4 ± 0.4
OL	33.3 ± 0.9	28.6 ± 0.5
IM	38.8 ± 0.8	30.4 ± 0.5
PC-OL	31.2 ± 1.9	24.2 ± 0.3
active cooling		
25°C	34.2 ± 0.1	25.5 ± 0.2
20°C	31.6 ± 1.8	21.7 ± 0.7
15°C	27.1 ± 1.4	15.8 ± 0.8

4.4 Effects of procedures to reduce reservoir heating during nebulization on aerosol performance

The recorded temperature profiles also revealed an impact of T_{RES} manipulation on nebulization time and thus nebulizer performance (Figure IV-14). Delivery efficiency (DE), OR and the resulting inhaled aerosol rate (IAR) were consequently assessed in dependence of the cooling procedures. The IAR is the principal measure regarding treatment time. As prolonged treatment times may have a negative impact on life quality of chronically ill patients and are associated with reduced compliance [7, 8], IAR was included into nebulizer performance evaluation. An acceptable procedure to reduce T_{RES} should not markedly reduce IAR or DE.

Manipulating T_{RES} had a distinct impact on OR and on DE (Figure IV-16). OR correlated with $T_{RES\ AVG}$ changes (R^2=0.8766). DE on the other hand correlated inversely with $T_{RES\ AVG}$ (R^2=0.9488). As a result, $T_{RES\ AVG}$ impact on IAR (R^2=0.5498) is largely compensated by the opposing effects on OR and DE. Only if the nebulizer is operated below a $T_{RES\ AVG}$ of 20°C, the negative influence on OR dominates, leading to a decreased IAR. Interestingly, neither DE (R^2=0.6153) nor OR (R^2=0.4599) correlate well with reservoir $T_{RES\ MAX}$. It has been shown previously that a higher solution viscosity decreases OR and increases DE of VM nebulizers (section 2). Given that lowering $T_{RES\ AVG}$ will result in a viscosity increase in the nebulized solution, a correlation described by the empirical Arrhenius-Andrade equation [24], the declining OR and rising DE can be explained by temperature induced viscosity changes. As previously

mentioned, this correlation also explains the impact of rising T_{RES} on the time resolved changes in OR and DE observed in section 2.5.

Manipulating T_{RES} for the sake of protein stability has the advantage to increase DE (Figure IV-17 B). This effect is particularly significant for active cooling to 20°C or below. The OR, on the other hand, remained unaffected unless T_{RES} was actively cooled to 15°C or 20°C. In this case, a significant drop in OR was observed (Figure IV-17 A). As a result, the IAR remained comparable for all nebulization methods except nebulization at 15°C, where the OR decrease is more pronounced than the distinct DE increase can compensate for. Although this apparent decline of IAR is not quite statistically significant (Figure IV-17 C). Of the simple 'passive' temperature reduction approaches, PC-OL seems the most promising as it rendered the best T_{RES} reduction and improved DE by 6% while maintaining IAR at the rate of normal nebulization.

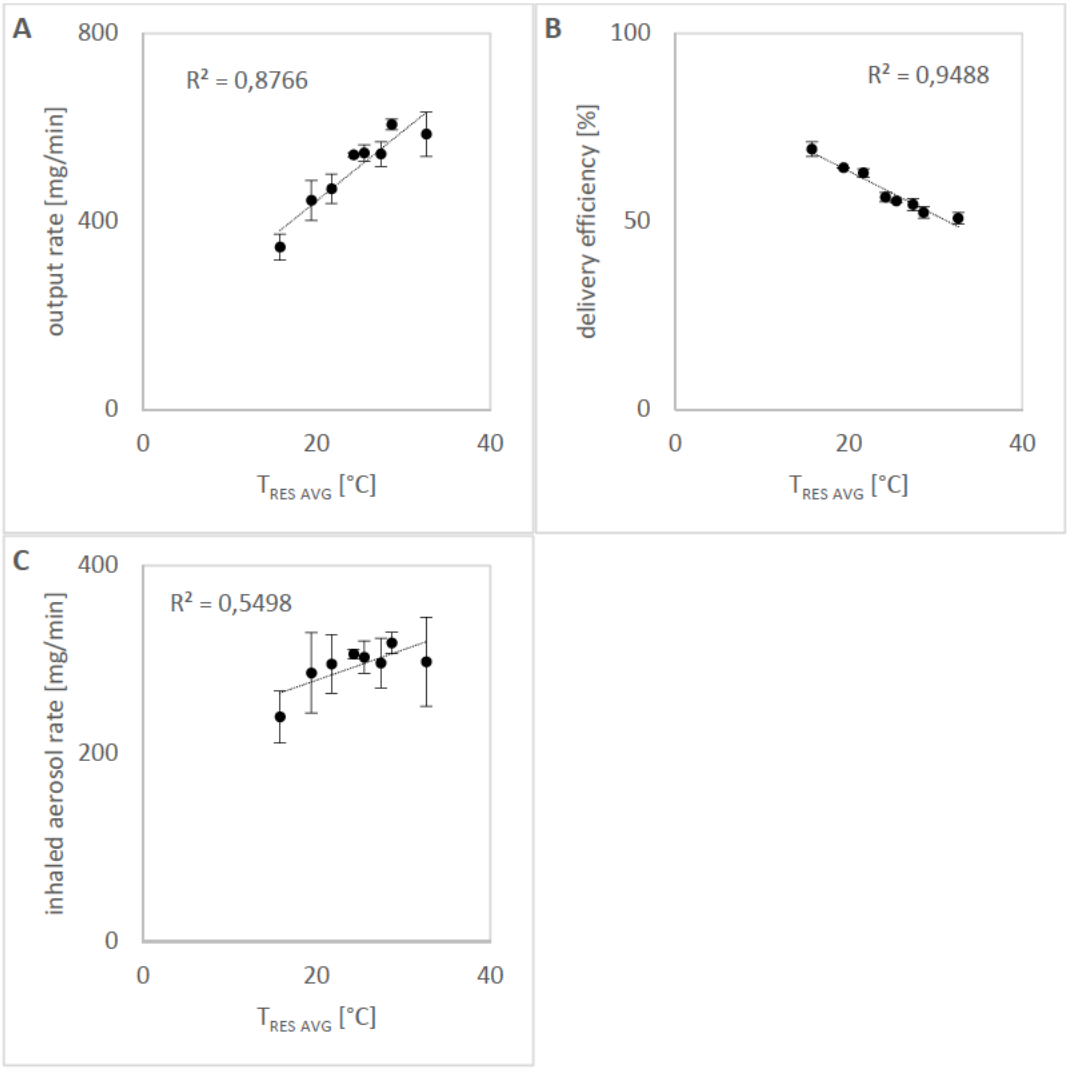

Figure IV-16: Correlation of $T_{RES\ AVG}$ to output rate (A, R^2=0.8766), delivery efficiency (B, R^2=0.9452) and inhaled aerosol rate (C, R^2=0.5758) respectively, n≥3 (mean ± SD).

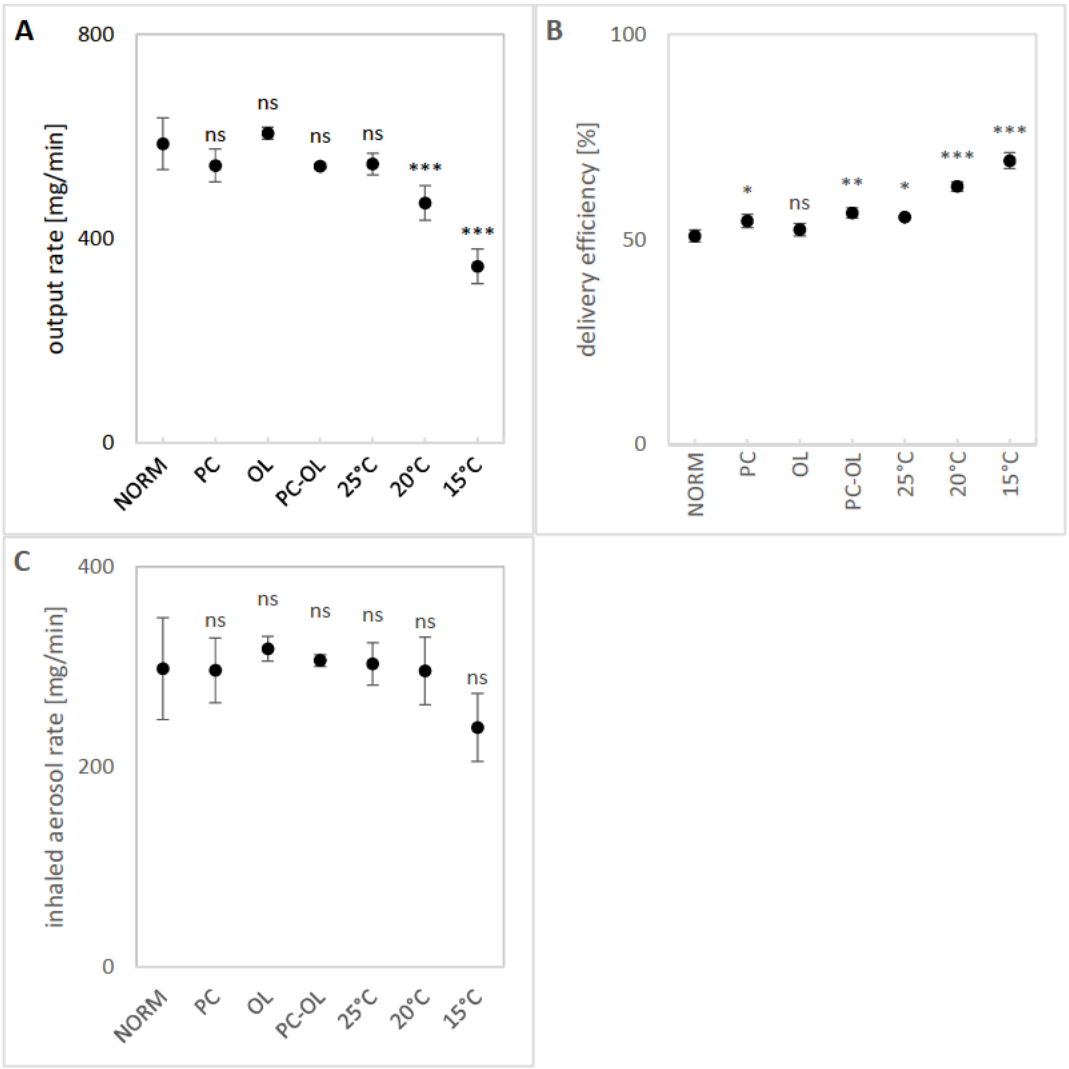

Figure IV-17: Impact and significance levels of tested nebulization procedures on output rate (A), delivery efficiency (B) and inhaled aerosol rate (C) for the nebulization of 4 mL saline with a PARI eFlow®, n=3 (mean ± SD).

Comparably beneficial nebulization conditions were observed for active cooling to 25°C. A further reduction in T_{RES} to 15°C increased DE by 18% at the expense of a 20% reduced IAR. The effect of reduced T_{RES} on protein stability upon nebulization was therefore investigated for PC-OL and active cooling to 15°C, with normal nebulization serving as reference.

4.5 Impact of regular and cooled nebulization on protein stability

To determine protein stability after nebulization, three different proteins were nebulized and assessed for remaining protein activity, monomer content and formation of soluble or insoluble aggregates. LDH served as a model protein that is very sensitive to the interfacial and thermal stress of nebulization [53, 54]. The sensitivity to thermal stress was also expressed in a T_m of 58.6°C as determined by differential scanning calorimetry. An IgG1 antibody was chosen as a

model protein with reported sensitivity to interfacial stress [3, 56, 57] but higher thermal stability and a T_m of 76.8°C. Additionally, degradation of SM101 with a T_m of 57.6°C was analyzed.

4.5.1 Impact of normal and cooled nebulization on protein aggregation

Initially, the contribution of thermal and interfacial stress to the aggregation of the three proteins during nebulization was investigated. Therefore, the protein solutions were nebulized either under normal conditions or at a constant T_{RES} of 15°C while turbidity was monitored by fractionated aerosol collection and analysis.

Upon nebulization under normal conditions, the turbidity of the LDH solution instantly increased to 69 mAU (Figure IV-18 A). With ongoing nebulization the turbidity linearly increased with rising T_{RES} and ended in a sharp rise up to 344 mAU for the last 400 µL nebulized.

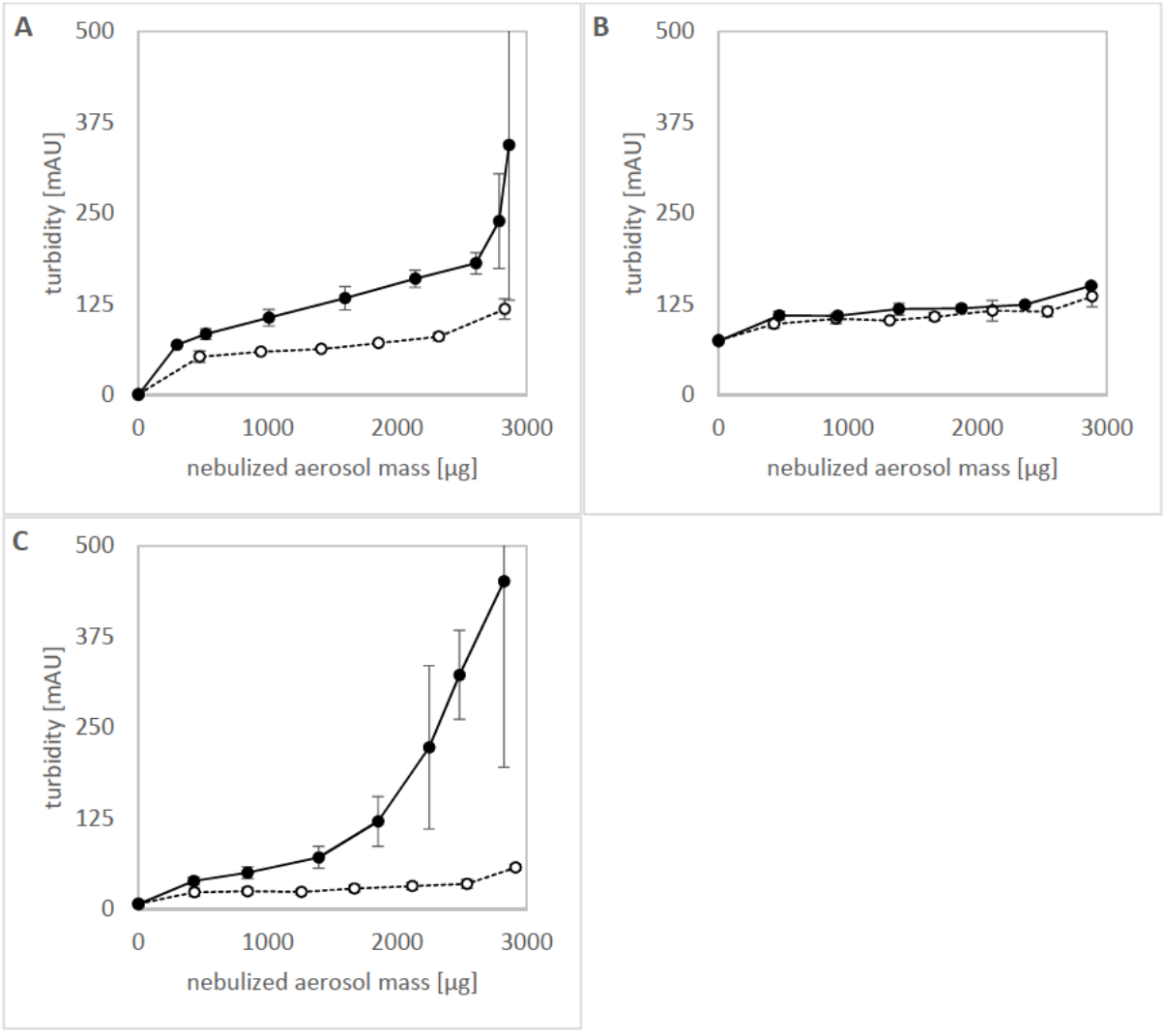

Figure IV-18: Progression of turbidity during nebulization of LDH (A), IgG1 (B) and SM101 (C) with normal nebulization (filled circles, solid line) or active cooling to 15°C (empty circles, dashed line), n=3 (mean ± SD).

When nebulized in the absence of thermal stress at 15°C, turbidity also initially rose above 50 mAU, while the further increase throughout nebulization was reduced and reached a maximum of only 118 mAU. In contrast, the extent of IgG1 aggregation after nebulization was not altered by active cooling (Figure IV-18 B). Regardless of T_{RES}, turbidity immediately increased by 35 mAU and only slowly increased during further nebulization by a maximum of 76 mAU. The initial rise in turbidity was less pronounced for SM101 but with increasing T_{RES} the increase in turbidity was very distinct, reaching turbidity values above 400 mAU (Figure IV-18 C). When thermal stress was mitigated by active cooling, SM101 aggregation during nebulization was almost completely prevented.

This data suggests that LDH aggregation is promoted by both thermal and interfacial stress of VM nebulization. Interfacial stress occurred instantly upon aerosol droplet generation and remained constant throughout operation. It is responsible for the immediate jump in turbidity and the constant turbidity throughout cooled nebulization. In contrast, the extent of thermal aggregation increased with increasing T_{RES} leading to rising turbidity for normal but not for cooled nebulization. IgG1 did not suffer from thermal stress during nebulization but exhibited constant turbidity values due to aggregation by interfacial stress. On the other hand, interfacial stress did not seem to contribute to SM101 aggregation during nebulization. Instead, thermal stress was the detrimental force. The susceptibility to thermal degradation and the resulting benefit from cooled nebulization can be predicted by the proteins T_m value. The use of T_m to predict nebulization stability of proteins was also suggested by Zeles-Hahn et al. [58]. Interestingly, thermal degradation of LDH and SM101 occurred at temperatures below their T_m, which confirms reports that onset temperatures for protein unfolding are considerably lower at the air-liquid interface than for bulk solutions [46]. Thermal and interfacial stress have also been reported responsible for LDH degradation during vibrating mesh spray drying, whereas potential cavitation by mesh vibration did not cause any harm [59].

While protein aggregation by thermal stress was effectively reduced by cooling, interfacial stress is usually prevented by the addition of protective excipients like nonionic surfactant that protect proteins by surface displacement [3]. The protective capabilities of passive and active cooling procedures were compared to the effect of PS20 addition to formulations of LDH and SM101.

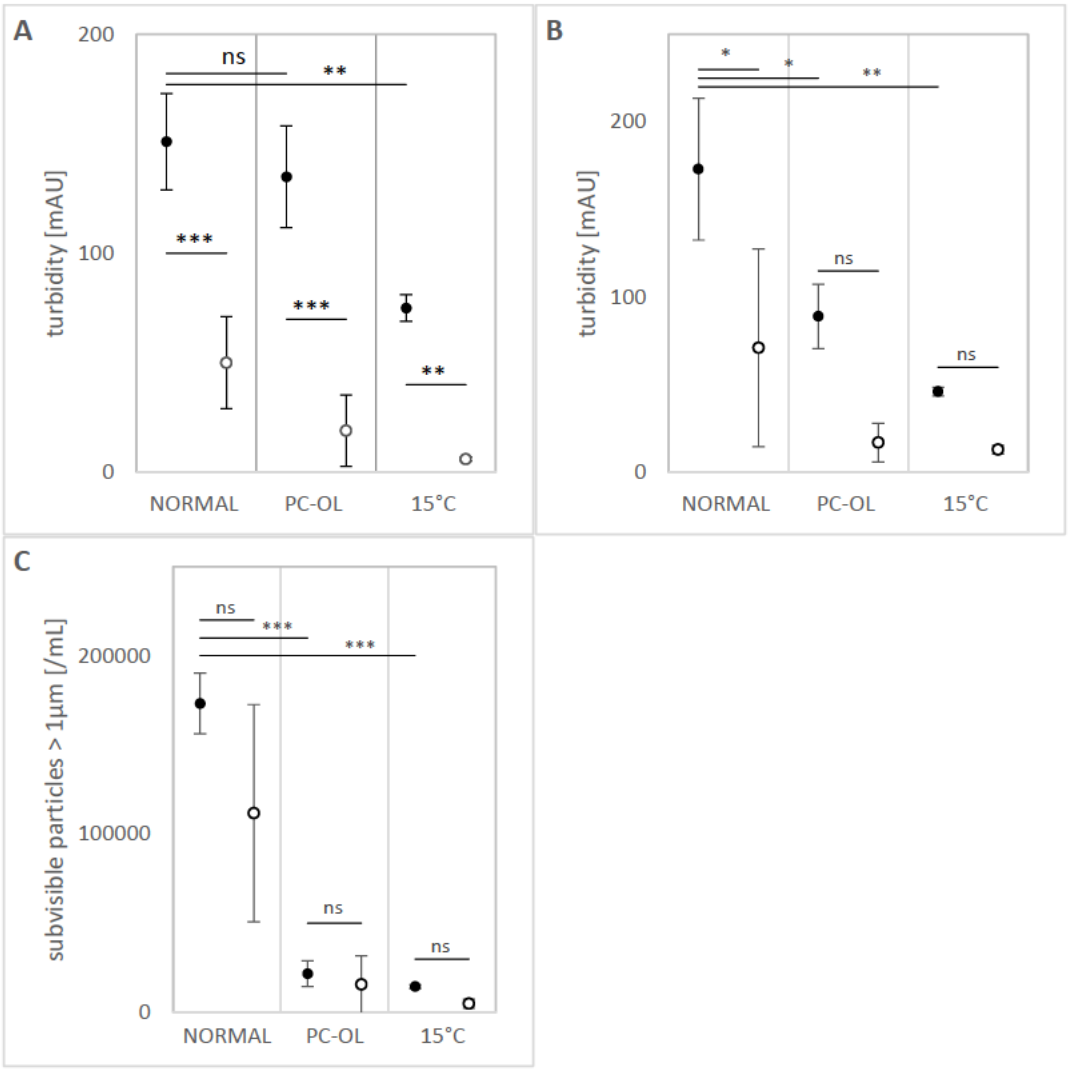

Figure IV-19: Effect and significance levels of passive or active cooling with (empty symbols) and without (filled symbols) addition of polysorbate 20 (PS20) on the aggregation of LDH (A) and SM101 (B and C) in respect to average turbidity (A and B) and subvisible particles > 1µm (C), n=3 (mean ± SD).

Based on polysorbate 80 concentrations protecting proteins during nebulization [37], LDH and IgG formulations were supplemented with 0.1% PS20. For SM101, 0.04% PS20 were added based on excipient screening results (Chapter V).

While cooling did not prevent IgG aggregation, the addition of 0.1% PS20 to the formulation led to a complete stabilization during nebulization with the normal procedure. Therefore, the combination of cooling and PS20 addition was not further tested for IgG.

Addition of PS20 very effectively reduced turbidity for LDH by 70% when nebulized normally (Figure IV-19 A) and the protective effect of PS20 was equally significant when additional passive or active cooling was applied. PC-OL alone did not significantly reduce LDH turbidity while active cooling reduced turbidity by 50%. Combining PS20 and either passive or especially active cooling enabled the almost complete prevention of LDH aggregation.

For SM101, active and passive reduction of T_{RES} are more effective measures to reduce aggregation than PS20 addition. Unlike the addition of 0.04% PS20 that did not cause a significant reduction of subvisible particle levels, both cooling procedures very effectively prevented the formation of subvisible particles (Figure IV-19 C). The extent of turbidity reduction by passive cooling was comparable to the effects of 0.04% PS20, while active cooling was even more protective (Figure IV-19 B). The combined use of active or passive cooling and PS20 most significantly prevented SM101 aggregation during nebulization. Nebulization did not result in the formation of soluble protein aggregates or fragments of LDH or SM101 as determined by size-exclusion chromatography.

For both proteins, cooled nebulization and the addition of a protective excipient are a necessity for the complete prevention of aggregation. As LDH is more sensitive toward interfacial stress, PS20 was very protective, while SM101 benefited more from nebulizer cooling. Active cooling and passive cooling strategies are appropriate for this purpose.

4.5.2 Impact of normal and cooled nebulization on LDH activity

The contribution of thermal and interfacial stress to LDH activity loss during VM nebulization was investigated respectively. Again, LDH was nebulized under normal conditions and at 15°C in the absence of thermal stress. The LDH activity in both the collected aerosol and the reservoir fluid was compared. In the reservoir fluid, LDH molecules are only exposed to thermal stress. When collected after VM nebulization, LDH molecules additionally underwent atomization and interaction with the newly created air/liquid interface.

During normal nebulization more than 25% LDH activity was lost instantly upon nebulization, of which 15% was already lost within the reservoir (Figure IV-20 A). With proceeding nebulization, LDH activity further deteriorated within the reservoir, which also reduced the remaining activity of the collected aerosol. Prevention of reservoir heating preserved the full LDH activity inside the reservoir for half of the nebulization process as shown for 15°C (Figure IV-20 B). Subsequently, LDH activity also decreased in the reservoir. Despite cooling, actual nebulization caused an immediate activity loss of 13% which gradually increased as LDH activity diminished inside the reservoir fluid.

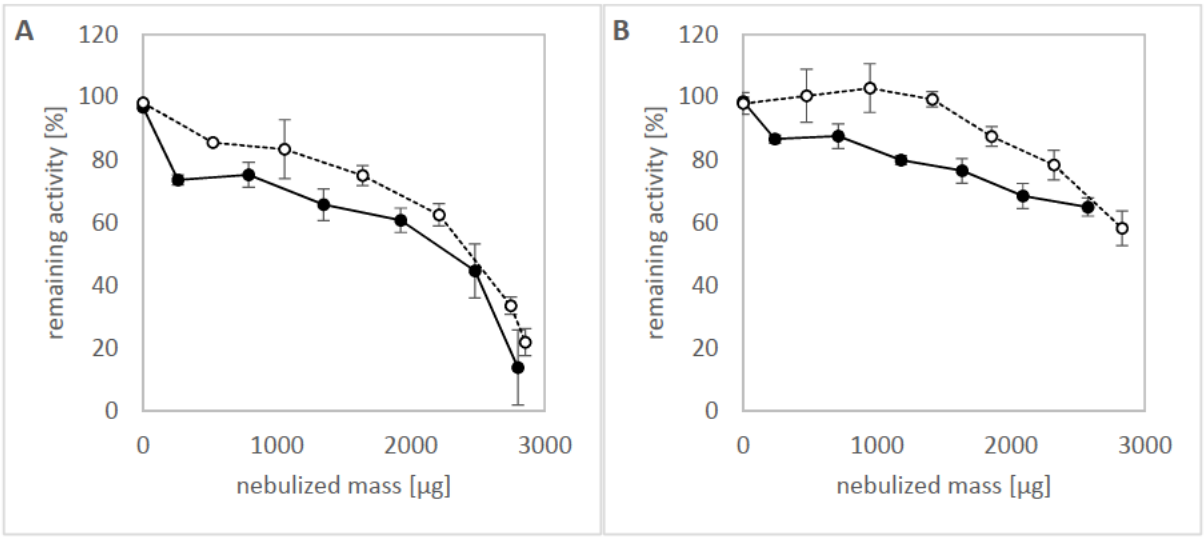

Figure IV-20: LDH activity in the reservoir (empty symbols, dashed line) and in the collected aerosol (filled symbols, solid line) during normal nebulization (A) and at 15°C (B), n=3 (mean ± SD).

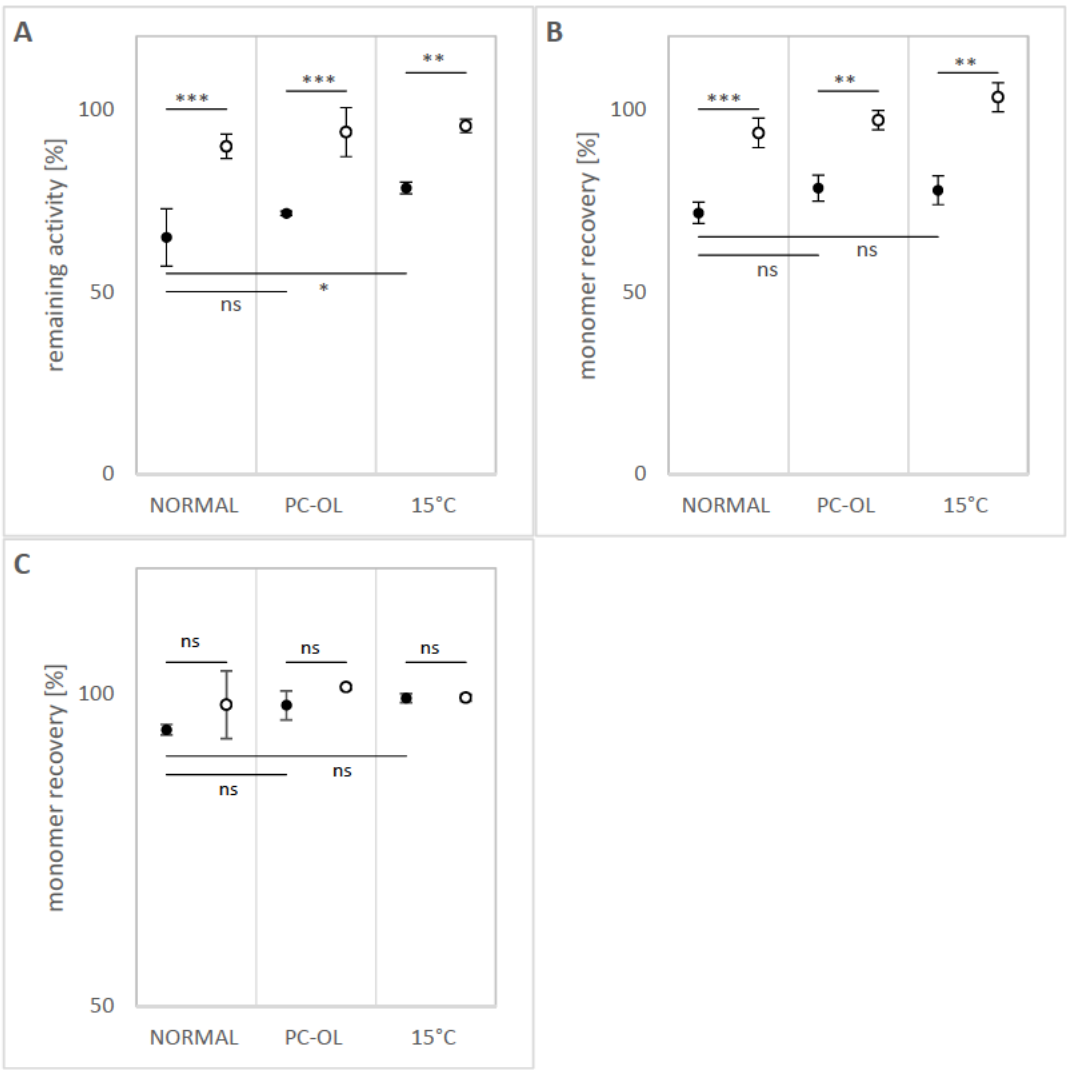

Figure IV-21: Effect and significance levels of passive or active cooling with (empty symbols) and without (filled symbols) addition of polysorbate 20 (PS20) on the activity of LDH (A) and the monomer recovery of LDH (B) and SM101 (C), n=3 (mean ± SD).

Similar to aggregation, LDH activity loss can be attributed to different factors. Thermal stress already occurs inside the reservoir before actual atomization. It increases with ongoing operation and rising T_{RES} and led to rising activity losses with advancing nebulization. Interfacial stress occurs upon actual nebulization and droplet formation and is responsible for an instantaneous but constant activity loss of approximately 13-25%. As witnessed for aggregation, cooling reduces thermal stress but cannot prevent interfacial LDH degradation. The contribution of thermal and interfacial stress to LDH degradation had already been shown with an US nebulizer [53].

The capability to preserve LDH activity during nebulization by passive or active cooling was compared to the stabilizing effects of 0.1% PS20. 35% LDH activity was lost after normal nebulization (Figure IV-21 A). With passive cooling, this loss was reduced to 29%, which was not quite significant due to high variability of remaining activity after normal nebulization. A significant protection of LDH activity was achieved with active cooling, which reduced activity loss to 22%. The addition of 0.1% PS20 to the LDH formulation on the other hand, resulted in very significant protection and reduced activity loss to 10%. Combining passive or active cooling with PS20 addition protected an additional 3.9-5.6% LDH activity respectively. Monomer recovery values confirmed these observations, indicating that loss of LDH monomers was responsible for reduced activity (Figure IV-21 B).

SM101 was much less affected from monomer loss with 94% recovery after normal nebulization (Figure IV-21 C). SM101 monomer loss was reduced below 2% by passive cooling or PS20 addition and below 1% by active cooling, though none of these effects was statistically significant.

Confirming the findings for aggregation, partial protection of LDH can be achieved by either reduction of T_{RES} or the addition of protective excipients but only a combination of both approaches can provide complete protection. Furthermore, the finding that SM101 suffers mostly from thermal stress, while LDH is susceptible to both interfacial and thermal stress, is reflected by the effectiveness of protein stabilization by either cooling or surfactant addition.

4.5.3 Impact of protein stability preserved by cooled nebulization on nebulizer performance

As demonstrated for LDH, cooled nebulization has a protective effect on protein activity (Figure IV-21 A), which in turn also affects the efficiency of nebulization based on the active delivery efficiency (aDE) and the active inhaled aerosol rate (aIAR).

With normal nebulization, 33% of the initially loaded dose remained active and respirable (Figure IV-22 A). The beneficial influence of passive or active cooling on DE and protein activity increased the fraction of active and inhalable protein aerosol to 40% with the PC-OL procedure and to 54% for a constant T_{RES} of 15°C. In other words, when nebulized at 15°C the reservoir may be loaded with 39% less material to deliver an equal dose as via normal nebulization. Although distinct cooling was associated with reduced OR (Figure IV-16A and Figure IV-17A) the time to deliver an equal dose would be unchanged as the aIAR remained comparable for cooled and normal nebulization (Figure IV-22 B).

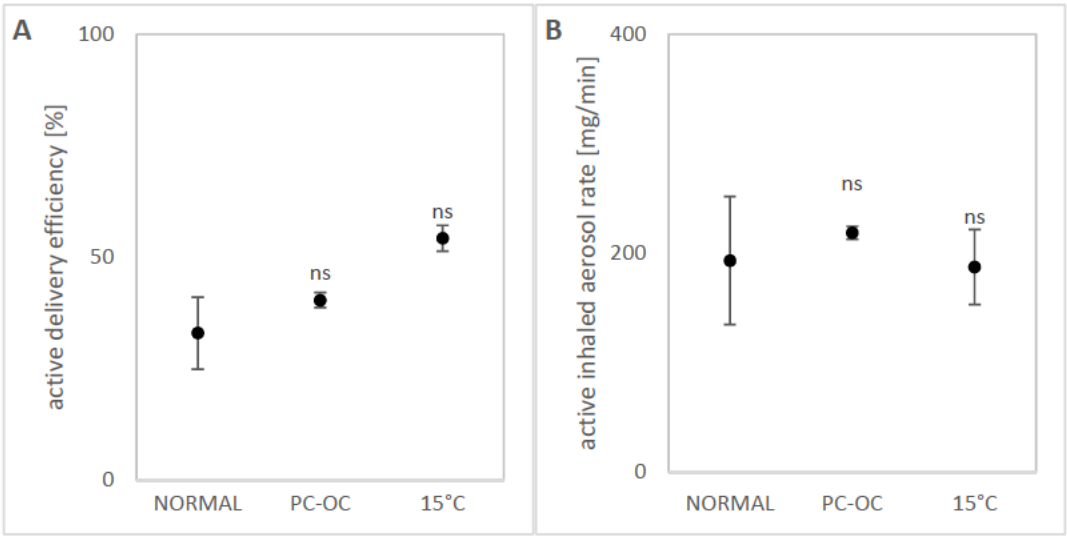

Figure IV-22: Impact and significance levels of normal and cooled nebulization on active delivery efficiency (aDE) (A) and active inhaled aerosol rate (aIAR) (B), n=3 (mean ± SD).

4.6 Conclusion

Despite contrary reports, a significant temperature rise was observed in the reservoir of vibrating mesh nebulizers during operation. To enable the use of advantageous VM nebulization for the pulmonary delivery of thermolabile protein drugs, various approaches to reduce the thermal stress of VM nebulization were evaluated. A simple 'passive' and an active cooling method were each

capable to prevent protein degradation by the thermal stress of VM nebulization without negatively influencing nebulizer performance.

Overloading the reservoir with pre-cooled solution is simple and easy to integrate into nebulization routine. It can significantly improve the stability of nebulized protein drugs by a reduction of T_{RES} as demonstrated for LDH and SM101. Peltier based active cooling is far more capable as it enables full control over T_{RES}, which offers a range of interesting applications. The influence of T_{RES} on aerosol characteristics was investigated. The observed effects can be attributed to temperature dependent viscosity changes. As demonstrated, thermal stress can be completely eliminated from VM nebulization, a capability that was exploited to investigate the contribution of thermal stress to protein degradation during VM nebulization. The relevance of thermal exposure during VM nebulization and the respective benefit from cooling, depend on the proteins susceptibility to thermal degradation, which can be predicted by its T_m. An IgG1 antibody of relative thermostability was not degraded by thermal stress and thus did not benefit from cooling, whilst the thermolabile SM101 was completely protected from severe aggregation by active cooling. LDH on the other hand, was shown to degrade by thermal and interfacial stress. While only the interfacial degradation was containable by surfactant addition, thermal degradation could be prevented by nebulizer cooling.

Cooled nebulization can also improve nebulizer performance as demonstrated for LDH. Higher remaining protein activity and an increased respirable aerosol fraction can reduce API consumption by up to 39%, while maintaining treatment times, an advantage that even stable but valuable drugs may benefit from. PC-OL cooling is readily applicable by any patient/user without additional requirements. The prototype setup for Peltier cooling is feasible for laboratory use and offers several opportunities for optimization, which would allow a more general application. The curved shape of the device reservoir did not allow direct attachment of a Peltier element but required the use of a bulky heat transducer. Better integration of the Peltier element into the reservoir design would allow a much more compact cooler setup. This would improve T_{RES} control, reduce energy consumption and heat dissipation. The already oversized fan cooled heat sink could be replaced by a smaller, passive one further reducing the complexity of the setup. The use of the presented procedures is recommended for the nebulization of thermolabile protein drugs.

5 Summary

The investigations summarized in this chapter aimed to thoroughly characterize vibrating mesh nebulization to provide the necessary prerequisites for efficient nebulization of stable protein solutions. As a result of these investigations, the PARI eFlow® was selected for nebulization, as it generates aerosols of the highest respirable fraction at the highest output rate among the tested devices. It was shown that both proteins and commonly employed excipients may influence the aerosol characteristics when applied in concentrations that markedly alter formulation viscosity. This can potentially improve the delivery efficiency at the cost of a reduced output rate. The temperature dependence of viscosity can explain a comparable impact of the reservoir temperature on nebulizer performance.

Thermal and interfacial stress were identified as the main detrimental factors in vibrating mesh nebulization. The significant temperature rise observed for the PARI eFlow® can prove very detrimental for nebulized proteins, depending on their susceptibility to thermal degradation. Protein unfolding temperatures are a suitable indicator to predict the thread of thermal degradation during vibrating mesh nebulization. In this context, the thermolability of SM101 was confirmed.

While interfacial stress can be controlled by the addition of stabilizing excipients like nonionic surfactants, procedures for the mitigation of thermal stress were proposed. Overloading the reservoir with pre-cooled solution is simple, effective and readily available without further requirements. Alternatively, Peltier based active cooling offers full control over reservoir temperatures and is capable of completely eliminating thermal stress from vibrating mesh nebulization. Use of these methods is recommended for the nebulization of heat sensitive proteins with the PARI eFlow®.

Failing to do so may entail extensive protein aggregation which can disrupt proper nebulizer operation. The responsible mesh occlusion can be detected early with a newly developed method, providing time resolved output rate data. This tool may be useful in the development of suspensions, nanoparticle or liposome formulations for vibrating mesh nebulizers, where obstruction of the membrane is also of concern.

The induction of protein degradation was also observed as a result of several procedures of aerosol cloud collection. While aerosol cloud re-condensation is mandatory for subsequent protein stability analytics, associated protein degradation must be avoided to obtain meaningful stability data. Based on according experiments, aerosol collection in 2 mL polypropylene test tubes was the most appropriate approach for this purpose.

Important prerequisites for protein nebulization have been clarified, so that the specific requirements for the development of inhalable protein formulation may be examined in the following chapter.

6 References

[1] T. Ghazanfari, A.M.A. Elhissi, Z. Ding, K.M.G. Taylor, The influence of fluid physicochemical properties on vibrating-mesh nebulization, International Journal of Pharmaceutics, 339 (2007) 103-111.

[2] J.C. Lee, S.N. Timasheff, The stabilization of proteins by sucrose, Journal of Biological Chemistry, 256 (1981) 7193-7201.

[3] T. Serno, E. Hartl, A. Besheer, R. Miller, G. Winter, The role of polysorbate 80 and HPbetaCD at the air-water interface of IgG solutions, Pharm Res, 30 (2013) 117-130.

[4] F.-C. Lintz, E. Walther, R. Waldner, M. Keller, Influence of viscosity and surface tension on the nebulization efficiency of a jet (LC PLUS) and a vibrating membrane type nebuilzer (e-Flow), in: AAPS Annual Meeting, Denver, 2001.

[5] U. Michaelis, R. Rudolph, G. Winter, H. Woog, Aqueous pharmaceutical preparations of G-CSF with a long shelf life, in, Google Patents, 1999.

[6] E. Ablinger, M. Hellweger, S. Leitgeb, A. Zimmer, Evaluating the effects of buffer conditions and extremolytes on thermostability of granulocyte colony-stimulating factor using high-throughput screening combined with design of experiments, International Journal of Pharmaceutics, 436 (2012) 744-752.

[7] G. Scheuch, M.J. Kohlhaeufl, P. Brand, R. Siekmeier, Clinical perspectives on pulmonary systemic and macromolecular delivery, Advanced Drug Delivery Reviews, 58 (2006) 996-1008.

[8] Z.M. Corden, C.M. Bosley, P.J. Rees, G.M. Cochrane, Home Nebulized Therapy for Patients with COPD Patient Compliance With Treatment and Its Relation to Quality of Life, CHEST Journal, 112 (1997) 1278-1282.

[9] J.P. Mitchell, M.W. Nagel, S. Nichols, O. Nerbrink, Laser Diffractometry as a Technique for the Rapid Assessment of Aerosol Particle Size from Inhalers, Journal of Aerosol Medicine, 19 (2006) 409-433.

[10] A.R. Clark, The use of laser diffraction for the evaluation of the aerosol clouds generated by medical nebulizers, International Journal of Pharmaceutics, 115 (1995) 69-78.

[11] A.J. Hickey, T.B. Martonen, Y. Yang, Theoretical relationship of lung deposition to the fine particle fraction of inhalation aerosols, Pharmaceutica Acta Helvetiae, 71 (1996) 185-190.

[12] R. Tandon, M. McPeck, G.C. Smaldone, Measuring Nebulizer Output Aerosol Production vs Gravimetric Analysis, CHEST Journal, 111 (1997) 1361-1365.

[13] A. Arzhavitina, H. Steckel, Surface active drugs significantly alter the drug output rate from medical nebulizers, International Journal of Pharmaceutics, 384 (2010) 128-136.

[14] O.M. McCallion, K.G. Taylor, M. Thomas, A. Taylor, Nebulization of Fluids of Different Physicochemical Properties with Air-Jet and Ultrasonic Nebulizers, Pharmaceutical Research, 12 (1995) 1682-1688.

[15] O.N.M. Mccallion, K.M.G. Taylor, M. Thomas, A.J. Taylor, Ultrasonic Nebulisation of Fluids with Different Viscosities and Surface Tensions, Journal of Aerosol Medicine, 8 (1995) 281-284.

[16] O.N.M. Mc Callion, M.J. Patel, Viscosity effects on nebulisation of aqueous solutions, International Journal of Pharmaceutics, 130 (1996) 245-249.

[17] O.N.M. Mc Callion, K.M.G. Taylor, M. Thomas, A.J. Taylor, The influence of surface tension on aerosols produced by medical nebulisers, International Journal of Pharmaceutics, 129 (1996) 123-136.

[18] S.S. Davis, Physico-chemical studies on aerosol solutions for drug delivery I. Water-propylene glycol systems, International Journal of Pharmaceutics, 1 (1978) 71-83.

[19] B.A. Salinas, H.A. Sathish, S.M. Bishop, N. Harn, J.F. Carpenter, T.W. Randolph, Understanding and modulating opalescence and viscosity in a monoclonal antibody formulation, J Pharm Sci, 99 (2009) 82-93.

[20] Z. Guo, A. Chen, R. Nassar, B. Helk, C. Mueller, Y. Tang, K. Gupta, A. Klibanov, Structure-Activity Relationship for Hydrophobic Salts as Viscosity-Lowering Excipients for Concentrated Solutions of Monoclonal Antibodies, Pharmaceutical Research, 29 (2012) 3102-3109.

[21] J. Jezek, M. Rides, B. Derham, J. Moore, E. Cerasoli, R. Simler, B. Perez-Ramirez, Viscosity of concentrated therapeutic protein compositions, Advanced Drug Delivery Reviews, 63 (2011) 1107-1117.

[22] M. Mathlouthi, J. Génotelle, Rheological properties of sucrose solutions and suspensions, in: M. Mathlouthi, P. Reiser (Eds.) Sucrose, Springer US, 1995, pp. 126-154.

[23] R. Saggin, J.N. Coupland, Rheology of xanthan/sucrose mixtures at ultrasonic frequencies, Journal of Food Engineering, 65 (2004) 49-53.

[24] E.N.d.C. Andrade, XLI. A theory of the viscosity of liquids. Part I, Philosophical Magazine Series 7, 17 (1934) 497-511.

[25] G. Beck, G.S. Habicht, Invertebrate Cytokinesa, Annals of the New York Academy of Sciences, 712 (1994) 206-212.

[26] K.M. Ahmed, W.-Q. Chen, J. John, S. Kang, G. Lubec, Complete sequencing of the recombinant granulocyte-colony stimulating factor (filgrastim) and detection of biotinylation by mass spectrometry, Amino Acids, 38 (2010) 1043-1049.

[27] K.C. Dee, D.A. Puleo, R. Bizios, Protein-Surface Interactions, An Introduction to Tissue-Biomaterial interactions, (2003) 37-52.

[28] S. Yadav, S.J. Shire, D.S. Kalonia, Viscosity behavior of high-concentration monoclonal antibody solutions: Correlation with interaction parameter and electroviscous effects, J Pharm Sci, 101 (2012) 998-1011.

[29] J.S. Lass, A. Sant, M. Knoch, New advances in aerosolised drug delivery: vibrating membrane nebuliser technology, Expert Opinion on Drug Delivery, 3 (2006) 693-702.

[30] K. Bechtold-Peters, H. Luessen, Pulmonary Drug Delivery: Basics, Applications and Opportunities for Small Molecules and Biopharmaceutics, ECV Editio Cantor Verlag, Aulendorf, 2007.

[31] M. Luisetti, P. Kroneberg, T. Suzuki, Z. Kadija, B. Muellinger, I. Campo, J. Gleske, G. Rodi, W.C. Zimlich, F. Mariani, F. Ferrari, M. Frey, B.C. Trapnell, Physical properties, lung deposition modeling, and bioactivity of recombinant GM-CSF aerosolised with a highly efficient nebulizer, Pulmonary Pharmacology & Therapeutics, 24 (2011) 123-127.

[32] P. Brand, I. Friemel, T. Meyer, H. Schulz, J. Heyder, K. Häu β inger, Total deposition of therapeutic particles during spontaneous and controlled inhalations, J Pharm Sci, 89 (2000) 724-731.

[33] R.W. Niven, Delivery of Biotherapeutics by Inhalation Aerosol, Critical Reviews™ in Therapeutic Drug Carrier Systems, 12 (1995) 151-231.

[34] H. Steckel, F. Eskandar, K. Witthohn, The effect of formulation variables on the stability of nebulized aviscumine, International Journal of Pharmaceutics, 257 (2003) 181-194.

[35] Sylvia Kiese, Astrid Papppenberger, Wolfgang Friess, Hanns-Christian Mahler, Shaken, not stirred: Mechanical stress testing of an IgG1 antibody, J Pharm Sci, 97 (2008) 4347-4366.

[36] Y.Y. Albasarah, S. Somavarapu, K.M.G. Taylor, Stabilizing protein formulations during air-jet nebulization, International Journal of Pharmaceutics, 402 (2010) 140-145.

[37] R.W. Niven, S.J. Prestrelski, M.J. Treuheit, A.Y. Ip, T. Arakawa, Protein nebulization II. Stabilization of G-CSF to air-jet nebulization and the role of protectants, International Journal of Pharmaceutics, 127 (1996) 191-201.

[38] A.M.A. Elhissi, M. Faizi, W.F. Naji, H.S. Gill, K.M.G. Taylor, Physical stability and aerosol properties of liposomes delivered using an air-jet nebulizer and a novel micropump device with large mesh apertures, International Journal of Pharmaceutics, 334 (2007) 62-70.

[39] L. Khatri, K.M.G. Taylor, D.Q.M. Craig, K. Palin, An assessment of jet and ultrasonic nebulisers for the delivery of lactate dehydrogenase solutions, International Journal of Pharmaceutics, 227 (2001) 121-131.

[40] A.Y. Ip, T. Arakawa, H. Silvers, C.M. Ransone, R.W. Niven, Stability of recombinant consensus interferon to air-jet and ultrasonic nebulization, J Pharm Sci, 84 (1995) 1210-1214.

[41] T. Scherer, D.E. Geller, L. Owyang, M. Tservistas, M. Keller, N. Boden, K.C. Kesser, S.J. Shire, A technical feasibility study of dornase alfa delivery with eflow® vibrating membrane nebulizers: Aerosol characteristics and physicochemical stability, J Pharm Sci, 100 (2011) 98-109.

[42] A. Wagner, K. Vorauer-Uhl, H. Katinger, Nebulization of Liposomal rh-Cu/Zn SOD with a Novel Vibrating Membrane Nebulizer, Journal of Liposome Research, 16 (2006) 113-125.

[43] T.W.J. Steele, X. Zhao, P. Tarcha, T. Kissel, Factors influencing polycation/siRNA colloidal stability toward aerosol lung delivery, European Journal of Pharmaceutics and Biopharmaceutics, 80 (2012) 14-24.

[44] M. Beck-Broichsitter, J. Gauss, C.B. Packhaeuser, K. Lahnstein, T. Schmehl, W. Seeger, T. Kissel, T. Gessler, Pulmonary drug delivery with aerosolizable nanoparticles in an ex vivo lung model, International Journal of Pharmaceutics, 367 (2009) 169-178.

[45] Y.-F. Maa, C.C. Hsu, Protein denaturation by combined effect of shear and air-liquid interface, Biotechnology and Bioengineering, 54 (1997) 503-512.

[46] R.J. Green, I. Hopkinson, R.A.L. Jones, Unfolding and Intermolecular Association in Globular Proteins Adsorbed at Interfaces, Langmuir, 15 (1999) 5102-5110.

[47] G. Narsimhan, F. Uraizee, Kinetics of Adsorption of Globular Proteins at an Air-Water Interface, Biotechnology Progress, 8 (1992) 187-196.

[48] J.G. Barnard, K. Babcock, J.F. Carpenter, Characterization and quantitation of aggregates and particles in interferon-beta products: potential links between product quality attributes and immunogenicity, J Pharm Sci, 102 (2013) 915-928.

[49] A. Rosenberg, Effects of protein aggregates: An immunologic perspective, The AAPS Journal, 8 (2006) E501-E507.

[50] J.C. Waldrep, R. Dhand, Advanced Nebulizer Designs Employing Vibrating Mesh/Aperture Plate Technologies for Aerosol Generation, Current Drug Delivery, 5 (2008) 114-119.

[51] J.B. Fink, D. Schmidt, J. Power, Comparison of a nebulizer using a novel aerosol generator with a standard ultrasonic nebulizer designed for use during mechanical ventilation, in: American Thoracic Society 97th International Conference, San Fransisco, CA, 2001.

[52] K. Schmid (2011): Spray drying of protein precipitates and Evaluation of the Nano Spray Dryer B-90. PhD thesis, Ludwig Maximilian University Munich: Faculty of Chemistry and Pharmacy.

[53] R.W. Niven, A.Y. Ip, S. Mittelman, S.J. Prestrelski, T. Arakawa, Some Factors Associated with the Ultrasonic Nebulization of Proteins, Pharmaceutical Research, 12 (1995) 53-59.

[54] R.W. Niven, A.Y. Ip, S.D. Mittelman, C. Farrar, T. Arakawa, S.J. Prestrelski, Protein nebulization: I. Stability of lactate dehydrogenase and recombinant granulocyte-colony stimulating factor to air-jet nebulization, International Journal of Pharmaceutics, 109 (1994) 17-26.

[55] L. Vecellio, The mesh nebuliser: a recent technical innovation for aerosol delivery, Breathe, 2 (2006) 252-260.

[56] C. Mück (2002): Analytik von Proteinaggregation mittels Coulter-Prinzip: Vergleich mit der Lichtblockade-Messung. Diploma Thesis, Ludwig Maximilian University Munich / University of Applied Sciences Albstadt-Sigmaringen, Germany.: Department of Pharmacy.

[57] K. Hellerbrand, A. Papadimitriou, G. Winter, Process for stabilizing proteins, US 6,238,664 B1, issued May 29, 2001.

[58] M. Zeles-Hahn, T.J. Anchordoquy, C.S. Lengsfeld, Observations on the impact of aerosolization on macromolecular therapeutics, in: European Conference on Liquid Atomization and Spray Systems, Como Lake, Italy, 2008, pp. 8-3.

[59] K. Schmid, C. Arpagaus, W. Friess, Evaluation of the Nano Spray Dryer B-90 for pharmaceutical applications, Pharm Dev Technol, 16 (2011) 287-294.

Chapter V Formulation development for vibrating mesh nebulization of pharmaceutical proteins

1 Introduction

The development of protein formulations for the purpose of pulmonary delivery involves some special aspects and limitations to consider. Like any formulation, inhalable protein formulations have to maintain protein stability during production, shelf live and handling. Additionally, proteins have to be protected from the detrimental forces occurring during aerosol generation, in case of vibrating mesh (VM) nebulization this is mainly thermal and interfacial stress (Chapter IV). As observed in chapter IV, stabilization may be achieved by stabilizing excipients and control of the nebulization conditions. Inhalative formulations underlie some restrictions. The pH must be in a range of pH 3.5-8.0 [1] and should ideally be above pH 5.0 [2]. Osmolality in the range of 150-549 mOsmol was well tolerated but isotonicity of pulmonary formulations has been recommended [2]. This limits the maximum concentration of osmotically active excipients often used for protein stabilization (e.g. salts, sugars, polyols) in a formulation. The influence of the formulation on aerosol properties (Chapter IV) has to be considered as well to maintain an efficient aerosol generation. Complicating matters, the range of excipients currently approved for pulmonary delivery is very limited (FDA inactive ingredient database for approved drugs, [3]).

In this chapter, aerosol formulation development is demonstrated at the example of SM101. Initially, a parenteral formulation of highly concentrated SM101 was developed and also tested for nebulization. In a second stage, a method for accelerated testing of nebulizer stress on protein stability was developed and its feasibility evaluated for different proteins. Aerosol formulation development based on this surrogate method was conducted for SM101. Finally the selected lead candidate formulations were tested against VM and jet nebulization.

2 Development of a highly concentrated parenteral formulation for SM101

2.1 Rationale for the optimization of the parenteral formulation

The current parenteral formulation of SM101 has been successfully employed during early phase Ib/IIa clinical trials of Primary Immune Thrombocytopenia (ITP) treatment, yet an increase in SM101 concentration seemed a reasonable approach to satisfy the growing demand of SM101 during upcoming clinical studies. Handling and patient treatment would be facilitated if the required SM101 doses could be delivered in smaller infusion volumes. Additionally, an improved production process for SM101 bulk material has been developed. Direct manufacturing of SM101 bulk material into the parenteral formulation is intended to improve bulk material stability. Therefore, the previous parenteral formulation had to be modified to increase SM101 concentration and provide sufficient freeze/thaw (F/T) stability for storage and shipment in frozen form.

Phosphate buffers, as found in the current formulation, may undergo significant pH shift during freezing [4], which can seriously compromise protein stability [5]. For histidine, buffering at the desired pH of 6.5, much less temperature dependent pH shift was reported [6]. Accordingly, histidine was chosen to replace the phosphate buffer in the formulation. Non-crystallizing cryoprotectants can reduce protein degradation during phase transition between the liquid and the frozen state [6]. The incorporated mannitol partially crystallizes during freezing [7] and may therefore not provide optimum SM101 F/T protection. Sucrose seemed to be a more appropriate excipient for cryoprotection and has already proven SM101 stabilizing potential during early formulation studies.

At the site of SuppreMol (Martinsried, Germany) in cooperation with Thomas Pohl, three formulation candidates were prepared at 10 and 20 mg/mL SM101 and evaluated regarding F/T stabilization and accelerated stability studies at 25°C and 40°C. Based on the current formulation, containing a phosphate buffer, 150 mM NaCl, 2% mannitol and 0.005% polysorbate 20 (PS20), formulation candidate A replaced the phosphate buffer by 20 mM histidine, pH 6.5 while the rest of the composition remained unchanged. Additional incorporation of 2% sucrose

and reduction of mannitol content to 1% was implemented in formulation candidate B. Finally candidate C was designed as a liquid formulation which would allow switching to lyophilization if necessary during later stages of the project. It was therefore formulated without NaCl but 6% sucrose and 2% mannitol instead (Table V-1).

Table V-1: SM101 formulations used throughout the experiments.

Formulation	Excipients	Concentration		Experiments
		mg/mL	mM	(SM101 concentration in mg/mL)
drug product (DP)	NaH_2PO_4	0.731	5.3	Chapter V:
	KH_2PO_4	0.272	2.0	parenteral formulation
	NaCl	8.766	150	development (5.0)
	D-Mannitol	20.0	109.8	
	Polysorbate 20	0.05	0.04	
histidine buffered saline (HBS)	L-Histidine	3.103	20.0	Chapter IV:
	NaCl	8.766	150.0	aerosol cloud collection (3.0)
				T_m and T_{agg} measurement (1.0)
				Chapter V:
				surrogate screening method (5.0)
				excipient screening (2.0 or 8.0)
candidate A	L-Histidine	3.103	20.0	Chapter V:
	NaCl	8.766	150.0	parenteral formulation
	D-Mannitol	20.0	109.8	development (10.0 or 20.0)
	Polysorbate 20	0.05	0.04	
parenteral formulation = candidate B	L-Histidine	3.103	20.00	Chapter IV:
	NaCl	8.766	150.00	T_m measurement (1.0)
	D-Mannitol	10.000	54.90	Chapter V:
	Sucrose	20.000	58.40	parenteral formulation
	Polysorbate 20	0.050	0.04	development (10.0 or 20.0)
				excipient screening (2.0 or 8.0)
				AKITA² nebulization (20.0)
candidate C	L-Histidine	3.103	20.0	Chapter V:
	D-Mannitol	20.0	109.8	parenteral formulation
	Sucrose	60.0	175.3	development (10.0 or 20.0)
	Polysorbate 20	0.05	0.04	
candidate 1	L-Histidine	3.103	20.00	Chapter V:
	NaCl	8.766	150.00	AKITA² nebulization (10.0 or 20.0)
	D-Mannitol	10.000	54.90	
	Sucrose	20.000	58.40	
	Polysorbate 20	0.400	0.32	
aerosol formulation (AF) = candidate 2	L-Histidine	3.103	20.00	Chapter V:
	NaCl	4.383	75.00	AKITA² nebulization (10.0)
	D-Mannitol	13.333	73.20	Chapter VI:
	Sucrose	26.667	77.90	MicroSprayer® (0.25, 0.5, 1.0)
	Polysorbate 20	0.400	0.32	Aeroneb® Pro nebulization (10.0)
				in vivo experiments (10.0)

2.2 Freeze / thaw stability

Samples of each formulation were subjected to 0, 1, 2, 4 or 6 F/T cycles and SM101 stability was assessed in respect to SM101 recovery and visible and subvisible aggregation.

2.2.1 SM101 content by UV280 and SE-HPLC

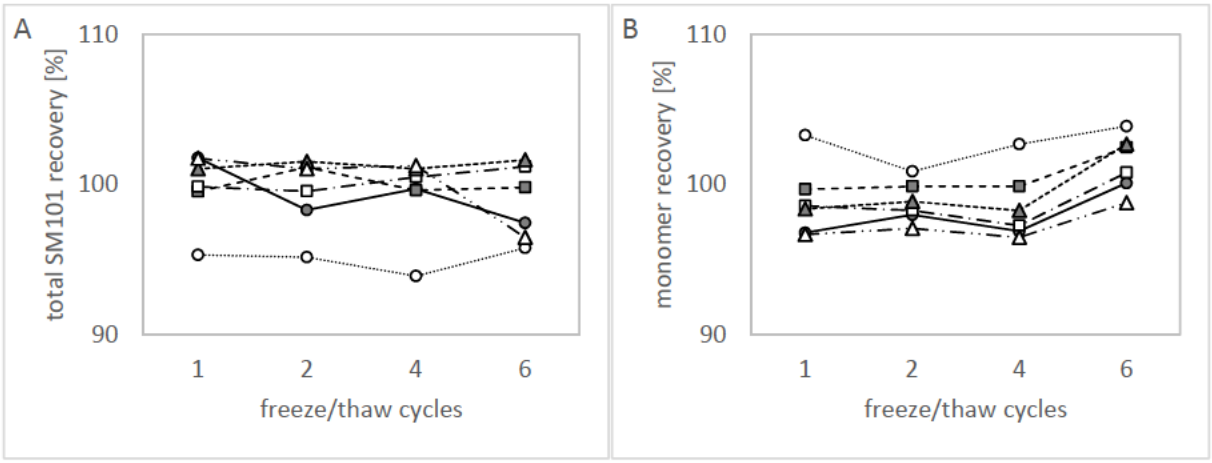

Figure V-1 A: Total SM101 recovery (UV/Vis) and B: monomer recovery (SE-HPLC) after 1, 2, 4 or 6 F/T cycles relative to unstressed reference samples (=100%) for the formulation candidates A (circle), B (square) and C (triangle) at 10 mg/mL (filled symbols) or 20 mg/mL SM101 (empty symbols) (n=1).

SM101 concentration after F/T remained unchanged for all formulations, except formulation A at 20 mg/mL SM101 (Figure V-1 A). There, SM101 content decreased by 5% after one F/T cycle but maintained this concentration after additional cycles. Taking into account, that this loss was not confirmed by SE-HPLC monomer recovery (Figure V-1 B), it was likely due to a mistaken preparation of the A20 sample instead of actual SM101 degradation. According to monomer recovery, no significant amounts of SM101 monomer were lost in any formulation after up to 6 F/T cycles.

2.2.2 SM101 aggregation

*Table V-2: Visual inspection scores after F/T cycles (mean of two observers); * changed into a score of 10 after 24h storage at 4°C.*

F/T cycles	*A 10 mg/mL*	*A 20 mg/mL*	*B 10 mg/mL*	*B 20 mg/mL*	*C 10 mg/mL*	*C 20 mg/mL*
0 (=ref.)	1	0	1	0	0	1
1	0	1	1	0	1	1*
2	0	1	1	0	1	1*
4	1	1	1	1	1	1*
6	1	1	1	1	1	10

F/T stress did not lead to a formation of soluble aggregates in any tested sample. However, the candidates differed in respect to insoluble aggregation. Increasing levels of subvisible particles > 1 µm were formed in formulation A10 with every F/T cycle, reaching more than 33000 particles per mL after 6 F/T cycles. No consecutive increase was found for formulation A20 with no more than 7900 particles per mL or formulation B10 and B20 which kept particle counts below 5000 per mL after up to 6 F/T cycles (Figure V-2 A). Candidates A and B remain within the compendial specifications for particles ≥ 10 µm exceeding no more than 31 or 15 particles respectively and for particles ≥ 25µm with no more than 1 or 10 particles respectively after up to 6 F/T cycles. After visual inspection hardly any visible particles were found in candidate formulations A and B after F/T but also in placebo and in non-frozen reference samples (Table V-2). Consequently, these findings were not assumed relevant regarding SM101 stability.

Unlike the candidates A and B, formulation C could not stabilize SM101 during repeated freeze/thaw cycles. At 20 mg/mL SM101, subvisible particle counts surged with repeated F/T cycles (Figure V-2 B), which was also apparent by visual inspection. Microscopic images revealed that the formed particles were no amorphous aggregates but of crystalline nature (Figure V-3 A). SDS-PAGE analysis of separated and washed precipitate confirmed that crystals were composed of SM101 (Figure V-3 B).

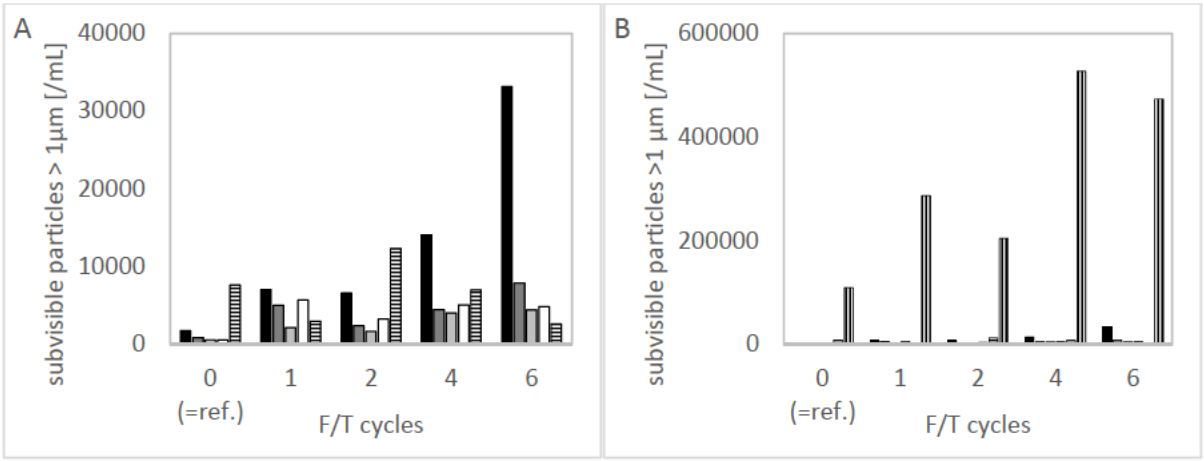

Figure V-2: Subvisible particles > 1µm for formulation candidates A at 10 mg/mL (black) and 20 mg/mL SM101 (dark grey), B at 10 mg/mL (light grey) and 20 mg/mL SM101 (white) and C at 10 mg/mL (horizontal stripes) and 20 mg/mL SM101 (vertical stripes) (n=1). Formulation C at 20 mg/mL is not displayed in figure A.

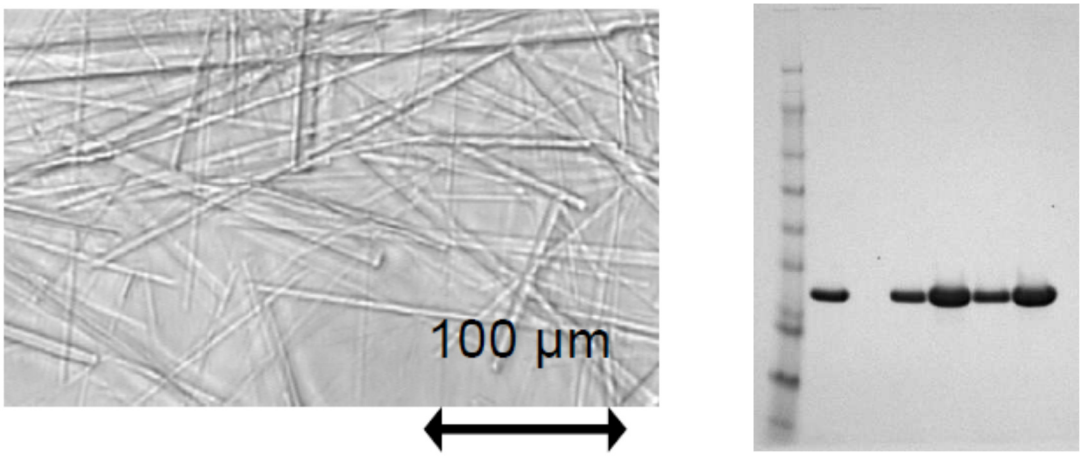

Figure V-3 A: Light-microscopic image of SM101 crystals formed in formulation C at 20 mg/mL SM101. B: SDS-PAGE of soluble and insoluble fraction: lane 1: molecular weight standard, lane 2: 4 µg SM101 reference, lanes 3+5: isolated and washed precipitate from formulation C, lanes 4+6: supernatant from formulation C. Pictures provided by Thomas Pohl (SuppreMol).

2.3 Storage stability

Formulation candidate C was not included into further testing due to the insufficient solubility of SM101. Accelerated storage stability testing was performed for the formulation candidates A and B. Samples were incubated for up to four weeks at 25°C and analyzed after 0, 1, 7, 14 or 28 days. During a one week storage at 40°C, samples were analyzed after 0, 1, 2, or 7 days.

SM101 concentration was analyzed with UV/Vis photometry and confirmed by SE-HPLC monomer recovery. Chemical degradation was assessed with RP-HPLC and charge variants were detected by CEX-HPLC. Soluble aggregates were detected with SE-HPLC, while insoluble aggregates were assessed with light obscuration and visual inspection.

2.3.1 SM101 content by UV280 and SE-HPLC

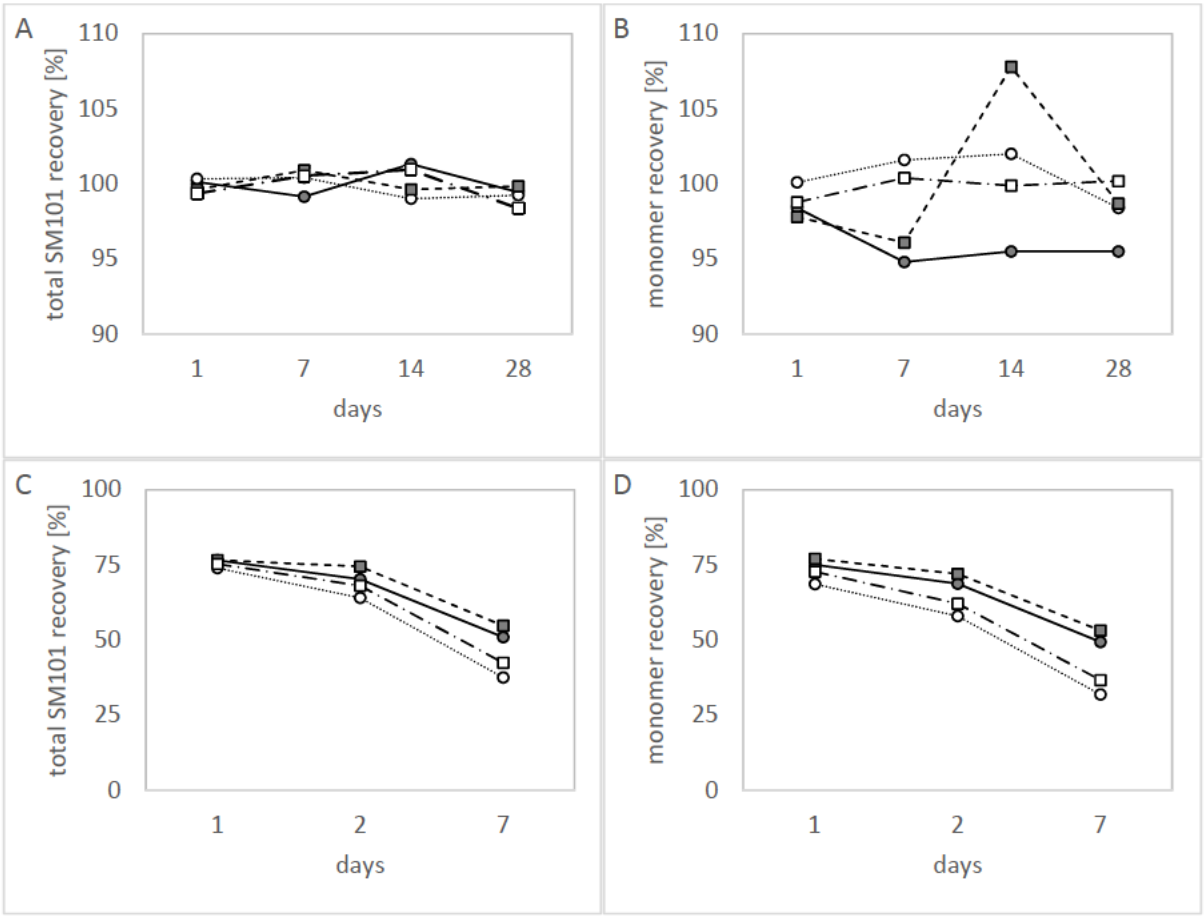

Figure V-4: Total SM101 recovery (UV/Vis)(A+C) and monomer recovery (SE-HPLC)(B+D) after storage at 25°C (A+B) or 40°C (C+D) relative to unstressed reference samples for the formulation candidates A at 10 mg/mL (● filled circle, solid line) or 20 mg/mL SM101 (○ empty circle, dotted line) and B at 10 mg/mL (■ filled square, dashed line) or 20 mg/mL SM101 (□ empty square, dash dotted line) (n=1).

Storage at 25°C for up to 4 weeks did not alter SM101 concentration or monomer content in formulation A or B (Figure V-4 A+B). When stored at 40°C though, SM101 content rapidly declined in all formulations (Figure V-4 C+D). Up to 25% and 31% monomer were lost after one day for the 10 mg/mL and 20 mg/mL formulations respectively. The influence of SM101 concentration was even more pronounced after seven days, when up to 51% monomer were lost in formulations containing 10 mg/mL SM101, compared to 68% loss in the formulations with 20 mg/mL SM101. While no formulation candidate could protect SM101 over a prolonged period of quiescent storage at 40°C, SM101 recovery was generally slightly higher for formulation B with up to 5% more SM101 being recovered.

2.3.2 Chemical degradation by RP-HPLC and CEX-HPLC

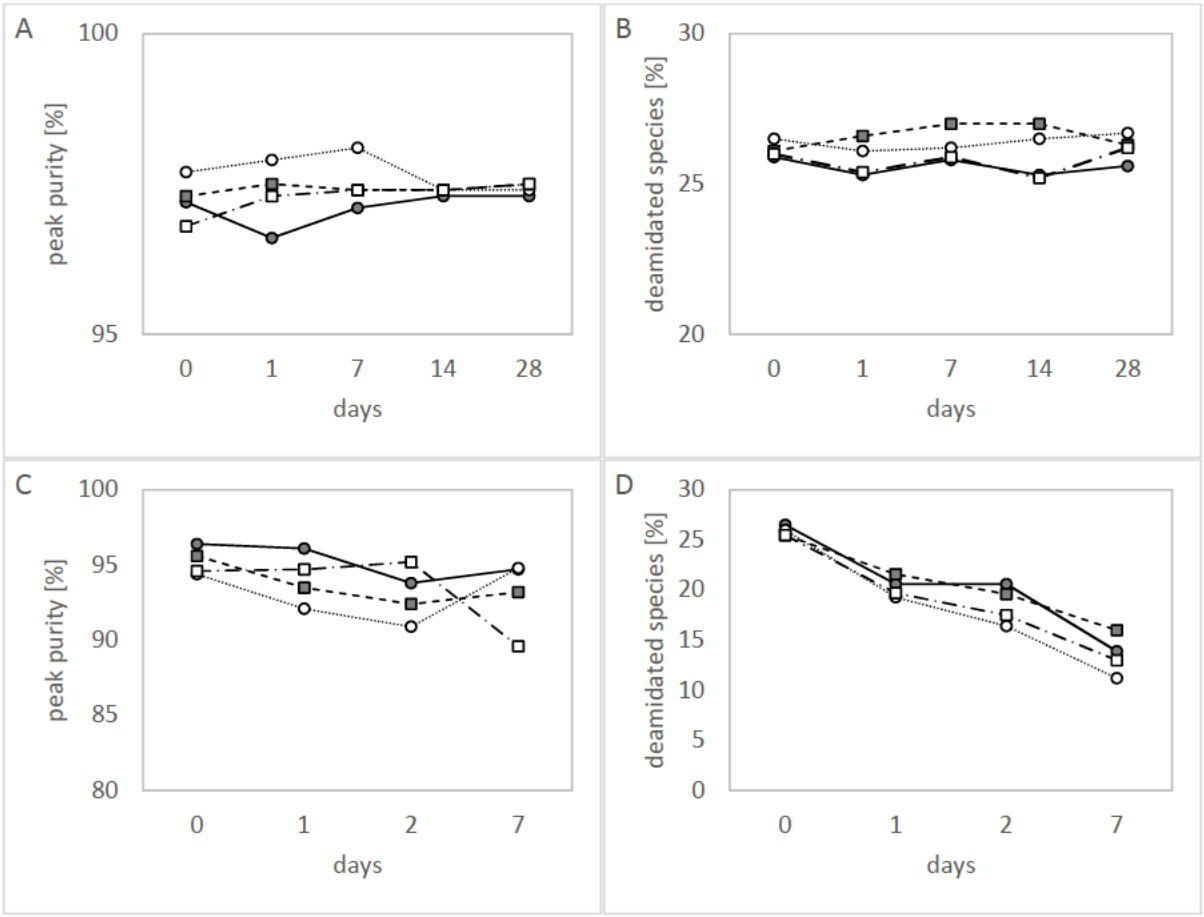

Figure V-5: Peak purity (RP-HPLC)(A+C) and deamidated species (CEX-HPLC)(B+D) after storage at 25°C (A+B) or 40°C (C+D) for the formulation candidates A at 10 mg/mL (● filled circle, solid line) or 20 mg/mL SM101 (○ empty circle, dotted line) and formulation candidates B at 10 mg/mL (■ filled square, dashed line) or 20 mg/mL SM101 (□ empty square, dash dotted line) (n=1).

Four weeks incubation at 25°C did not cause chemical degradation or covalent modification of SM101 in formulation A or B, as judged by RP-HPLC (Figure V-5 A+C) and CEX-HPLC (Figure V-5 B+D). At 40°C, RP-HPLC peak purity decreased by up to 8% during one week incubation, indicating the occurrence of chemical modifications. Deamidated SM101 species seemed more susceptible to degradation at 40°C as the fraction of charge variants gradually decreased from 26% in the starting material to 11-16% during seven days storage. The samples containing 20 mg/mL SM101 suffered slightly higher losses in peak purity and amount of deamidated species, although the difference was less pronounced compared to the one observed for monomer recovery. Formulation candidates A and B do not differ regarding RP- and CEX-HPLC results. Overlays of the chromatogram of the formulation B at 20 mg/mL SM101 are displayed for 25°C and 40°C storage for RP-HPLC (Figure V-6) and CEX-HPLC (Figure V-7) analysis.

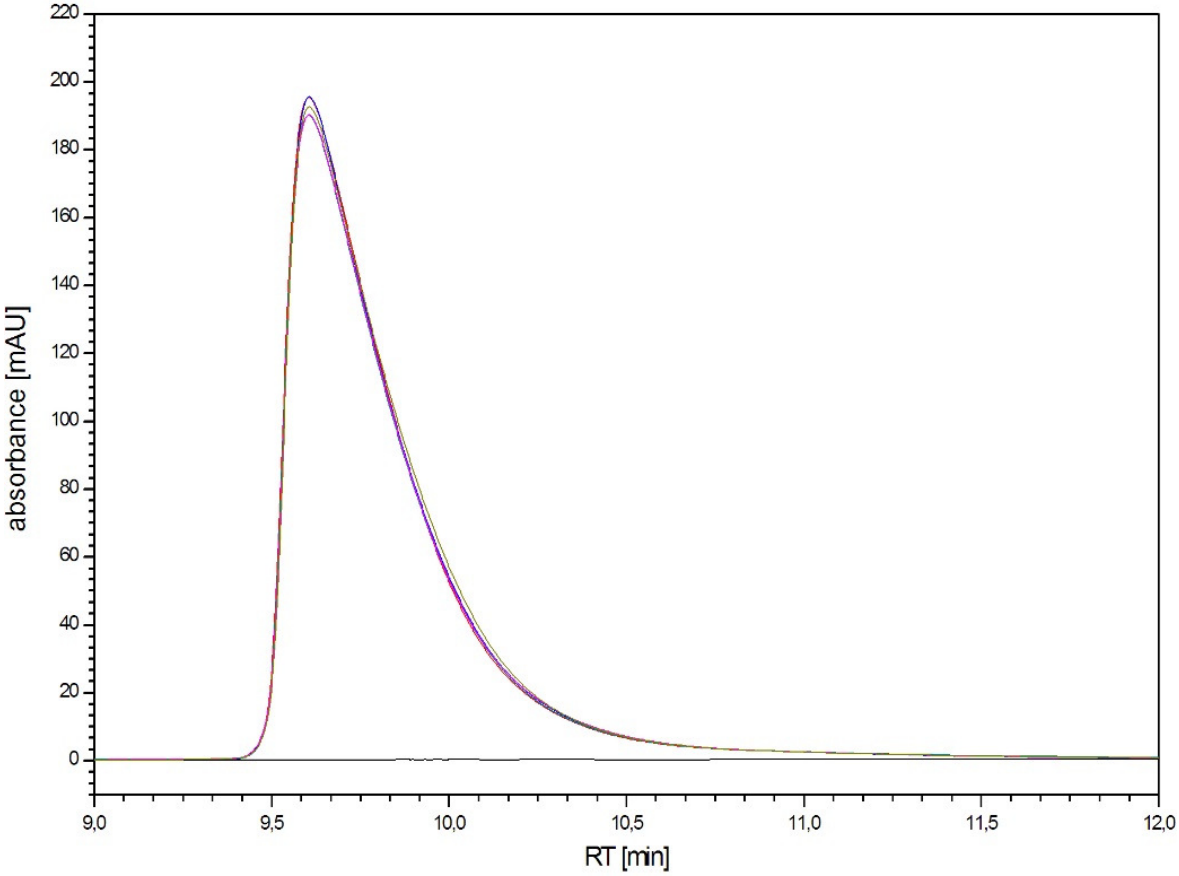
absorbance [mAU]
RT [min]
0
20
40
60
80
100
120
140
160
180
200
220
9,0
9,5
10,0
10,5
11,0
11,5
12,0

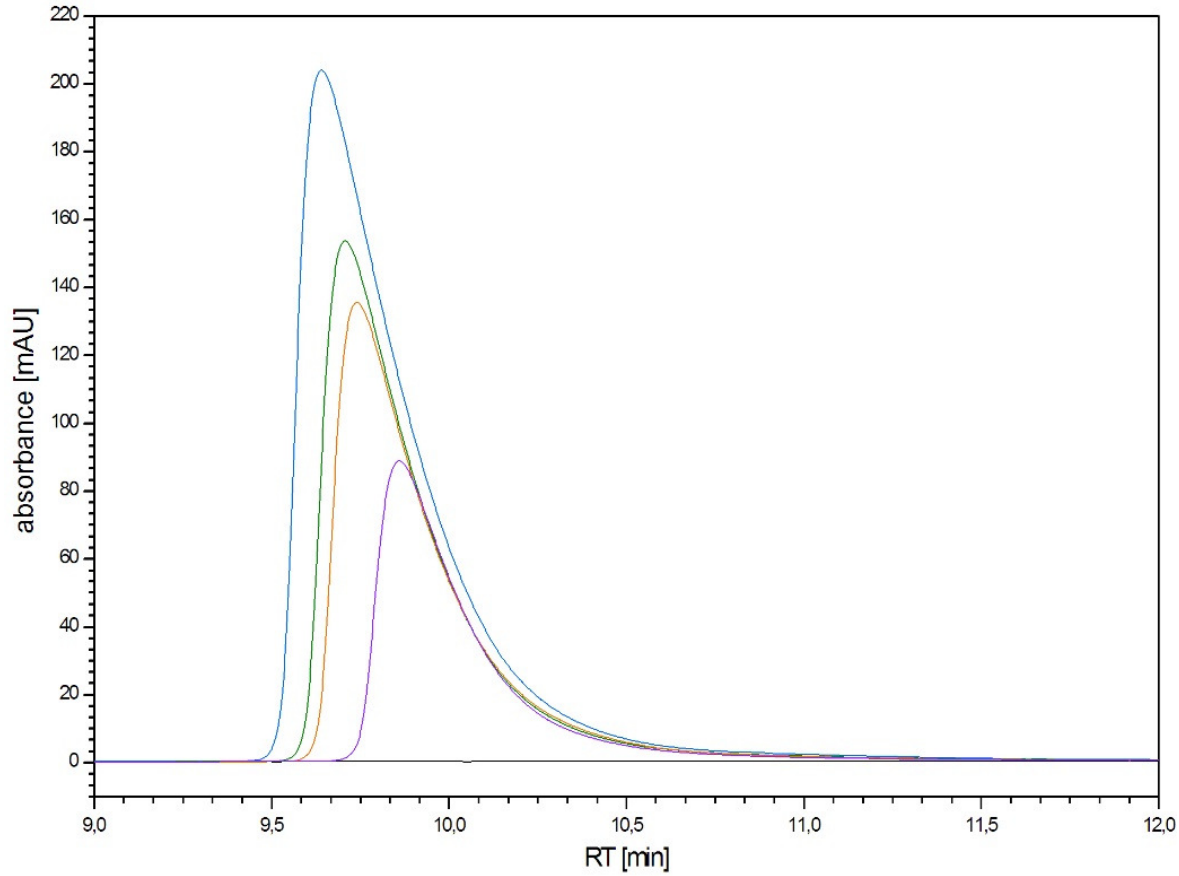
absorbance [mAU]
RT [min]
0
20
40
60
80
100
120
140
160
180
200
220
9,0
9,5
10,0
10,5
11,0
11,5
12,0

Figure V-6: RP-HPLC chromatogram overlays for samples of formulation candidate B at 20 mg/mL SM101 stored for 0 days (blue), 1 day (green), 2 days (yellow), 7 days (purple), 14 days (red) or 28 days (orange) at 25°C (A) or 40°C (B).

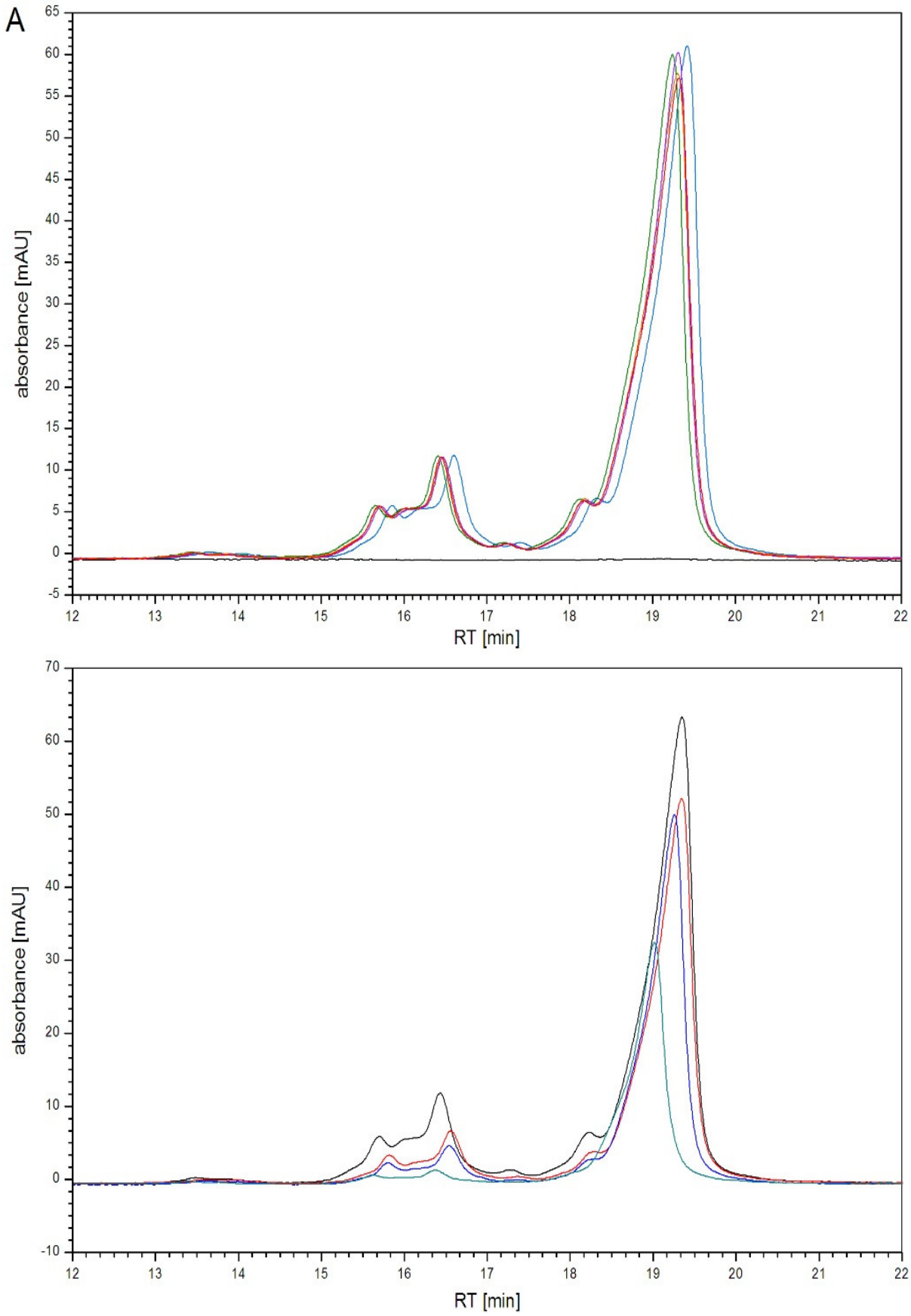

Figure V-7: CEX-HPLC chromatogram overlay for samples of formulation B20 stored for 0 days (black), 1 day (red), 2 days (blue), 7 days (green), 14 days (yellow) or 28 days (purple) at 25°C (A) or 40°C (B).

2.3.3 SM101 aggregation

Incubation at 40°C led to the formation of large amounts of insoluble aggregates, while no soluble aggregation was observed. All tested formulations were cloudy with a large number of visible particle after only 24h incubation at 40°C (Table V-3). The massive formation of particles > 200 µm prevented the use of light obscuration to detect subvisible particle counts. There was no apparent difference between the formulation candidates or SM101 concentration.

Storage at 25°C did not lead to the formation of soluble aggregates or an increase in visible particles over 4 weeks. In regard to subvisible particles > 1 µm, formulation candidate B was more stabilizing than candidate A. The particle count slightly increased over time reaching up to 38534 particles in candidate A and 17232 particles in candidate B with a SM101 concentration of 10 mg/mL (Figure V-8). At 20 mg/mL SM101, less subvisible particles formed. In formulation A, a maximum of 21103 particles per mL were observed, while the particle count of formulation B did not rise over the 10588 particles per mL found in the reference during the entire storage period. All formulations complied with compendial limits regarding particles ≥ 10 µm and ≥ 25 µm [8].

Table V-3: Visual inspection scores after storage at 25°C or 40°C (mean of two observers).

	A *10 mg/mL*	*A* *20 mg/mL*	*B* *10 mg/mL*	*B* *20 mg/mL*
Storage at 25°C				
0d (=ref.)	0	0	1	1
1d	0	0	1	0
7d	0	1	1	1
14d	1	1	0	1
28d	1	1	0	0
Storage at 40°C				
0d (=ref.)	1	0	1	0
1d	10	10	10	10
2d	10	10	10	10
7d	10	10	10	10

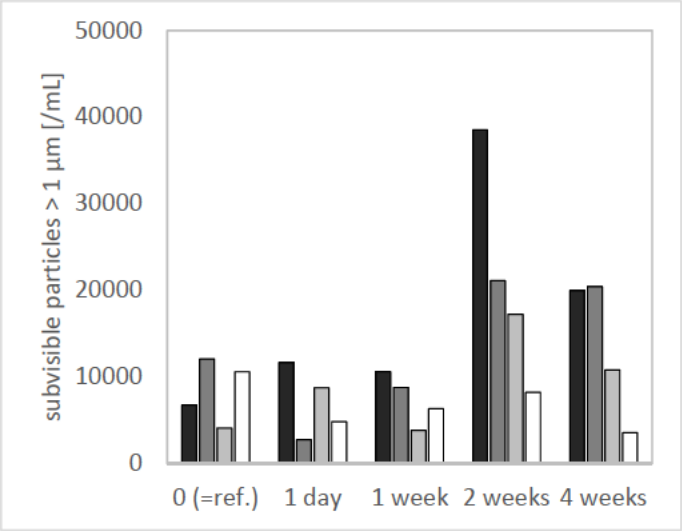

Figure V-8: Subvisible particles > 1µm after storage at 25°C in candidate A containing 10 mg/mL (■ black) or 20 mg/mL (■ dark grey) SM101 and candidate B containing 10 mg/mL (■ light grey) or 20 mg/mL (□ white) SM101 (n=1).

2.4 Candidate choice

Both formulation candidates A and B demonstrated their ability to protect SM101 during up to 6 F/T cycles and 28 days storage at 25°C. A lack of sufficient amounts of NaCl in the formulation as in candidate C decreased SM101 solubility below the desired concentration of 20 mg/mL. In candidate A, SM101 showed the tendency to form increasing amounts of subvisible particles during repeated F/T and with ongoing storage, which was not the case if formulated in candidate B. Therefore, formulation B containing 20 mg/mL SM101 was evaluated in an external long term stability study. Formulation B was chosen as the new parenteral formulation of SM101 and used for direct manufacturing of SM101 bulk into this formulation.

The observed thermolability of SM101 was further characterized by differential scanning calorimetry and UV/Vis spectroscopy. SM101 degradation was irreversible with a T_m of 57.6°C for SM101 in HBS buffer and comparable 58.0°C for formulation candidate B. Values determined with UV/Vis spectroscopy were comparable with a T_{agg} of 55.2°C and 55.6°C for the HBS formulation and candidate B respectively. While the determined T_m values range well above 40°C, the unfolding curve depicted for candidate B (Figure V-9 A) shows an onset of unfolding at approximately 40°C. An additional experiment with 5 mg/mL SM101 in HBS confirmed that SM101 thermal degradation occurred between 35° and 40°C. At temperatures of 35°C or below,

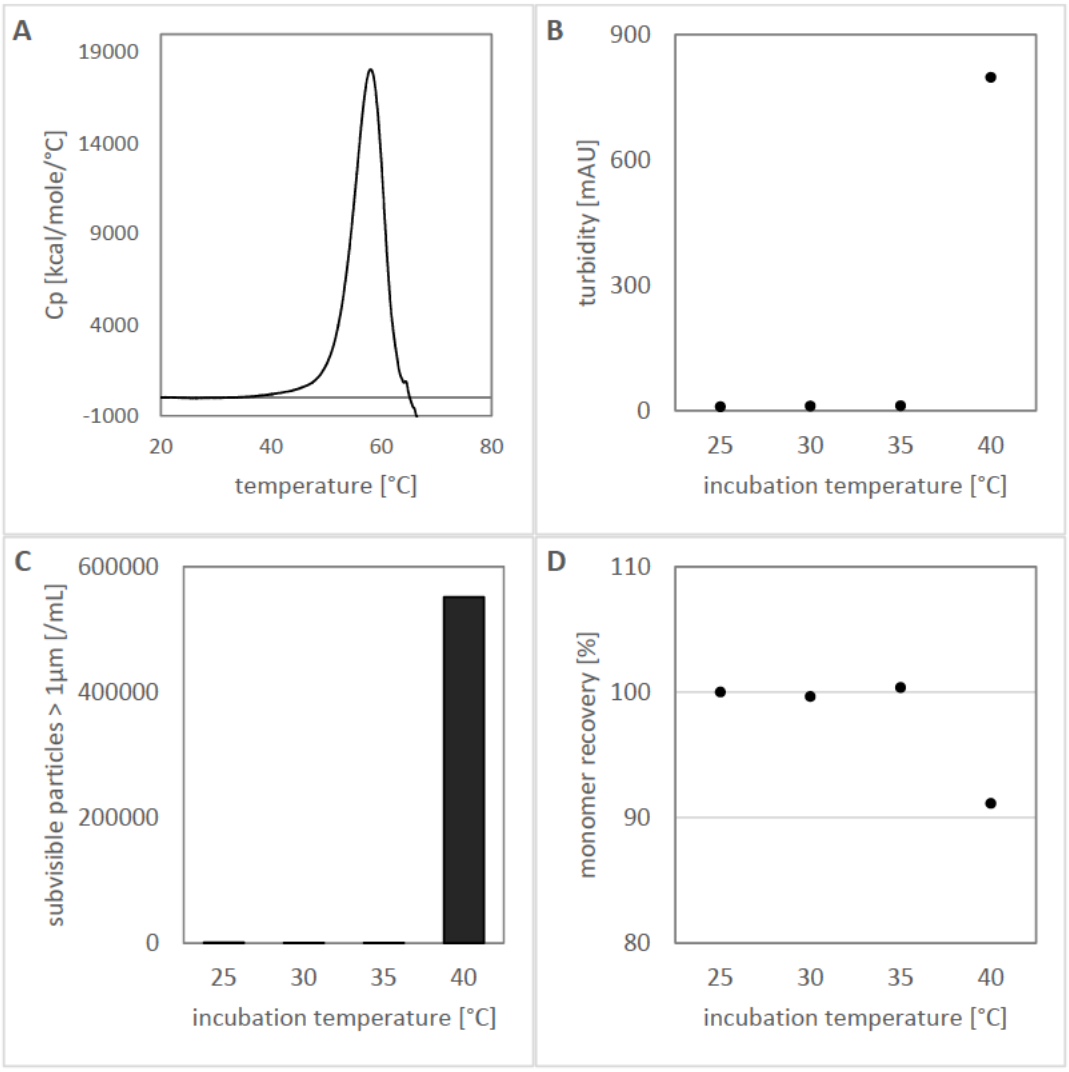

Figure V-9: Unfolding curve (A), turbidity (B), subvisible particles > 1 µm (C) and monomer recovery (D) of SM101 after 7 days storage at 25, 30, 35 or 40°C (n=1).

SM101 did not degrade during one week incubation, while heavily aggregating when incubated at 40°C (Figure V-9 B-D).

2.5 Nebulization of the parenteral formulation

The potential of the new parenteral formulation to stabilize SM101 during nebulization with a PARI eFlow® was evaluated. Nebulization resulted in 50% loss of activity, as indicated by the doubling of the IC50, although only 3% monomer were lost (Table V-4). It was accompanied with heavy aggregate formation as determined by light obscuration and turbidity. No soluble aggregates or SM101 fragments were observed with SE-HPLC. Unlike the collected aerosol, SM101 degradation did not occur inside the reservoir.

Table V-4: Protein stability (n=3, mean ± SD) and activity (n=1, value ± error from fitting) data for 20 mg/mL SM101 in the new parenteral formulation after nebulization of 1.2 mL from a reservoir of a PARI eFlow® nebulizer filled with 2.2 mL.

Method	*Parameter*	*Unit*	*pre-nebulization*	*post-nebulization*	*reservoir*
Light obscuration	Particles >1µm	[mL^{-1}]	1474	187750 ± 17558	n.d.
	Particles >10µm		14	645 ± 517	
	Particles >25µm		1	11 ± 12	
UV/Vis spectroscopy	Turbidity, OD_{350}	[mAU]	30 ± 1	149 ± 43	29
SE-HPLC	Monomer recovery	[%]	100 ± 0.0	97.1 ± 1.5	100.6
	Monomer fraction		100	100	100
FACS potency	$IC50_{sample}/IC50_{reference}$		0.8 ± 0.2	2.0 ± 0.5	n.d.

The parenteral formulation did not stabilize SM101 toward VM nebulization, although the formulation was suitable to protect SM101 during handling and shelf-life as investigated with conventional accelerated and real time stress studies including freeze-thaw and storage at various temperatures during parenteral formulation development. Consequently, a dedicated formulation for the purpose of nebulization and pulmonary delivery needed to be developed.

2.6 Conclusion

This section summarizes the work done in cooperation with T. Pohl to improve the parenteral formulation of SM101 resulting in a fourfold increase in SM101 concentration. While this formulation was proven to stabilize SM101 during freeze/thaw and storage, nebulization with a PARI eFlow® resulted in severe degradation. Development of a dedicated aerosol formulation of SM101 will therefore have to integrate the nebulization process in order to be successful.

3 Development of a dedicated aerosol formulation for SM101

3.1 Introduction

The implementation of the nebulization process into stress testing is mandatory for the development of stable protein formulations for nebulization. Due to long nebulization times as well as laborious handling and cleaning procedures which are not easily parallelized or automated,

formulation screening with nebulizers is a time consuming task. Additionally, API consumption may be too high in early development considering limited availability and the high manufacturing costs of the protein bulk drug substance. This framework may significantly limit the number of formulation parameters tested during development. Nebulization stress testing could be accelerated, while consuming less API material if the main stress factors occurring during nebulization were mimicked in a controllable manner by a surrogate method allowing generation of multiple samples in parallel. Such an accelerated stress test may be used to predict stabilizing formulation conditions allowing the selection of few promising formulation candidates, which are then thoroughly tested employing the real nebulizer in question.

As observed during characterization of the PARI eFlow® (Chapter IV), generation of air-liquid interface and heat are the main stress forces contributing to protein degradation during nebulization. In an effort to design a surrogate stress method for this nebulizer in order to accelerate formulation development with reduced protein consumption, the generation of comparable stress conditions by simple controllable means was pursued.

Air-liquid interfacial stress is classically generated by sample agitation via shaking or vortexing [9, 10]. Generated air-liquid interface is maximized when using half-filled reaction tubes [11] placed horizontally. Alternatively, bubbling of gas through liquid has been employed [12, 13] but involves a more complex setup. Agitation in an incubator at defined elevated temperatures may be used to emulate nebulizer heat up. In this study we aimed to develop a method based on vigorous agitation at elevated temperatures to imitate nebulization conditions in a simple and controllable manner, able to predict the stabilizing potential of different excipient classes allowing higher throughput stress testing. The surrogate method was initially developed for SM101. Formulation development for SM101 was demonstrated based on this technique, comprising an excipient screening and formulation optimization based on the surrogate method and statistical design. Two formulation candidates were created and ultimately challenged by real nebulization experiments to verify and evaluate the results attained by the surrogate method. Finally, we investigated if the proposed surrogate method is applicable for the formulation development of other protein drugs. For this purpose, lactic dehydrogenase (LDH) and granulocyte-colony stimulating factor (G-CSF) were chosen, exhibiting distinctly different protein characteristics than SM101 and a history in nebulization [14, 15].

3.2 Development of a surrogate method to simulate nebulization stress

In order to save both time and valuable SM101 material, a surrogate method allowing stress testing without nebulization was to be developed based on generation of multiple samples in parallel by agitation at elevated temperatures. The surrogate conditions should render similar protein degradation as nebulization. Therefore, a test set of three SM101 formulations and the model excipient PS20 were first nebulized and later used to identify suitable agitation conditions. PS20 was chosen as a model excipient for its potential to stabilize proteins during nebulization by occupation of the air-liquid interface [16]. All formulations contained 5 mg/mL SM101 in HBS, pH 6.5 but varying amounts of PS20, assuming that the formulation without PS20 would show marked instability, whereas the one with 0.05% PS20, above the critical micelle concentration, would be well stabilized and the third formulation including 0.005% PS20 would be in between. This setup enabled a three-point calibration of the surrogate method settings, which are agitation time and incubation temperature, while agitation speed was fixed at 1450rpm. The initial test settings for shaking time and incubation temperature were inspired by the conditions observed during nebulizer operation, which typically took approximately 5 minutes resulting in average reservoir temperatures of 30-35°C (Chapter IV).

Subvisible particle (r^2=0.9996) and turbidity (r^2=0.912) values after nebulization are well met when a 1 mL sample is agitated for ten minutes at 30°C in 2.0 mL PP caps (Figure V-10 A+B). To further reduce the sample volume, 0.65 mL PP caps requiring only 325 µL sample were tested and consequently light obscuration analysis was dropped due to its high sample demand per analysis (>1.2 mL) and its low throughput. Turbidity after nebulization also correlated for samples agitated in 0.65 mL PP caps (Figure V-10 C). Analogous to 2.0 ml PP caps, shaking at 30°C for 10 min resulted in the best correlation (r^2=0.973) to nebulization data. When shaking was performed at 35°C, matching values (r^2=0.924) were reached already after 5 min, while at 25°C, 15 min shaking was required (r^2=0.9027). As implied by nebulization of the parenteral formulation (Table V-4), SEC data did not reveal significant changes in monomer or soluble aggregate content for both nebulized and agitated samples. Interestingly, SM101 degradation behavior after nebulization was very well matched with surrogate method settings closely resembling conditions found during nebulization, suggesting that the developed surrogate stress method is able to generate a comparable amount of stress at the air-liquid interface and by heat.

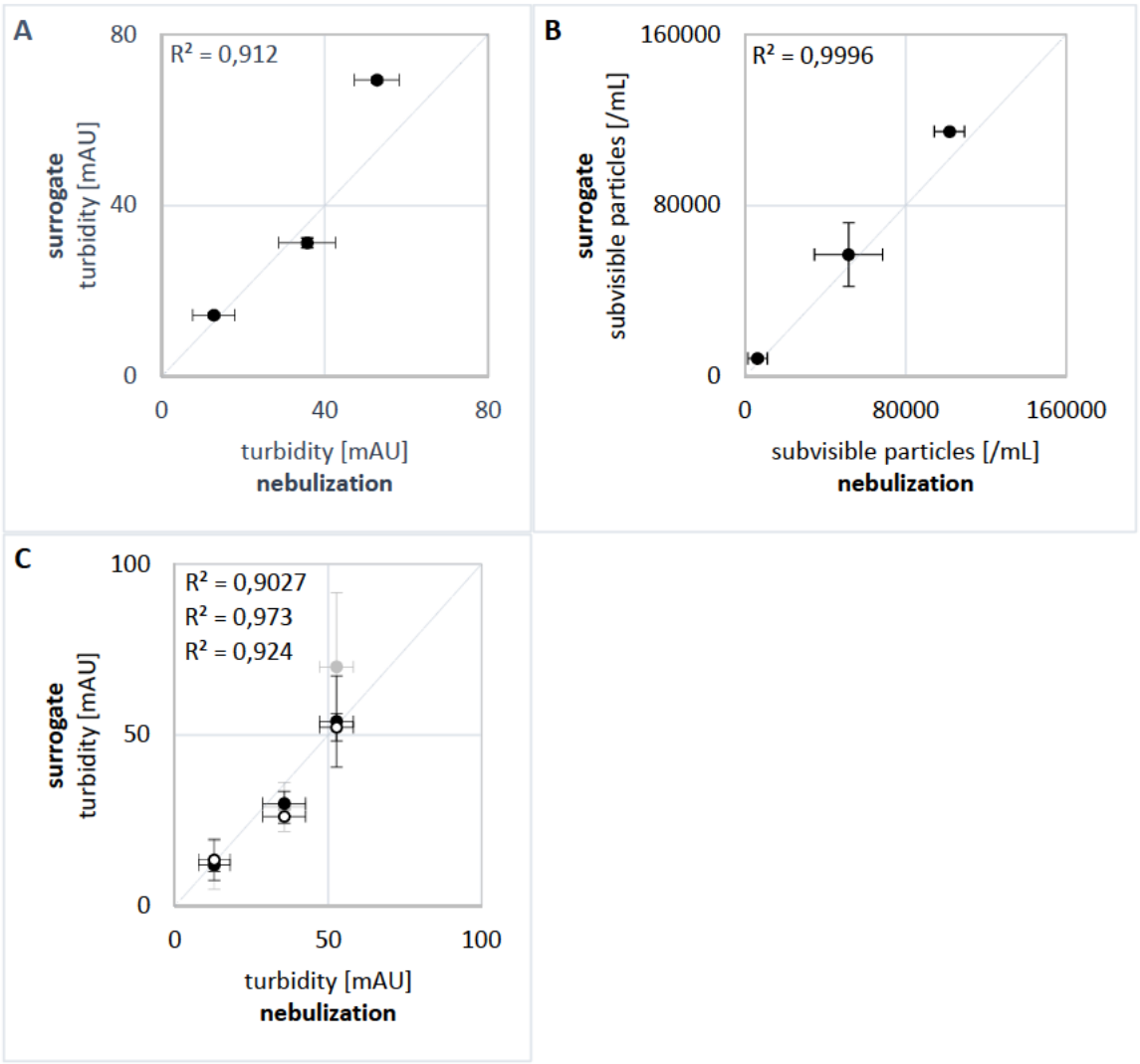

Figure V-10: Correlation of nebulization and surrogate agitation for SM101 formulations containing 0%, 0.005% or 0.05% PS20 (n=3, mean ± SD). Samples agitated for 10 minutes at 30°C in 2 mL PP caps correlated in respect to turbidity (A; R^2=0.9120) and subvisible particles ≥ 1 µm (B; R^2=0.9996). Samples agitated in 0.65 mL PP caps (C) correlated with respect to turbidity when agitated for 5 minutes at 35°C (○ white, R^2=0.9240), 10 minutes at 30°C (● black, R^2=0.9730) or 15 minutes at 25°C (● grey, R^2=0.9027). The main diagonal is shown for easier orientation.

In order to make reasonable use of the surrogate method, good predictions must be possible for different classes of excipients. That in mind, excipients representing different stabilizing mechanisms were selected to verify the predictive power of the surrogate stress method. Agitation for 10 minutes at 30°C in 0.65 mL PP caps was used. Besides 0.005% and 0.05% PS20, 0.035%, 0.35% and 3.5% hydroxypropyl-β-cyclodextrin (HPβCD), 0.1% and 1.0% polyethylene glycol 8000 (PEG 8000) and 2%, 5% and 8% L-arginine were tested. HPβCD was selected for its stabilizing potential [17] and reported low toxicity in pulmonary application *in vitro* and *in vivo* [18, 19]. The stabilizing mechanism is not yet fully understood but as opposed to non-ionic surfactants, it does not include surface displacement [20]. PEGs were also reported to protect proteins against degradation by nebulization [16]. Addition of PEGs results in preferential

hydration of proteins by steric exclusion of the PEG molecules from native proteins [21, 22]. Furthermore, it has been suggested that PEG sterically hinders monomer to monomer interactions at the air-water interface thus preventing further aggregation [16]. Although the amino acid arginine is frequently used during protein refolding and for suppression of aggregation the stabilizing mechanism is still object of discussion and research. Proposed theories include suppression or deceleration of protein interactions [23, 24].

The surrogate results accurately predict nebulization induced SM101 degradation for all tested excipients (Figure V-11) except for the concentration dependent effect of arginine on SM101. Upon nebulization, 2% arginine caused drastic SM101 aggregation while 8% arginine increased SM101 stability, which was both correctly predicted by the surrogate. The addition of 5% arginine however was predicted to stabilize SM101 (21 mAU) but instead led to increased aggregation (99 mAU) upon nebulization. Such arginine-protein ratio dependent stabilizing and destabilizing effects of arginine have been reported before [25]. Despite this discrepancy, the observed correlation between surrogate and nebulization was excellent (R^2=0.9725). The formulations containing 0.35% or 3.5% HPβCD and 0.05% PS20 or 1.0% PEG 8000 are the most stabilizing.

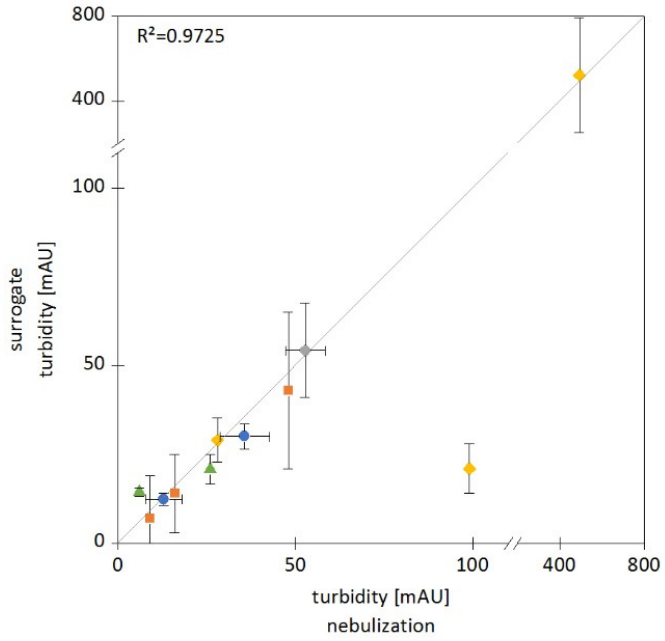

Figure V-11: Correlation of turbidity after nebulization (n=5 for drug substance and PS20 formulations, mean ± SD; n=1 for other excipients) and surrogate method (n=3 for all formulations, mean ± SD) for PS20 (● blue circle), HP-β-CD (■ orange square), PEG8000 (▲ green triangle), L-arginine (◆ yellow diamond) and without added excipient (◆ grey diamond) (R^2 = 0.9725).

3.3 Surrogate based formulation development for SM101

Consequently, we developed a formulation for nebulization of SM101 based on the new surrogate method by screening for stabilizing excipients followed by formulation optimization via the surrogate method and statistical experimental design. Based on these results, two formulation candidates were selected, which were tested with an advanced vibrating mesh nebulizer based on PARI eFlow® technology the AKITA² APIXNEB. Additionally an AKITA jet nebulizer was used as an alternative and SM101 stability compared after the nebulization with either device.

3.3.1 Single excipient screening

To identify excipients that protect SM101 during nebulization, formulations with a single excipient added were treated with the surrogate method. Additionally, excipients that may preserve SM101 stability during quiescent storage were tested for their effects during nebulization. Solution turbidity was used as read out after subtracting the turbidity values of equally treated corresponding placebo formulations. The parenteral SM101 formulation and SM101 in HBS without any excipient added served as references. While finally aiming at a SM101 concentration of approx. 20 mg/mL, screening was performed at 2 mg/mL and 8 mg/ml due to limited SM101 availability which saved valuable protein but enables a statement on protein concentration effects and an outlook toward the intended concentration range.

Non-formulated SM101 in HBS served as a reference. Additionally the excipient effects were compared to the SM101 parenteral formulation that contains 0.005% PS20, 2% sucrose and 1% mannitol to identify conditions outperforming it in regard to SM101 stabilization.

At 2 mg/mL non-formulated SM101 exhibited a turbidity of 40 mAU which was reduced to 12 mAU by the parenteral formulation. All tested excipients provided equal or even better protection of SM101 (Figure V-12 A). At 8 mg/mL non-formulated SM101 exhibited a turbidity of 119 mAU (Figure V-12 B). The parenteral formulation partially protected SM101 and reduced the turbidity to 26 mAU. PS80 or PS20 at 0.005% reduced the turbidity compared to non-formulated SM101 but did not outperform the parenteral formulation. Better protection of SM101 was achieved by higher concentrations of PS80 and PS20 with turbidity values as low as 9 mAU and 8 mAU respectively. Comparable protection was also achieved with HPβCD and PEG 8000.

Addition of sugars, polyols or amino acids to 8 mg/mL SM101 mostly resulted in reduction of turbidity compared to non-formulated SM101 (Figure V-12 C). The level of protection granted by the PS20 containing parenteral formulation was not achieved though. Interestingly, the tested sugars and polyols seem to exhibit a concentration dependent effect on SM101 stability, where high or low concentrations result in less turbidity than the intermediate concentration. Accordingly, mannitol and sucrose were not protective at 2% but at 1% and 5%. The addition of glycine had inconsiderable effects.

Comparing different excipients to the parenteral formulation of SM101 revealed that nonionic surfactants but also HPβCD and PEG 8000 are potent protectors of SM101 against the interfacial stress during surrogate screening. For improved SM101 stabilization, there is no need to substitute the excipients of the starting formulation if excipient concentrations are adjusted to suitable values. None of the tested excipients outperformed 0.02%-0.05% PS20 regarding SM101 stabilization. Adjusting of sucrose and mannitol content may also be beneficial for improved SM101 protection.

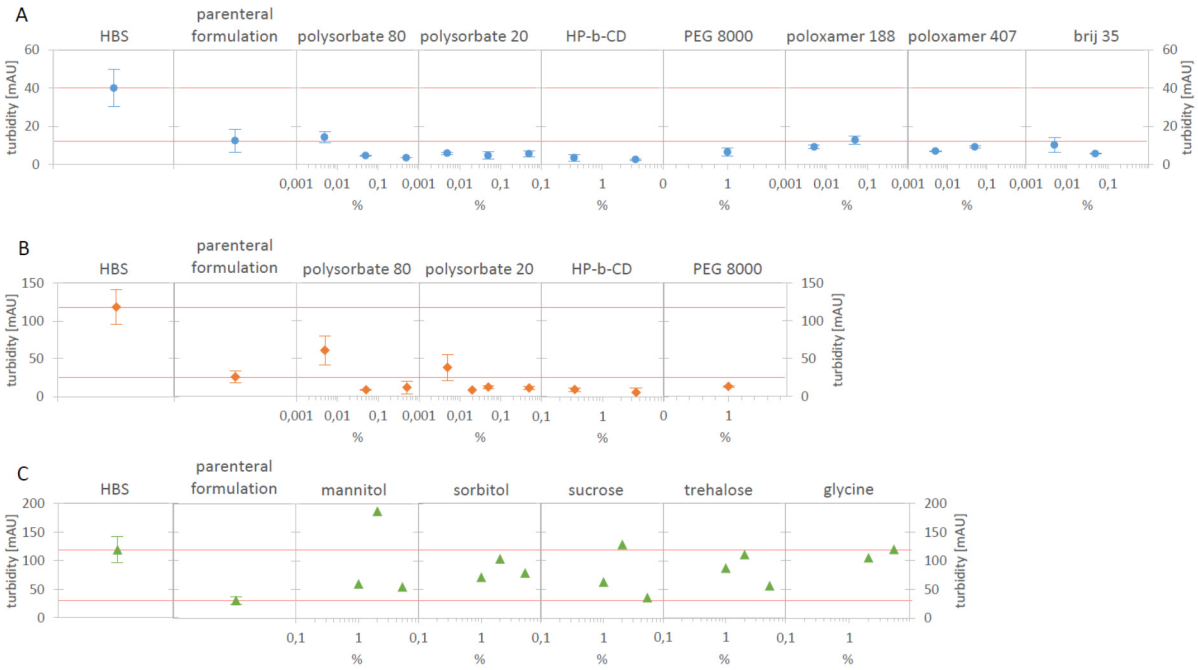

Figure V-12: Turbidity of formulations containing 2 mg/mL (A, n=2, mean ± SD) or 8 mg/mL (B, n=2, mean ± SD and C, n=1) SM101 with one excipient added at the concentration indicated. SM101 in HBS (n=3) or the new parenteral formulation (n=3) served as references and their respective turbidity values are indicated with dotted lines for easier distinction of stabilizing from non-stabilizing formulations.

3.3.2 Formulation optimization via statistical experimental design

After selecting the excipients based on the screening results, statistical experimental design was applied to find optimum ingredient concentrations, allowing economic use of resources by combining design of experiment (DoE) with the material saving surrogate method. A central composite face-centered design (CCF) was chosen to generate a response surface model as the basis to identify optimum formulation candidates. Four factors with three concentration levels each (low, mid, high) (Table V-5) were investigated. All formulations based on a 20 mM histidine buffer at pH 6.5. The ratio of sucrose and mannitol was fixed at 2:1 and the factor was labeled "Sugar" although mannitol is none. Since a reduction of tonicity toward more physiologic values was an additional aim of this optimization, the effect of NaCl concentration was included into the investigation. In total the DoE consisted of 27 runs including a centered triplicate. The stability indicating response parameter was turbidity after surrogate stressing with values for equally treated placebo formulations subtracted.

Table V-5: List of factors and concentration levels included in a CCF DoE conducted for the optimization of the SM101 starting formulation. The concentrations found in the parenteral formulation are in italics.

factor	name	low	intermediate	high
SM101	SM101	4 mg/mL	12 mg/mL	*20 mg/mL*
polysorbate 20	PS20	*0.005%*	0.0275%	0.05%
sodium chloride	SALT	50mM	100mM	*150mM*
sucrose:mannitol (fixed ratio 2:1)	SUGAR	1.5 %	*3.0 %*	4.5 %

DoE model quality can be evaluated by a set of coefficients calculated by Modde software. Model fit (R^2=0.919), model prediction (Q^2=0.828), model validity (=0.904) and reproducibility (=0.860) all indicated good model quality allowing to base further decisions about formulation optimization on DoE generated data.

As already suggested by single excipient screening (Figure V-12), PS20 and SM101 concentration are the main impact factors regarding SM101 stability after surrogate stressing (Figure V-13). While increasing PS20 concentrations had a positive impact on SM101 stability, rising SM101 concentration led to increased aggregation. As indicated by $PS20^2$, there is an optimum PS20 concentration predicted at 0.04% (Figure V-14 A) instead of a merely linear relationship. The concentration dependent effect of "sugar" content that was already apparent during excipient

screening of sugars and polyols (Figure V-12 C), i.e. low and high levels of "sugar" led to less turbidity than intermediate levels, is indicated by $SUGAR^2$. Since linear fitting of the "sugar" data points would result in a flat line of no apparent slope, the linear SUGAR factor is insignificant and the effect of sucrose:mannitol content in the formulation is only revealed after the introduction of this quadratic term (Figure V-14 B). Sodium chloride (SALT) content did not have a significant effect on turbidity after stressing but manipulated how "sugar" addition affected turbidity. When sodium chloride content was low, increasing the "sugar" concentration was protective but in the presence of the high sodium chloride concentration rising the "sugar" concentration would increase turbidity, though the overall magnitude of this effect was small compared to the influence of PS20 and SM101. The SALT:SUGAR interaction factor (Figure V-14 C) accounts for this antagonistic interaction.

The response surface of the main impact factors SM101 and PS20 concentration (Figure V-15) visualizes the described effects and demonstrated that the composition of the parenteral formulation is not optimal regarding the stabilization of SM101 during surrogate stressing. Based on this data, two formulation candidates were identified that have a much better stabilization potential. Their formulation is summarized in Table V-1. PS20 concentration was set to the optimum at 0.04% in candidate 1, for an easily implementable but significant improvement of SM101 protection. Since SM101 concentration was retained at 20 mg/mL, the formulation remained hyperosmolar with 424 mOsmol. Candidate 2 was selected as a compromise between best possible stabilization by adjusting both PS20 and SM101 content but maintaining an acceptably high SM101 concentration of 10mg/mL. Additionally, candidate 2 exhibits near isotonic osmolality of 324 mOsmol, which was achieved by cutting sodium chloride content to half and instead increasing SUGAR concentration to 4.0%, which should also further improve SM101 stability (SALT:SUGAR antagonism, Figure V-14C).

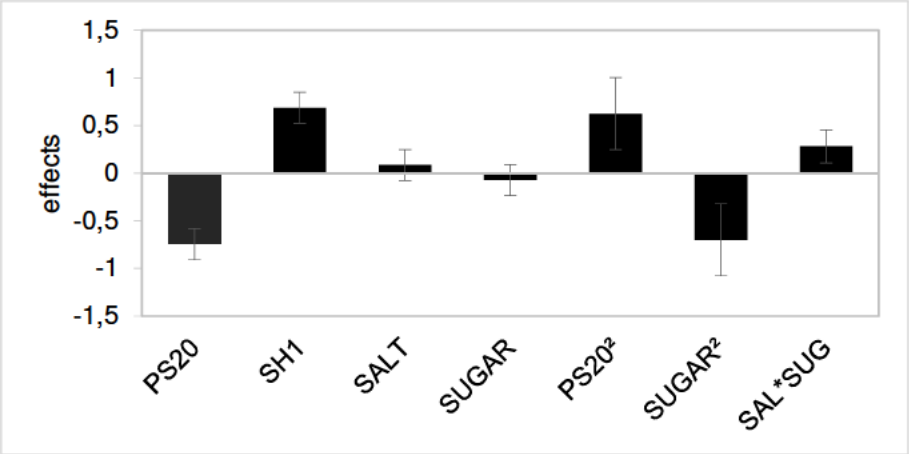

Figure V-13: The plot illustrates the effect of raising ingredient concentration from low to high level (Table V-5) on the turbidity after surrogate stress for all single and for relevant quadratic and interaction factors. The error bars indicate the 95% confidence level.

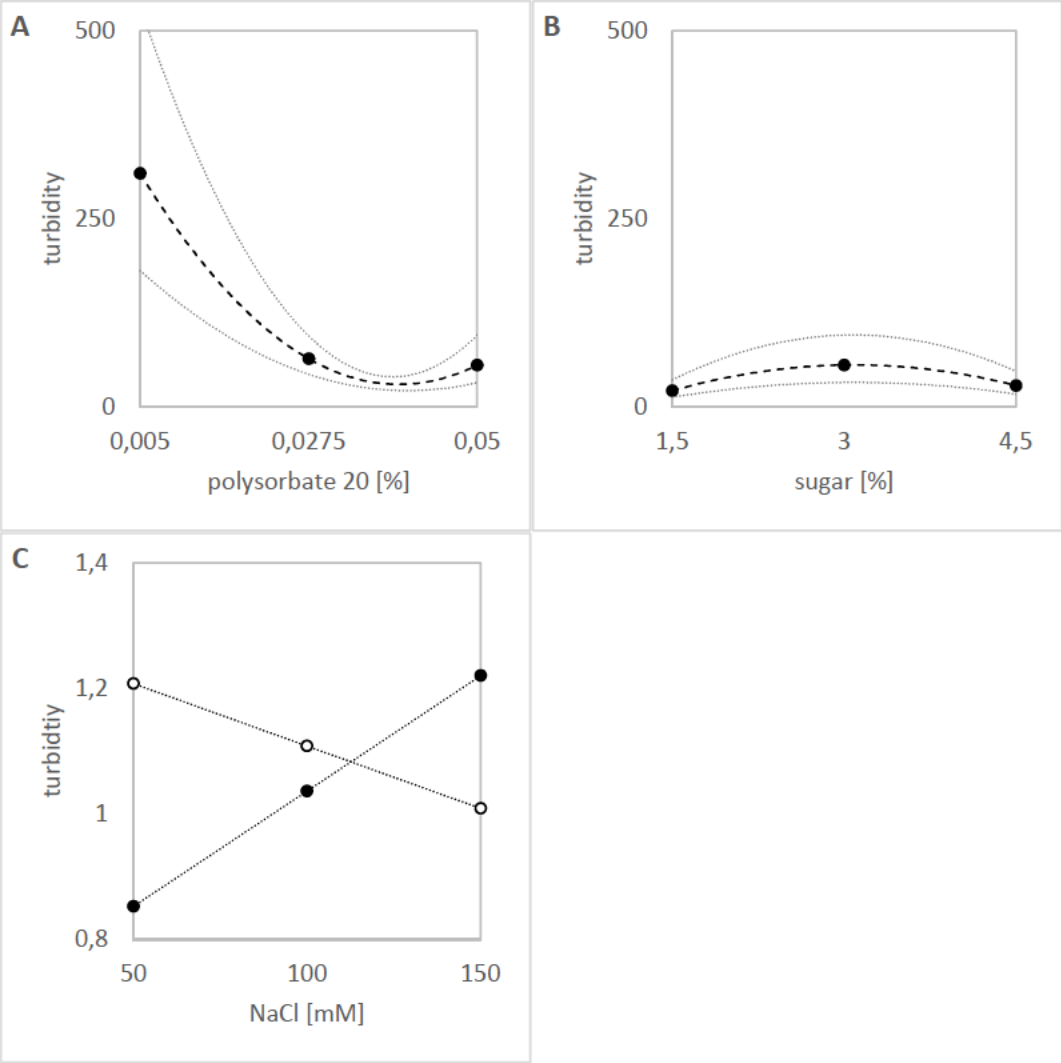

Figure V-14: Impact of the factors PS20 (A) and sugar content (B) on turbidity illustrated by respective prediction plots (dashed line) with the 95% confidence interval (dotted lines). Interaction of sugar and salt content regarding turbidity is illustrated by an interaction effects plot (C) for 1.5% (empty symbols) or 4.5% (filled symbols) sugar content.

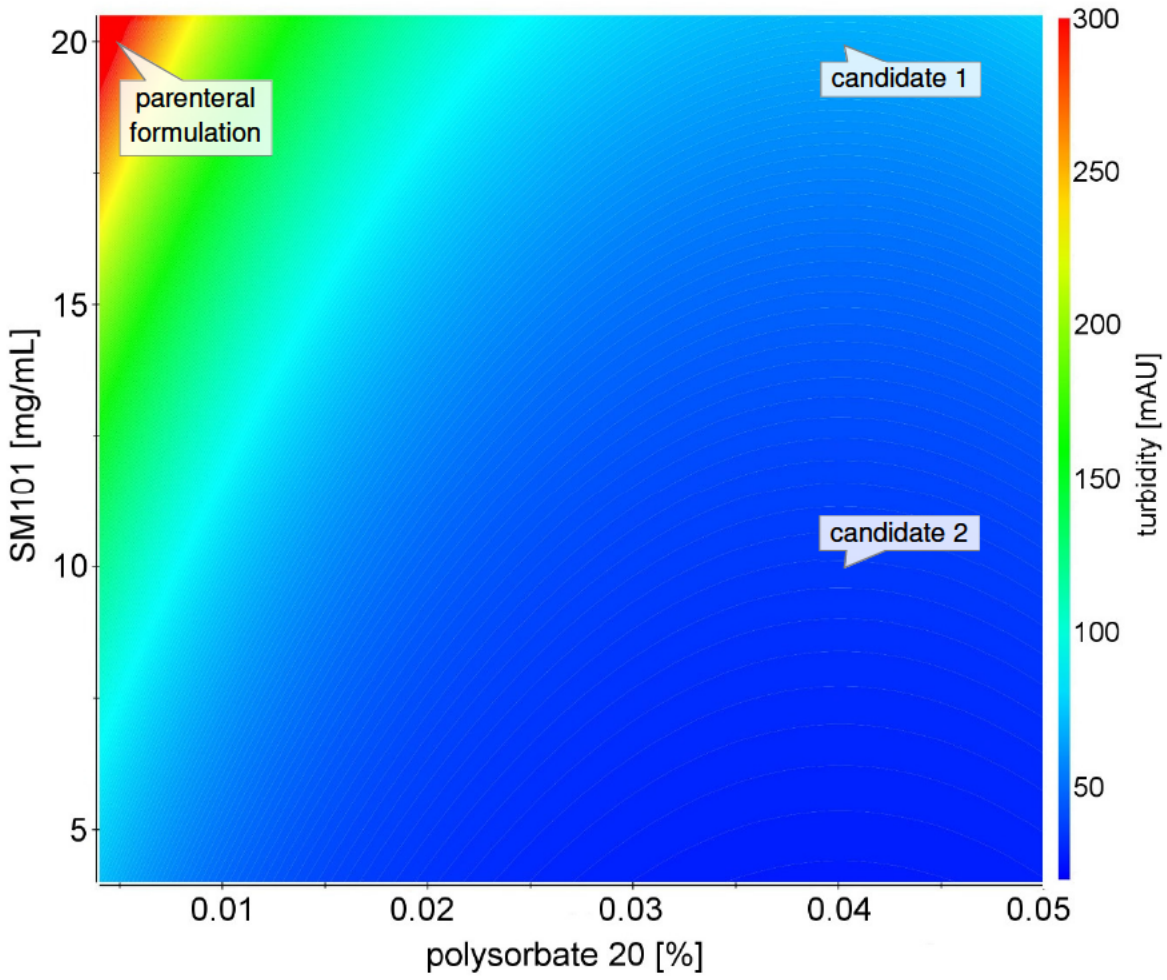

Figure V-15: Response surface plot illustrating the influence of the main impact factors SM101 and PS20 concentration on turbidity. The reference formulation and two formulation candidates are marked up. Sodium chloride and total sugar content are set to 150mM and 3% respectively as found in the parenteral formulation and candidate 1.

3.3.3 Formulation candidate testing by vibrating mesh nebulization

In the ultimate step of formulization development, the lead candidates selected based on the surrogate method were nebulized with an AKITA² APIXNEB (Activaero, 35285 Gemünden/Wohra) nebulizer. It combines PARI eFlow® vibrating mesh technology with nebulizer controlled breathing patterns for the benefit of a high and more reproducible pulmonary deposition [26, 27].

After nebulization and re-condensation, the SM101 samples were analyzed for biologic potency, SM101 monomer content and aggregation (Figure V-16). As already observed during the preliminary nebulization experiments (Table V-4), the parenteral formulation is not capable of maintaining sufficient SM101 activity and stability. After nebulization, SM101 inhibitory potency

was reduced to 60% of a non-nebulized reference. Interestingly, this is not caused by SM101 monomer loss as only a minor decline of 3.4% was detected by SE-HPLC analysis, indicating that this monomeric population must also be severely damaged or that the degraded protein interferes with the assay. During nebulization, SM101 heavily aggregated, forming a very milky solution with large visible particles, making light obscuration analysis essentially impossible. Aerosol generation ceased prematurely after nebulization of only 1.5 mL as the vibrating mesh increasingly occluded by large aggregates (see Chapter IV.2.6).

Both formulation candidates showed a major improvement regarding SM101 stability and delivered clear solutions free of visible particles after aerosol re-condensation. Light obscuration and turbidity revealed some degree of aggregation for candidate 1 and only very little aggregation for candidate 2. Both candidates would even comply with Ph. Eur. demands regarding subvisible particles ≥ 10µm and ≥ 25 µm for parenterals. SE-HPLC showed no formation of soluble aggregates and no loss in SM101 monomer concentration for the two candidate formulations. Regarding biologic potency, nebulization of candidate 1 resulted in a slight reduction of activity by 14% but is safely within internal specification (67-200% activity). Candidate 2 maintained full SM101 potency after nebulization (106%).

As predicted by DoE surrogate data (Figure V-15), formulation candidate 2 slightly outperformed candidate 1 regarding protection of SM101 during nebulization. Unlike the parenteral formulation, both developed formulation candidates deliver stable and active SM101 to the nebulizer mouthpiece. The predictions made on the basis of the DoE surrogate approach were confirmed by the real nebulization results. According to the DoE results, enhanced stabilization is mainly caused by increasing PS20 content and SM101 concentration reduction. To investigate if the minor improvements in SM101 stability predicted for salt and sucrose:mannitol content (Figure V-14) also contribute to the better performance of candidate 2 over candidate 1, both candidate formulations were also nebulized containing only 10 mg/mL SM101 with the PARI eFlow® nebulizer.

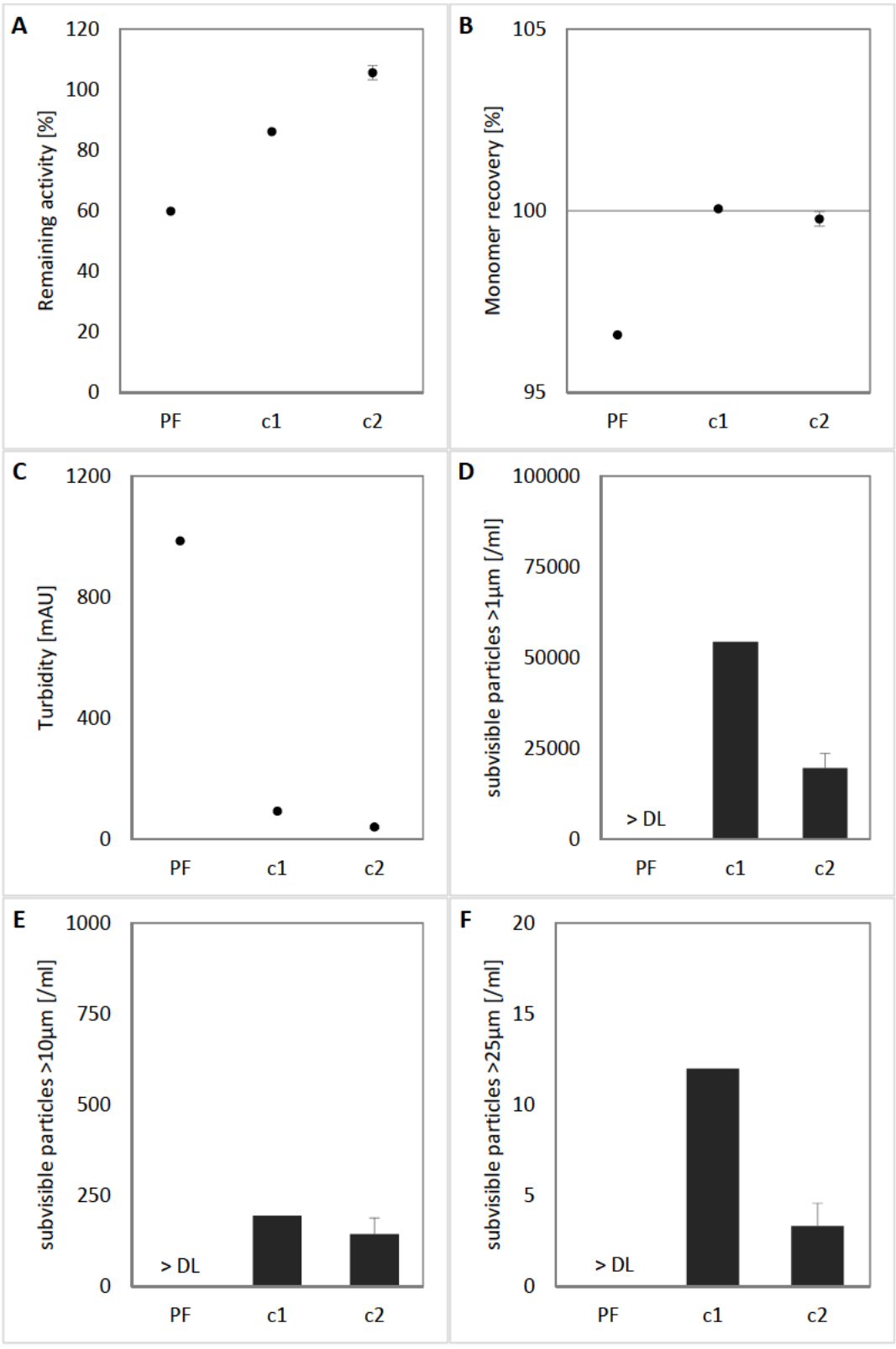

Figure V-16: Remaining activity (A), monomer recovery (B), turbidity (C) and subvisible particle data (D-F) for the parenteral formulation (PF; 20 mg/mL SM101, n=1) and the two lead formulation candidates 1 (C1; 20 mg/mL SM101, n=1) and 2 (C2; 10 mg/mL SM101, n=3, mean ± SD) after nebulization with the AKITA² nebulizer (> DL = above detector limit).

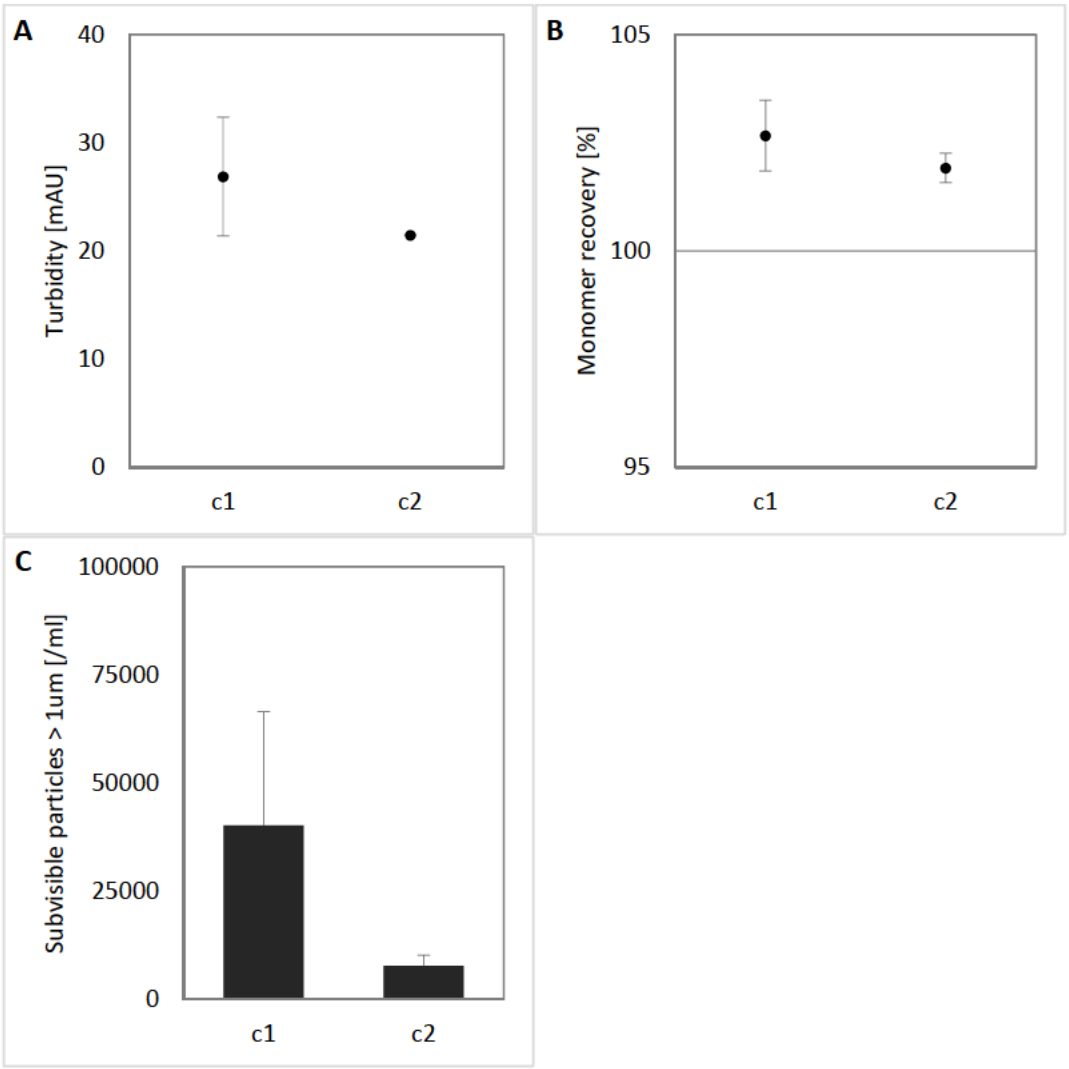

Figure V-17: Turbidity (A), monomer recovery (B) and subvisible particles > 1µm (C) after nebulization of candidate 2 (C2) and candidate 1 (C1) containing 10 mg/mL SM101 (n=3, mean ± SD).

Both formulations show the same stability according to turbidity and monomer content after nebulization (Figure V-17). But subvisible particle levels indicate better stabilization of SM101 if salt and sugar content is optimized according to DoE suggestion as is the case for candidate 2. Candidate 1 with 10 mg/mL SM101 showed increased subvisible particle counts for two out of three samples, causing high standard deviation. With these findings, all predicted factor effects of the surrogate based DoE (Figure V-13) are confirmed by nebulization including PS20, SM101 and SUGAR:SALT optimum.

3.4 Comparison of vibrating mesh and jet nebulization

3.4.1 SM101 stability after vibrating mesh and jet nebulization

Since reservoir heating during VM nebulization appeared to be the major contributor to SM101 degradation, jet nebulization of the lead formulation candidates was performed in comparison to VM nebulization. Jet nebulization does not suffer from reservoir heating, instead, the constant air stream leads to a temperature reduction in the reservoir accompanied by solvent evaporation. While high temperatures are avoided, up-concentration of the API and excipients resulting from evaporation may introduce another source of protein instability.

Conditions during jet nebulization were distinctly different from these of VM nebulization. At the end of nebulization, the temperature of the residual solution had fallen to 15.9-17.5°C as opposed to 31.9-35.2 °C found for VM nebulization. The cool down resulted from solvent evaporation, which also led to a 20.3-22.5% increase in osmolality of the residual liquid. While the pH was not affected by excipient up-concentration, SM101 concentration rose by 15.5-16.3% (Figure V-19 B), a common phenomenon in jet nebulization [28].

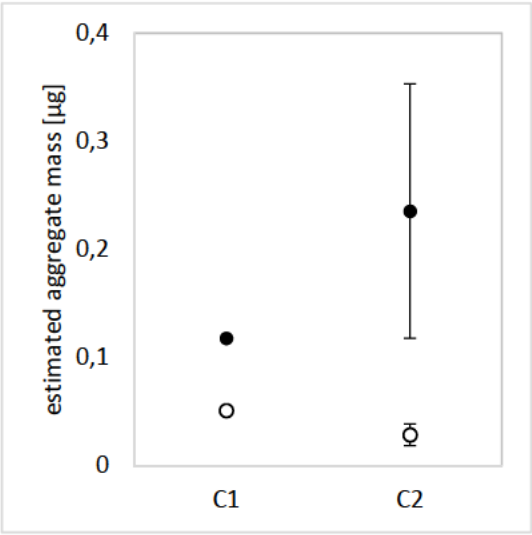

Figure V-18: Aggregate mass calculated from subvisible particles within 1 – 200 µm for candidate 1 (C1, n=1) and candidate 2 (C2, n=3) after nebulization with the AKITA² (empty symbols) or the AKITA jet nebulizer (filled symbols).

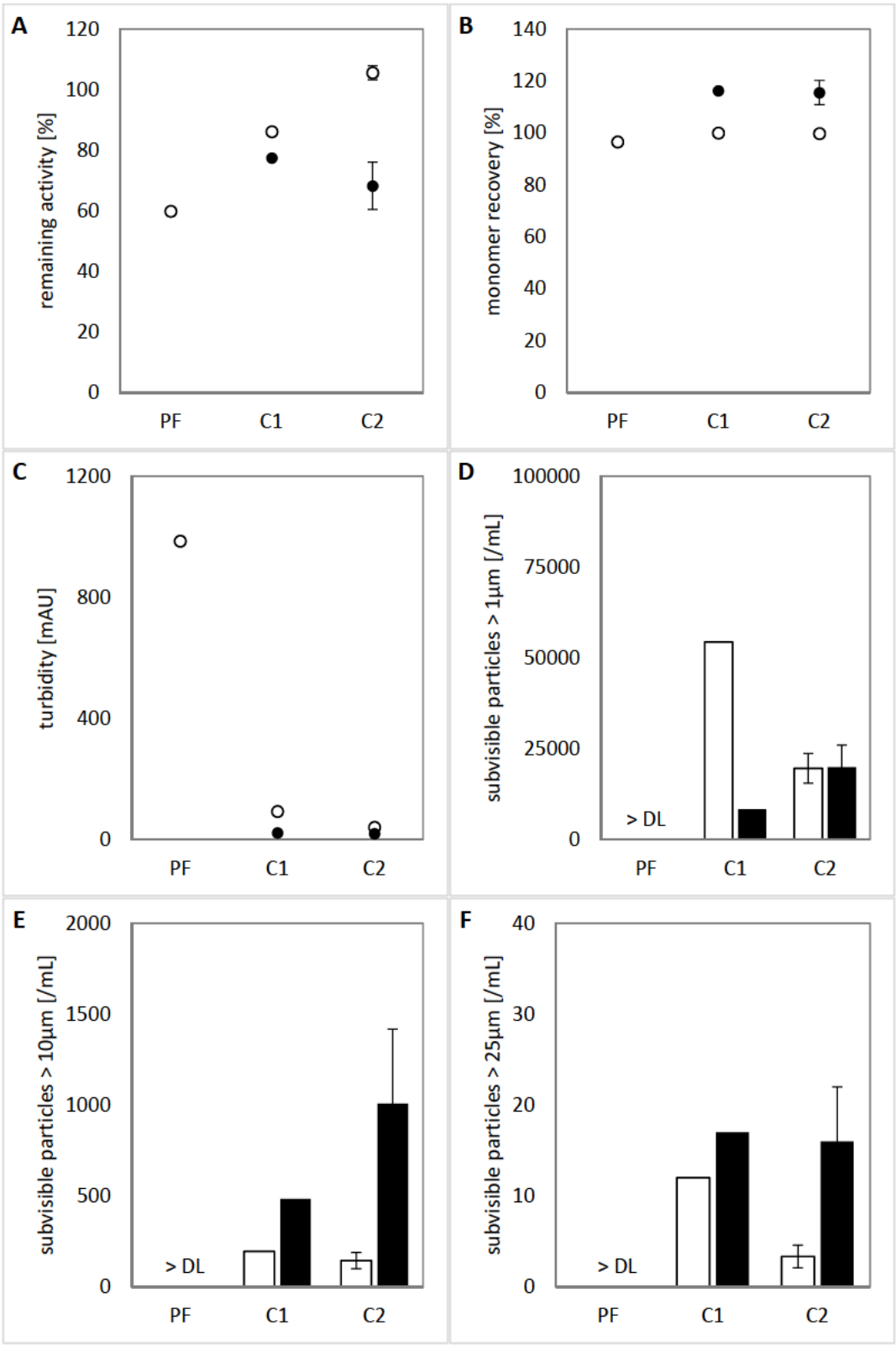

Figure V-19: Remaining activity (A), monomer recovery (B), turbidity (C) and subvisible particle data (D-F) for the parenteral formulation (PF; 20 mg/mL SM101, n=1) and the two lead formulation candidates 1 (C1; 20 mg/mL SM101, n=1) and 2 (C2; 10 mg/mL SM101, n=3, mean ± SD) after nebulization with AKITA² (empty symbols and columns) and the AKITA jet nebulizer (filled symbols and columns) (> DL = above detector limit).

Although high temperatures were avoided, the remaining activity of SM101 after jet nebulization was inferior compared to VM nebulization (Figure V-19 A). This was also confirmed by aggregate analytics. Although the total count of subvisible particles > 1 µm was equal or reduced (Figure V-19 D), jet nebulization led to an increased formation of larger subvisible particles especially in the 10-25 µm range (Figure V-19 E+F). Here, up to 7 fold more particles formed compared to VM nebulization. Consequently, the aggregate mass estimated according to a protocol suggested by Barnard et al. [29], was up to 8 fold increased with jet nebulization (Figure V-18). Increased aggregation was not obvious from turbidity results (Figure V-19 C), which can be explained by the fact that light scattering decreases with increasing particle size. Thus, the larger subvisible particles contribute less to turbidity [30]. Interestingly, candidate 1 provided better protection of SM101 during jet nebulization, while candidate 2 was superior during VM nebulization. One should note though that the absolute IC50 values determined by the cell based potency assay are prone to inter-assay variations. Due to technical restrictions, the assay was only performed once for the parenteral formulations and candidate 1 therefore the absolute values obtained should be regarded as a trend.

3.4.2 Aerosol characteristics of vibrating mesh and jet nebulization

The formulation candidates do not differ in respect to aerosol characteristics (Table V-6). While the median droplet size was smaller for the jet nebulizer, the VM nebulization generated aerosols of narrower size distribution, leading to comparable fine particle fractions of at least 70.5% or 67.8% for the AKITA² or the AKITA jet respectively. The total output rate was slightly higher for the AKITA jet but if SM101 activity was also considered the AKITA² was more efficient.

Table V-6: Aerosol characterization of SM101 formulation candidates nebulized with an AKITA² APIXNEB (n=1) or an AKITA Jet nebulizer (n=1).

Device		AKITA² APIXNEB		AKITA Jet	
Formulation		C1	C2	C1	C2
VMD (=d[v,50])	[µm]	4.16	4.11	3.69	3.89
Span		0.86	0.86	1.42	1.41
FPF	[%]	70.5	71.7	70.8	67.8
total output rate[1)]	[mg/min]	n.d.	132 (329)	130 (325)	145 (363)
API output rate[1)]	[mg/min]	n.d.	1.32 (3.29)	2.60 (6.5)	1.45 (3.63)
active API output rate	[mg/min]	2.2 (5.6)	1.4 (3.5)	2.0 (5.0)	1.0 (2.5)

[1)] In parentheses the rate in respect to the actual inhalation phase is shown.

3.5 Conclusion

This study demonstrates how the newly developed surrogate method can be used to replace laborious nebulization and thereby accelerate the development process for inhalable protein formulations and drastically reduce material demand (4mL nebulization versus 0.35mL surrogate). As was demonstrated for vibrating mesh nebulizers relying on PARI eFlow® technology (PARI eFlow® and AKITA²) and the protein SM101, a method mimicking nebulizer related stress factors by agitation at elevated temperatures is feasible and allows predictions about the stabilizing potential of various excipients and in doing so can predict their necessary concentration for protein stabilization.

It is generally advisable to use more than one analytical method to investigate different aspects of protein degradation like loss of protein content, aggregation, structural changes or loss of biologic activity. Based on this surrogate stress method, the successful development of a formulation dedicated to nebulization of SM101 was demonstrated. Its high quality of correlation enabled prediction of stability influencing factors by means of statistical design. All predictions made were confirmed by nebulization with an AKITA² vibrating mesh nebulizer.

Especially aerosol formulation candidate 2 preserves the activity and stability of SM101 after nebulization, which fulfills a major requirement for future *in vivo* studies. It could also be demonstrated that VM nebulization was less detrimental than jet nebulization of SM101 with the tested formulation candidates. Nevertheless, with candidate 1, a formulation providing sufficient stability during jet nebulization is also available in case jet nebulization of SM101 should become necessary.

Within the scope of this study, the general applicability of the suggested procedure for other nebulizers was not evaluated. Therefore any such extrapolation should be accompanied by further testing, which may be accomplished by following the procedures presented in this section. For other vibrating mesh nebulizer models, we expect the adaption of the surrogate method to be straight forward as principle of operation, generated droplet size and therefore encountered stress upon nebulization should be similar. The incubation temperature may need to be adjusted based upon temperatures measured inside the device reservoir during operation. Transfer to ultrasonic (US) nebulizers might also be possible, as comparable stress factors - namely reservoir heating

and interface generation - occur. Otherwise, protein stability threatening effects of excessive recirculation and evaporation, which are not modeled by the surrogate method may cause a significantly altered protein degradation pattern. The latter is especially applicable to jet nebulizers, which may hence not be well simulated by the proposed surrogate method.

Caution toward extrapolation is also advised regarding the applicability of surrogate screening to other proteins, which was therefore further evaluated for two additional proteins.

4 Feasibility of the surrogate screening method for other proteins

4.1 Selection of model proteins to test with the surrogate method

The power of the surrogate method for formulation development was successfully demonstrated for SM101. Therefore, two further model proteins lactic dehydrogenase (LDH) and granulocyte-colony stimulating factor (G-CSF) were selected to examine a wider applicability of the surrogate method for protein stability prediction during VM nebulization. Both proteins exhibit distinctly different characteristics compared to SM101 (Table V-7).

As suggested in chapter IV and by Zeles-Hahn et al., T_m may be used to evaluate protein stability to atomization [31]. All selected proteins exhibit a T_m below 60°C but onset of melting (see Table V-7) occurs at a higher temperatures for G-CSF compared to LDH and especially SM101. G-CSF is of comparable molecular weight but mainly helical structure compared to the mostly beta-strand structure of SM101. Unlike SM101 or G-CSF, LDH is a tetrameric protein of 140 kDa of the alpha and beta protein folding class [32]. LDH is often used as a model for interfacial stress (lyophilization, spray drying, nebulization) and has a history of nebulization [14, 15], where it was proven highly susceptible to degradation by jet or US nebulization. While nebulization at ambient temperatures is already detrimental, additional heat during US nebulization acts synergistically, whereas heating alone is not problematic up to 45°C [33]. Comparable behavior was observed for VM spray drying [34]. A tendency of G-CSF to degrade during jet nebulization is also described in literature [15].

Table V-7: Molecular weight, protein unfolding temperature (T_m) and structural classification (SCOP, [32]) of the proteins used in this study.

	SM101	LDH	G-CSF
Molecular weight	20 kDa	140 kDa	19.9 kDa
T_m (onset)	57.6°C (39.2°C)	58.6°C (43.3°C)	59.7°C (52.5°C)
SCOP class	all beta	alpha and beta (tetrameric)	All alpha

4.2 Surrogate screening for G-CSF

G-CSF formulations of pH 4.2 and below did not exhibit significant degradation during vibrating mesh nebulization. But at pH 4.4, nebulization with the PARI eFlow® and agitation for 45 minutes at 30 °C in the surrogate setup yielded a reasonable correlation with respect to turbidity (Figure V-20 A, r^2=0.8250) and G-CSF monomer recovery (Figure V-20 B, r^2=0.8813) for formulations containing either 0%, 0.001%, 0.005% or 0.05% PS20. Agitation for only 10 minutes, i.e. the setting used for SM101, failed to generate significant G-CSF degradation. Increasing the incubation temperature to 40°C instead of prolonging agitation time during surrogate screening did not result in turbidity comparable to nebulization.

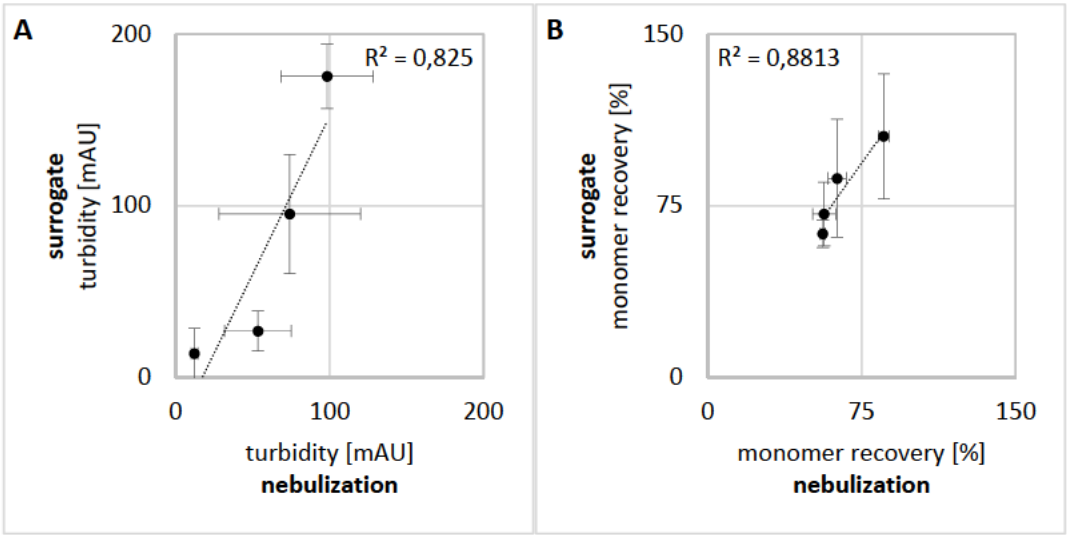

Figure V-20: Correlation of nebulization (n=4, mean ± SD) and surrogate (45min, 30°C; n=3, mean ± SD) for G-CSF formulations containing 0%, 0.001%, 0.005% and 0.05% PS20 with respect to turbidity (A, R^2=0.8250) and SEC monomer recovery (B, R^2=0.8813).

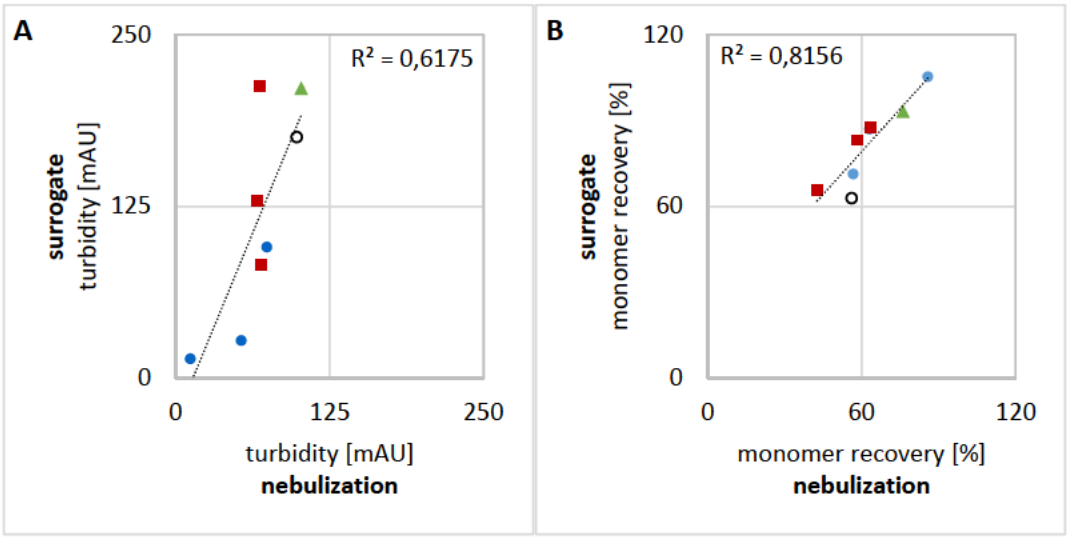

Figure V-21: Correlation of nebulization (n=4) and surrogate (n=3) for G-CSF formulations containing PS20 (● blue circle), HPβCD (■ red squares), PEG 8000 (▲ green triangle) or no excipient (○ empty circle) with respect to turbidity (A, R^2= 0.6175) and SEC monomer recovery (B, R^2=0.8156). Error bars are omitted to retain clarity.

Expanding the comparison of surrogate testing and nebulization to additional G-CSF formulations containing HPβCD or PEG 8000 revealed a reasonable correlation in SEC monomer recovery (R^2=0.8156, Figure V-21 B). Notably, the values from surrogate testing are on average about 20% higher than after nebulization. For most of the tested formulations, turbidity after agitation correlated well with values after nebulization (Figure V-21 A). Only surrogate results for HPβCD containing formulations did not fit to turbidity after nebulization (R^2=0.6175). While surrogate results suggested a concentration dependent reduction of G-CSF turbidity, the amount of HPβCD present during nebulization did not alter the extent of G-CSF stabilization. This discrepancy may result from HPβCD's mechanism of protection, which remains unclear. The surrogate method correctly identified 0.05% PS20 as the only tested formulation capable of maintaining low turbidity and high monomer recovery of G-CSF during nebulization.

4.3 Surrogate screening for LDH

Nebulization and surrogate testing of LDH formulations containing 0%, 0.01% or 0.1% PS20 produced comparable results for turbidity (R^2=0.9544), SEC monomer recovery (R^2=0.9046) and remaining activity (R^2=0.8277) (Figure V-22). As already observed for G-CSF, neither the SM101 derived surrogate setting (10 minutes, 30°C) nor increasing the incubation temperature to 35°C provoked significant LDH degradation. Instead, LDH samples had to be agitated for 60

minutes at 30°C. These settings were then tested with additional LDH formulations containing either PS20, HPβCD or PEG 8000 in different concentrations.

In the surrogate test, the addition of 0.1% PS20, 3.5% HPβCD or 1% PEG 8000 was most protective for LDH as predicted by monomer recovery, remaining activity, turbidity (Figure V-23) and visual inspection results alike, while lower excipient concentrations only partially stabilized LDH. These results corresponded well to the situation found after nebulization, demonstrating that the surrogate setup is a valuable tool for the simulation of the nebulization process during formulation development for an additional protein.

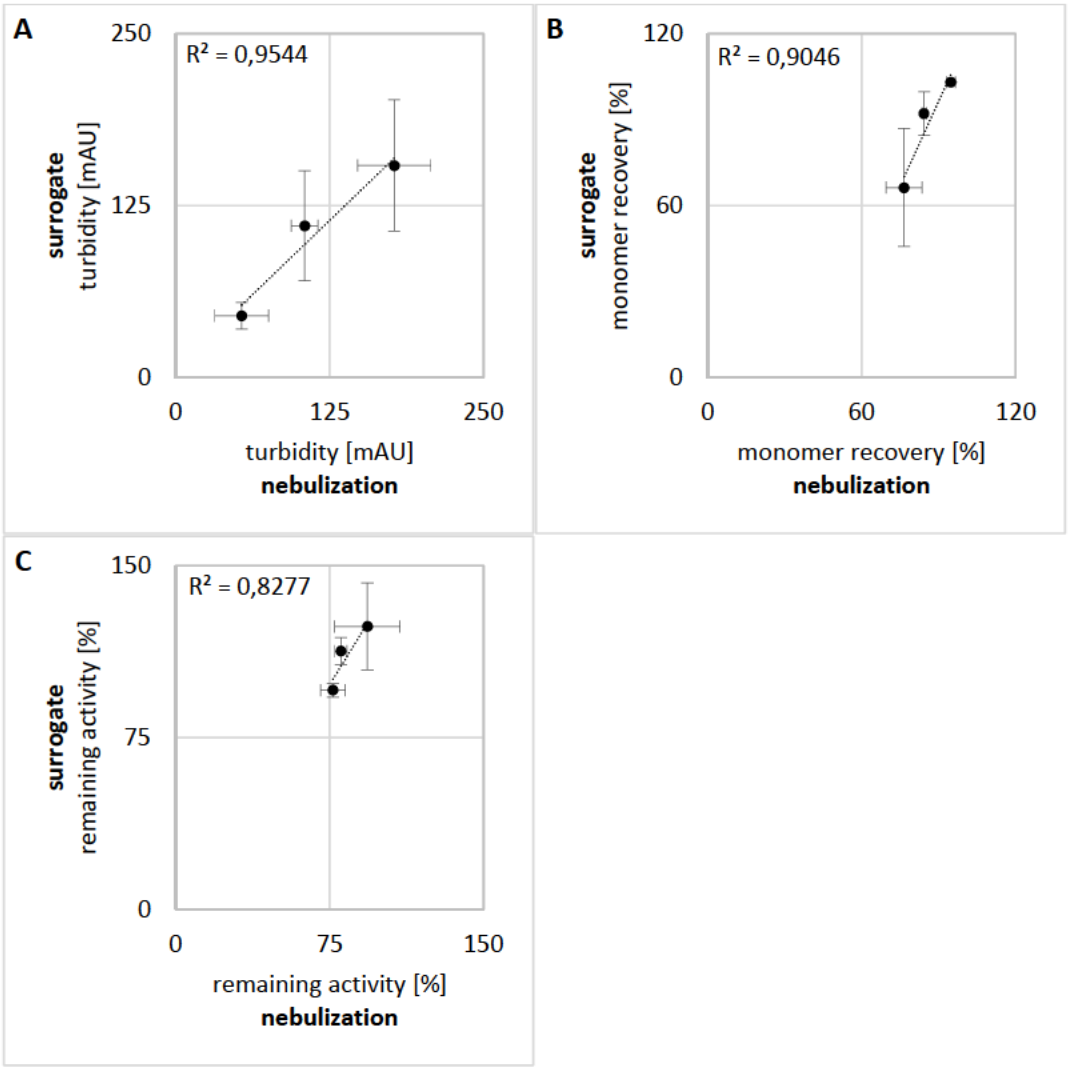

Figure V-22: Correlation of nebulization and surrogate agitation for 60 minutes at 30°C for LDH formulations containing 0%, 0.01% or 0.1% PS20 in respect to turbidity (A, R^2=0.9544), monomer recovery (B, R^2=0.9046) and remaining activity (C, R^2=0.8277)(n=3, mean ± SD).

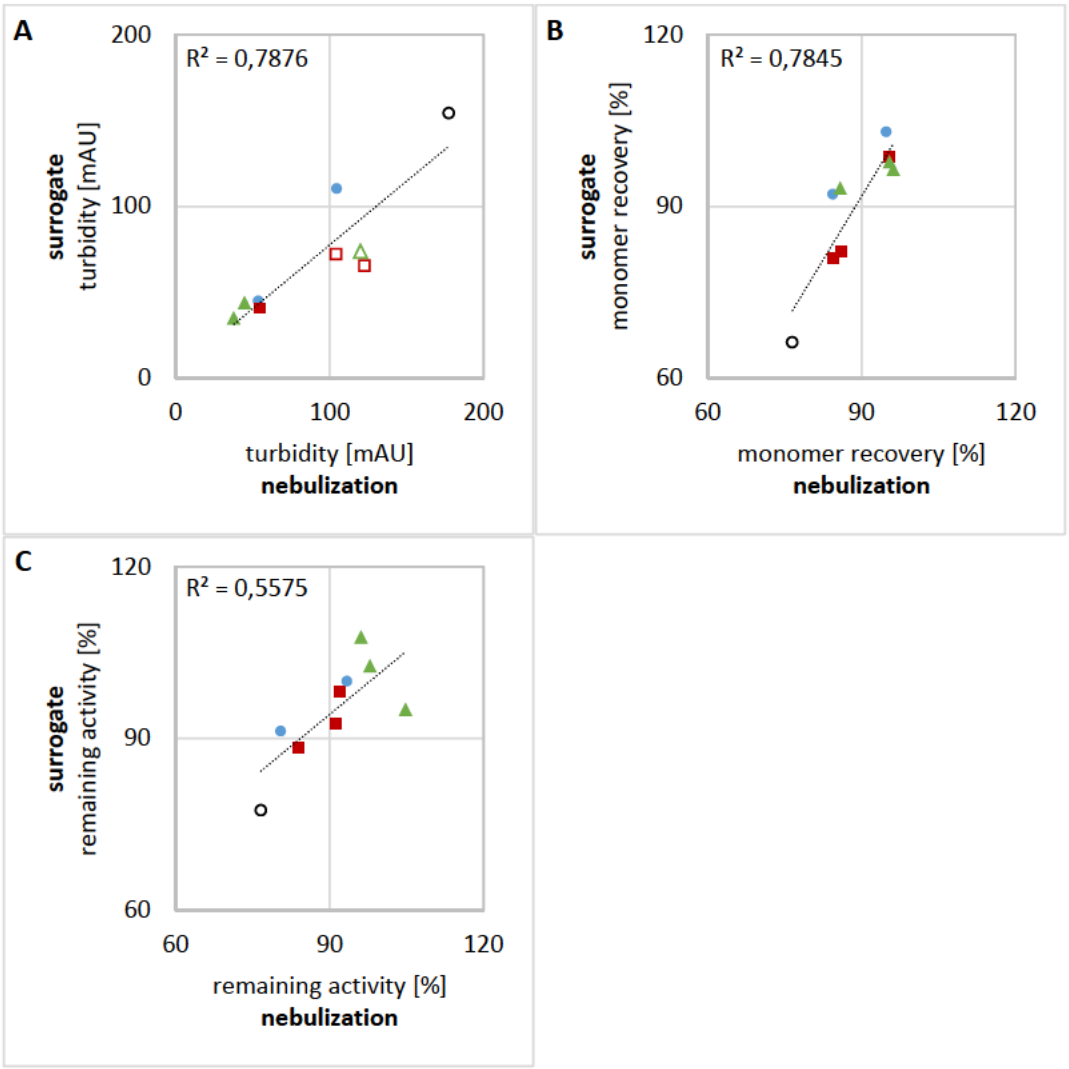

Figure V-23: Correlation of nebulization (n=3) and surrogate agitation for 60 minutes at 30°C (n=3) for LDH formulations containing either PS20 (● blue circle), HPβCD (■ red square), PEG 8000 (▲ green triangle) or no excipient (○ empty circle) with respect to turbidity (A, R^2=0.7876), SEC monomer recovery (B, R^2=0.7845) and remaining activity (C, R^2=0.5575). Formulations exhibiting inconsistent visual inspection results are shown as empty symbols in figure A. Error bars are omitted to retain clarity.

Three of the tested formulations that only partially stabilized SM101 including 0.01% PEG 8000, 0.035% HPβCD and 0.35% HPβCD exhibited inconsistent results after nebulization and surrogate testing in respect to visual inspection and turbidity (marked as empty symbols in Figure V-23 A). After surrogate testing the visual inspection score was distinctly higher (10) than after nebulization (2). As opposed to this, turbidity after surrogate was lower than after nebulization, indicating that insoluble LDH aggregates agglomerated into visible particles that contribute less to turbidity [30] during surrogate testing but remained in the subvisible range after nebulization.

4.4 Universal surrogate screening

Although the experiments, which are necessary to find optimum surrogate settings, also require some time and material, even after the extensive surrogate method development and verification for SM101 an overall reduction of SM101 consumption greater factor two was achieved. Even though protein specific method adjustment can be realized with relatively little effort, it would be very convenient to operate the surrogate method with one standard setting. A suggestion for such universal settings is the use of a prolonged agitation time of 60 minutes independent of the protein investigated. To prove this assumption both G-CSF and SM101 were briefly screened with the LDH derived method settings of 60 minute agitation at 30°C.

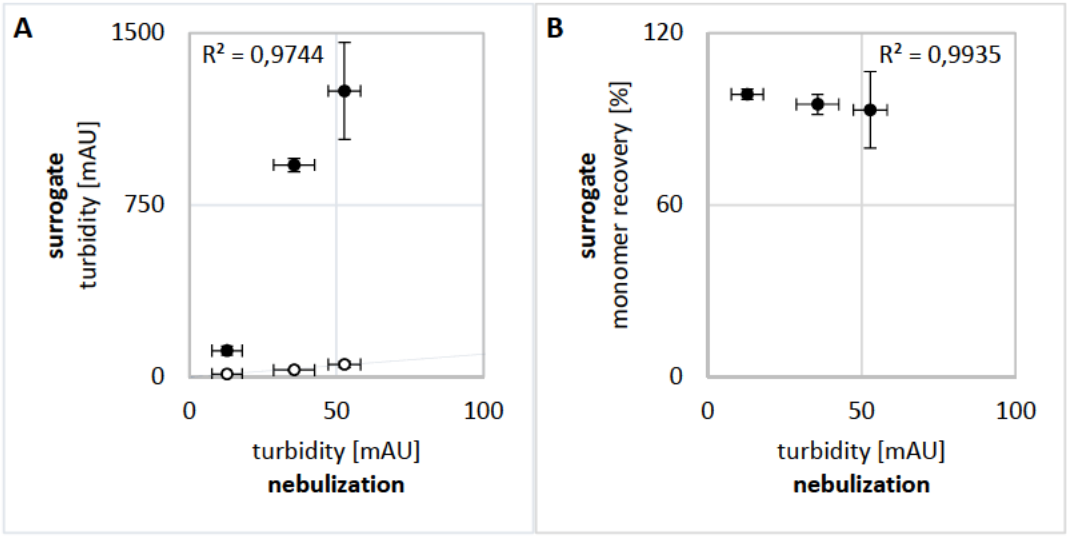

Figure V-24: Correlation of nebulization and universal surrogate setting (60 min at 30°C) for SM101 formulations (n=3, mean ± SD) including 0%, 0.005% or 0.05% PS20 with respect to turbidity (A, R^2=0.9744) and monomer loss (B, R^2=0.9935). Main diagonal and original SM101 surrogate screening (white) shown for orientation.

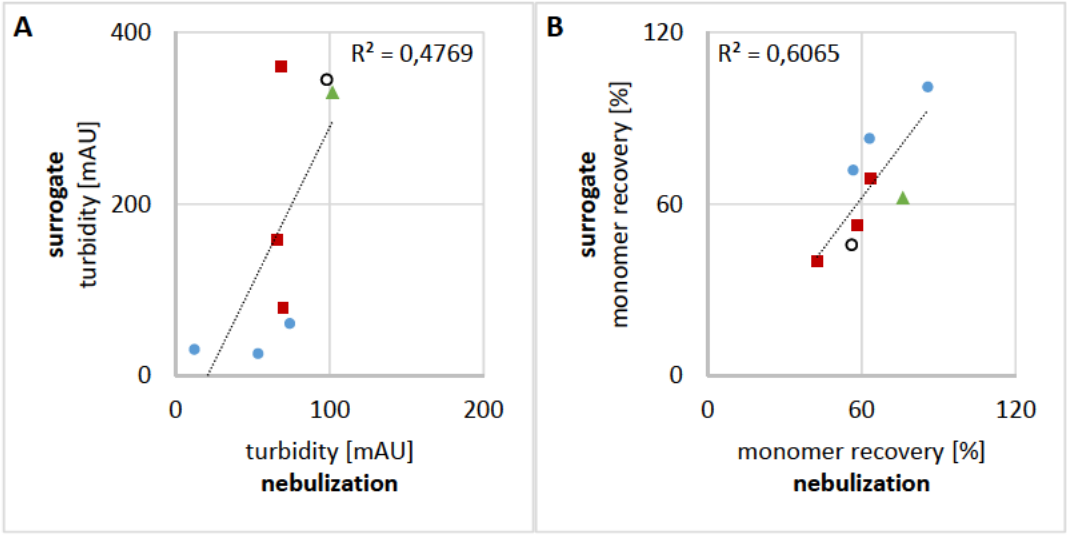

Figure V-25: Correlation of nebulization (n=3) and universal surrogate (60 min 30°C; n=3) in turbidity (A, R^2= 0.4769) and monomer recovery (B, R^2=0.6065) for G-CSF formulations including PS20 (● blue circle), HPβCD (■ red square), PEG 8000 (▲ green triangle) or no excipients (○ empty circle). Error bars are omitted to retain clarity.

As was to be expected, SM101 turbidity after 60 minute agitation was more than tenfold higher compared to nebulization. Nevertheless, both sets of turbidity values followed a common trend (R^3=0.9744) (Figure V-24). Additionally, monomer recovery data also revealed formulation dependent SM101 stability, as extensive agitation caused monomer loss that inversely correlated to turbidity after nebulization (R^2=0.9935). A rough approximation of G-CSF stability after nebulization was possible by combining the results of turbidity and monomer recovery after agitation (Figure V-25). Using this standard surrogate method results in inferior prediction accuracy but allows a fast, rough assessment of expected formulation stability toward nebulization.

4.5 Conclusion

Applicability of the surrogate screening method previously developed for SM101 was evaluated for the model proteins G-CSF and LDH. The results reveal, that the surrogate approach is also feasible for these proteins. The best correlation was achieved after protein specific adjustment of the surrogate settings. In the case of G-CSF and LDH, prolonging the agitation time was more expedient than altering incubation temperature. Protein specific adjustment can be skipped when a set of standard settings for the surrogate method is used, allowing a fast and rough assessment of expected formulation stability upon nebulization.

5 Summary

This chapter deals with the importance of a dedicated development of nebulized protein formulations. The example of SM101 clearly demonstrated that the nebulization procedure has to be an integral part of formulation development. As elucidated in chapter IV, vibrating mesh nebulization, as well as other nebulization techniques, induces significant stress that differs in its extent and factor combination from regular conditions experienced by parenteral formulations. It is therefore not covered by the range of standard stress testing. Conducting thorough nebulizations for the testing of excipients and formulation may evolve into an excessive task if several candidates shall be tested, due to long nebulization times, limited possibilities for automation or parallelization and high API consumption. A solution to these issues has been demonstrated with the surrogate method proposed in this chapter. Based on the simulation of the two major stress factors of vibrating mesh nebulization interface and heat by simple and controllable means, it allows the high throughput screening of excipient and formulation candidates. Application of the surrogate screening to three different proteins revealed that predictions could be improved with protein specific sets of surrogate screening parameters. On the other hand, universal test parameters were defined, which allowed the rapid screening of all tested proteins without the need of prior parameter optimization.

Concerning SM101, an optimized parenteral formulation with improved handling was developed for upcoming clinical trials. Based on the surrogate screening, a dedicated aerosol formulation was developed that enables the efficient vibrating mesh nebulization of 10 mg/mL SM101 without loss of activity or aggregation. This formulation will be used during *in vivo* studies of SM101 efficacy in mice.

6 References

[1] Ph.EUR., Preparations for Inhalation, in: B. European Directorate for the quality of Medicine (EDQM), Belgium (Ed.) 0671, European Directorate for the quality of Medicine (EDQM), Ph.Eur., 2008, pp. 1048-1053.

[2] R. Beasley, P. Rafferty, S.T. Holgate, Adverse reactions to the non-drug constituents of nebuliser solutions, British Journal of Clinical Pharmacology, 25 (1988) 283-288.

[3] FDA, Inactive Ingredient Database for Approved Drug Products, FDA, Center for Drug Evaluation and Research, Office of Generic Drugs, Silver Spring, MD, USA. Retrieved 09/03/2013 from http://www.accessdata.fda.gov/scripts/cder/iig/index.cfm.

[4] A.P. MacKenzie, The physico-chemical basis for the freeze-drying process, Developments in biological standardization, 36 (1976) 51-67.

[5] J.C. Kasper, W. Friess, The freezing step in lyophilization: Physico-chemical fundamentals, freezing methods and consequences on process performance and quality attributes of biopharmaceuticals, European Journal of Pharmaceutics and Biopharmaceutics, 78 (2011) 248-263.

[6] P. Kolhe, E. Amend, S. K. Singh, Impact of freezing on pH of buffered solutions and consequences for monoclonal antibody aggregation, Biotechnology Progress, 26 (2010) 727-733.

[7] Y.R. Gokarn, A.A. Kosky, E. KRAS, A. McAuley, R.L. Remmele Jr, Chapter 17, Excipients for protein drugs, in: A.C.M.V. Katdare (Ed.) Excipient Development for Pharmaceutical, Biotechnology and Drug Delivery Systems, Informa Helthcare, New York, USA, Informa Helthcare, New York, USA, 2006.

[8] Ph.EUR., Partikelkontamination - Nicht sichtbare Partikeln, in: EMEA (Ed.) 6.0/2.9.19, Ph. Eur. 6.0, pp. 4.

[9] A. Hawe, M. Wiggenhorn, M. van de Weert, J.H.O. Garbe, H.-C. Mahler, W. Jiskoot, Forced degradation of therapeutic proteins, J Pharm Sci, 101 (2012) 895-913.

[10] Sylvia Kiese, Astrid Papppenberger, Wolfgang Friess, Hanns-Christian Mahler, Shaken, not stirred: Mechanical stress testing of an IgG1 antibody, J Pharm Sci, 97 (2008) 4347-4366.

[11] A. Eppler, M. Weigandt, A. Hanefeld, H. Bunjes, Relevant shaking stress conditions for antibody preformulation development, European Journal of Pharmaceutics and Biopharmaceutics, 74 (2010) 139-147.

[12] Y.-F. Maa, C.C. Hsu, Protein denaturation by combined effect of shear and air-liquid interface, Biotechnology and Bioengineering, 54 (1997) 503-512.

[13] S. Dasnoy, N. Dezutter, D. Lemoine, V. Le Bras, V. Préat, High-Throughput Screening of Excipients Intended to Prevent Antigen Aggregation at Air-Liquid Interface, Pharmaceutical Research, 28 (2011) 1591-1605.

[14] L. Khatri, K.M.G. Taylor, D.Q.M. Craig, K. Palin, An assessment of jet and ultrasonic nebulisers for the delivery of lactate dehydrogenase solutions, International Journal of Pharmaceutics, 227 (2001) 121-131.

[15] R.W. Niven, A.Y. Ip, S.D. Mittelman, C. Farrar, T. Arakawa, S.J. Prestrelski, Protein nebulization: I. Stability of lactate dehydrogenase and recombinant granulocyte-colony stimulating factor to air-jet nebulization, International Journal of Pharmaceutics, 109 (1994) 17-26.

[16] R.W. Niven, S.J. Prestrelski, M.J. Treuheit, A.Y. Ip, T. Arakawa, Protein nebulization II. Stabilization of G-CSF to air-jet nebulization and the role of protectants, International Journal of Pharmaceutics, 127 (1996) 191-201.

[17] T. Serno, J.F. Carpenter, T.W. Randolph, G. Winter, Inhibition of agitation-induced aggregation of an IgG-antibody by hydroxypropyl-beta-cyclodextrin, J Pharm Sci, 99 (2009) 1193-1206.

[18] L.B. Salem, C. Bosquillon, L.A. Dailey, L. Delattre, G.P. Martin, B. Evrard, B. Forbes, Sparing methylation of [beta]-cyclodextrin mitigates cytotoxicity and permeability induction in respiratory epithelial cell layers in vitro, Journal of Controlled Release, 136 (2009) 110-116.

[19] L. Matilainen, T. Toropainen, H. Vihola, J. Hirvonen, T. Järvinen, P. Jarho, K. Järvinen, In vitro toxicity and permeation of cyclodextrins in Calu-3 cells, Journal of Controlled Release, 126 (2008) 10-16.

[20] T. Serno, E. Hartl, A. Besheer, R. Miller, G. Winter, The role of polysorbate 80 and HPbetaCD at the air-water interface of IgG solutions, Pharm Res, 30 (2013) 117-130.

[21] R. Bhat, S.N. Timasheff, Steric exclusion is the principal source of the preferential hydration of proteins in the presence of polyethylene glycols, Protein Science, 1 (1992) 1133-1143.

[22] T. Arakawa, S.N. Timasheff, Mechanism of polyethylene glycol interaction with proteins, Biochemistry, 24 (1985) 6756-6762.

[23] T. Arakawa, D. Ejima, K. Tsumoto, N. Obeyama, Y. Tanaka, Y. Kita, S.N. Timasheff, Suppression of protein interactions by arginine: A proposed mechanism of the arginine effects, Biophysical Chemistry, 127 (2007) 1-8.

[24] D. Shukla, B.L. Trout, Interaction of Arginine with Proteins and the Mechanism by Which It Inhibits Aggregation, The Journal of Physical Chemistry B, 114 (2010) 13426-13438.

[25] D. Shah, A.R. Shaikh, X. Peng, R. Rajagopalan, Effects of arginine on heat-induced aggregation of concentrated protein solutions, Biotechnology Progress, 27 (2011) 513-520.

[26] M. Luisetti, P. Kroneberg, T. Suzuki, Z. Kadija, B. Muellinger, I. Campo, J. Gleske, G. Rodi, W.C. Zimlich, F. Mariani, F. Ferrari, M. Frey, B.C. Trapnell, Physical properties, lung deposition modeling, and bioactivity of recombinant GM-CSF aerosolised with a highly efficient nebulizer, Pulmonary Pharmacology & Therapeutics, 24 (2011) 123-127.

[27] P. Brand, I. Friemel, T. Meyer, H. Schulz, J. Heyder, K. Häu β inger, Total deposition of therapeutic particles during spontaneous and controlled inhalations, J Pharm Sci, 89 (2000) 724-731.

[28] H. Steckel, F. Eskandar, Factors affecting aerosol performance during nebulization with jet and ultrasonic nebulizers, European Journal of Pharmaceutical Sciences, 19 (2003) 443-456.

[29] J.G. Barnard, S. Singh, T.W. Randolph, J.F. Carpenter, Subvisible particle counting provides a sensitive method of detecting and quantifying aggregation of monoclonal antibody caused by freeze-thawing: Insights into the roles of particles in the protein aggregation pathway, J Pharm Sci, 100 (2011) 492-503.

[30] H. Mach, C.R. Middaugh, Ultraviolet spectroscopy as a tool in therapeutic protein development, J Pharm Sci, 100 (2011) 1214-1227.

[31] M. Zeles-Hahn, T.J. Anchordoquy, C.S. Lengsfeld, Observations on the impact of aerosolization on macromolecular therapeutics, in: European Conference on Liquid Atomization and Spray Systems, Como Lake, Italy, 2008, pp. 8-3.

[32] A.G. Murzin, John-Marc Chandonia, Antonina Andreeva, Dave Howorth, Loredana Lo Conte, Bartlett G. Ailey, Steven E. Brenner, Tim J. P. Hubbard, C. Chothia., SCOP: Structural Classification of Proteins., http://scop.mrc-lmb.cam.ac.uk/scop/. Retrieved 11/27/2012 from http://scop.mrc-lmb.cam.ac.uk/scop/.

[33] R.W. Niven, A.Y. Ip, S. Mittelman, S.J. Prestrelski, T. Arakawa, Some Factors Associated with the Ultrasonic Nebulization of Proteins, Pharmaceutical Research, 12 (1995) 53-59.

[34] K. Schmid (2011): Spray drying of protein precipitates and Evaluation of the Nano Spray Dryer B-90. PhD thesis, Ludwig Maximilian University Munich: Faculty of Chemistry and Pharmacy.

Chapter VI SM101 *in vivo* efficacy study

1 Introduction

After successful development of a formulation allowing efficient pulmonary delivery of SM101 via nebulization (Chapter V), the ultimate stage of the thesis aimed at the demonstration of *in vivo* efficacy of pulmonary delivered SM101. Preparations for *in vivo* efficacy testing comprised the choice of a disease model adequate to demonstrate SM101 efficacy in mice and the characterization of different pulmonary administration procedures suitable for such small animals.

All *in vivo* experiments were performed by Otmar Schmid and his group at the Comprehensive Center of Pulmonology (Neuherberg, Germany). Lung deposition and distribution investigation described in 2.3 are part of the master thesis of Juliane Freitag [1]. *In vitro* evaluation of protein stability and aerosol characteristics was performed by Sebastian Hertel at the department of Pharmaceutical Technology and Biopharmaceutics, Ludwig-Maximilian-University in Munich, Germany.

Skokowa et al. had used a version of sFcγRIIB essentially equal to SM101 to examine its effect on a type III hypersensitivity reaction, also known as Arthus reaction, provoked in the lungs of mice [2]. The Arthus reaction is initiated by the binding of immune complexes (IC) by Fc-receptors on the surface of immune competent cells [3] and is therefore applicable for SM101 efficacy testing. The used mouse model relied on the induction of the immune reaction by intratracheal instillation (i.t.) of anti-OVA IgG antibody immediately followed by i.v. injection of ovalbumin (OVA) antigen. Skokowa et al. reported that i.t. administered sFCγRIIB can prevent the inflammatory cascade in the lungs of mice. It was shown that the IC resulting from antibody-antigen binding, initially activated alveolar macrophages (AM) eliciting an inflammatory response. If sFcγRIIB was administered to the lungs immediately after antibody and antigen administration, no inflammatory response occurred. Skokowa suggested that

sFCγRIIB bound IC by their Fc part and prevented Fc receptor mediated activation of AM or other Fc receptor bearing immune competent cells.

While the so called reverse passive Arthus reaction [4, 5] is a common model to induce IC-triggered hypersensitivity (type III) [6], the suggested setup may be not suitable to evaluate the efficacy of SM101 *in vivo*. Skokowa et al. delivered both antibody and antigen in an opposite to physiologic manner. Antigen was administered via i.v. injection while it is naturally inhaled in pulmonary Arthus type reactions like the Farmer's lung disease. Antibodies, on the other hand, are naturally secreted by plasma cells and infiltrate the site of immune reactions from the systemic circulation. But in the study, they were administered through the lungs. This interchange has serious consequence for the model. The delivery of both antibody and sFcγRIIB through the lungs increases the possibility of direct binding of sFCγRIIB to the Fc part of the IgG before encounter of antibody and antigen, i.e. in the lung lining fluid. So, instead of formation of IC as the initial step triggering the Arthus reaction, antigen-antibody binding does not occur and the entire disease model is interrupted. The condition to be treated with sFcγRIIB would not be induced in the first place. This may falsely be mistaken as therapeutic efficacy of SM101. It was therefore necessary to modify the protocol used by Skokowa et al. to a non-reverse Arthus reaction to enable a meaningful evaluation of SM101 efficacy *in vivo*.

A second need for optimization originates from the importance of homogeneous distribution of the pulmonary delivered agents in this disease model. The spatial distribution of drug delivered into the lungs by i.t. instillation is non-uniform and patchy and is confined to central lung regions [7, 8]. As a consequence, an immune response to OVA antigen — the foundation of this disease model — will only be provoked in those patches of lung tissue to which OVA antigen (in case of a non-reverse Arthus reaction) or anti-OVA antibody (in case of a reverse Arthus reaction) has been delivered. Brain et al. [9] could show that the non-uniformity of i.t. instillation is mostly random, meaning that a subsequent instillation may not cover the same lung patches as the previous one. Therefore, after subsequent delivery of antibody, antigen and the treatment (SM101) three situations may occur: A patch of lung tissue, e.g. an alveolus, received both the trigger (antigen or antibody) and treatment fluids as intended. An alveolus received only the treatment fluid but no trigger, which is merely ineffective. Finally, the delivery of only the triggering fluid while missing the treatment may be problematic. In such regions, an

inflammatory cascade will be triggered even if SM101 was efficacious. Due to the averaging of the inflammatory response indicators over the entire lung by bronchoalveolar lavage fluid (BALF) collection and analysis, this would result in significant noise and attenuate SM101 efficacy results. Therefore different methods of pulmonary drug delivery to mice were compared regarding efficiency and reproducibility of aerosol deposition and the homogeneity of spatial distribution in the lungs. Ultimately, the stability of SM101 as well as antigen and antibody towards the respective administration methods was examined.

2 Small animal aerosol delivery with a pneumatic MicroSprayer®

2.1 Introduction

Aerosol delivery to small laboratory animals like mice is a complicated endeavor. Most of these animals are nose-breathers which together with the small size of their airways results in poor delivery efficiency to the lungs [9]. Aerosol delivery with common nebulization techniques requires the use of special equipment like exposure chambers, where a large fraction of the aerosol may not be inhaled but deposits on the skin or pelt and may be ingested during grooming [9]. The actual dose deposited in the lungs depends on the breathing pattern, aerosol droplet size and airway and alveolar dimensions [9]. The exact dose is therefore not easily assessed and may lack reproducibility.

Therefore, instead of inhalation, pulmonary delivery to small animals is often accomplished by oro-tracheal (o.t.) instillation of a liquid. This approach is considerably simpler and does not require special equipment like inhalers and exposure chambers. Dose delivery is very efficient and the administered dose can be precisely controlled and calculated. Large doses can be administered in a short timeframe. Instillation can therefore be considered time and material saving. Accidental drug ingestion or topical exposure is ruled out. On the other hand, i.t. instillation is non-physiological and as mentioned above results in non-uniform and patchy drug distribution, which is confined to central lung regions [7, 8]. Delivery of large volumes may lead to pooling of liquid

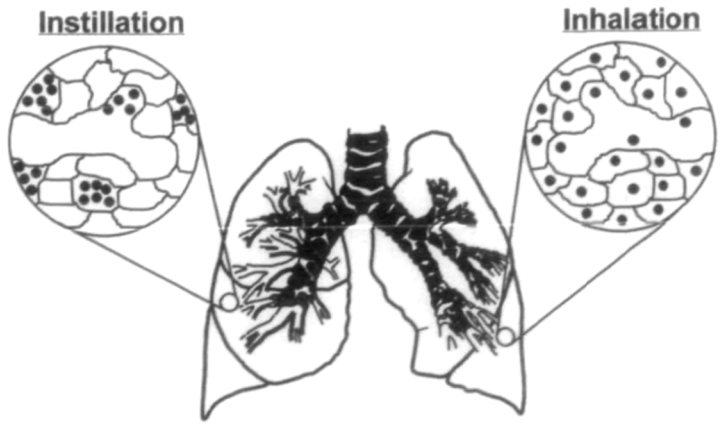

Figure VI-1. Differences in particle distribution following an instillation or inhalation exposure, illustrating the decreased homogeneity of an instilled dose. Taken from [10].

in lung parenchyma [11]. Inhalation is associated with a wider and more homogeneous spatial distribution to central and peripheral regions [9] as illustrated in Figure VI-1 [10].

An alternative approach to small animal aerosol delivery is i.t. aerosolization. The MicroSprayer®, a high pressure syringe with a special needle that generates an aerosol from its tip, uses the pressure of manual actuation to creates a coarse aerosol of 15 30µm [12] directly in the trachea. This method combines some of the advantages of instillation with those of inhalation. Since it involves intubation, a skilled operator is required but otherwise no special equipment is necessary. Dosing is reproducible and the precise delivered dose is known. The spatial distribution is expected to be more homogeneous compared to instillation but may depend on the operator. No detailed investigation of lung deposition and distribution in comparison with instillation or nebulization has been reported. Aiming to improve the reproducibility of aerosol application and to eliminate the influence of the individual operator, a pneumatic actuator for automatic operation of the MicroSprayer® has been developed by the group of O. Schmid (CPC). The newly developed actuator is customizable regarding the preset sprayed volume and the pneumatic actuation pressure. Additionally, the tip of the MicroSprayer® is held in a fixed position during spraying which can reduce the risk of injuring intubated animals by accidental movements during actuation. In a first stage, the pneumatic actuator was compared to manual operation of the MicroSprayer® *in vitro* with regard to the aerosol droplet size distribution. In subsequent experiments, *in vivo* lung deposition and spatial distribution were compared after instillation, MicroSprayer® aerosolization and vibrating mesh (VM) nebulization.

2.2 *In vitro* comparison of manual and pneumatic actuation of a MicroSprayer®

Aerosol characteristics of physiologic saline were compared for manual actuation by three different operators and by pneumatic actuation. Pneumatic actuation was performed at pressures of 2-8 bar. Aerosol characteristics were analyzed in a time resolved manner via laser diffraction.

When actuated manually, the droplet size profile featured a sharp initial drop by 30-40 µm before reaching a constant droplet size during the remaining spray time (Figure VI-2 A). This final droplet size was significantly influenced by the operator, ranging from 20-30 µm thus varying by up to 50%. The standard deviation for manual use by one operator was in a range of 1-4 µm.

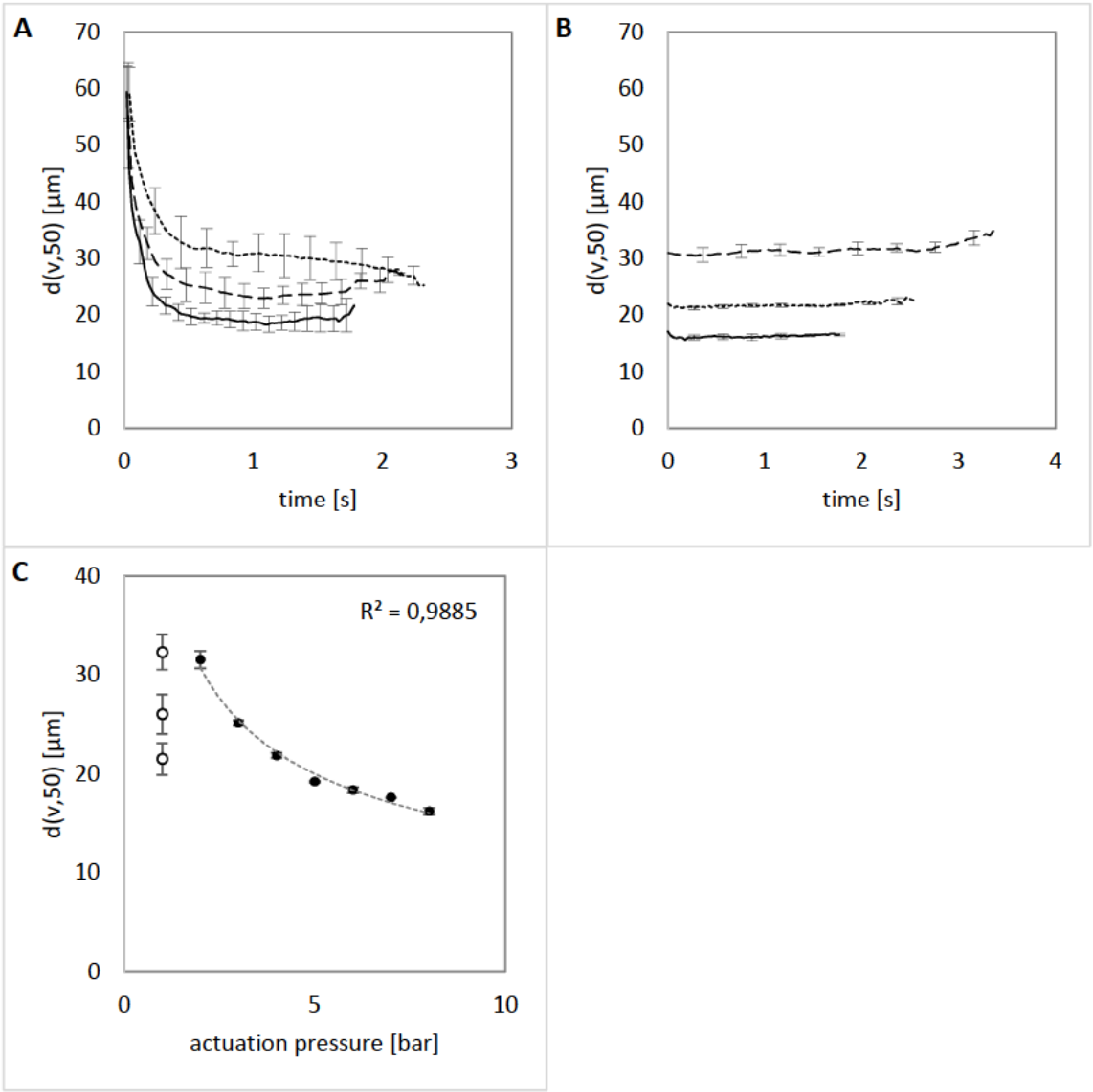

Figure VI-2: Course of d[v,50] after manual actuation (A) by three different operators or pneumatic actuation (B) at 2 (dashed line), 4 (dotted line) or 8 bar (solid line)(n=4, mean ± SD; SD is only displayed for every 10th data point to retain clarity). (C) Droplet size of the MicroSprayer® in dependence of actuation pressure of pneumatic actuation (filled circles) compared to manual actuation (empty circles) (n=4, mean ± SD).

Droplet size profiles after pneumatic actuation did not exhibit the initial decrease observed for manual operation but instead generated droplets of very constant diameter throughout the entire spraying duration (Figure VI-2 B). The d[v,50] was very reproducible and inversely proportional to the pneumatic actuation pressure (Figure VI-2 C). Increasing actuation pressure also shortened spray times. Increasing the actuation pressure in steps of 1 bar in a range of 2-8 bar resulted in a continuous decrease in VMD from 32µm to 16µm. The observed impact of actuation pressure on droplet size may also explain the observed variability of manual actuation, since the manual pressure applied is dependent on the operator. The speed and force of pneumatic actuation had to be accounted for when setting the actuation distance of the piston, in order to prevent a bold collision between the piston and the syringe barrel. This resulted in a volume of 67 µL remaining in the MicroSprayer® after pneumatic actuation compared to only 13 µL residual volume after manual operation, so that the charged volume had to be adapted accordingly. During manual actuation however, the last fraction of loaded solution left the MicroSprayer® as 1-2 large droplets instead of an aerosol spray which did not occur with pneumatic actuation.

According to these *in vitro* data, the newly designed pneumatic actuator improves the uniformity and reproducibility of MicroSprayer® generated aerosols and mitigates individual operator impact. It can further be utilized to control the droplet size in a range of 16-32 µm.

2.3 Impact of the application method on lung distribution and deposition in mice

If and how the effect of pneumatic actuation pressure influences aerosol deposition *in vivo* was subject of the following investigation. Fluorescently labelled SM101 was administered to CL57/B6 mice by either i.t. instillation, vented intubated nebulization (IVN) with an Aeroneb® Pro VM nebulizer or pneumatically actuated MicroSprayer® (MS) aerosolization, while the latter was performed with actuation pressures of either 2.2 or 4.0 bar. Immediately after administration, mice were sacrificed, the lungs excised and examined with respect to the deposited lung dose and spatial distribution of the administered drug between the lung lobes. Fluorescence detection for the five lobes and the trachea was initially performed with an IVIS 100 CCD imaging system. To confirm IVIS results, the same lung lobes were subsequently homogenized and the contained amount of fluorescent dye determined from the supernatant. Alexa Fluor® 750 was used as a

fluorescent marker since its emission spectrum lies in the near-infrared region where tissue attenuation is minimized. The IVIS utilizes fluorescent reflective imaging and is capable of *in vivo* imaging. It is regularly used to visualize tumor development or inflammatory processes. Fluorescence imaging of excised murine lungs to examine drug deposition and distribution has been previously suggested [13] and may be an alternative to scintigraphic methods that are usually not suitable for imaging of small animals.

2.3.1 Lung deposition

Determination of the fraction of SM101-Alexa750 found inside the lungs revealed that use of the MicroSprayer® yielded a deposition efficiency equal to that after instillation of the same solution (Figure VI-3). A lower standard deviation indicated better reproducibility with the MicroSprayer®. The pressure of pneumatic actuation did not have a major impact on lung deposition, whereas the lower pressure resulted in a slightly higher recovery of SM101-Alexa750 in the murine lungs. Relative lung deposition after IVN was only 2.1% or 2.2% according to lung homogenate and IVIS respectively. The data does not allow a direct conclusion on the deposition efficiency in regard to the initially loaded dose. In a separate experiment, a pristine lung augmented with the exact initial dose served as the 100% reference. A deposition efficiency in the range of 73-88% was observed for i.t. instillation.

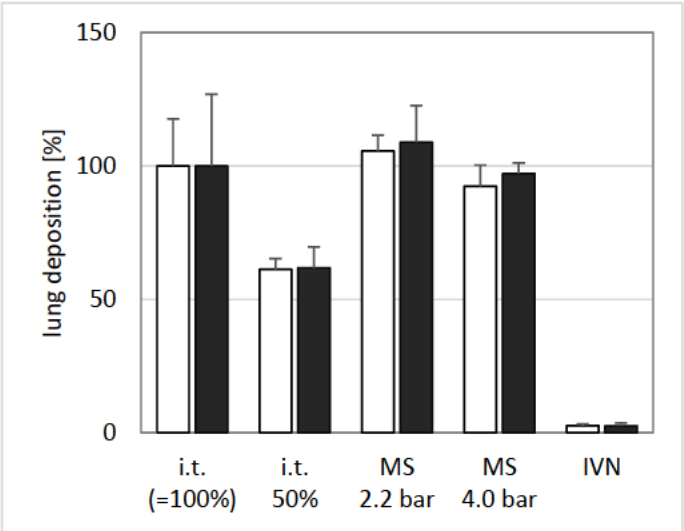

Figure VI-3: Relative fluorescence intensity of SM101-Alexa750 conjugate deposited in murine lungs in comparison to i.t. instillation (=100%) determined by IVIS (black bars) or from supernatant of homogenized lungs (white bars), n=4 (mean ± SD).

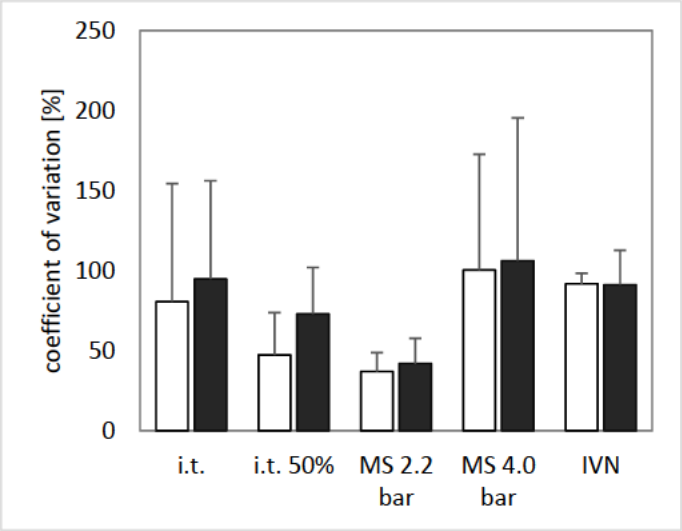

Figure VI-4: Uniformity of distribution among lung lobes expressed as the coefficient of variation of the mass-normalized fluorescence intensity of each of the 5 lobes, calculated with IVIS (black bars) or lung homogenate (white bars) data, n=4 lungs (mean ± SD).

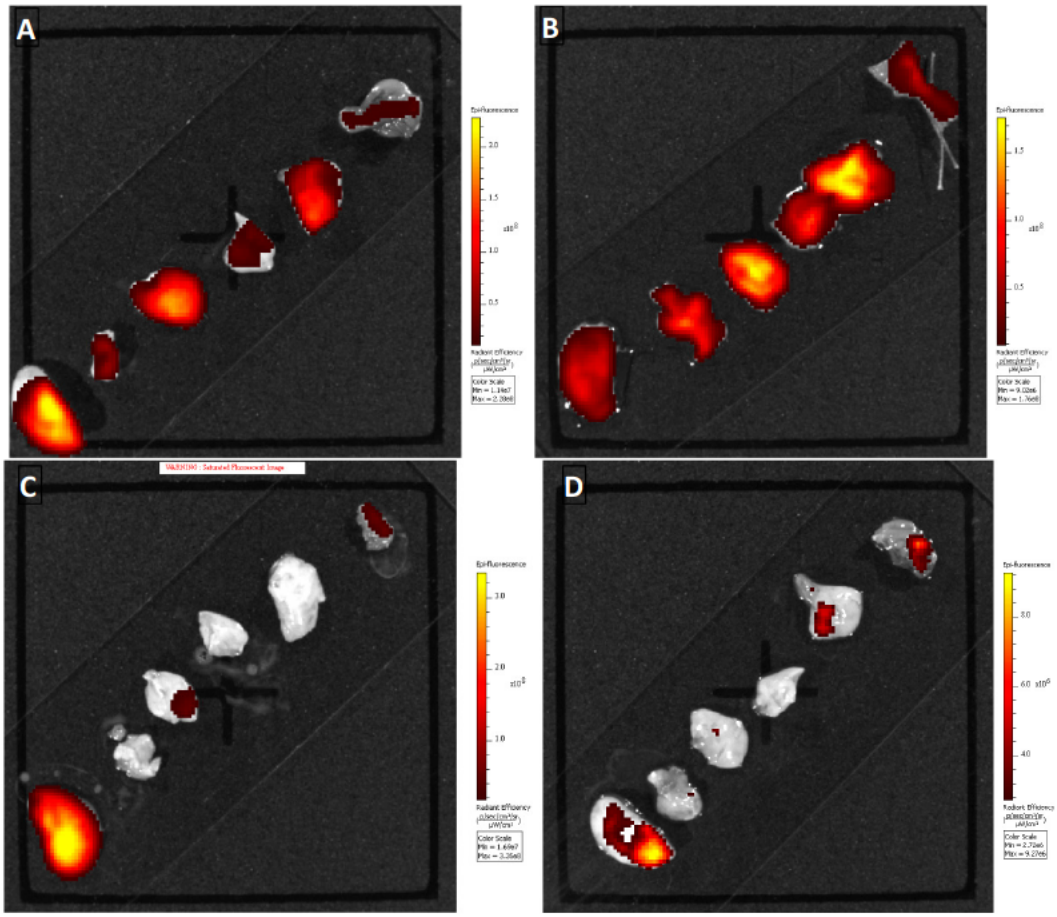

Figure VI-5: IVIS scans of murine lungs after i.t. instillation (A), MS 2.2 bar (B), MS 4.0 bar (C) and IVN (D) of SM101-Alexa750. The lobes are ordered from the lower left to the upper right: lobe 1 to 5 and the trachea in the upper right corner.

2.3.2 Lobes distribution

For information about the spatial distribution of the administered SM101-Alexa750, the lobes were segregated and fluorescence intensity assessed for each lobe individually. Values were normalized for lobe mass and the coefficient of variation among the five lobes of each lung calculated (Figure VI-4). Unlike lung deposition, the inter-lobal distribution was influenced by the actuation pressure of the pneumatic MicroSprayer®. Actuation at 4 bar resulted in a non-uniform aerosol distribution among the lobes comparable to the situation found for instillation with inter-lobe variability in a range of 80-110%. MicroSprayer® actuation at 2.2 bar, on the other hand, cut inter-lobe variability by more than half to approximately 40% as consistently determined by IVIS and in the homogenate. Inter-lobe variability after IVN was comparable to i.t. instillation.

IVIS scans (Figure VI-5) and individual lobe data after homogenization (Figure VI-6) reveal that the high variation coefficients for instillation, 4 bar microspraying and IVN mainly resulted from non-uniform distribution in some lungs (Figure VI-6: instillation lung 4; MS 4 bar lungs 1 and 3; IVN lungs 2 and 4). In these lungs SM101-Alexa750 was only delivered into the left or the right bronchus. As visible in Figure VI-7, the murine lung consists of 5 lobes whereas lobe 1 is the only lobe attached to the left bronchus, while lobes 2 to 5 are attached to the right bronchus. IVIS scans of lung 3 of MS 4.0 bar and lung 4 of IVN (Figure VI-5 C and D) clearly demonstrate this observation. Only lobe 1 exhibited notable fluorescence signals, while lobes 2-5 did not receive significant amounts of the dye. These results were confirmed by the distribution data calculated from lung homogenate measurements (Figure VI-6). IVIS scans and homogenate data reveal that pneumatic microspraying at 2.2 bar resulted in the most homogeneous inter lobe distribution of fluorescence intensity of all measured lung samples.

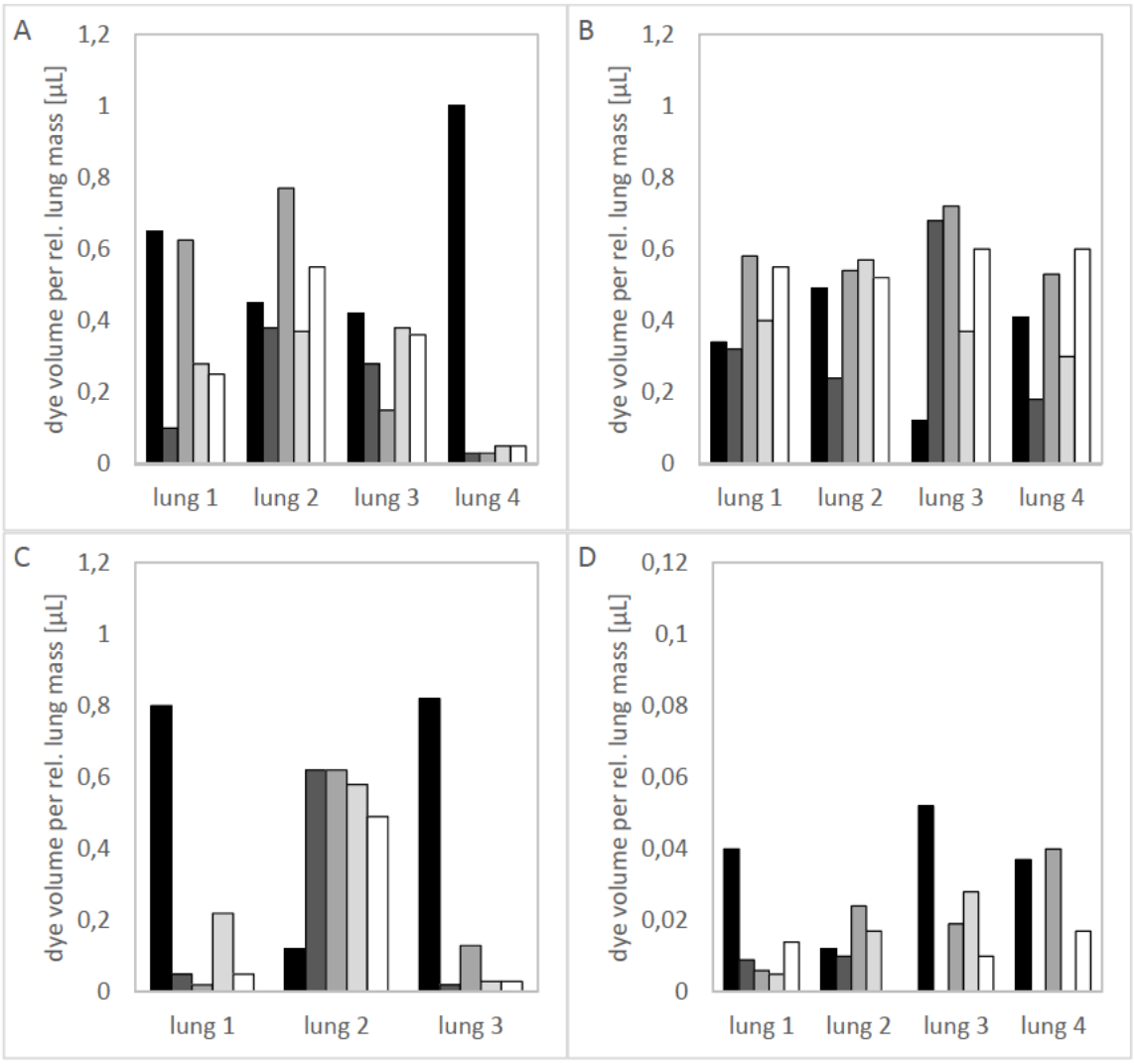

Figure VI-6: Deposited dye volume normalized for relative lung mass of individual lobes (5 lobes per lung) after i.t. instillation (A), Microspraying at 2.2 bar (B) or 4.0 bar (C) and IVN (D).

The one-sided pulmonary distribution observed for i.t. instillation and IVN may be caused by improper placement of the intubation tube leading to dye distribution biased for one bronchus. The observed impact of MS actuation pressure on lung distribution is contrary to what may be expected from the correlation of actuation pressure and *in vitro* droplet size. While a more uniform drug distribution may be anticipated from the finer aerosol size generated with increasing actuation pressure, the opposite was observed: At low pressure actuation of the MS, spatial distribution was more uniform compared to instillation. These advantages over instillation were completely offset when actuated at a high pressure. An explanation may be provided by aerosol spray velocity that is also influenced by actuation pressure. As shown in Figure VI-2, doubling the actuation pressure from 2 to 4 bar resulted in a decrease of the spray time, e.g. the time necessary to move the MicroSprayer® piston from start to end position from 3.3 s to 2.5 s. In consequence, aerosol velocity may have increased by 33%, assuming that piston speed directly

translates to droplet velocity. The probability of droplet impaction, the predominant deposition mechanism in the prevalent droplet size range, increases with rising velocity (inertial Impaction ~ d^2 * v). High aerosol velocity in combination with a suboptimal, angled position of the MS aerosolizer tip inside the trachea could force all aerosol into only one bronchus, resulting in one-sided distribution as observed for high pressure MS administration.

After completion of the experiment, malfunctioning of the Aeroneb® Pro nebulizer utilized for IVN was noted. The median droplet size was found to range above 8 µm instead of the 5.0 µm determined for functioning devices. A significant impact on lung deposition is to be expected, since aerosol deposition in the ventilation tubes connecting the nebulizer to the lung will be increased for an increased droplet size and less aerosol will leave the distal end of the intubation tube and enter the lung. The deposition data determined for IVN in the course of this study are therefore considered as too low. In fact, while a deposition of approximately 2% was found (Figure VI-3) in this study, experiments with another Aeroneb® Pro resulted in a deposition range of 10-20% (O. Schmid 2014, personal communication).

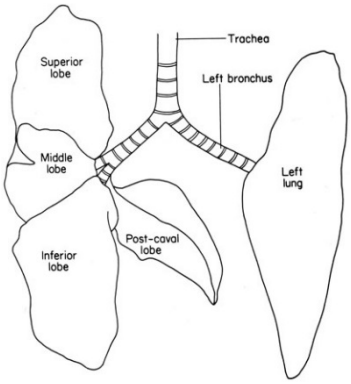

Figure VI-7: Allocation of the five lobes of a murine lung into one left lobe and four right lobes.

2.4 Conclusion

The comparison of i.t. aerosolization with a MicroSprayer® against plain i.t. instillation showed that the MicroSprayer® allows an equally high dosing efficiency, with slightly improved dosing reproducibility. Furthermore, the inter-lobe distribution is more uniform after MicroSprayer® administration if the actuation pressure is kept below 4 bar. Actuation at 4 bar diminished uniformity of distribution to a level found after instillation. Precise control of MS actuation is not possible during manual use but can only be ascertained with the newly developed pneumatic actuator. Otherwise, no evidence was found of any favorable *in vivo* effect of droplet size

reduction from approximately 32 µm to 20 µm by increasing pneumatic actuation pressure. Instead, advantageous distribution after low pressure actuation may be a consequence of the resulting slow aerosol velocity.

Due to malfunctioning of the Aeroneb® Pro used for IVN, the obtained results are no basis for valid assumption on the deposition and distribution characteristics of this pulmonary application method in murine lungs. A problem observed for i.t. instillation, high pressure microspraying and IVN was undesired one-sided drug deposition. It is therefore very important to place the intubation tube and the tip of the cannula or aerosolizer in an optimum position in the trachea to avoid one-sided pulmonary delivery. The MicroSprayer® is a suitable tool for pulmonary administration of liquids, where the exact dosing of instillation and the uniform distribution of nebulization have to be combined.

IVIS results for lung deposition and lobe distribution were essentially identical to the data obtained from the lung homogenate. It is an attractive orthogonal method, allowing fast generation of pulmonary deposition and distribution data without the need of laborious sample preparation that may be a potential source of artifacts, e.g. through deterioration of sensitive fluorescent dyes. More research seems vindicated to fully exploit the full potential of the IVIS for ex vivo or *in vivo* imaging of small animal pulmonary drug delivery.

3 Stability of proteins toward microspraying and low volume vibrating mesh nebulization

3.1 Introduction

As demonstrated in chapter IV, atomization can cause proteins to denature depending on its sensitivity to the encountered stress. It was therefore a necessity to investigate the different methods for pulmonary application in mice regarding their impact on the stability of the employed proteins.

For the Arthus disease model, stability after pulmonary delivery has to be assured not only for the treatment protein SM101 but also for anti-OVA IgG antibody or OVA antigen in the case

of the reverse or non-reverse (direct) passive Arthus model respectively. Insufficient stability of OVA or anti-OVA IgG may lead to a failure of the disease model. SM101 degradation on the other hand, would impact on the results of treatment efficacy. As demonstrated for VM nebulizers in chapter IV, protein aggregation may also lead to a failure of the atomization device. Analogously, protein aggregates and adsorption may impair proper function of the small orifice of the MS.

While plain i.t. instillation was assumed to cause no significant protein degradation, the MicroSprayer® may impact protein stability by detrimental forces like interfacial stress or shear stress during mechanical atomization in the aerosol tip and was therefore object of investigation. The setup available for aerosol delivery relies on vented intubated nebulization (IVN) and was originally built around an Aeroneb® Pro nebulizer but may be customized to integrate different VM nebulizers. Three different models were therefore characterized regarding nebulizer performance under the operating conditions intended for the *in vivo* study. The nebulization conditions differ in respect to charged volume and nebulization procedure. Instead of reservoir overloading and the nebulization of 3-4 mL, volumes as small as 100 µL were charged into the reservoir and nebulized completely. Based on aerosol performance, a suitable nebulizer was selected to be used for stability testing of SM101, OVA and anti-OVA IgG under these nebulization conditions.

3.2 Choice of a nebulizer for vented intubated nebulization during in *vivo* studies

Comparison of aerosol characteristics with placebo aerosol formulation showed that VM nebulizer models of different manufactures exhibit significantly different aerosol performance, an observation already made during previous investigations (Chapter IV). The PARI eFlow® generated aerosol at the highest output rate that was more than double that of the Aeroneb® Pro or Solo model (Figure VI-8 A). The PARI eFlow® also outperformed the Aeroneb models concerning fine particle fraction (FPF), although the difference was less marked (Figure VI-8 B). As already elaborated on in chapter IV, the superior aerosol performance of the PARI eFlow® is accompanied by significant heating inside the medication reservoir. Heating was less distinct or insignificant for the Aeroneb® Pro and Solo respectively (Figure VI-8 C).

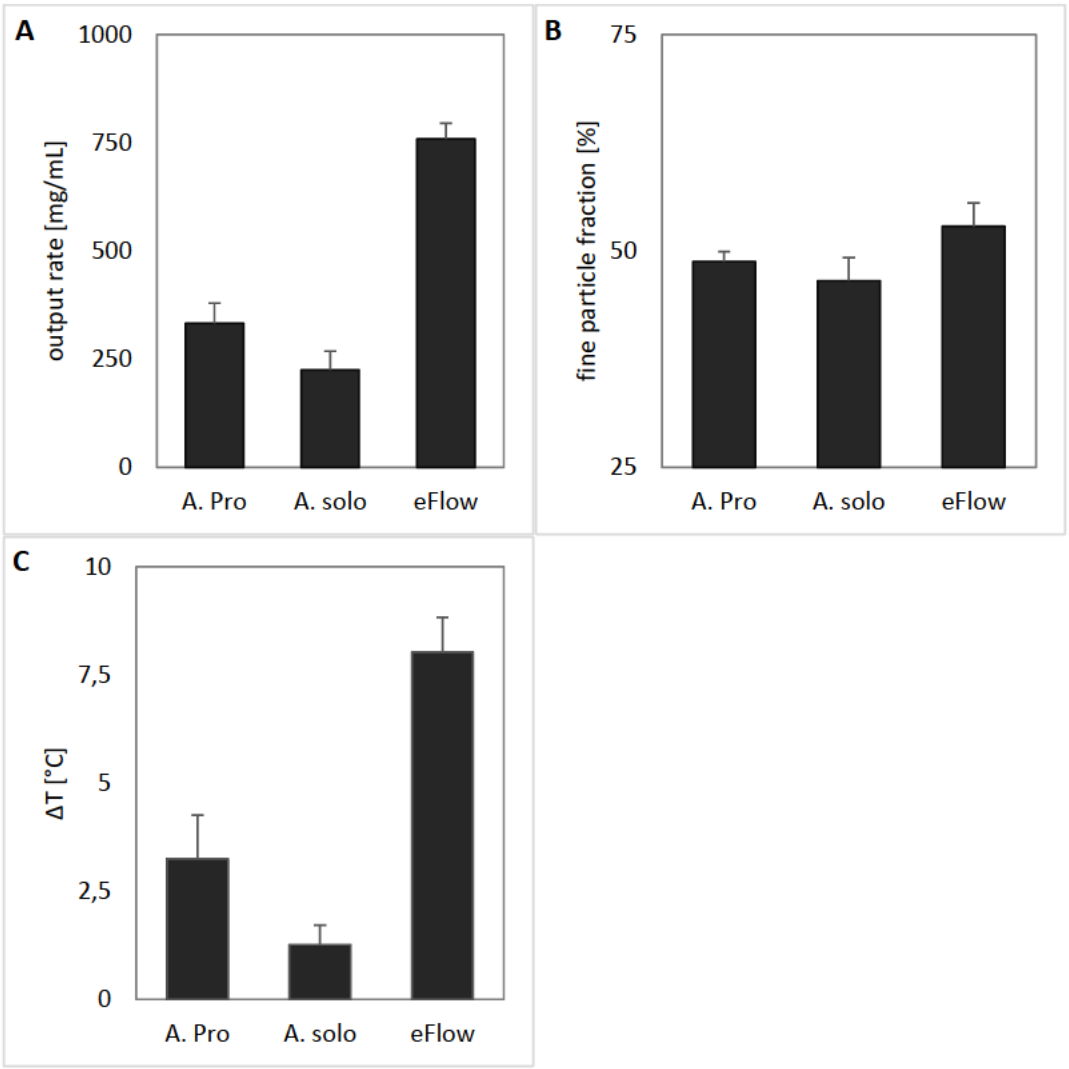

Figure VI-8: Comparison of the characteristics output rate (A), fine particle fraction (B) and reservoir temperature change upon operation (C) of three vibrating nebulizers for application during in vivo studies.

Since no measures to manage reservoir temperature (Chapter IV) during the *in vivo* study were designated in order to keep handling as simple as possible, the Aeroneb® Pro nebulizer was selected for use with the study as a compromise between heating and aerosol performance. Furthermore, no adaption to the existing apparatus for IVN was necessary.

3.3 SM101

3.3.1 MicroSprayer®

In tentative experiments 200 µL formulations of different SM101 concentrations were atomized, so that a total of 50 µg, 100 µg or 200 µg SM101 were sprayed with a MicroSprayer® that was actuated with a pneumatic pressure of 2.2 bar. Stability after atomization of the according

concentrations of 0.25, 0.5 and 1.0 mg/mL SM101 was assessed in either HBS buffer or the previously developed aerosol formulation (Chapter V).

None of the tested formulations and concentrations exhibited an increased turbidity after MS atomization (Figure VI-9 A), indicating that no significant aggregation of SM101 occurred. When formulated in HBS a concentration dependent loss of SM101 monomer was observed after MS atomization. At the lowest SM101 concentration of 0.25 mg/mL 7% monomer was lost. Increasing the SM101 content to 0.5 mg/mL or 1.0 mg/mL reduced the monomer loss to 3.4% or 1.2% respectively (Figure VI-9 B). This observation was confirmed by SM101 concentration measurements with a UV/Vis photometer (Figure VI-9 C). Atomization of SM101 formulated in the aerosol formulation prevented any monomer loss.

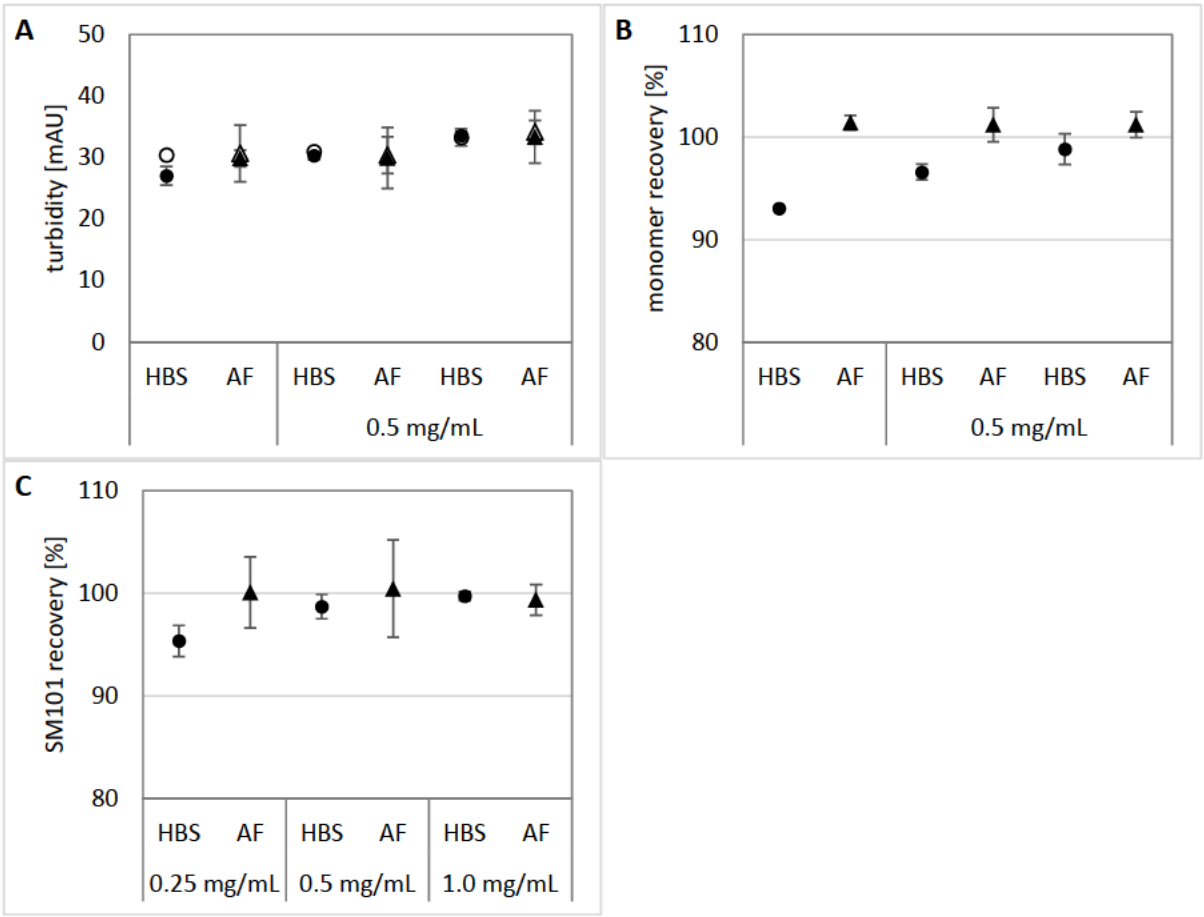

Figure VI-9: Turbidity (A), monomer recovery (B) and SM101 recovery (C) of 0.25, 0.5 or 1.0 mg/mL SM101 in HBS (circle) or aerosol formulation (triangle) before (empty symbols) and after (filled symbols) pneumatic atomization with a MicroSprayer® with 2.2 bar actuation pressure, n=3 (mean ± SD).

3.3.2 Aeroneb® Pro

Assuming a deposition of approximately 10% of the charged dose into the murine lung by IVN with an Aeroneb® Pro, 100µL of 10 mg/mL SM101 had to be nebulized to deliver 100 µg SM101. SM101 stability after nebulization under this low volume conditions was investigated and the parenteral formulation and the aerosol formulation were tested. Nebulization of 100µL of the parenteral formulation led to the distinct SM101 aggregation as observed by turbidity (Figure VI-10 A) and subvisible particles > 1 µm (Figure VI-10 B). The soluble aggregate content was not significantly altered, while monomer recovery decreased to 98.4% (Figure VI-10 C). When formulated in the aerosol formulation (AF), 100% SM101 monomer was recovered and aggregation was completely prevented according to turbidity and light obscuration data.

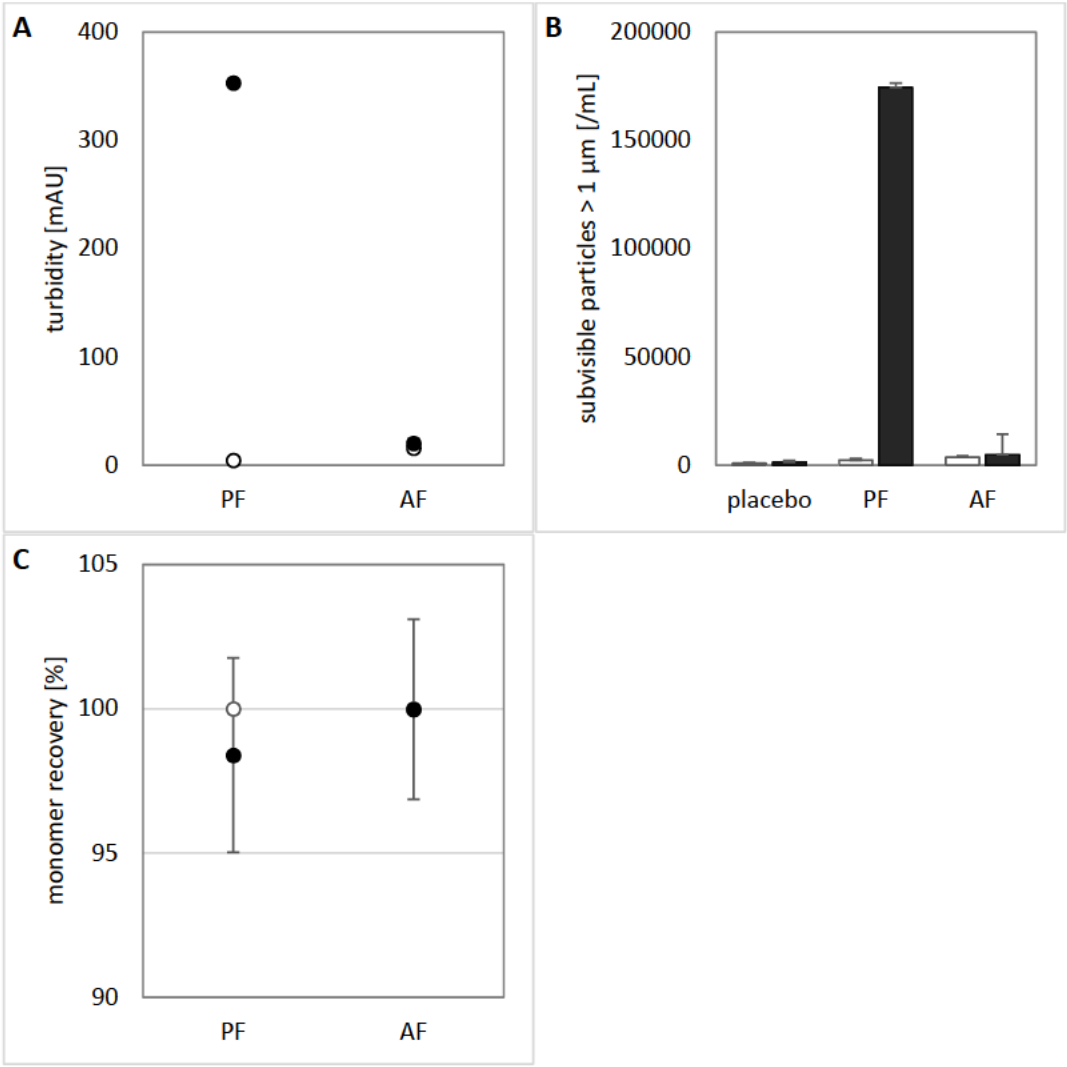

Figure VI-10: Turbidity (A), subvisible particles (B) and monomer recovery (C) of 10 mg/mL SM101 in the parenteral formulation (PF, n=2) or the aerosol formulation (AF, n=4) before (empty) and after (filled) vibrating mesh nebulization with an Aeroneb® Pro (mean ± SD).

3.4 OVA

3.4.1 MicroSprayer

The stability of OVA after atomization with a MicroSprayer® was tested under the conditions intended for use during *in vivo* experiments. Therefore, 200 µL of 2 mg/mL OVA formulated in PBS was atomized for a total delivery of 400 µg OVA antigen. OVA stability was not negatively affected by atomization, with a monomer recovery of 99.4±1.0% (Table VI-1). The fraction of soluble aggregates remained essentially unchanged with 17.8±0.4% observed prior and 16.9±0.9% after atomization. Accordingly, turbidity remained essentially unchanged as well.

Table VI-1: Stability of 2 mg/mL OVA in PBS after atomization with a MicroSprayer® regarding monomer recovery and soluble aggregation determined by SE-HPLC and turbidity, n=3 (mean ± SD).

	before atomization	after atomization
Monomer recovery [%]	100.0 ± 0.6	99.4 ± 1.0
Soluble aggregates [%]	17.8 ± 0.4	16.9 ± 0.9
Turbidity [mAU]	39 ± 2	40 ± 0

3.4.2 Aeroneb® Pro

Stability of OVA to VM nebulization with an Aeroneb® Pro was tested for OVA concentrations of 4.0 and 10.0 mg/mL formulated in PBS. Nebulization led to a loss of 11.8% or 7.4% monomer respectively (Figure VI-11 C). The soluble aggregate content remained constant at 8.0±0.1%. Turbidity increased by 20 mAU for both OVA concentrations indicating some aggregate formation (Figure VI-11 A). According to LO data, a slight increase in subvisible particles > 1µm was observed but did not exceed that found for nebulized placebo and was therefore considered to consist mainly of non-proteinaceous material (Figure VI-11 B). Visual inspection of the collected aerosol revealed that instead of dispersed subvisible particles, a coherent transparent gel had formed on the inner surface of the polypropylene (PP) tube used for aerosol collection. After aspiration of the supernatant the gel was pelleted by centrifugation and the residual mass was determined after drying for three hours at 80°C. The residual mass of 0.65 mg and 1.05 mg found for 4 mg/mL and 10 mg/mL OVA made up 5-8% of the OVA content of the initially charged solution (Figure VI-11 D). In some occasions the nebulization times notably increased, suggesting that the gel occluded part of the nebulizer mesh, thus preventing proper operation comparable to the mesh occlusion described in Chapter IV.2.6.

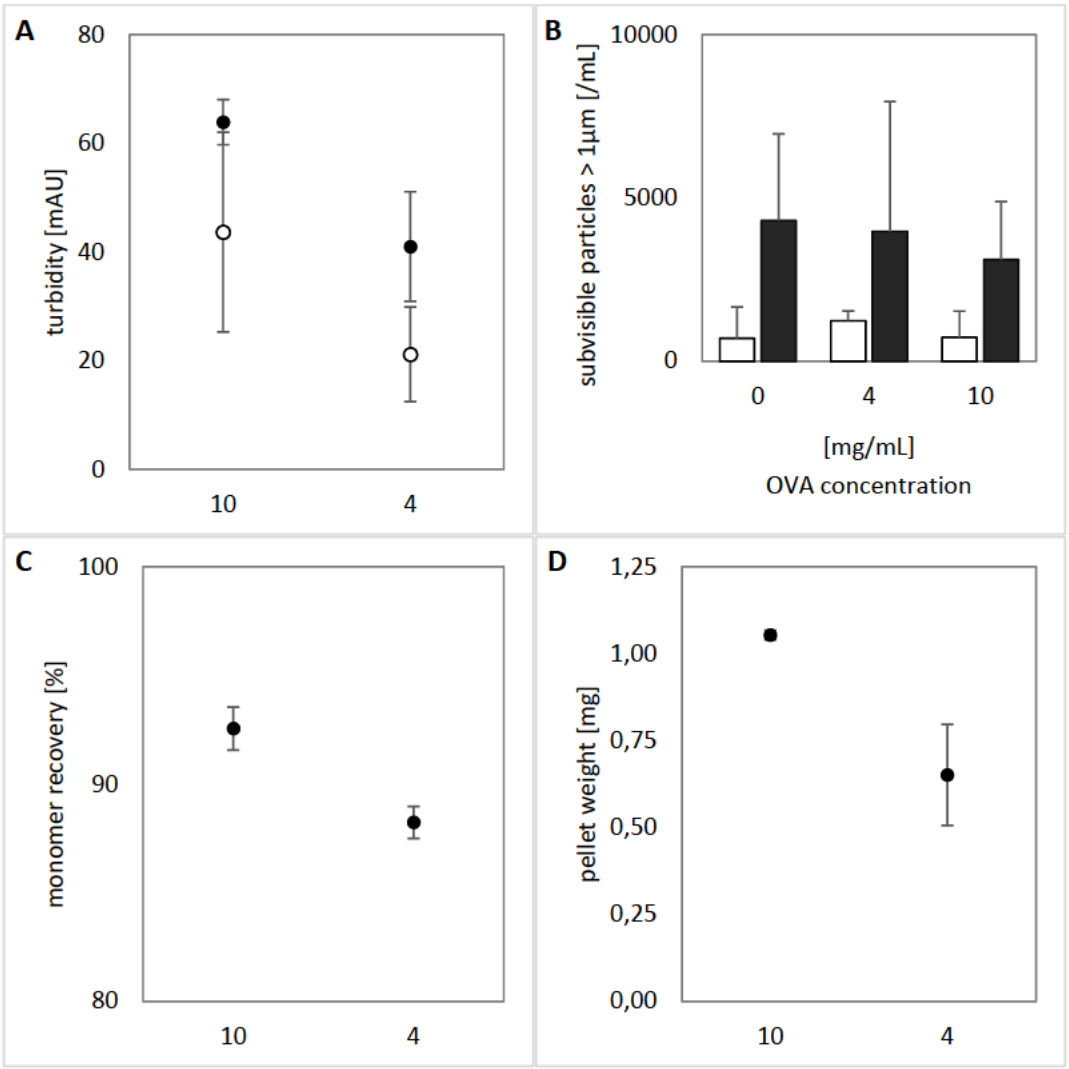

Figure VI-11: Turbidity (A), subvisible particles > 1 µm (B), monomer recovery (C) and aggregate pellet residue (D) of 0, 4.0 and 10.0 mg/mL OVA formulated in PBS before (white) and after nebulization with an Aeroneb® Pro (black), n=3 (mean ± SD).

Heat-induced gelation of OVA and other globular proteins is a common phenomenon [14, 15] with significance in food processing. OVA gels are formed by cross-linking of branched linear OVA aggregates [16] by means of hydrogen bonds, ionic and hydrophobic interactions and disulfide bonds [17]. Branching of aggregates and thus gelation can be controlled by pH and ionic strength [16, 17].

Two different approaches for OVA stabilization were compared. Either 0.04% PS20 were added to the PBS buffer to protect OVA from interfacial degradation or OVA was formulated with reduced ionic strength in a 10 mM potassium phosphate buffer at pH 7.4 instead of PBS. Both formulations prevented OVA gelation but while a decrease in ionic strength also reduced OVA aggregation and kept monomer loss at 4.4%, addition of PS20 provoked an increase of both

turbidity (Figure VI-12 A) and subvisible particles > 1 µm (Figure VI-12 B). This was accompanied with 8.3% monomer loss for the PS20 containing formulation (Figure VI-12 C).

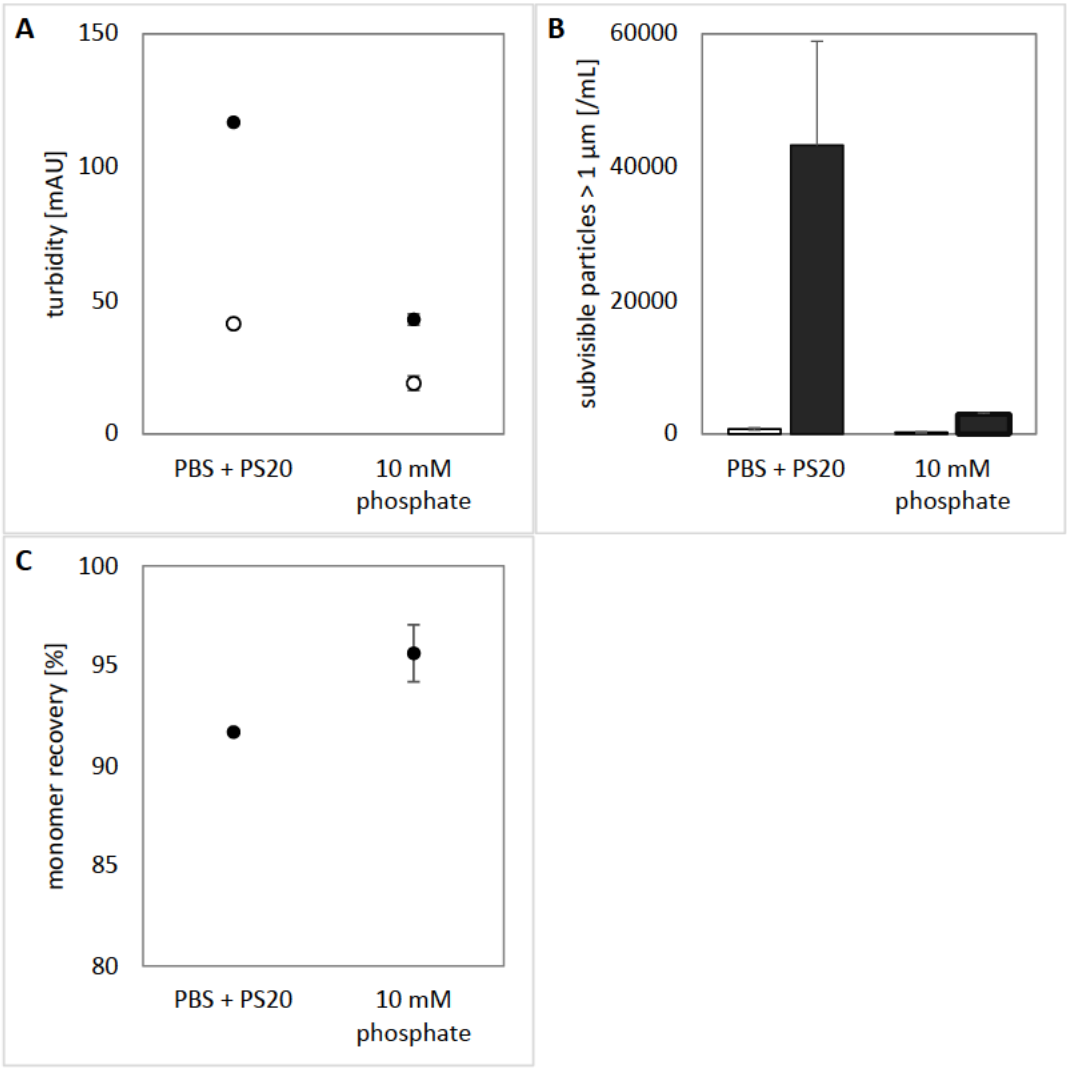

Figure VI-12: Stability of 10 mg/mL OVA formulated in PBS+PS20 and 4mg/mL OVA formulated in 10mM phosphate buffer before (white) and after nebulization with an Aeroneb® Pro (black), n=3 (mean ± SD).

3.5 Polyclonal anti-OVA IgG

3.5.1 Aeroneb® Pro

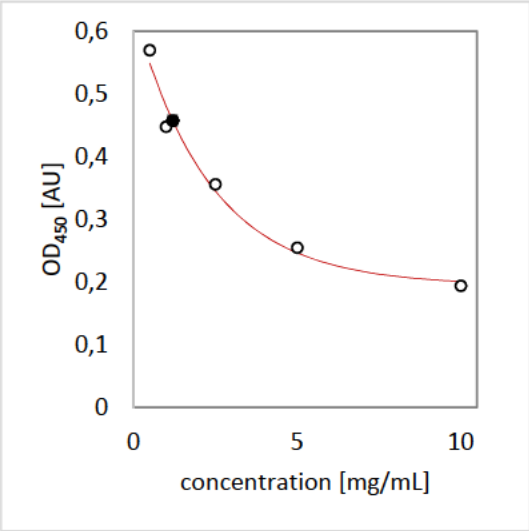

Figure VI-13: Calibration curve of an anti-OVA IgG specific ELISA assay in a range of 0.5-10.0 mg/mL anti-OVA IgG. The respective OD_{450} for anti-OVA IgG before and after nebulization with an Aeroneb® Pro is displayed (filled symbol) and both point overlay, n=3 (mean ± SD).

The polyclonal anti-OVA IgG was purchased in rabbit whole serum and used without further processing. The serum contained a total protein content of 70.8 mg/mL of which 4.2 mg/mL were polyclonal anti-OVA IgG. As analyzed by SEC, the total protein fraction contained 74% rabbit albumin and 17% immunoglobulins. 400 µL of the serum were nebulized with an Aeroneb® Pro and collected for stability analysis. The serum was examined with an ELISA assay specific for rabbit anti-OVA IgG to compare OVA binding activity before and after nebulization. The assay was calibrated and fitted in a range of 0.5-10.0 mg/mL anti-OVA IgG (Equation VI-1 and Figure VI-13). OVA binding activity was not affected by nebulization and remained at 100.0±11.0% (n=3, mean ± SD).

$$concentration_{anti-OVA\ IgG} = 0.43851 * e^{-\frac{OD450}{2.34038}} + 0.19485$$ *Equation VI-1*

Additionally, the protein mixture in the serum was analyzed by SEC regarding recovery of the immunoglobulin monomer peak and regarding aggregate formation by light obscuration and turbidity. Monomer recovery of the immune globulin peak at a retention time of 14.92 minutes was 98.1±0.7% (n=3, mean ± SD). The number of subvisible particle approximately doubled after nebulization but did not rise above levels reached with placebo controls (Figure VI-14 A).

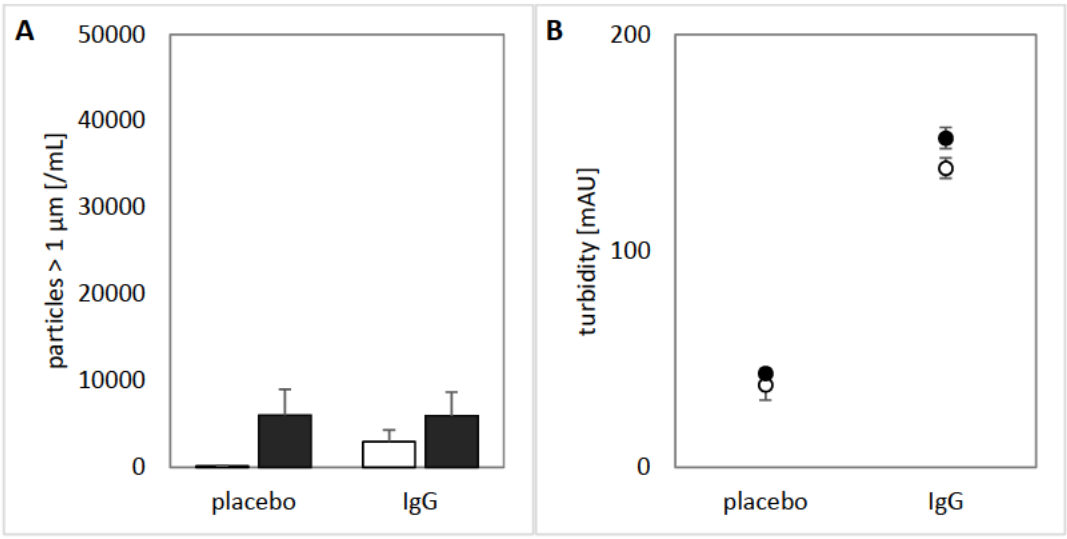

Figure VI-14: Aggregation of anti-OVA IgG in rabbit whole serum in respect to subvisible particles > 1 µm (A) and turbidity (B) before (white) and after (black) nebulization with an Aeroneb® Pro, n=3 (mean ± SD).

The pristine serum had a turbidity of 138 mAU which slightly increased by 14 mAU after nebulization. At the same time placebo turbidity increased by 5 mAU due to nebulization (Figure VI-14 B).

3.6 Conclusion

Investigation of SM101 stability during potential aerosol delivery procedures for *in vivo* studies confirmed that the aerosol formulation previously developed (Chapter V) is capable to deliver stable SM101 with the Penn-Century MicroSprayer® and with the Aeroneb® Pro nebulizer under the conditions intended for *in vivo* application. Once again, the parenteral formulation failed to protect SM101 under the tested nebulization conditions.

Anti-OVA IgG antibody retained its full OVA binding capacity and did not aggregate after nebulization with an Aeroneb® Pro. The antibody may therefore be used as purchased without further need of formulation development.

OVA antigen stability depended upon the administration method. While delivery with the MS did not negatively affect OVA stability, vibrating mesh nebulization of PBS formulated OVA caused monomer loss and OVA gel precipitation on surfaces including the vibrating mesh. The gelation phenomenon may severely impair the IVN procedure as gel formation on the vibrating mesh or the ventilation tubing used for intubation would prevent efficient aerosol generation and delivery. OVA gelation and aggregation were shown to be avoided when formulations of low ionic

strength are used instead of PBS. Simply reducing salt content to lower the ionic strength is not a viable option though, since salts, in this case sodium chloride, are also important for tonicity adjustment. Pulmonary formulations should be isosmotic to avoid airway irritation [18], which is especially important considering the large volume of solution delivered to the small murine lung. Plain reduction of salt content would render the formulation hypotonic though. A reduction of ionic strength must therefore be compensated by tonicity regulation with non-ionic tonicity modifiers like sugars or polyols. Alternatively, pulmonary delivery of OVA may easily be achieved by i.t. instillation or MS atomization instead of VM nebulization.

As a consequence, OVA and SM101 may not be used in the same formulation and formulations must not be mixed prior to administration since the higher ionic strength (Chapter V.2) and the polysorbate 20 content (Chapter V.3) required for SM101 stabilization would provoke OVA instability.

4 *In vivo* studies of SM101 efficacy

Based on this preparative work, the feasibility of SM101 efficacy testing with a non-reverse pulmonary Arthus disease model was evaluated by O. Schmid and his group at the Comprehensive Pneumology Center (CPC, Neuherberg, Germany). The model was based on the protocol employed by Skokowa et al. [2] but the delivery route for antigen and antibody were interchanged. OVA antigen was administered to the lungs via i.t. instillation, while anti-OVA antibody was given systemically via the tail vein. In a preliminary experiment, reverse and non-reverse Arthus reaction were induced and the impact compared. Therefore, the BALF was characterized in terms of total cell number and differential cell count of neutrophils, macrophages and lymphocytes as inflammation markers and red blood cell (RBC) counts to determine hemorrhage.

The differential cell count showed a distinct increase in neutrophils content in the BALF for the reverse and the non-reverse (direct) disease model (Figure VI-15). The lymphocyte population was not affected and the macrophage count was slightly increased after the reversed but not the direct model. According to RBC data, both models induce hemorrhage. While the RBC of the

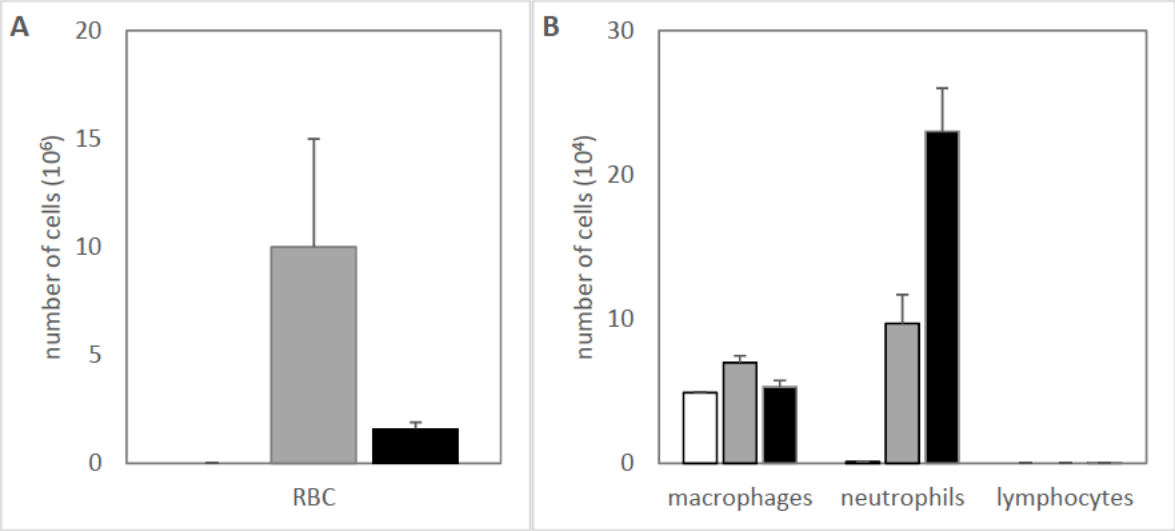

Figure VI-15: RBC (A) and differential cell count (B) for mice that received a protocol for the induction of either reverse (grey) or non-reverse (black) Arthus reaction compared to untreated mice (white)(n=3, mean ± SD).

direct model was an order of magnitude lower than for the reverse Arthus reaction, this was not statistically significant. Hemorrhage and inflammation, as reported for the reverse pulmonary Arthus reaction by Skokowa et al., have been achieved for the reverse and for the more physiological correct direct Arthus reaction model in mice.

The direct Arthus disease model was subsequently used to test SM101 efficacy *in vivo*. Therefore, mice were assigned to five different groups as listed in Table VI-2. Additionally to the systemic application of anti-OVA IgG and the i.t. instillation of OVA-antigen, SM101 or the respective placebo formulation were administered via IVN with a VM nebulizer. Mice in the "positive control" group received antigen and antibody but no SM101 in order to control if an Arthus reaction was induced. The "OVA control" group received only antigen and placebo formulation to distinguish potential non-specific immune response by OVA alone. Similarly the "lung control" group received the pulmonary administered OVA antigen and SM101 but no anti-OVA antibody. As a reference mice were assigned to a "home cage control" group and left untreated.

Table VI-2: Animal groups for first inhalation experiment

#	n	Group Name	*1st application (i.v.) anti-OVA IgG (100µl)*	*2nd application (i.t.) OVA-Antigen (50µl)*	*3rd application (nebulization) (100µl)*
1	3	Home Cage Control (HCC)	-	-	-
2	4	OVA Control	-	40µg	Placebo
3	5	Lung Control (LC)	-	40µg	SM101 (100µg)
4	5	Positive Control	420µg	40µg	Placebo
5	5	Treatment	420µg	40µg	SM101 (100µg)

Treatment and control group response was assessed from differential cell count of the BALF. As in the previous experiment, inflammation was monitored by total cell, macrophage and neutrophils cell count and hemorrhage was determined from erythrocyte numbers (Figure VI-16). The “positive control” group exhibited an increase in the total cell (TC) count, which was significant in respect to the “lung control” but not compared to the “OVA control” group since TC was slightly but not significantly increased compared to the home cage control (HCC) and lung control (LC) groups. Macrophage count in the “positive control” and the “OVA control” group were slightly increased above HCC and LC levels but differences between the groups were not significant. In the negative control groups, the vast majority of TC are macrophages as expected in normal BALF. The differential neutrophil count was significantly increased for the “positive control” group. In the OVA control group a slight yet insignificant rise was observable. Confirming the preliminary experiment, an inflammatory response was induced by the immune complex in the positive control group. The slight neutrophils increase for the OVA control group may indicate some inflammation caused by OVA alone but the fact that endotoxin free OVA was used and no neutrophil rise was observable after OVA application in the LC group do not support this assumption. SM101 inhalation reduced neutrophil numbers and macrophage counts to levels equal or below negative control groups.

The erythrocyte count suggests that no hemorrhage was induced in the positive control group, contradicting findings of the preliminary experiments (Figure VI-15). Instead, the erythrocyte count was significantly increased in the treatment group. Notably, no rise in erythrocytes was found for the lung control group that received the same dose of SM101 nor in any of the groups receiving placebo formulation by IVN. Furthermore, no hemorrhage occurred after reverse Arthus reaction treatment with sFcγRIIB by Skokowa et al. The erythrocyte count observed for the treatment group was comparable to the number found in the positive control group during an antigen and antibody dose finding experiment (Figure VI-17). Due to these observations, hemorrhage does not seem to stem from SM101 or the placebo formulation alone. One possibility may be tissue rupture related to IVN or subsequent animal preparation. The occurrence and accumulation merely in mice of the treatment group would be improbable though or linked to a yet unapparent circumstance. In combination with the failed positive control, no statement about the effect of SM101 on hemorrhage is legitimate.

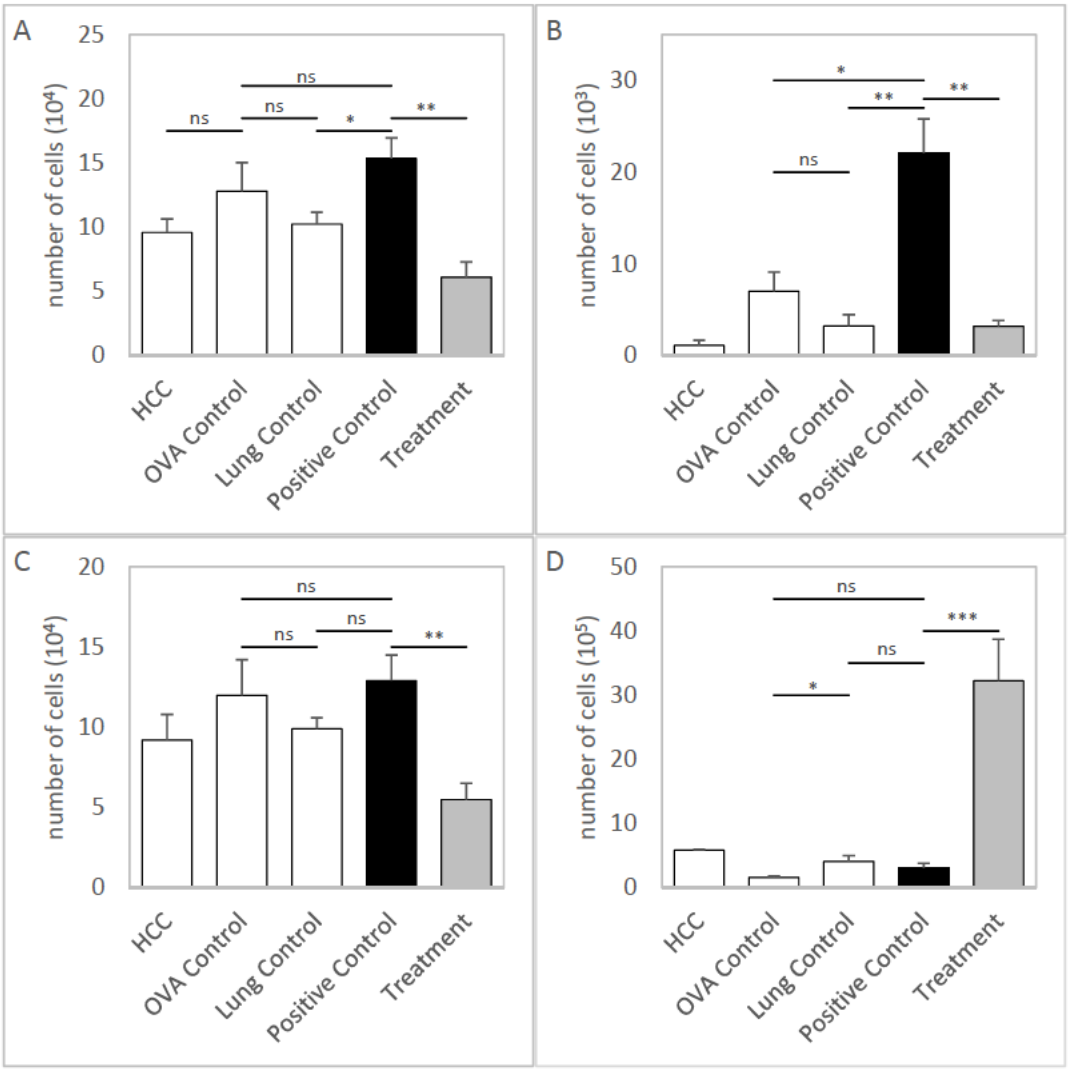

Figure VI-16: Total cell count (A), neutrophils (B), macrophages (C) and RBC (D) in the BALF of mice after the first inhalation experiment (n≥3 see Table III-10, mean ± SD).

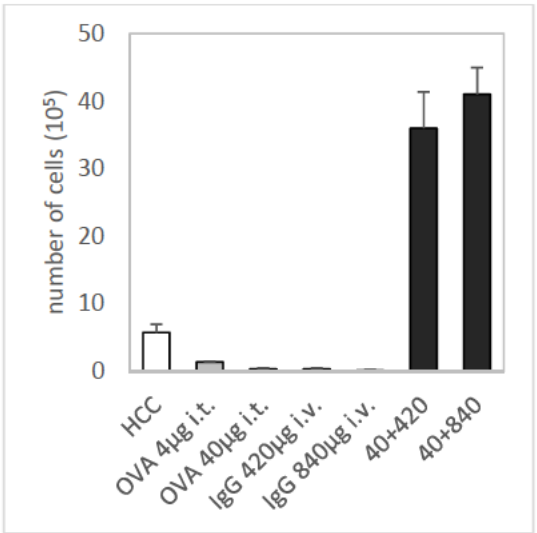

Figure VI-17: Erythrocyte count after administration of different amounts of OVA (light grey bars, i.t. instillation of 4 or 40 µg), anti-OVA IgG (dark grey bars, 420 or 840 µg i.v.) or administration of both (black bars), or none (white bar, HCC=home cage control)(n=3, mean ± SD).

Table VI-3: Animal groups for the second inhalation experiment

#	n	Group Name	1st application (i.v.) anti-OVA IgG (100µl)	2nd application (i.t.) OVA-Antigen (50µl)	3rd application (nebulization) (100µl)
1	4	Home Cage Control (HCC)	-	-	-
2	5	OVA Control	-	40µg	Placebo
3	5	Lung Control	-	40µg	SM101 (100µg)
4	5	Positive Control	420µg	40µg	Placebo
5	5	Treatment-inhal.	420µg	40µg	SM101 (100µg)
6	5	Treatment-i.t.	420µg	40µg	SM101 (100µg) (i.t.)

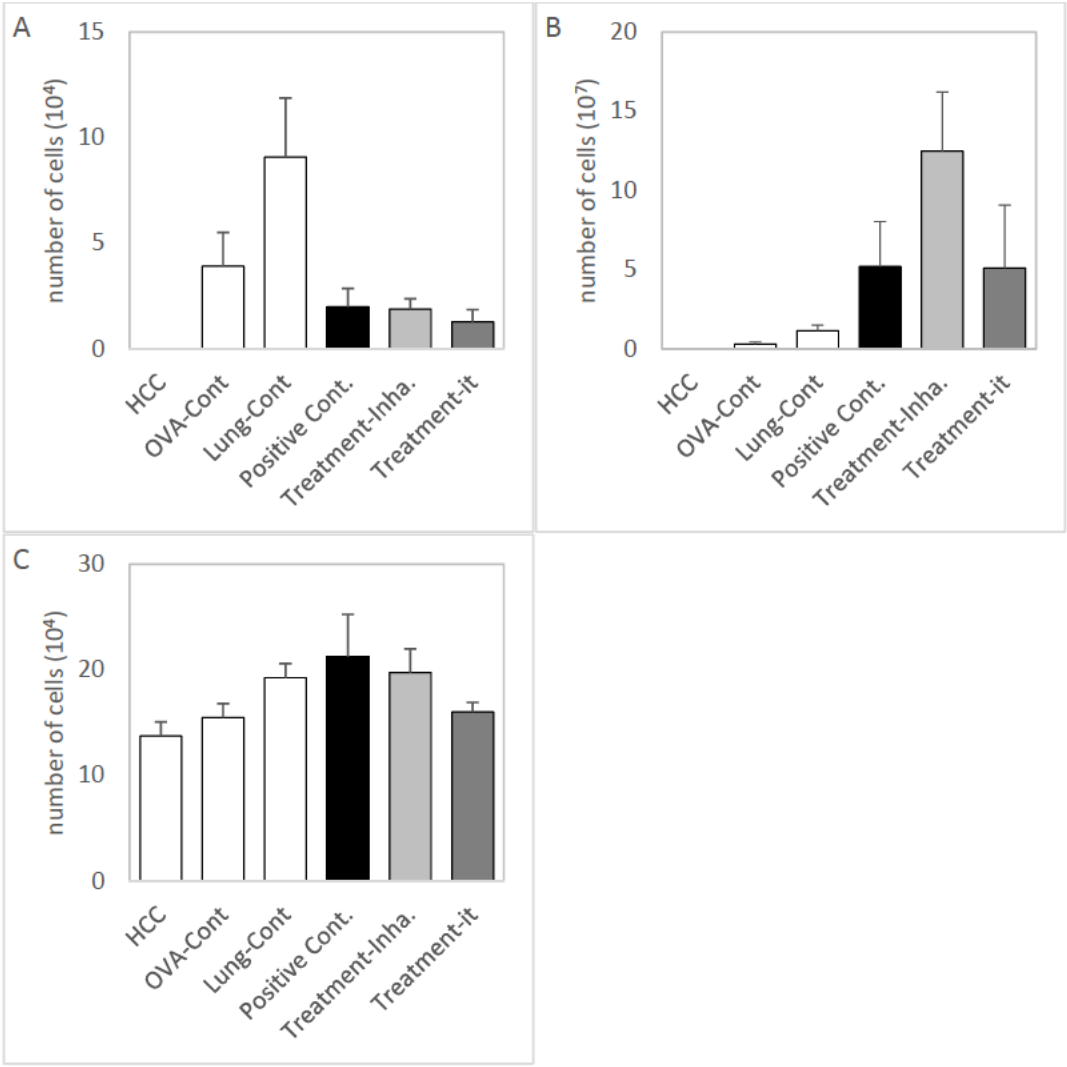

Figure VI-18: Count of neutrophils (A), RBC (B) and total cells (C) in the BALF after the second inhalation experiment (n=5, mean ± SD).

As a consequence of the ambiguous situation, the study was repeated. To the current control and treatment groups a sixth group was added that resembled the treatment group except that SM101 was delivered via i.t. instillation but not via IVN (Table VI-3).

While the total cell count may represent reasonable relations between the groups, the differential neutrophils count in the positive and negative control groups clearly shows that induction of the direct pulmonary Arthus reaction failed (Figure VI-18). Neutrophil count in the OVA control and especially the lung control group were distinctly increased. In contrast, neutrophils count in the positive control group was markedly lower than in these two negative control groups, where only an insignificant rise in neutrophils, as observed in the first iteration of the study, was expected. Notably though, in absolute numbers the positive control closely matches the results of the first experiment. Erythrocyte counts for the positive control and both treatment groups were one to two orders of magnitude higher compared to the first experiment. Even the lung control group exhibited an erythrocyte count well above the highest count observed in the first set of experiments.

4.1 Conclusion

Upon evaluation of these results, it had to be concluded that deduction of statements about SM101 efficacy or safety were not legitimate with the current data. The proposed protocol failed to induce a direct pulmonary Arthus reaction in mice in a reproducible manner. While preliminary experiments resulted in the infliction of inflammatory and hemorrhagic response as expected for a type III hypersensitivity reaction, in the subsequent study conducted with treatment groups, respective controls signaled a failure of either hemorrhagic response (first experiment) or inflammation (second experiment). The reasons for failure remain to be elucidated. To improve the robustness and reliability of the direct pulmonary Arthus reaction model, a detailed characterization of the influence of the different application regimes in direct and reverse pulmonary Arthus reaction on physiological processes should be considered in future research.

The apparent difficulties to reproducibly induce a direct pulmonary Arthus reaction may be a reason why only one study utilized a comparable direct pulmonary model on rabbits [19], while the reverse Arthus reaction, as used by Skokowa et al., is a standard model for pulmonary type III hypersensitivity reactions. Alternatively a disease model relying on active sensitization by repeated antigen exposure instead of passive sensitization by antibody administration may be established for *in vivo* efficacy testing of SM101.

5 Summary

Work related to SM101 efficacy testing *in vivo* is presented in this chapter. This included efforts to establish an animal disease model suitable for this purpose and the characterization of pulmonary delivery methods that may be used for small laboratory animals.

Comparison of pulmonary application methods demonstrated the benefit a MicroSprayer® can offer in small animal studies by combining the efficient delivery of an exact dose of i.t. instillation and the uniform aerosol distribution within the lung that more realistically resembles inhalation. This merging however, relies on actuation by a well-defined and constant pressure as accomplished by the developed pneumatic actuator.

SM101 efficacy may be studied by treatment of an immune complex (IC) mediated hypersensitivity reaction (type III). The pulmonary model of a reverse passive Arthus reaction is commonly used to induce such a reaction and has previously been employed to demonstrate sFcγRIIB efficacy to prevent inflammation and hemorrhage. However, the setup of the reverse model is considered futile in the case of SM101. Due to its mechanism of binding IC by the antibodies Fc-part, the rapid consecutive delivery of both the sensitizing antibody and SM101 by the pulmonary route may lead to premature SM101-IgG binding before IC were formed and a hypersensitivity reaction was induced. Therefore, a protocol to induce a more physiologically correct, direct (non-reverse) pulmonary Arhus disease in mice was developed. SM101 delivery remained by pulmonary route while the antibody was delivered systemically. The stability of antigen, antibody and SM101 to the pulmonary delivery procedures employed by either reverse or direct Arthus reaction was tested and ascertained. Yet, while inflammation and hemorrhage developed as expected in positive control groups during preliminary trials, the disease model failed to reliably induce a type III hypersensitivity reaction during consecutive and repeated attempts of SM101 efficacy investigation. The study results therefore do not support a legitimate statement on SM101 efficacy. The question of SM101 efficacy to treat pulmonary IC mediated hypersensitivity reactions could therefore not be conclusively settled within this work.

6 References

[1] J. Freitag (2012): Quantitative Bestimmung von fluoreszenz-gekoppelten Nanopartikeln und Proteinen in biologischen Materialien. Master Thesis, Universität Rostock: UMR/ZIM, Klinik I, Abt. Pneumologie.

[2] J. Skokowa, S.R. Ali, O. Felda, V. Kumar, S. Konrad, N. Shushakova, R.E. Schmidt, R.P. Piekorz, B. Nurnberg, K. Spicher, L. Birnbaumer, J. Zwirner, J.W.C. Claassens, J.S. Verbeek, N. van Rooijen, J. Kohl, J.E. Gessner, Macrophages Induce the Inflammatory Response in the Pulmonary Arthus Reaction through Gαi2 Activation That Controls C5aR and Fc Receptor Cooperation, J Immunol, 174 (2005) 3041-3050.

[3] D.L. Sylvestre, J.V. Ravetch, Fc receptors initiate the Arthus reaction: redefining the inflammatory cascade, Science (New York, N.Y.), 265 (1994) 1095-1098.

[4] Z. Ovary, O.G. Bier, Study of Arthus Reaction and of Cutaneous Anaphylaxis Induced Passively in the Rat, Experimental Biology and Medicine, 81 (1952) 584-586.

[5] B. Benacerraf, E.A. Kabat, A Quantitative Study of the Arthus Phenomenon Induced Passively in the Guinea Pig, The Journal of Immunology, 64 (1950) 1-19.

[6] J. Köhl, J.E. Gessner, On the role of complement and Fc γ-receptors in the Arthus reaction, Molecular Immunology, 36 (1999) 893-903.

[7] J.N. Pritchard, A. Holmes, J.C. Evans, N. Evans, R.J. Evans, A. Morgan, The distribution of dust in the rat lung following administration by inhalation and by single intratracheal instillation, Environmental Research, 36 (1985) 268-297.

[8] A.M. Dorries, P.A. Valberg, Heterogeneity of phagocytosis for inhaled versus instilled material, The American review of respiratory disease, 146 (1992) 831-837.

[9] J.D. Brain, D.E. Knudson, S.P. Sorokin, M.A. Davis, Pulmonary distribution of particles given by intratracheal instillation or by aerosol inhalation, Environmental Research, 11 (1976) 13-33.

[10] M. Osier, G. Oberörster, Intratracheal Inhalation vs Intratracheal Instillation: Differences in Particle Effects, Toxicological Sciences, 40 (1997) 220-227.

[11] S.E. Beck, B.L. Laube, C.I. Barberena, A.C. Fischer, R.J. Adams, K. Chesnut, T.R. Flotte, W.B. Guggino, Deposition and expression of aerosolized rAAV vectors in the lungs of Rhesus macaques, Molecular therapy : the journal of the American Society of Gene Therapy, 6 (2002) 546-554.

[12] L.A. Davies, S.C. Hyde, D.R. Gill, Plasmid Inhalation: Delivery to the Airways, in: DNA-Pharmaceuticals, Wiley-VCH Verlag GmbH & Co. KGaA, 2006, pp. 145-164.

[13] D. Yi, A. Price, A. Panoskaltsis-Mortari, A. Naqwi, T.S. Wiedmann, Measurement of the distribution of aerosols among mouse lobes by fluorescent imaging, Analytical Biochemistry, 403 (2010) 88-93.

[14] W.S. Gosal, S.B. Ross-Murphy, Globular protein gelation, Current Opinion in Colloid & Interface Science, 5 (2000) 188-194.

[15] C.H. Wang, S. Damodaran, Thermal gelation of globular proteins: influence of protein conformation on gel strength, Journal of Agricultural and Food Chemistry, 39 (1991) 433-438.

[16] M. Weijers, R.W. Visschers, T. Nicolai, Light Scattering Study of Heat-Induced Aggregation and Gelation of Ovalbumin, Macromolecules, 35 (2002) 4753-4762.

[17] F.S.M. Van Kleef, Thermally induced protein gelation: Gelation and rheological characterization of highly concentrated ovalbumin and soybean protein gels, Biopolymers, 25 (1986) 31-59.

[18] R. Beasley, P. Rafferty, S.T. Holgate, Adverse reactions to the non-drug constituents of nebuliser solutions, British Journal of Clinical Pharmacology, 25 (1988) 283-288.

[19] P.R. Cannon, T.E. Walsh, C.E. Marshall, Acute local anaphylactic inflammation of the lungs, The American journal of pathology, 17 (1941) 777-784.

Chapter VII Conclusion and Outlook

The overall objective of this thesis (**Chapter I**) was to investigate the suitability of vibrating mesh (VM) nebulization for the pulmonary delivery of sensitive pharmaceutical proteins. Emphasis was put on the interaction of protein, formulation and device regarding protein stability and nebulizer performance.

This issue derived from literature reports of advantageous properties of VM nebulization for the pulmonary delivery of small molecular drugs and the assumption that biopharmaceuticals may especially benefit from these improvements. Promising results, however, were so far only available for a handful of stable biopharmaceuticals and no comprehensive investigation about the impact of VM nebulization on protein stability had been carried out (**Chapter II**).

Basic stimulus and motivation for this work was to prove the feasibility of pulmonary delivery of stable and active SM101 (a soluble FcγRIIB) by VM nebulization, the development of a respective liquid formulation and *in vivo* efficacy testing. The presented solutions to issues raised throughout this quest are also applicable to the nebulization of biopharmaceuticals in general. The work conducted in this thesis is therefore a valuable contribution to the field of pulmonary protein delivery.

Materials and methods employed throughout the entire thesis are summarized in **Chapter III**.

Chapter IV summarizes work conducted to establish prerequisite tools necessary for a thorough investigation of VM nebulization, meaningful protein stability assessment after nebulization and the efficient pulmonary delivery of delicate biopharmaceuticals.

Initially, different VM nebulizers were tested regarding aerosol performance and found that the PARI eFlow® outperformed other models in generating aerosols of high respirable fraction at the highest output rate. Additionally, the PARI eFlow® did not suffer any performance losses upon decreasing surface tension, which was observed for the other tested nebulizers. This is of special importance, accounting for the surface activity of many protein molecules and of surfactants the most important group of excipients in liquid aerosol formulations. It could be shown that the

performance altering impact of viscosity, previously reported for various fluids of less importance in protein formulation, does also occur for commonly employed excipients and proteins themselves and must be considered in formulation design.

Besides aerosol performance, protein stability after nebulization is the most critical issue for successful pulmonary protein delivery. Since analytical methods rely on a bulk liquid, aerosol condensation and collection is a requirement. A comparison of collection methods mentioned in literature revealed that essentially all methods have the potential to alter protein stability. Protein degradation by collection may thereby be significantly greater than damage by actual nebulization. The investigation showed that aerosol collection in small volume reaction caps was related to the least protein degradation. It is very important to evaluate the impact of the planned collection procedure on protein stability before commencing with a study.

Significant heating was observed in the medication reservoir during PARI eFlow® operation. The resulting thermal stress was shown to be a major cause for the degradation of proteins during nebulization. The second major detrimental force identified was interfacial stress by atomization. The contribution of thermal degradation was investigated through nebulization at defined temperatures, which was accomplished with a newly developed prototype of a micro Peltier cooled nebulizer. These investigations also revealed a significant impact of nebulization temperature on key aerosol characteristics like droplet size and respirable fraction as well as output rate, which is related to the temperature dependence of viscosity. While a shrinking droplet size with reduced temperature is advantageous in terms of an increased respirable fraction, it is also accompanied by a decrease in output rate. Overall these contrary effects compensate, so that a defined drug dose could be delivered to the lungs in a comparable time frame but requiring less nominal dose if the nebulization temperature was lowered. Controlling the temperature in the medication reservoir is thus not only mandatory for maintaining the stability and activity of delicate proteins during VM nebulization, as demonstrated for LDH and SM101, but may also pose an attractive approach to improve the efficiency of pulmonary delivery. It may be worth to foster the development of the current prototype towards a VM nebulizer with fully integrated Peltier cooling.

Besides the powerful yet elaborate application of Peltier cooling, the temperature in the medication reservoir can also be managed by simple and readily available procedures. A

combination of overloading the medication reservoir and pre-cooling the solution efficiently reduced the reservoir temperature and protected heat sensitive SM101 during VM nebulization. This procedure is therefore highly recommended for VM nebulization of sensitive biopharmaceuticals.

Observed throughout this thesis and also reported in literature, protein nebulization often results in higher order aggregation. The impact of subvisible proteinaceous particles on the functionality of the micron-sized mesh was therefore assessed. A newly developed gravimetrical method for time resolved output rate measurement revealed how mesh occlusion by insufficiently stabilized proteins impairs nebulizer operation. This emphasizes the importance to assess and reduce protein aggregation during VM nebulization by means of formulation and reservoir temperature management. Time resolved output rate determination is a valuable tool for early detection of beginning mesh occlusion which may also be of interest for the development of particulate formulations for VM nebulization.

Based on the accomplished foundation, development of a liquid protein formulation for VM nebulization by a nebulizer specific high-throughput method was explored in **Chapter V**.

Initially, a parenteral formulation of SM101 was optimized to contain a fourfold increased protein concentration of 20 mg/mL. The failure of this formulation to protect SM101 during VM nebulization illustrated that integration of the nebulization process into formulation development is an essential requirement. To avoid laborious nebulization trials and conserve valuable resources, a high throughput screening method was developed that simulates the stress factors of VM nebulization identified in chapter IV. Thermal and interfacial stress was simply generated by vigorous agitation in half-filled reaction caps, while incubated at elevated temperatures. Agitation time and incubation temperature served to control the amount of stress generated. For SM101, settings remarkably resembling actual nebulization conditions allowed the precise prediction of the protective properties of a broad range of excipients with various stabilizing mechanisms. Notably, a direct match of screening results and actual nebulization required protein specific adjustment of screening method parameters. Therefore, universal method parameters were proposed that enabled a rapid screening for the three model proteins SM101, LDH and G-CSF.

The development of a dedicated aerosol formulation for VM nebulization of SM101 was entirely based on the newly developed screening method in conjunction with statistical experimental design. The main formulation factors determining SM101 stability were the concentrations of the surfactant PS20 and of the protein in the formulation. Hence, two lead formulation candidates were identified: One candidate (C1) contained the optimum amount of PS20 but conserved SM101 concentration to 20 mg/mL, while the other candidate (C2) contained the ideal PS20 concentration and a reduced SM101 content of 10 mg/mL. Both candidates were finally submitted to VM nebulization and the results of the screening thereby fully confirmed. Both candidates are a significant improvement compared to the parenteral formulation, whereas C2 was slightly more stable than C1, enabling efficient nebulization of SM101 without loss of activity or aggregation. Despite its reduced SM101 concentration, C2 was therefore designated to be used for all further testing of SM101.

In parallel, SM101 stability in both formulation candidates was also assessed after jet nebulization. Despite the absence of thermal stress, the recovered SM101 was less active after jet nebulization, emphasizing the eligibility of VM nebulization for sensitive biopharmaceuticals.

Work related to *in vivo* testing of SM101 efficacy is summarized in **Chapter VI**, which included efforts to establish an animal disease model suitable for this purpose and the characterization of pulmonary delivery methods applicable to small laboratory animals.

Comparison of pulmonary application methods demonstrated the benefit a MicroSprayer® can offer in small animal studies by combining the efficient delivery of an exact dose as by i.t. instillation and the uniform aerosol distribution within the lung that more realistically resembles inhalation. This merging however relies on actuation by a well-defined and constant pressure as accomplished by the developed pneumatic actuator.

SM101 efficacy may be studied by treatment of an immune complex (IC) mediated hypersensitivity reaction (type III). The pulmonary model of a reverse passive Arthus reaction is commonly used to induce such a reaction. It has previously been employed to demonstrate sFcγRIIB efficacy to prevent inflammation and hemorrhage. However, the setup of the reverse model was considered futile in the case of SM101. Due to its mechanism of binding IC by the antibodies Fc-part, the rapid consecutive delivery of both the sensitizing antibody and SM101

by the pulmonary route may lead to premature SM101-IgG binding, before IC were formed and a hypersensitivity reaction was induced. Therefore, a protocol to induce a more physiologically correct, direct (non-reverse) pulmonary Arhus reaction in mice was developed. SM101 delivery remained by pulmonary route while the antibody was delivered systemically. The stability of antigen, antibody and SM101 to the pulmonary delivery procedures employed by either reverse or direct Arthus reaction was tested and ascertained. Yet, while inflammation and hemorrhage developed as expected in positive control groups during preliminary trials, the disease model failed to reliably induce a type III hypersensitivity reaction during consecutive and repeated attempts of SM101 efficacy investigation. Therefore, the study results do not support a legitimate statement on SM101 efficacy.

To put it in a nutshell (**conclusion**), VM nebulization can be considered the preferential means of aerosol generation for liquid biopharmaceutical formulations. VM nebulizers have a low impact on protein stability and can be recommended for the pulmonary delivery of delicate biopharmaceuticals, provided that measures for temperature management inside the medication reservoir are adopted where necessary. Furthermore, they allow efficient and fast pulmonary delivery of large drug doses, especially when the latest device generation of highly efficient and reproducible breath-controlling VM nebulizers are employed.

While the applicability of VM nebulization for pulmonary delivery of SM101 was demonstrated, the question of SM101 efficacy to treat pulmonary IC mediated hypersensitivity reactions could not be conclusively settled within the frame of this work and should be the subject of further research. Emphasize should be put on the establishment of a robust animal model of a pulmonary type III hypersensitivity reaction. While further optimization of the non-reverse passive Arthus reaction protocol is an option worth pursuing, an alternative may be the induction of a hypersensitivity reaction by active sensitization through repeated antigen exposure.

Appendix

Associated publications

Original research and review articles

Hertel S., Pohl T., Friess W., Winter G., Prediction of protein degradation during vibrating mesh nebulization via a high throughput screening method, European Journal of Pharmaceutics and Biopharmaceutics, Available online 4 April 2014, http://dx.doi.org/10.1016/j.ejpb.2014.03.020.

Hertel S., Pohl T., Friess W., Winter G., That's cool! Nebulization of thermolabile proteins with a cooled vibrating mesh nebulizer, European Journal of Pharmaceutics and Biopharmaceutics, Available online 15 March 2014, http://dx.doi.org/10.1016/j.ejpb.2014.03.001.

Hertel S., Winter G., Friess W., Protein Stability in Pulmonary Drug Delivery via Nebulization, submitted to Advanced Drug Delivery Reviews

Proceedings and Abstracts contributed to international conferences

Hertel S., Friess W., Winter G., Comparison of Aerosol Collection Methods for Liquid Protein Formulations, RDD Europe 2011 (2011), Vol 2, pp 345-350

Hertel S., Friess W., Winter G., Degradation of thermolabile proteins during vibrating mesh nebulization is prevented by reservoir overloading, 8th World Meeting on Pharmaceutics, Biopharmaceutics and Pharmaceutical Technology, Istanbul, Turkey, March 19th - 22th, 2012.

Hertel S., Wurst F., Patzak M., Friess W., Winter G., High-throughput stability screening method for vibrating-mesh nebulization of protein formulations, 8th World Meeting on Pharmaceutics, Biopharmaceutics and Pharmaceutical Technology, Istanbul, Turkey, March 19th - 22th, 2012.